frontiers | Research Topics

Degradation, ecological restoration and adaptive management of estuarine wetlands under intensifying global changes, volume II

Edited by
Tian Xie, Milko Alberto Jorquera, Laibin Huang and Junhong Bai

Published in
Frontiers in Marine Science

ISSN 1664-8714
ISBN 978-2-8325-5113-4
DOI 10.3389/978-2-8325-5113-4

About Frontiers

Frontiers is more than just an open access publisher of scholarly articles: it is a pioneering approach to the world of academia, radically improving the way scholarly research is managed. The grand vision of Frontiers is a world where all people have an equal opportunity to seek, share and generate knowledge. Frontiers provides immediate and permanent online open access to all its publications, but this alone is not enough to realize our grand goals.

Frontiers journal series

The Frontiers journal series is a multi-tier and interdisciplinary set of open-access, online journals, promising a paradigm shift from the current review, selection and dissemination processes in academic publishing. All Frontiers journals are driven by researchers for researchers; therefore, they constitute a service to the scholarly community. At the same time, the *Frontiers journal series* operates on a revolutionary invention, the tiered publishing system, initially addressing specific communities of scholars, and gradually climbing up to broader public understanding, thus serving the interests of the lay society, too.

Dedication to quality

Each Frontiers article is a landmark of the highest quality, thanks to genuinely collaborative interactions between authors and review editors, who include some of the world's best academicians. Research must be certified by peers before entering a stream of knowledge that may eventually reach the public - and shape society; therefore, Frontiers only applies the most rigorous and unbiased reviews. Frontiers revolutionizes research publishing by freely delivering the most outstanding research, evaluated with no bias from both the academic and social point of view. By applying the most advanced information technologies, Frontiers is catapulting scholarly publishing into a new generation.

What are Frontiers Research Topics?

Frontiers Research Topics are very popular trademarks of the *Frontiers journals series*: they are collections of at least ten articles, all centered on a particular subject. With their unique mix of varied contributions from Original Research to Review Articles, Frontiers Research Topics unify the most influential researchers, the latest key findings and historical advances in a hot research area.

Find out more on how to host your own Frontiers Research Topic or contribute to one as an author by contacting the Frontiers editorial office: frontiersin.org/about/contact

Degradation, ecological restoration and adaptive management of estuarine wetlands under intensifying global changes, volume II

Topic editors

Tian Xie — Beijing Normal University, China

Milko Alberto Jorquera — University of La Frontera, Chile

Laibin Huang — University of California, Davis, United States

Junhong Bai — Beijing Normal University, China

Citation

Xie, T., Jorquera, M. A., Huang, L., Bai, J., eds. (2024). *Degradation, ecological restoration and adaptive management of estuarine wetlands under intensifying global changes, volume II*. Lausanne: Frontiers Media SA.

doi: 10.3389/978-2-8325-5113-4

Table of contents

frontiers | Frontiers in Marine Science

TYPE Editorial
PUBLISHED 25 June 2024
DOI 10.3389/fmars.2024.1429612

OPEN ACCESS

EDITED AND REVIEWED BY
Heliana Teixeira,
University of Aveiro, Portugal

*CORRESPONDENCE
Tian Xie
tianxie@bnu.edu.cn

RECEIVED 08 May 2024
ACCEPTED 23 May 2024
PUBLISHED 25 June 2024

CITATION
Ren Y, Xie T and Ning Z (2024) Editorial: Degradation, Ecological Restoration and Adaptive Management of Estuarine Wetlands under Intensifying Global Changes, Volume II. *Front. Mar. Sci.* 11:1429612. doi: 10.3389/fmars.2024.1429612

Editorial: Degradation, Ecological Restoration and Adaptive Management of Estuarine Wetlands under Intensifying Global Changes, Volume II

Yongning Ren[1], Tian Xie[1,2]* and Zhonghua Ning[1]

[1]State Key Joint Laboratory of Environmental Simulation and Pollution Control, School of Environment, Beijing Normal University, Beijing, China, [2]Yellow River Estuary Wetland Ecosystem Observation and Research Station, Ministry of Education, Shandong, China

KEYWORDS

anthropogenic pressures, eco-hydrological processes, ecosystem resistance and resilience, nature-based solutions, ecological networks

Editorial on the Research Topic
Degradation, Ecological Restoration and Adaptive Management of Estuarine Wetlands under Intensifying Global Changes, Volume II

This editorial focuses on the specific Research Topic "*Degradation, ecological restoration, and adaptive management of estuarine wetlands under intensifying global change*." We offer an overview and conclusions on the state-of-the-art research aimed at addressing the challenges encountered by estuarine wetlands under multiple pressures.

Estuarine wetlands provide various critical ecosystem services, including providing habitats for organisms, preventing seawater intrusion, biodiversity conservation, and microclimate regulation, in addition to nutrient cycling and carbon sequestration. Estuaries host numerous mega-cities which are characterized by intense human activity. The associated human disturbance has altered the structure and function of estuarine ecosystems through land reclamation, pollution, overfishing, and altered flows.

Moreover, estuarine wetlands are facing increasing threats from the effects of global climate change, including more frequent tsunamis, rising sea levels, and large-scale biological invasions. These environmental stressors not only affect primary and secondary productivity, community composition, distribution, and biodiversity within estuaries but also disrupt natural ecohydrological and biogeochemical processes, ultimately leading to the disruption of ecosystem services.

Multiple pressures on estuarine wetlands

High-intensity human reclamation is a key driver of the large-area loss and degradation of estuarine wetlands. The reduction of natural coastlines and the increase in the proportion of artificial coastlines in China has been a major source of concern. High-intensity reclamation not only causes coastline hardening but also decreases offshore

suspended sediment concentrations and aggravates natural coastline erosion (Li et al.). In addition, reclamation and the construction of dams affects tidal processes resulting in changes in key habitat factors such as salinity, moisture content and hydrological connectivity (Man et al.) in estuarine wetlands. Furthermore, considering estuarine wetlands are major carbon (C) pools (Li et al.), shifts in nutrient accumulation, salinity, and mineral factors in wetland sediments would affect the soil organic C (SOC) stability (Zhao et al.).

Fragmentation of plant patches caused by activities such as establishment of aquaculture ponds, ports, and farmland are some of the key pressures suffered by estuarine wetlands following reclamation (Zhang et al.), and they decrease the stability of estuarine wetland plant communities. Furthermore, in the wake of current extreme climate events, the risks of degradation and ecosystem collapse increase. The impacts of reclamation activities on wetland plants are observed over the entire life cycle of plants, including hindering seed diffusion, limiting plant seed germination, and causing the death of plant seedlings. Therefore, once plant communities are degraded, self restoration is difficult and permanent bare spots are likely to be established (Wang et al.). Strategies for the restoration of bare patches should be explored by coastal wetland managers.

Estuarine wetlands represent important breeding fields or wintering grounds for birds, such as along the East Asia-Australia Flyway (EAAF). However, the degradation of estuarine wetlands due to reclamation has led to the disappearance of suitable breeding grounds and habitats for birds and has placed numerous species at risk (Jordán et al.). Fish spawning grounds, feeding grounds, nursery grounds, and migration channels are hotspots for fish diversity conservation; however, comprehensive information on the shoreline morphology of remaining habitats and the relationships among habitat factors is still lacking, which hampers the targeted protection of key species (Xu et al.) and their habitats (Xu et al.; Zhou et al.).

Aquatic environment pollution in estuarine wetlands is another major stress factor. The concentrations of pollutants in estuaries are often higher than the local background values upstream due to the high intensity of human activities and complex hydrological processes in the estuaries (Yu et al.). The accumulation of pollutants such as heavy metals in estuarine wetland sediment and enrichment of animal and plant nutrients cause high ecological risks (Wang et al.).

As a highly open land–sea transition zone, estuarine wetlands are at high risk of invasion by alien species. Globally, most of the major estuaries, especially those with human development footprints, experience biological invasion. In China, *S. alterniflora* is the most invasive plant in estuarine wetlands. *S. alterniflora* is present in almost all estuaries in China from the southern tropical zone to the northern temperate zone. *S. alterniflora* has a strong capacity to expand following colonization in areas with high habitat invasibility and can expand outward through asexual reproduction (Yan et al.). In addition, *S. alterniflora* can establish along the tidal creek through seed dispersal. *S. alterniflora* invasion would influence the structure and function of wetland ecosystems considerably.

Biological adaptation to multiple pressures

In estuaries, the functional traits of wetland plants, including biomass, plant height, root–stem–leaf proportions, morphology, photosynthesis rate, nutrient contents, and functional enzyme activity, would adapt to the habitat conditions (Liu et al.). An increase in salinity in estuarine wetlands would reduce plant biomass (Mao et al.; Song et al.), in addition to plant investment in vegetative parts, while increasing their investment in reproductive parts to ensure the survival of their progeny (Wu et al.). Changes in plant functional traits can be employed as indicators of the degree of environmental stress (Wu et al.), in addition to plant adaptability to habitat change and the prediction of the evolution trends of plant community distribution and structure in future under environmental stress.

The effects of environmental stress on biological communities are also reflected in shifts in competitive relationships between species and in food chains. For example, interspecific relationships may shift from mutual competition to common resistance following an increase in environmental stress. In addition, changes in the distribution patterns and species compositions of plant–macroinvertebrates communities caused by environmental stress in estuarine wetlands (Li et al.) would directly affect foraging, concealment behavior of birds, and adaptability of birds to habitats (Lu et al.).

The effects of climate change and multiple pressures caused by high-intensity human activities on plant–soil relationships and root microbes are more subtle. Usually, plant–soil relationships are influenced by the morphological characteristics of the underground root system and the biochemical function of the root system (An et al.) With advancements in the development of underground ecological observation technologies, differences in the growth and development of plant roots and their capacity to absorb water and ions under different salinity and mineralization conditions have been observed in estuarine wetlands. Similarly, the allelopathy of plant roots and the secretion of allelochemicals in soil would change, in turn affecting soil physicochemical properties and affecting the responses of plant–soil interactions to external stress (Cui et al.). The bioturbation of soil or sediment by benthos, especially burrowing organisms such as crabs, would modify the sediment structure and cause the vertical migration of nutrients. Furthermore, crabs feed on plants, establishing plant –benthos–soil interactions (Xie et al.). Root microbes are more susceptible to environmental changes, and rhizosphere microbial community composition and functional diversity varies significantly across freshwater and saline water gradients (Ma et al.). Changes in microbial functional groups imply changes in organic matter mineralization and greenhouse gas emissions.

Ecological restoration to mitigate impacts

Estuarine wetland restoration projects are increasingly undertaken to mitigate the negative impacts of estuarine degradation. Such projects aim to re-establish various ecological attributes, including community structure (species diversity and habitat) and ecological processes (energy flow and nutrient cycling), which are associated with increased resilience and resistance of the estuarine ecosystems to abiotic and biotic stress factors. Increasingly adopted restoration practices, including wetland restoration (Li et al.) and efficient ecological management, improve the C storage capacity of wetlands and increase the blue C storage of estuarine wetlands.

Ecological restoration practices do not always yield satisfactory results, particularly in the wake of intensifying global change and socioeconomic change (Gibbons and Quijón). Ecologists, biologists, and environmental science researchers have been investigating effective solutions for application in the restoration of degraded estuarine wetland ecosystems globally. The concepts of "nature –based solutions," "adaptive management (Li et al.)," or "ecological networks" seem to offer great prospects and are currently being applied to estuarine ecosystem restoration based on risk and climate change adaptation and mitigation strategies.

New perspectives on monitoring wetlands restoration

Following the implementation of ecological restoration, assessing the results of these efforts will be crucial. Updating restoration techniques and adjusting restoration measures will be essential through thorough monitoring of the entire ecological restoration process. This requires a deep understanding of the ecosystem throughout the restoration process. The distribution patterns, community structures, and functional traits of animals and plants in estuarine wetlands are the products of long-term adaptation of animals and plants to the highly dynamic nature of estuaries and their oscillating environmental conditions (Sui et al.).

The interaction between freshwater and saline water associated with the interaction between runoff and tidal current in estuarine wetlands shapes estuarine wetland habitat characteristics. The interaction between runoff and tidal current is a dynamic equilibrium state, resulting in continuous fluctuation or periodic pulse that control estuarine wetland habitat factors. Plants that are most sensitive to changes in habitat factors usually exhibit hierarchical spatial self-organization under stress (Wang et al.). However, changes in habitat elements caused by multiple pressures, such as runoff, sediment change, and sea level rise, exceed the adaptive threshold of animals and plants, which transform multiple homeostasis states in biological communities and cause community degradation (Duan et al.).

In the face of high-intensity short-term pressures, such as storm surges and human reclamation activities, animal and plant communities will undoubtedly exhibit major responses (Fan et al.). Afterward, the animal and plant communities would recover, and when the stress intensity exceeds the resistance threshold of the animal and plant communities, artificial restoration strategies are required to reconstruct the community. Compared with artificial restoration, enhancing the adaptability and self-recovery capacity of biotic communities is a natural solution.

As the world enters the United Nations Decade on Ecosystem Restoration (2021–2030), countries and organizations globally are paying greater attention to innovative ecological restoration approaches that could facilitate the achievement of the full potential of such ecosystems in delivery of social and ecological value, and in turn, sustainable development. Therefore, it is essential to explore how anthropogenic disturbance and climate change are affecting estuarine wetlands and the latest restoration frameworks that can guide future practice toward conservation and restoration of the biodiversity of estuarine wetlands.

Author contributions

YR: Writing – original draft. TX: Funding acquisition, Resources, Supervision, Validation, Visualization, Writing – original draft, Writing – review & editing. ZN: Writing – review & editing.

Funding

The author(s) declare financial support was received for the research, authorship, and/or publication of this article. This Research Topic was supported by National Natural Science Foundation of China (52271256).

Conflict of interest

The authors declare that the research was conducted in the absence of any commercial or financial relationships that could be construed as a potential conflict of interest.

Publisher's note

References

Fan, W., Xu, Z., Dong, Q., Chen, W., and Cai, Y. (2023). Remote sensing-based spatiotemporal variation and driving factor assessment of chlorophyll-a concentrations in China's Pearl River Estuary. *Front. Mar. Sci.* 10. doi: 10.3389/fmars.2023.1226234

Gibbons, E. G., and Quijón, P. A. (2023). Macroalgal features and their influence on associated biodiversity: implications for conservation and restoration. *Front. Mar. Sci.* 10. doi: 10.3389/fmars.2023.1304000

Jordán, F., Jordán, F., Capelli, G., Capelli, G., Primicerio, R., and Bodini, A. (2024). Strongly asymmetric interactions and control regimes in the Barents Sea: a topological food web analysis. *Front. Mar. Sci.* 11. doi: 10.3389/fmars.2024.1301612

Liu, X., Wang, G., Zhang, H., Han, G., Li, K., and Wang, A. (2023). Inconsistent stoichiometry and growth responses of two coexisting dominant species to various N and P supplies in a supratidal wetland of the Yellow River Delta. *Front. Mar. Sci.* 10. doi: 10.3389/fmars.2023.1113629

Man, Y., Zhou, F., Wang, Q., and Cui, B. (2023). Quantitative evaluation of sea reclamation activities on tidal creek connectivity. *Front. Mar. Sci.* 10. doi: 10.3389/fmars.2023.1164065

Mao, P., Lin, Q., Pang, Y., Wang, K., Ni, R., Han, X., et al. (2023). Eco-physiological response mechanism of Tamarix chinensis to soil water changes in coastal wetlands of the Yellow River Delta. *Front. Mar. Sci.* 10. doi: 10.3389/fmars.2023.1231928

Wang, Y., Wang, X., Khan, S., Zhou, D., and Ke, Y. (2023). Evaluation of mangrove restoration effectiveness using remote sensing indices - a case study in Guangxi Shankou Mangrove National Natural Reserve, China. *Front. Mar. Sci.* 10. doi: 10.3389/fmars.2023.1280373

Wu, W., Grimes, E., and Suir, G. (2023). Impact of freshwater diversions on vegetation in coastal wetlands based on remote sensing derived vegetation index. *Front. Mar. Sci.* 10. doi: 10.3389/fmars.2023.1202300

Xu, Y., Huang, F., Zhou, M., Gu, R., Zhu, J., Rong, Q., et al. (2023a). Recognizing topological attributes and spatiotemporal patterns in spotted seals (Phoca largha) trophic networks based on eDNA metabarcoding. *Front. Mar. Sci.* 10. doi: 10.3389/fmars.2023.1305763

Xu, Y., Huo, X., Jordán, F., Zhou, M., Cai, Y., and Sun, J. (2023b). Identifying marine food web homogenization patterns. *Front. Mar. Sci.* 10. doi: 10.3389/fmars.2023.1245513

frontiers | Frontiers in Marine Science

TYPE Original Research
PUBLISHED 19 January 2023
DOI 10.3389/fmars.2023.1113629

OPEN ACCESS

EDITED BY
Laibin Huang,
University of California, Davis, United States

REVIEWED BY
Jiang Bao Xia,
Shandong Key Laboratory of Eco-Environmental Science for the Yellow River Delta, Binzhou University, China
Hao Chen,
Institute of Oceanology, Chinese Academy of Sciences (CAS), China

*CORRESPONDENCE
Guangmei Wang
gmwang@yic.ac.cn

SPECIALTY SECTION
This article was submitted to Marine Ecosystem Ecology, a section of the journal Frontiers in Marine Science

RECEIVED 08 December 2022
ACCEPTED 04 January 2023
PUBLISHED 19 January 2023

CITATION
Liu X, Wang G, Zhang H, Han G, Li K and Wang A (2023) Inconsistent stoichiometry and growth responses of two coexisting dominant species to various N and P supplies in a supratidal wetland of the Yellow River Delta.
Front. Mar. Sci. 10:1113629.
doi: 10.3389/fmars.2023.1113629

Inconsistent stoichiometry and growth responses of two coexisting dominant species to various N and P supplies in a supratidal wetland of the Yellow River Delta

Xiaoling Liu[1], Guangmei Wang[1]*, Haibo Zhang[1], Guangxuan Han[1], Kexin Li[1,2] and Andong Wang[3]

[1]CAS Key Laboratory of Coastal Environmental Processes and Ecological Remediation, Yantai Institute of Coastal Zone Research (YIC), Chinese Academy of Sciences (CAS), Shandong Key Laboratory of Coastal Environmental Processes, YICCAS, Yantai, China, [2]Key Laboratory of Forest Ecosystem Process of Beijing, Beijing Forestry University, Beijing, China, [3]Administration Bureau of the Yellow River Delta National Nature Reserve, Dongying, China

The availability and stoichiometry ratio of nitrogen (N) and phosphorus (P) play vital roles in plant trophic dynamics and primary production. However, the responses of these plant traits to varying N and P supplies remain largely unclear for supratidal wetland herbs. Here, we conducted a 4-year field manipulation experiment in a supratidal wetland in the Yellow River Delta. The changes in aboveground biomass, leaf N and P concentrations and N:P ratios of two dominant herbs (*Suaeda glauca* and *Phragmites australis*) were examined at 3 overall nutrient supply levels (low, medium and high) combined with 3 N:P supply ratios (5:1, 15:1 and 45:1). The results showed that the leaf trophic dynamics of the two dominant species rely on the overall supply level as well as on the N:P supply ratio, while the aboveground biomass of both species was only significantly influenced by the overall supply level. With the increase in supply level, *S. glauca* gained an advantage over *P. australis* in aboveground biomass competition. The leaf N and P concentrations of both species raised with the respective increasing nutrient inputs, and N:P improved with the increasing supply ratio. The leaf stoichiometry of *S. glauca* was more strongly influenced by the various N and P supplies than that of *P. australis*. Specifically, the gap of nutrient contents between the two species widened as nutrient availability improved, with the dominance of *S. glauca* increasing while that of *P. australis* decreasing. This species-specific response may explain the altered aboveground biomass of the two species. Our findings suggested that changing the N and P supply can potentially influence primary productivity by changing leaf nutrient status, indirectly affecting the shifts in plant dominance and community composition in supratidal wetland ecosystems.

KEYWORDS

N and P supply, dominant species, aboveground biomass, leaf nutrient stoichiometry, supratidal wetland

1 Introduction

Nitrogen (N) and phosphorus (P) are essential nutrients controlling plant growth and primary production (Elser et al., 2007; Sardans and Peñuelas, 2012). In terrestrial ecosystems, the increase in N deposition due to fossil fuel burning and anthropogenic fertilizer input has not been paralleled by a proportional increase in P inputs (Venterink and Güsewell, 2010; Peñuelas et al., 2012), leading to changes in the ambient N and P supply status from both aspects of overall supply level and relative supply ratio (Elser et al., 2009; Carnicer et al., 2015). Normally, plants respond to these changes at metabolic and physiological levels (Elser et al., 2010; Wang et al., 2018; Chen et al., 2020) and further alter the elemental composition and growth rate of plants (Sardans and Peñuelas, 2012). As responses are frequently species-specific (Mayor et al., 2014), patterns of plant competition and dominant species in the plant community may be changed (Bobbink et al., 2010).

Plants can optimize nutrient acquisition and conservation strategies to acclimate to altered nutrient availability and elemental stoichiometry (Yan et al., 2014; Huang et al., 2018a; Jin et al., 2020). Accordingly, the concentrations and stoichiometric ratio of N and P in plants are widely used to reflect the plant nutrient status and nutrient supply of ecosystems (Sardans and Peñuelas, 2012). Notably, many previous studies have focused on green leaves (Mayor et al., 2014; Yan et al., 2018; Liu et al., 2021). Leaf nutrient dynamics are a more reliable indicator of plant adaptive strategies than total nutrient concentrations (Yang, 2018; Xu et al., 2021); moreover, their species-specific responses could explain the changes in community structure (Wan et al., 2020). To date, the effects of altered absolute nutrient availability on leaf N and P stoichiometry have been well demonstrated (Lü et al., 2013; Jing et al., 2017; Huang et al., 2018b). Evidence from grasslands, wetlands, and forests indicates that enriched N and P availability generally increased the respective nutrient concentrations in the leaves (Yuan and Chen, 2015), which will in turn have important feedbacks on productivity (Li et al., 2016; Huang et al., 2018b). The N:P supply ratio is also perceived as a key factor affecting leaf nutrient traits, which could influence the trade-offs in the nutrient allocation of different species and may explain their distinct performances under competition (Venterink and Güsewell, 2010; Yuan et al., 2013); however, relatively little attention has been given to it. Considering that the environmental N and P status had been changed from both the overall supply level and the supply ratio, it is necessary to distinguish the respective and interactive effects of the two aspects on the leaf nutrient status thus to predict future changes in the productivity and community composition.

Wetlands are experiencing an increase in reactive N and P loadings globally (Jordan et al., 2011; Wolf et al., 2013; Hu et al., 2017), and the plant trophic dynamics under the changing external environment have been extensively studied in wetland ecosystems (Yuan and Chen, 2015). Nonetheless, the response of plant stoichiometry to varying N and P supplies, and its role in vegetation community structure shifts, are still elusive due to different climate, vegetation and soil properties (Yue et al., 2017; Gao et al., 2018; Wan et al., 2020). Given these uncertainties, more studies are urgently needed to further reveal the plant ecological stoichiometry responses to altered nutrient supply conditions in wetlands.

The Yellow River Delta wetland, the most efficiently conserved and youngest wetland ecosystem in the warm temperature zone in China, is regarded as vulnerable to climate change and anthropogenic impacts (Yu et al., 2016). During the last several decades, jointly influenced by atmospheric deposition and regional economic development, the region has been undergoing increasing N and P inputs, which has significant impact on plant communities (Yu et al., 2014; Li et al., 2017). Generally, the adaptive capacity of plants to environmental change varies with species evolutionary history, and may lead a change in interspecific competition, thus shifting the community composition (Peñuelas et al., 2008; Sardans and Peñuelas, 2014; Sardans et al., 2015). *Suaeda glauca* and *Phragmites australis* are two dominant species in the supratidal wetland of this area but have received little attention in previous studies. Comparatively, *S. glauca* is an annual forb and is restricted to the upland of the Yellow River Delta (He et al., 2012), while *P. australis* is a perennial and widespread wetland grass (Guo et al., 2018). Although our previous study based on a field-stimulated experiment showed how the two species respond to various N and P supplies (Liu et al., 2019), it mainly focused on the variation in their dominance, while the species-specific responses of leaf nutrient status and plant biomass remain unclear.

In this study, we examined the effects of nutrient supply level and N:P supply ratio on the aboveground biomass and leaf nutrient stoichiometry of *P. australis* and *S. glauca* using the same field-stimulated experiment (Liu et al., 2019). The primary objectives of this study were to (*i*) clarify the main and interactive effects of nutrient supply level and supply ratio on the aboveground biomass and leaf nutrient stoichiometry of two dominant species, (*ii*) assess the linkage between aboveground biomass and leaf nutrient stoichiometry in two dominant species, and (*iii*) compare the plant growth strategies employed by two dominant species in response to various N and P supplies. Our previous findings suggest that the plant community composition in this area was only affected by the overall nutrient supply level, in which *S. glauca* became increasingly dominant with increasing supply level and thus suppressed other species, including *P. australis*. In addition, the N:P supply ratio and overall supply level both significantly affected the concentrations of soil inorganic N and available P and the N:P ratio, with the soil resource availability being more affected by the supply level and the soil N:P ratio being overridingly influenced by the N:P supply ratio (Liu et al., 2019). We therefore hypothesized that (*i*) the aboveground biomass of both species was only significantly influenced by the overall supply level, while the leaf nutrient stoichiometry relied on the overall supply level as well as on the N:P supply ratio (*H1*); (*ii*) the aboveground biomass of *S. glauca* was positively associated with the altered leaf nutrient contents, while the performance of *P. australis* was the opposite, and there was no significant relationship between the N:P and aboveground biomass of both species (*H2*); and (*iii*) *S. glauca* exhibited relatively greater plasticity in plant growth strategies than *P. australis*, leading to its dominance in the plant community under increased nutrient inputs (*H3*).

2 Materials and methods

2.1 Experimental site

This study was conducted in the Yellow River Delta Ecology Research Station of Coastal Wetland (37°45'52" N, 118°58'52" E), Chinese Academy of Sciences. The study site has a warm-temperate

and continental monsoon climate with a mean annual temperature and precipitation of 12.9°C and 560 mm, respectively. This area is periodically flooded from July to September, and nearly 70% of the annual precipitation is concentrated in this period. The soil type is a saline-alkali soil with a pH of 7.20–7.89 and conductivity of 1.64–3.15 ms cm^{-1}. The dominant plant species at the experimental site are *S. glauca*, *P. australis* and *Suaeda salsa*, comprising more than 90% of the total aboveground biomass.

2.2 Experimental design

In July 2014, a N and P addition experiment was installed to simulate future nutrient supply changes in this wetland. Detailed information about the experimental design has been reported in a previous study (Liu et al., 2019). Briefly, there were nine fertilization treatments combined with 3 overall nutrient supply levels (low, medium, high) and 3 N:P supply ratios (5:1, 15:1, 45:1) with four replicates for each treatment, and one control treatment (CK) was also set up with six replicates, for a total of 42 plots (Figure 1). Each plot was 3.5 × 3.5 m in size and was laid out separated by 1 m aisles. Starting in 2015, fertilizer was applied twice each year with 50% of the supply in early April and 50% in late June. N and P were supplied as urea and dihydrogen phosphate (NaH_2PO_4) dissolved in 6 L water, respectively, and the CK plots received an equal amount of water.

2.3 Field sampling and measurement

In late July 2018, peak aboveground biomass was estimated by clipping at ground level in three 0.3 m × 0.3 m random quadrats within each plot and sorting the biomass into different species. After clipping, living biomass was oven-dried at 75 °C for 48 h to a consistent weight and then weighed and ground. Dominant species *S. glauca* and *P. australis* were sampled in all experimental plots (Figure 2), while another dominant species *S. salsa* was not sampled in 3/4 of the high nutrient supply experimental plots due to its low occurrence. Therefore, we only measured the N and P concentrations of *S. glauca* and *P. australis*. Total N concentrations in plant leaf were analyzed by a C/N analyzer (Vario Micro, Germany). For total P concentration, powders of plant leaf samples were digested with H_2SO_4-H_2O_2 and then determined by the molybdenum blue method on a continuous-flow autoanalyzer (AA3, Seal Analytical, Germany).

2.4 Statistical analysis

Data were tested for normality using Levene's test. Two-way ANOVA was employed to examine the effects of supply level, supply ratio and their interactions on aboveground biomass, N concentration, P concentration and the N:P ratio of the two species. The ANOVAs were followed by S-N-K *post hoc* tests to determine the difference level (if necessary). Independent samples t-test was used to compare the mean values of the parameters between the two species under different N and P supplies. The Pearson coefficient was calculated to detect the relationship between the community biomass and aboveground biomass of the two species and the correlation among the N and P concentrations, the N:P ratio and the aboveground biomass of the two species. Structural equation model (SEM) was further constructed with Amos 21.0 software (SPSS Inc., IBM Co., Armonk, NY, USA) to examine direct and indirect hypothetical relationships among supply level, supply ratio, plant N and P concentrations, plant N:P ratios and plant biomass. In these analyses, the data were fit to the model using maximum likelihood estimation. All statistical analyses were performed with SPSS 17.0 (SPSS Inc., Chicago, IL, USA). The significance level was set as 0.05.

3 Results

3.1 Effects on aboveground biomass

The increase in aboveground biomass of *S. glauca* (B_{Sg}) occurred in all N and P addition plots compared to the control plots (Figure 3A). In contrast, the aboveground biomass of *P. australis*

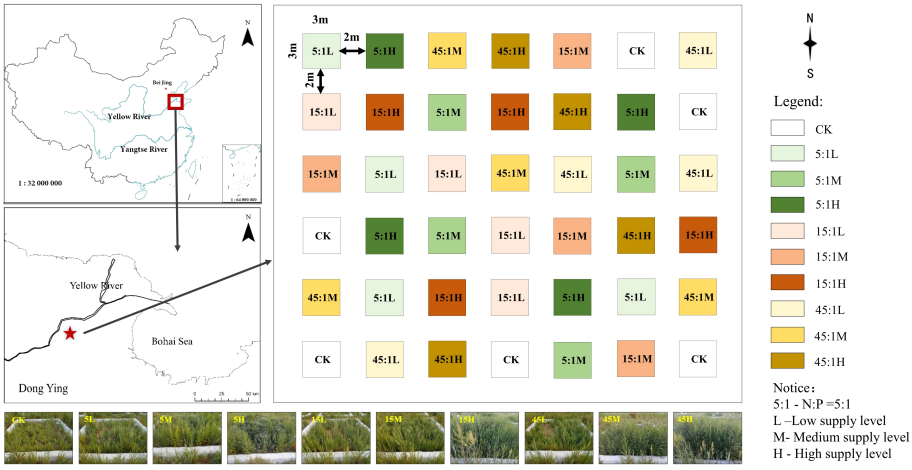

FIGURE 1
Location and layout of the experimental plots.

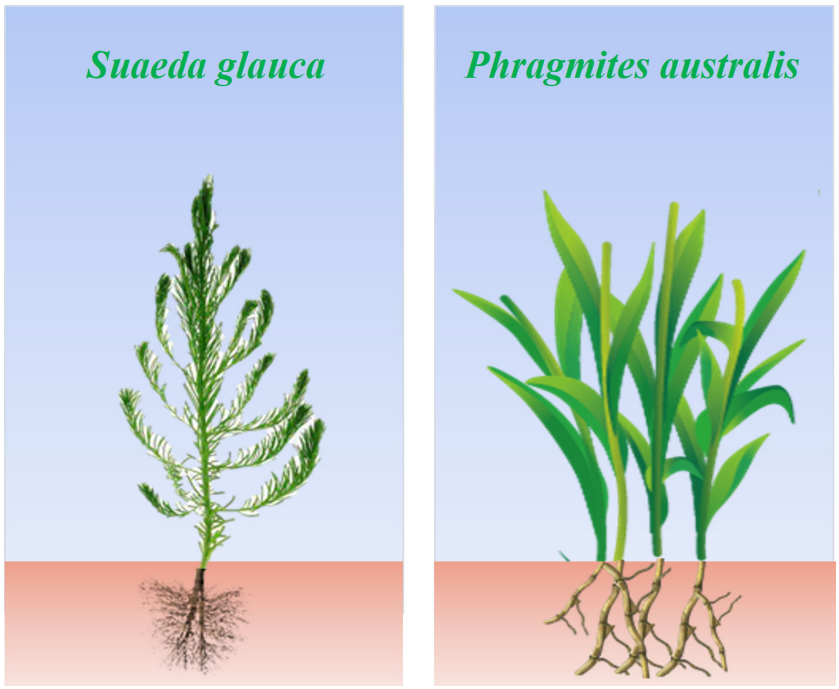

FIGURE 2
S. glauca is a C3 annual forb with fibrous roots; *P. australis* is a C4 perennial rhizome grass.

(B_{Pa}) decreased with N and P addition, except for the 5:1 M and 45:1 M treatments (Figure 3B). Both B_{Sg} and B_{Pa} were significantly affected by the N and P supply level rather than the supply ratio, and no significant supply level × supply ratio interaction was observed (Table 1). Compared with the control treatment, B_{Sg} increased strongly at the medium and high supply level, while B_{Pa} decreased significantly at the low and high supply level (Figure 4A). With the rise of the overall supply level, B_{Sg} increased significantly between all gradual supply levels. For B_{Pa}, there was no difference between the low and medium supply level, while it decreased significantly at the high supply level. Relative to B_{Pa}, $B_{Sg}$was lower at the low supply level, nearly equal at the medium supply level, and higher at the high supply level (Figure 4A).

The plant community structure in the control plots was co-dominated by *S. glauca* (20.8%) and *P. australis* (57.6%) with over 75% of the total aboveground biomass (Figure 4B). However, these two dominant species showed opposite patterns in relative aboveground biomass along the nutrient supply gradient. When the supply level reached a high level, *S. glauca* became the single-dominant species, accounting for 88.4% of the total aboveground biomass, while *P. australis* deceased to only 10.9%. Further linear regression analysis showed that the community biomass response was positively correlated with B_{Sg} (P<0.001, Supplementary Figure S1) and negatively correlated with B_{Pa}(P=0.005, Supplementary Figure S1).

3.2 Effects on N and P stoichiometry

For both *S. glauca* and *P. australis*, all of the N and P addition treatments had greater N and P concentrations than the control

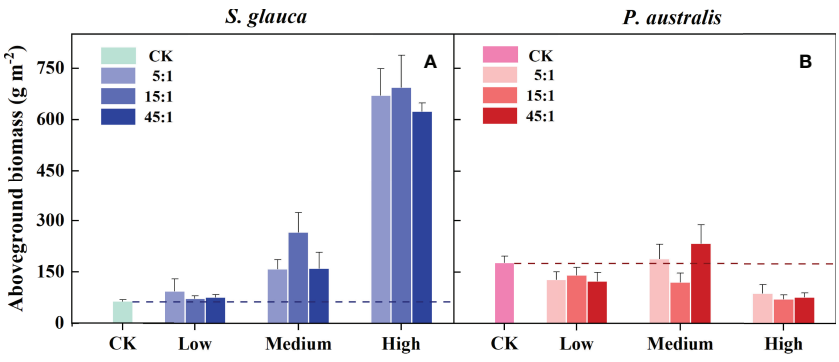

FIGURE 3
Effects of N and P addition on aboveground biomass of *S. glauca* **(A)** and *P. australis* **(B)**. CK=control. Different bars indicate the mean value (± SE) for each treatment (N and P addition, n=4; CK, n=6).

TABLE 1 Two-way ANOVA for the aboveground biomass of *S. glauca* and *P. australis* using the overall supply level (SL) and N:P supply ratio (SR) as the main effects. P-values in bold indicate significant differences at P < 0.05.

Source	*df*	*S. glauca*		*P. australis*	
		F	*P*	*F*	*P*
Supply Level (SL)	2	111.763	**<0.001**	8.638	**<0.001**
Supply Ratio (SR)	2	0.991	0.384	0.984	0.387
SL×SR	4	0.526	0.717	1.416	0.256

Significant P values are marked in bold (P < 0.05).

treatment (Figures 5A–D). However, foliar nutritional traits responded differently to changing N and P supply conditions between *S. glauca* and *P. australis*. Two-way ANOVA showed that the effects of supply level and supply ratio on the N and P concentrations of *S. glauca* were significant, and there was a significant supply level × supply ratio interaction. For *P. australis*, the P concentration was significantly affected by the supply level and supply ratio, while the N concentration was only significantly affected by the supply level, and no significant supply level × supply ratio interaction was observed (Table 2). In terms of the N:P ratio, the supply ratio rather than the supply level had a significant effect on both species, and a significant supply level × supply ratio interaction was observed only for *S. glauca*. The N and P concentrations of the two species tended to increase with increasing supply level. With the increase in the supply ratio, the N concentration and N:P ratio also increased, while the P concentration declined (Figures 5E–F, Supplementary Figure S2).

Overall, changing the supply conditions affected the foliar nutritional traits of *S. glauca* more than those of *P. australis*, which could be indicated by the *F* value (Table 2). Correspondingly, the N and P concentrations of *S. glauca* among the 3 supply levels and 3 supply ratios were all significantly different, and there were significant differences in N:P among the 3 supply ratio gradients. Otherwise, the N and P concentrations of *P. australis* increased significantly only at the high supply level, and only the high supply ratio significantly increased the N:P ratio and decreased the P concentration. At the medium and high supply level, the N and P concentrations of *S. glauca* were significantly higher than those of *P. australis*. Furthermore, the N concentration of *S. glauca* was significantly higher than that of *P. australis* at the 45:1 supply ratio, and the P concentration was significantly higher at the 5:1 and 15:1 supply ratio. Compared with the N:P ratio of *P. australis*, that of *S. glauca* was higher at the 45:1 supply ratio and lower at the 5:1 and 15:1 supply ratio (Supplementary Figure S2).

3.3 Linkages between nutrient stoichiometry and aboveground biomass

The SEM results indicated that the supply level had a significant positive direct effect on the leaf N and P concentrations of *S. glauca* and *P. australis* (Figure 6). In addition, the supply ratio had a significant negative direct effect on the leaf P concentrations of *S. glauca* and *P. australis*, whereas it had a significant positive direct effect on the leaf N concentration of *S. glauca*. The leaf N concentrations of *S. glauca* and *P. australis* showed significant positive correlations with the N:P ratios of the corresponding species, which is contrary to the observed relationship between leaf P concentration and the N:P ratio. Regression analysis suggested that the variation in the N:P ratio was primarily determined by foliar P for both species (Supplementary Figure S3). The two dominant species showed opposite patterns in the relationship between leaf nutrient concentrations and aboveground biomass. The N and P concentrations of *S. glauca* had a positive direct effect on the biomass of *S. glauca*, but the N and P concentrations of *P. australis* had a negative direct effect on the biomass of *P. australis* (Figure 6, Supplementary Figure S4). However, there were no significant correlations between the aboveground biomass of the two species and the N:P ratio of the corresponding species.

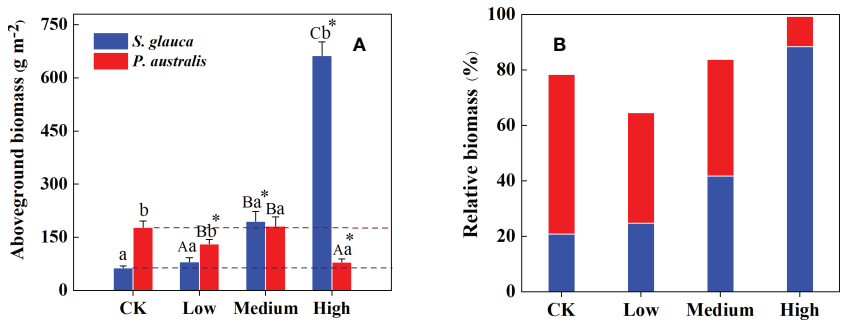

FIGURE 4
Mean aboveground biomass **(A)** and relative biomass **(B)** of *S. glauca* and *P. australis* under different treatments. Data show the mean ± SE (supply level treatment, n=12; control treatment, n=6). Different capital letters represent significant differences in plant biomass among the three supply level treatments at the 0.05 level. Different lowercase letters represent significant differences between *S. glauca* and *P. australis* under the same treatments at the 0.05 level. * denotes a significant difference between the control treatment and the supply level treatment at the 0.05 level.

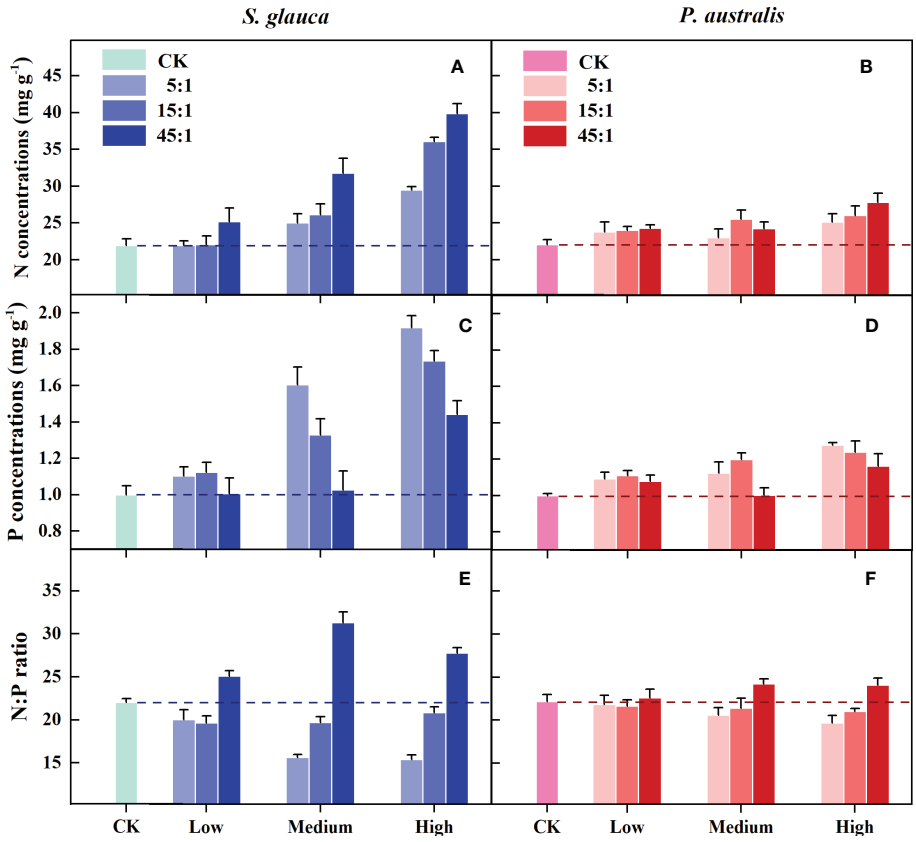

FIGURE 5
Effects of N and P addition on the N **(A, B)** and P concentrations **(C, D)** and the N:P ratio **(E, F)** of S. glauca and P. australis. Different bars indicate the mean value (± SE) for each treatment (N and P addition, n=4; CK, n=6). Green and red indicate positive and negative relationships corrected to red and green indicate positive and negative relationships.

4 Discussion

4.1 Effects of the overall supply level and supply ratio on plant aboveground biomass

The responses of *S. glauca* and *P. australis* to N and P supply were inconsistent from the perspective of plant biomass. Overall, N and P supply had a positive effect on the biomass of *S. glauca* and a negative effect on that of *P. australis* (except for the 5:1 M and 45:1 M treatments). The results correspond principally with our first hypothesis (*H1*), the biomass of both species was mainly affected by the supply level rather than either the supply ratio or the interactive effect. Correlation analysis of species biomass and soil properties demonstrated that B_{Sg} was significantly correlated with soil available P (R^2 = 0.309, n =36, P<0.01) and the available N:P ratio (R^2 = 0.130, n =36, P=0.031), while B_{Pa} was negatively correlated with soil conductivity (R^2 = 0.185, n =36, P=0.009). Correspondingly, our previous analysis showed that the supply level affected the soil available P, available N:P ratio and soil conductivity more than the supply ratio in the 4th study year (Liu et al., 2019), which could help

TABLE 2 Two-way ANOVA for N and P concentrations and the N:P ratio of *S. glauca* and *P. australis* using the overall supply level (SL) and N:P supply ratio (SR) as the main effects. P-values in bold indicate indicate significant differences at P < 0.05.

Species	Source	*df*	N concentration		P concentration		N: P ratio	
			F	*P*	*F*	*P*	*F*	P
S. glauca	SL	2	67.543	**<0.001**	49.602	**<0.001**	0.984	0.387
	SR	2	21.272	**<0.001**	19.099	**<0.001**	157.139	**<0.001**
	SL×SR	4	2.691	0.052	2.783	**0.047**	13.126	**<0.001**
P. australis	SL	2	4.221	**0.025**	7.773	**0.002**	0.303	0.741
	SR	2	1.605	0.219	4.297	**0.024**	9.663	**<0.001**
	SL×SR	4	0.768	0.555	1.149	0.355	1.276	0.304

Significant P values are marked in bold (P < 0.05).

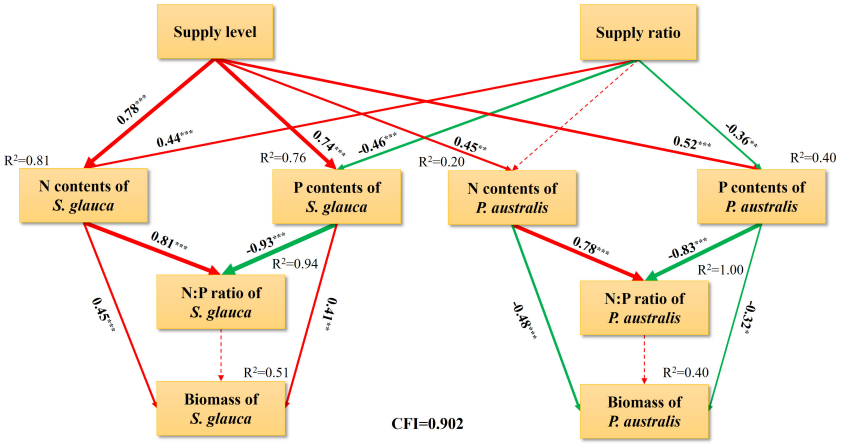

FIGURE 6
Structural equation model (SEM) considering the underlying causal relationships among leaf N and P contents, N:P ratio and biomass of *S. glauca* and *P. australis* under various N and P supplies. CFI, confirmatory fit index. Bold and dashed lines indicate significant ($P<0.05$) and nonsignificant ($P>0.05$) pathways, respectively. The width of arrows indicates the strength of the causal effect, while arrows colored red and green indicate positive and negative relationships respectively. The numbers listed within arrows are the standardized path coefficients. The R^2 values represent the proportion of the variance explained for each variable. Significance levels are as follows: $^*P < 0.05$, $^{**}P < 0.01$, and $^{***}P < 0.001$.

explain the stronger effects of the supply level on plant aboveground biomass.

As frequently observed in previous studies, grasses and forbs may have contrasting biomass responses to nutrient inputs (Xia and Wan, 2008; Li et al., 2019). Grasses often have high resource use ability and consequently become increasingly dominant with nutrient supply (Zhang et al., 2018a; Su et al., 2020). However, the response of the grass species *P. australis* in our study is some different. The dominance shifted from *P. australis* in low nutrient condition to *S. glauca* in high nutrient condition, indicating *S. glauca* was well acclimated to nutrient enrichment. Shifts in species dominance may favor acquisitive rather than conservative resource use strategies (Lan and Bai, 2012). *P. australis*, as a C3 species with conservative resource-use strategies, might perform poorer than *S. glauca* (C4 species) when exposed to the same changing nutrient conditions (Wang et al., 2015; Zhang et al., 2018b). That is, *S. glauca*, with faster-growing traits, tends to have a high aboveground competitive ability following nutrient enrichment, which indirectly causes a reduction of *P. australis* dominance. Additionally, the enhancement of *S. glauca* led to the positive response of plant community biomass to nutrient addition (Supplementary Figure S1), which confirmed that the growth of *S. glauca* was the main driver of changes in the plant community (Liu et al., 2019).

4.2 Effects of the overall supply level and supply ratio on plant N and P stoichiometry

Generally, the varying supplies of N and P had significant effects on plant N and P uptake (Fujita et al., 2010; Chen et al., 2020), which could further mediate plant stoichiometry (Zhan et al., 2017). For instance, a pot-culture study showed that the N:P supply ratio had a significant effect on the N and P concentrations and the N:P ratio of wetland grasses through a direct effect on nutrient uptake, whereas the supply level only affected the N:P ratio with a slight effect (Güsewell, 2005). Partly consistent with hypothesis 1 (*H1*), our results indicated that the leaf N and P concentrations of *S. glauca* and *P. australis* were affected more by the supply level than by the supply ratio, while the plant N:P ratio only varied as a function of the supply ratio. Given the positive feedback between soil nutrient availability and plant nutrient contents (Fan et al., 2015; Lü et al., 2015; Su et al., 2021), the inconsistent result with the previous study (Liu et al., 2019) was probably caused by the fact that supply level mainly affected soil resource availability, while the N:P supply ratio overridingly influenced the variations of the soil N:P. Moreover, we found that supply level and supply ratio significantly interacted to affect the N and P concentrations and N:P of *S. glauca*. This observation highlights the importance of the synergistic effects of supply level and supply ratio on plant stoichiometry (Güsewell and Bollens, 2003; Venterink and Güsewell, 2010), although the underlying mechanism remains unclear.

From the perspective of plant stoichiometry, species with distinct resource use strategies may exhibit different responses to the same changes in environmental conditions (Lü et al., 2015; Li et al., 2019; Qi et al., 2015). Consistent with previous results (Mao et al., 2016; Huang et al., 2018a), the N and P concentrations of both *S. glauca* and *P. australis* were significantly enhanced with corresponding increasing N and P input amounts. Theoretically, *P. australis* is a clonal rhizome grass with strong root reproduction and could benefit from relatively rapid extensive growth to have more chances to access different available nutrients (Cao et al., 2021). Unlike the extensiveness of *P. australis* root growth, *S. glauca* is a forb with fibrous roots, and its forage range for obtaining soil available nutrients is relatively limited. Unexpectedly, in contrast to the pattern observed with *S. glauca*, *P. australis* exhibited a lower variability in N and P concentrations with the input of corresponding elements, suggesting the relatively stable access of *P. australis* to N and P despite the nutrient supply gradients (Li et al., 2014; Lü et al., 2015). The nutrient supply had a greater effect intensity on the leaf nutritional traits of *S. glauca* than that of *P. australis* after fertilization annually for four

years. By comparing variations in the N:P ratio of the two species along the supply ratio gradient, we found that P limitation was transformed to N-P colimitation in *S. glauca* under decreased N:P supply ratios, whereas *P. australis* remained P limited (Güsewell, 2004) (Supplementary Figure S2). These results supported the idea that grasses with stronger homeostasis are generally less sensitive to varying N and P supplies than forbs (Yu et al., 2011; Luo et al., 2016). Accordingly, leaf stoichiometry of *P. australis* spanned a much smaller range than the nutrient availability gradient due to the plant's regulatory control (Qi et al., 2015), and that in *S. glauca* could better reflect variation in the N and P supply.

4.3 Plant growth strategies under varying supplies of N and P

In this study, variation in leaf N:P ratios was primarily determined by the response of leaf P concentration, which emphasized the important role of P in affecting plant growth in the supratidal wetland in the Yellow River Delta (Liu et al., 2019). Concretely, the leaf N:P ratios of the two dominant species improved with increasing N concentrations and decreasing P concentrations. Based on this, both the leaf N and P concentrations of the two species increased with increasing supply level, and the leaf N:P ratio remained relatively constant, indicating a higher access of the species to both nutrients and no change in its relative access to N and P (Lü et al., 2015). Alternatively, with an increasing N:P supply ratio, the leaf N concentration improved, while the P concentration exhibited an opposite change trend thus directly determined the positive response of the leaf N:P ratio to the supply ratio. In accordance with the growth rate hypothesis (Elser et al., 2000), changes of plants N:P ratio under changing environments would directly affect biomass accumulation, while our results do not support this view. Our observations suggest that the aboveground biomass of the two dominant species was significantly affected by the supply level rather than the supply ratio, while the leaf N:P ratio was significantly affected by the supply ratio rather than the supply level, which may indirectly result in no significant correlations between the aboveground biomass and the leaf N:P ratio of the two species.

Although species-level stoichiometry exhibited a similar response trend under varying nutrient statuses, the altered leaf nutrients of the two species in turn have divergent feedbacks to plant aboveground biomass (Huang et al., 2018b). Consistent with our expectation (*H2*), the aboveground biomass of *S. glauca* increased with increasing leaf N and P concentrations, while that of *P. australis* increased with reducing leaf N and P concentrations, which may be partially attributed to the differences in their growth strategies. With acquisitive resource-use strategies, *S. glauca* showed high leaf nutrient contents, corresponding to high aboveground competitive ability (Lan and Bai, 2012). In contrast, *P. australis* with conservation resource-use strategies exhibited disadvantages in competition, and even increased leaf nutrient contents were insufficient to increase biomass accumulation. Rather, a previous study found that the nutrient contents of grasses affected their biomass positively, while forbs showed an opposite trend (Li et al., 2019). Considering that our results are contrary to the typical expectations (Fujita et al., 2014; Luo et al., 2016), more empirical evidence is needed to clarify the competitive strategies between these two functional groups.

Together, these results supported our third hypothesis (*H3*) that *S. glauca* exhibited relatively greater plasticity in growth strategies than *P. australis*. Our SEM consistently showed that *S. glauca* has stronger positive feedback under nutrient enrichment (Figure 6) and therefore contributes to increasingly dominance when facing elevated N and P inputs. This finding might provide an underlying mechanism for the changes in the plant community structure from the *S. glauca* and *P. australis* co-dominant community to the *S. glauca* single-dominant community under N and P enrichment.

5 Conclusion

Unbalanced N and P supply as well as absolute nutrient status significantly influenced the leaf stoichiometry of both *S. glauca* and *P. australis*, however, the aboveground biomass of the two species was only significantly affected by the overall supply level. Nutrient enrichment promoted the growth of *S. glauca* but decreased the biomass of *P. australis* in the coexist community, owing to the strong competitiveness of *S. glauca* to resources. There was both convergence and divergence in the responses of the leaf stoichiometry of *S. glauca* and *P. australis* to various N and P supplies. The plasticity of nutrient resorption in *S. glauca* was much higher than that of *P. australis*, although the leaf N and P concentrations of the two species were both significantly enhanced with the increase in corresponding nutrient availability. Furthermore, the altered nutrient concentrations of the two species in turn have contrasting feedbacks to aboveground biomass due to the substantial differences in growth strategies. Comparatively, *S. glauca* with acquisitive resource-use strategies might become increasingly dominant under increasing nutrient inputs in the supratidal wetland in the Yellow River Delta. These species-specific responses are contrary to the typical expectations of competitive outcomes between grasses and forbs in nutrient supply conditions. The results can provide a scientific basis for adaptive management of wetlands under evolving nutrition change. As the prescribed fertilization was only performed for four years in this study, continuous monitoring is needed to test whether the results still be constant under longer-term fertilization.

Data availability statement

The original contributions presented in the study are included in the article/Supplementary Material. Further inquiries can be directed to the corresponding author.

Author contributions

XL and GW designed the project and wrote the manuscript with contributions from GH and AW. HZ, KL and XL performed the

experiment and data analysis. All authors contributed to the article and approved the submitted version.

Funding

This work was funded by Joint Funds of the National Natural Science Foundation of China (U2243207), the Strategic Priority Research Program of the Chinese Academy of Sciences, China (XDA23050202), International Science Partnership Program of the Chinese Academy of Sciences (121311KYSB20190029) and the Habitat and Bird Dynamics Monitoring Project of the Yellow River Delta National Reserve (Y991021021).

Acknowledgments

We would like to thank the support from Yellow River Delta Ecological Research Station of Coastal Wetland, CAS, and thank Changli Yang for field work. We thank the reviewers for helpful comments on revision of this manuscript.

Conflict of interest

The authors declare that the research was conducted in the absence of any commercial or financial relationships that could be construed as a potential conflict of interest.

Publisher's note

Supplementary material

The Supplementary Material for this article can be found online at: https://www.frontiersin.org/articles/10.3389/fmars.2023.1113629/full#supplementary-material

References

Bobbink, R., Hicks, K., Galloway, J., Spranger, T., Alkemade, R., Ashmore, M., et al. (2010). Global assessment of nitrogen deposition effects on terrestrial plant diversity: a synthesis. *Ecol. Appl.* 20, 30–59. doi: 10.1890/08-1140.1

Cao, J. R., Yang, L. Y., Pang, S., Yang, J. J., Hu, Y. C., Li, Y. C., et al. (2021). Convergent nitrogen uptake patterns and divergent nitrogen acquisition strategies of coexisting plant species in response to long-term nitrogen enrichment in a temperate grassland. *Environ. Exp. Bot.* 185, 104412. doi: 10.1016/j.envexpbot.2021.104412

Carnicer, J., Sardans, J., Stefanescu, C., Ubach, A., Bartrons, M., Asensio, D., et al. (2015). Global biodiversity, stoichiometry and ecosystem function responses to human-induced C–N–P imbalances. *J. Plant Physiol.* 172, 82–91. doi: 10.1016/j.jplph.2014.07.022

Chen, Z. F., Xiong, P. F., Zhou, J. J., Lai, S. B., Jian, C. X., Wang, Z., et al. (2020). Photosynthesis and nutrient-use efficiency in response to n and p addition in three dominant grassland species on the semiarid loess plateau. *Photosynthetica* 58, 1028–1039. doi: 10.32615/ps.2020.056

Elser, J. J., Andersen, T., Baron, J. S., Bergström, A.-K., Jansson, M., Kyle, M., et al. (2009). Shifts in lake N:P stoichiometry and nutrient limitation driven by atmospheric nitrogen deposition. *Sci. (80-.).* 326, 835–837. doi: 10.1126/science.1176199

Elser, J. J., Bracken, M. E. S., Cleland, E. E., Gruner, D. S., Harpole, W. S., Hillebrand, H., et al. (2007). Global analysis of nitrogen and phosphorus limitation of primary producers in freshwater, marine and terrestrial ecosystems. *Ecol. Lett.* 10, 1135–1142. doi: 10.1111/j.1461-0248.2007.01113.x

Elser, J. J., Fagan, W. F., Kerkhoff, A. J., Swenson, N. G., and Enquist, B. J. (2010). Biological stoichiometry of plant production: metabolism, scaling and ecological response to global change. *New Phytol.* 186, 593–608. doi: 10.1111/j.1469-8137.2010.03214.x

Elser and O'Brien, Dobberfuhl and Dowling (2000). The evolution of ecosystem processes: growth rate and elemental stoichiometry of a key herbivore in temperate and arctic habitats. *J. Evol. Biol.* 13, 845–853. doi: 10.1046/j.1420-9101.2000.00215.x

Fan, H. B., Wu, J. P., Liu, W. F., Yuan, Y. H., Hu, L., and Cai, Q. K. (2015). Linkages of plant and soil C:N:P stoichiometry and their relationships to forest growth in subtropical plantations. *Plant Soil* 392, 127–138. doi: 10.1007/s11104-015-2444-2

Fujita, Y., de Ruiter, P. C., Wassen, M. J., and Heil, G. W. (2010). Time-dependent, species-specific effects of N:P stoichiometry on grassland plant growth. *Plant Soil* 334, 99–112. doi: 10.1007/s11104-010-0495-y

Fujita, Y., Venterink, H. O., van Bodegom, P. M., Douma, J. C., Heil, G. W., Hölzel, N., et al. (2014). Low investment in sexual reproduction threatens plants adapted to phosphorus limitation. *Nature* 505, 82–86. doi: 10.1038/nature12733

Gao, Y. H., Cooper, D. J., and Zeng, X. Y. (2018). Nitrogen, not phosphorus, enrichment controls biomass production in alpine wetlands on the Tibetan plateau, China. *Ecol. Eng.* 116, 31–34. doi: 10.1016/j.ecoleng.2018.02.016

Guo, X., Yu, T., Li, M. Y., and Guo, W. H. (2018). The effects of salt and rainfall pattern on morphological and photosynthetic characteristics of *Phragmites australis* (Poaceae) [1]. *J. Torrey Bot. Soc* 145, 212–224. doi: 10.3159/TORREY-D-17-00003.1

Güsewell, S. (2004). N : P ratios in terrestrial plants: variation and functional significance. *New Phytol.* 164, 243–266. doi: 10.1111/j.1469-8137.2004.01192.x

Güsewell, S. (2005). Responses of wetland graminoids to the relative supply of nitrogen and phosphorus. *Plant Ecol.* 176, 35–55. doi: 10.1007/s11258-004-0010-8

Güsewell, S., and Bollens, U. (2003). Composition of plant species mixtures grown at various N:P ratios and levels of nutrient supply. *Basic Appl. Ecol.* 4, 453–466. doi: 10.1078/1439-1791-00174

He, Q., Cui, B. S., Bertness, M. D., and An, Y. (2012). Testing the importance of plant strategies on facilitation using congeners in a coastal community. *Ecology* 93, 2023–2029. doi: 10.1890/12-0241.1

Huang, J. Y., Wang, P., Niu, Y. B., Yu, H. L., Ma, F., Xiao, G. J., et al. (2018a). Changes in C:N:P stoichiometry modify n and p conservation strategies of a desert steppe species glycyrrhiza uralensis. *Sci. Rep.* 8, 12668. doi: 10.1038/s41598-018-30324-w

Huang, J. Y., Yu, H. L., Liu, J. L., Luo, C. K., Sun, Z. J., Ma, K. B., et al. (2018b). Phosphorus addition changes belowground biomass and C:N:P stoichiometry of two desert steppe plants under simulated n deposition. *Sci. Rep.* 8, 3400. doi: 10.1038/s41598-018-21565-w

Hu, M. J., Wilson, B. J., Sun, Z. G., Ren, P., and Tong, C. (2017). Effects of the addition of nitrogen and sulfate on CH_4 and CO_2 emissions, soil, and pore water chemistry in a high marsh of the Min river estuary in southeastern China. *Sci. Total Environ.* 579, 292–304. doi: 10.1016/j.scitotenv.2016.11.103

Jing, H., Zhou, H. X., Wang, G. L., Xue, S., Liu, G. B., and Duan, M. C. (2017). Nitrogen addition changes the stoichiometry and growth rate of different organs in pinus tabuliformis seedlings. *Front. Plant Sci.* 8, 1922. doi: 10.3389/fpls.2017.01922

Jin, X. M., Yang, L. X., Yang, X. G., Guan, Q. X., Ma, Z. S., Pan, J., et al. (2020). Effects of n and p fertilization on the biomass and ecological stoichiometric characteristics of agropyron michnoi in sandy grasslands. *Chem. Ecol.* 36, 938–952. doi: 10.1080/02757540.2020.1821672

Jordan, S. J., Stoffer, J., and Nestlerode, J. A. (2011). Wetlands as sinks for reactive nitrogen at continental and global scales: A meta-analysis. *Ecosystems*. 14, 144–155. doi: 10.1007/s10021-010-9400-z

Lan, Z. C., and Bai, Y. F. (2012). Testing mechanisms of n-enrichmentinduced species loss in a semiarid inner mongolia grassland: Critical thresholds and implications for long-term ecosystem responses. *Philos. Trans. R. Soc B Biol. Sci.* 367, 1606. doi: 10.1098/rstb.2011.0352

Li, X. Y., Chen, H. T., Jiang, X. Y., Yu, Z. G., and Yao, Q. Z. (2017). Impacts of human activities on nutrient transport in the yellow river: The role of the water-sediment regulation scheme. *Sci. Total Environ.* 592, 161–170. doi: 10.1016/j.scitotenv.2017.03.098

Li, Y., Niu, S. L., and Yu, G. R. (2016). Aggravated phosphorus limitation on biomass production under increasing nitrogen loading: A meta-analysis. *Glob. Change Biol.* 22, 934–943. doi: 10.1111/gcb.13125

Liu, Y. L., Li, L., Li, X. Y., Yue, Z. W., and Liu, B. (2021). Effect of nitrogen and phosphorus addition on leaf nutrient concentrations and nutrient resorption efficiency of

two dominant alpine grass species. *J. Arid Land*. 13, 1041–1053. doi: 10.1007/s40333-021-0080-7

Liu, X. L., Wang, G. M., Ran, Y. N., Qi, D. H., Han, G. X., Guan, B., et al. (2019). Overall supply level, not the relative supply of nitrogen and phosphorus, affects the plant community composition of a supratidal wetland in the yellow river delta. *Sci. Total Environ*. 695, 133866. doi: 10.1016/j.scitotenv.2019.133866

Li, J. J., Yang, C., Liu, X. L., and Shao, X. Q. (2019). Inconsistent stoichiometry response of grasses and forbs to nitrogen and water additions in an alpine meadow of the qinghai-Tibet plateau. *Agric. Ecosyst. Environ*. 279, 178–186. doi: 10.1016/j.agee.2018.12.016

Li, L. P., Zerbe, S., Han, W. X., Thevs, N., Li, W. P., He, P., et al. (2014). Nitrogen and phosphorus stoichiometry of common reed (Phragmites australis) and its relationship to nutrient availability in northern China. *Aquat. Bot*. 112, 84–90. doi: 10.1016/j.aquabot.2013.08.002

Lü, X. T., Freschet, G. T., Kazakou, E., Wang, Z. W., Zhou, L. S., and Han, X. G. (2015). Contrasting responses in leaf nutrient-use strategies of two dominant grass species along a 30-yr temperate steppe grazing exclusion chronosequence. *Plant Soil* 387, 69–79. doi: 10.1007/s11104-014-2282-7

Luo, X., Mazer, S. J., Guo, H., Zhang, N., Weiner, J., and Hu, S. J. (2016). Nitrogen: phosphorous supply ratio and allometry in five alpine plant species. *Ecol. Evol*. 6, 8881–8892. doi: 10.1002/ece3.2587

Lü, X. T., Reed, S., Yu, Q., He, N. P., Wang, Z. W., and Han, X. G. (2013). Convergent responses of nitrogen and phosphorus resorption to nitrogen inputs in a semiarid grassland. *Glob. Change Biol*. 19, 2775–2784. doi: 10.1111/gcb.12235

Mao, R., Chen, H. M., Zhang, X. H., Shi, F. X., and Song, C. C. (2016). Effects of P addition on plant C : N : P stoichiometry in an N-limited temperate wetland of northeast China. *Sci. Total Environ.* 559, 1–6. doi: 10.1016/j.scitotenv.2016.03.158

Mayor, J. R., Wright, S. J., and Turner, B. L. (2014). Species-specific responses of foliar nutrients to long-term nitrogen and phosphorus additions in a lowland tropical forest. *J. Ecol.* 102, 36–44. doi: 10.1111/1365-2745.12190

Peñuelas, J., Sardans, J., Ogaya, R., and Estiarte, M. (2008). Nutrient stoichiometric relations and biogeochemical niche in coexisting plant species: Effect of simulated climate change. *Polish J. Ecol*. 56, 613–622.

Peñuelas, J., Sardans, J., Rivas-Ubach, A., and Janssens, I. A. (2012). The human-induced imbalance between C, N and P in earth's life system. *Glob. Change Biol*. 18, 3–6. doi: 10.1111/j.1365-2486.2011.02568.x

Sardans, J., Janssens, I. A., Alonso, R., Veresoglou, S. D., Rillig, M. C., Sanders, T. G. M., et al. (2015). Foliar elemental composition of European forest tree species associated with evolutionary traits and present environmental and competitive conditions. *Glob. Ecol. Biogeogr*. 24, 240–255. doi: 10.1111/geb.12253

Sardans, J., and Peñuelas, J. (2012). The role of plants in the effects of global change on nutrient availability and stoichiometry. *Plant Physiol.* 160, 1741–1761. doi: 10.1104/pp.112.208785

Sardans, J., and Peñuelas, J. (2014). Climate and taxonomy underlie different elemental concentrations and stoichiometries of forest species: the optimum "biogeochemical niche". *Plant Ecol.* 215, 441–455. doi: 10.1007/s11258-014-0314-2

Su, Y., Le, J. J., Ma, X. F., Li, K. H., Gong, Y. M., Ahmed, Z., et al. (2020). Plant community composition altered by long-term nitrogen addition has minor contribution to plant nutrient status at the community level. *Appl. Ecol. Environ. Res.* 18, 6469–6484. doi: 10.15666/aeer/1805_64696484

Su, Y., Ma, X. F., Le, J. J., Li, K. H., Han, W. X., and Liu, X. J. (2021). Decoupling of nitrogen and phosphorus in dominant grass species in response to long-term nitrogen addition in an alpine grassland in central Asia. *Plant Ecol.* 222, 261–274. doi: 10.1007/s11258-020-01103-3

Venterink, H. O., and Güsewell, S. (2010). Competitive interactions between two meadow grasses under nitrogen and phosphorus limitation. *Funct. Ecol.* 24, 877–886. doi: 10.1111/j.1365-2435.2010.01692.x

Wang, W. Q., Sardans, J., Wang, C., Zeng, C. S., Tong, C., Asensio, D., et al. (2015). Ecological stoichiometry of c, n, and p of invasive phragmites australis and native cyperus malaccensis species in the minjiang river tidal estuarine wetlands of China. *Plant Ecol.* 216, 809–822. doi: 10.1007/s11258-015-0469-5

Wang, J. Y., Wang, J. N., Guo, W. H., Li, Y. G., Wang, G. G., and Wu, T. G. (2018). Stoichiometric homeostasis, physiology, and growth responses of three tree species to nitrogen and phosphorus addition. *Trees - Struct. Funct.* 32, 1377–1386. doi: 10.1007/s00468-018-1719-7

Wan, S. Z., Yang, G. S., and Mao, R. (2020). Responses of leaf nitrogen and phosphorus allocation patterns to nutrient additions in a temperate freshwater wetland. *Ecol. Indic.* 110, 105949. doi: 10.1016/j.ecolind.2019.105949

Wolf, K. L., Noe, G. B., and Ahn, C. (2013). Hydrologic connectivity to streams increases nitrogen and phosphorus inputs and cycling in soils of created and natural floodplain wetlands. *J. Environ. Qual.* 42, 1245–1255. doi: 10.2134/jeq2012.0466

Xia, J. Y., and Wan, S. Q. (2008). Global response patterns of terrestrial plant species to nitrogen addition. *New Phytol.* 179, 428–439. doi: 10.1111/j.1469-8137.2008.02488.x

Xu, L. C., Xing, A. J., Du, E. Z., Shen, H. H., Yan, Z. B., Jiang, L., et al. (2021). Effects of nitrogen addition on leaf nutrient stoichiometry in an old-growth boreal forest. *Ecosphere* 12, e03335. doi: 10.1002/ecs2.3335

Yang, H. (2018). Effects of nitrogen and phosphorus addition on leaf nutrient characteristics in a subtropical forest. *Trees - Struct. Funct.* 32, 383–391. doi: 10.1007/s00468-017-1636-1

Yan, Z. B., Kim, N., Han, W. X., Guo, Y. L., Han, T. S., Du, E. Z., et al. (2014). Effects of nitrogen and phosphorus supply on growth rate, leaf stoichiometry, and nutrient resorption of arabidopsis thaliana. *Plant Soil.* 388, 147–155. doi: 10.1007/s11104-014-2316-1

Yan, Z. B., Li, X. P., Tian, D., Han, W. X., Hou, X. H., Shen, H. H., et al. (2018). Nutrient addition affects scaling relationship of leaf nitrogen to phosphorus in *Arabidopsis thaliana*. *Funct. Ecol.* 32, 2689–2698. doi: 10.1111/1365-2435.13219

Yuan, Z. Y., and Chen, H. Y. H. (2015). Negative effects of fertilization on plant nutrient resorption. *Ecology* 96, 373–380. doi: 10.1890/14-0140.1

Yuan, Y. F., Guo, W. H., Ding, W. J., Du, N., Luo, Y. J., Xu, F., et al. (2013). Competitive interaction between the exotic plant *Rhus typhina L.* and the native tree *Quercus acutissima* Carr. in northern China under different soil N : P ratios. *Plant Soil* 372, 389–400. doi: 10.1007/s11104-013-1748-3

Yue, K., Fornara, D. A., Yang, W. Q., Peng, Y., Li, Z. J., Wu, F. Z., et al. (2017). Effects of three global change drivers on terrestrial C:N:P stoichiometry: a global synthesis. *Glob. Change Biol.* 23, 2450–2463. doi: 10.1111/gcb.13569

Yu, Q., Elser, J. J., He, N. P., Wu, H. H., Chen, Q. S., Zhang, G. M., et al. (2011). Stoichiometric homeostasis of vascular plants in the inner Mongolia grassland. *Oecologia*. 166, 1–10. doi: 10.1007/s00442-010-1902-z

Yu, J. B., Ning, K., Li, Y. Z., Du, S. Y., Han, G. X., Xing, Q. H., et al. (2014). Wet and dry atmospheric depositions of inorganic nitrogen during plant growing season in the coastal zone of Yellow River Delta. *Sci. World J.* 2014, 1–8. doi: 10.1155/2014/949213

Yu, J. B., Zhan, C., Li, Y. Z., Zhou, D., Fu, Y. Q., Chu, X. J., et al. (2016). Distribution of carbon, nitrogen and phosphorus in coastal wetland soil related land use in the modern yellow river delta. *Sci. Rep.* 6, 2–10. doi: 10.1038/srep37940

Zhang, H. X., Gao, Y. Z., Yohannis, B. L., Baskin, J. M., Baskin, C. C., Lü, X. T., et al. (2018a). Divergent responses to water and nitrogen addition of three perennial bunchgrass species from variously degraded typical steppe in Inner Mongolia. *Sci. Total Environ.* 647, 1344–1350. doi: 10.1016/j.scitotenv.2018.08.025

Zhang, J. J., Yan, X. B., Su, F. L., Li, Z., Wang, Y., Wei, Y. N., et al. (2018b). Long-term N and P additions alter the scaling of plant nitrogen to phosphorus in a Tibetan alpine meadow. *Sci. Total Environ.* 625, 440–448. doi: 10.1016/j.scitotenv.2017.12.292

Zhan, S. X., Wang, Y., Zhu, Z. C., Li, W. H., and Bai, Y. F. (2017). Nitrogen enrichment alters plant N: P stoichiometry and intensifies phosphorus limitation in a steppe ecosystem. *Environ. Exp. Bot.* 134, 21–32. doi: 10.1016/j.envexpbot.2016.10.014

frontiers | Frontiers in Marine Science

TYPE Original Research
PUBLISHED 09 May 2023
DOI 10.3389/fmars.2023.1164065

OPEN ACCESS

EDITED BY
Laibin Huang,
University of California, Davis, United States

REVIEWED BY
Jiakai Liu,
Beijing Forestry University, China
Weiqing Meng,
Tianjin Normal University, China

*CORRESPONDENCE
Qing Wang
wq@bnu.edu.cn
Baoshan Cui
cuibs@bnu.edu.cn

RECEIVED 12 February 2023
ACCEPTED 24 April 2023
PUBLISHED 09 May 2023

CITATION
Man Y, Zhou F, Wang Q and Cui B (2023) Quantitative evaluation of sea reclamation activities on tidal creek connectivity. *Front. Mar. Sci.* 10:1164065. doi: 10.3389/fmars.2023.1164065

Quantitative evaluation of sea reclamation activities on tidal creek connectivity

Ying Man[1,2], Fangwen Zhou[1,3], Qing Wang[2,4]* and Baoshan Cui[1,2]*

[1]State Key Joint Laboratory of Environmental Simulation and Pollution Control, School of Environment, Beijing Normal University, Beijing, China, [2]Yellow River Estuary Wetland Ecosystem Observation and Research Station, Ministry of Education, Dongying, Shandong, China, [3]Operation Management Department, China Construction Eco-Environmental Group Co., LTD, Beijing, China, [4]Research and Development Center for Watershed Environmental Eco-Engineering, Beijing Normal University, Zhuhai, China

Deltas are in a dynamic balance due to the impact of fluvial and coastal flooding, and hydrological connectivity plays an important role. In recent decades, the dynamic equilibrium has been influenced by upstream and local human activities, including sea reclamation activities. However, in most instances, the influence of human activities has not been explicitly distinguished and quantified in detail. In this paper, the influence of sea reclamation activities on hydrological connectivity in the Yellow River Delta was quantified by parameterizing the resistance surfaces (a spatial layer that assigns a value to each landscape feature, indicating the degree to which that variable impedes or promotes movement) that includes sea reclamation activities. By optimizing a functional relationship between landscape features and hydrological connectivity (water flow movement patterns), the values in the resistance surfaces could be assigned. We first calculated hydrological distances among bifurcations from 1985 to 2020 with a 5-year interval representing the hydrological connectivity of each tidal creek. The sea reclamation activities in the YRD were classified into four: reclaimed land, sea enclosure activity, freshwater resource facilities, and engineering in the oil field to create resistance surfaces. We identified that the periods of 1990–1995 and 2000–2005 were under the most severe influence of sea reclamation activities. Sea enclosure activity, freshwater resource facilities, and engineering in oil fields played major roles in composing resistance surfaces. Mariculture (quantified relative resistance value, 1.00), reservoir (0.92), agriculture (0.91), and river (0.97) were the features with the highest resistance values in the initial and mature development stages. The formation of resistance (costs to movement) was due to human activities and natural factors, for example, the evolution of tidal creeks. To develop the resource in tidal flats sustainably, systematic monitoring and sufficient conservation awareness were required. This study contributed to coastal management and planning by providing a quantified assessment of different types of sea reclamation activities.

KEYWORDS

tidal creek, hydrological connectivity, resistance surface, coastal wetland, reclamation activities

1 Introduction

The hydrological connectivity of tidal creeks plays an important role in maintaining the dynamic balance in deltas. By transferring nutrients, dissolved oxygen, sediment, propagules, and other substances to coastal salt marsh vegetation (Nelson et al., 2017; Wu et al., 2020; Wang et al., 2021), tidal creeks contribute to the health and ecological processes of coastal ecosystems (Nelson et al., 2017). By transporting water and sediment, the stability of tidal flats is maintained by stably developed tidal creeks. In turn, stable landform environments promote the development of coastal salt marsh vegetation, reaching equilibrium with the mutual promotion of vegetation-landform-tidal creek systems (Xie et al., 2017). Through this process, deltas are in dynamic balance (Tessler et al., 2015). However, in recent decades, the dynamic balance is often influenced by upstream and local human activities, such as the construction of upstream reservoirs (Chen et al., 2013b), floodplain engineering, and local sea reclamation activities. Once the dynamic balance is interrupted, deltas become vulnerable to disturbances such as sea level rise.

Studies of the influences of human activities on tidal creeks have focused on various aspects of the tidal creek response. Regarding the morphology characteristics and connectivity, the responses of tidal creeks to upstream construction (Chen et al., 2013a), land reclamation (Shi et al., 2016; Xie et al., 2020; Fan et al., 2021), or other coastal developments (Chen and Han, 2015; Xie et al., 2020; Fan et al., 2021) have been studied, including the sedimentary changes to land use (Sanger et al., 2004; Darrow et al., 2017–). Regarding the water environment, the variations in water quality due to the influence of pollution have been studied using simulations (Buzzelli, 2008; Boynton et al., 2014) and experiment methods (DiDonato et al., 2009; Boynton et al., 2014; Wessel et al., 2021). The biological responses to coastal development have also been studied, including the changes to zooplankton (Li et al., 2012), nekton, macrobenthos (Lerberg et al., 2000; Washburn and Sanger, 2011), and fish (Bilkovic, 2011).

In most studies, however, human activities have not been classified specifically, and their influence has not been quantified. Rather, human activities have largely been considered rough categorical variables, such as urban or suburban (Lerberg et al., 2000), and summarized as rough indexes according to population density (Holland et al., 2004) or impervious land cover (Sanger et al., 2015). In fact, human activities are more detailed, particularly considering that multiple activities can coexist in one area.

In this paper, we distinguished the different types of sea reclamation activities that influenced tidal creeks and quantified these influences on the Yellow River Delta (YRD). We modeled each tidal creek as a hydrological network, with its edges represented as hydrological distance. Using this network as the observed data, we optimized the resistance surface based on the resistance theory and random walk theory. Through this process, different human activities were modeled as a series of randomly assigned resistance surfaces (Spear et al., 2010), on which commute distances (details in Materials and methods) were calculated to reflect water flow movement among sites of bifurcation in the tidal creeks. By comparing the hydrological distances with commute distances using a generalized linear mixed model, the best-fitted commute distances were selected, as well as the resistance surface. The framework and its application provided a quantitative assessment of the influence of human activities on hydrological connectivity at multiple temporal and spatial scales.

2 Materials and methods

2.1 Study area

The YRD (36° 24.0′–36° 48.2′ N; 117° 59.8′–120° 36.1′ E) is situated to the south of Bohai Bay in eastern China (Figure 1). It is not only the youngest delta in China's warm temperate zone but also the largest delta with the most complete preservation (Song, 2015). The case study area is representative of coastal wetlands in the high-efficiency eco-economic zone of the Yellow River Delta, which extends from the mouth of the Taoer River in Zhanhua to the Qimu Cape in Longkou. Most areas of the YDR are dominated by irregular semidiurnal tides, while the tide in areas from the north of Doying Port to the south of the current course of the Yellow River is a diurnal tide (Yang et al., 2015; Weikang et al., 2018). The Yellow River has changed its channel courses multiple times, and the deposition of new subdeltas and the erosion of abandoned subdeltas have occurred successively (Zhang et al., 2018). In the study area, the mean tidal range on the north and south coasts is about 1–2 m, while that on the east coast near the current course is 0.76 m and that on the south coast is 0.61–1.68 m (Yang et al., 2015; Zhou et al., 2016; Wang et al., 2017). Changes to the coastline on the north coast were influenced by reclamation activities in recent decades, with maximum expansion rates up to 123.98 km^2 (Fan et al., 2018).

2.2 Subzone division

As the drainage area of one tidal creek is much smaller compared to the entire YRD, there is no need to optimize the entire resistance surface of the YRD each time, especially considering the huge operand of the genetic algorithm. According to different hydrological conditions, patterns of human activity, and natural resources, we divided the entire area into six zones (Figure 1). The different hydrological conditions were mainly due to the change of courses of the Yellow River into the sea in different periods in history. Zone 1 was located on the northwest coast of the study area and mainly contains the Ancient YRD due to the flow of the Yellow River into the sea in 1855 through the Taoer River. Zone 2 mainly contains the delta lobe of the Diaokou course, has suffered significant erosion since it was abandoned in 1976. Zone 3 was the subdelta of the Yellow River that flows into the sea in Stream Shenxian and courses south and north of it from 1953 to 1976. Zone 4 contained the National Reserve of the YRD, which was built in 1992 to protect coastal wetlands. Zone 5 contained the southern abandoned subdelta formed at the beginning of this century from the south of the current course of the Qingshui Sream to the southern plain of Laizhou Bay. Zone 6 mainly contained Laizhou Bay.

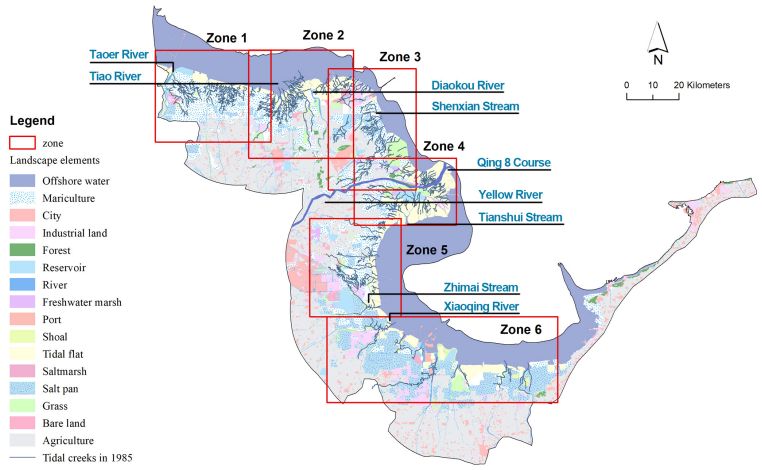

FIGURE 1
Study area and subzone divisions. The Yellow River Delta study area with landscape elements and tidal creeks in 1985.

2.3 Framework of landscape resistance quantification

2.3.1 Hydrological distance calculation

We used hydrological distance to measure the hydrological connectivity of tidal creeks, which was the shortest distance between pairs of sites computed along the stream network (Ganio et al., 2005; Ver Hoef et al., 2006). We focused on tidal creek changes in each 5-year period; the branching sites (e.g., confluence sites) in the beginning year were selected as objective sites (nodes). The hydrological distances between the objective sites in the ending year were selected as edges. Hydrological distances between lost objective sites were set to an infinite value (9999) to show the two sites were unconnected. By quantifying the changes between lost nodes caused by landscape features, their influence on hydrological connectivity could be reflected. The Spatial Tools for the Analysis of the River Systems (STARS) toolbox in ArcGIS 10.5 (Peterson and Ver Hoef, 2014) and the R package Spatial Stream Network (SSN) were used to calculate the hydrological distances between objective sites in tidal creeks, which referred to river system (Ver Hoef et al., 2014). The direction of the ebb tide was taken as the direction of tidal creek networks to be consistent with the terms defined in the river system in the software. The detailed steps for calculation were as follows.

First, the STARS toolbox was used to identify the topological relationships between features in the tidal creek data. Because the topological relationships were the basis for analyzing connectivity, adjacency, and directional relationships in a network, they were not stored in the format of extracted tidal creeks (shapefile) (Peterson and Ver Hoef, 2014). Specifically, the polyline to landscape network tool was used to transform the extracted tidal creek data from polyline format to landscape network format. Tools to check network topology, clean braided channels, and identify complex confluences were then used to eliminate topological errors in the tidal creek networks. Considering that the tidal creek segment may change during the 5-year period, the snap points to landscape network edges tool was used to ensure the objective sites were located on the tidal creek segment. After these preprocessing steps, the upstream distances tool of edges and sites was used for calculating upstream distances that were defined as the length of the continuous line from any location on the tidal creek network to its outlet (the most downstream location of the tidal creek network) (Peterson and Ver Hoef, 2014). Upstream distance based on edges was calculated between the stream outlet and the most downstream points. An upstream distance based on edges was calculated between the stream outlet and selected sites. Both were needed in the calculation of hydrological distances between objective sites. The Create SSN object tool was used to store the information of upstream distance in a.ssn object that can be statistically computed and graphed in an R environment (Peterson and Ver Hoef, 2014). At the same time, this tool also generated network identifiers (IDs) and binary IDs in the.ssn object. Network IDs could distinguish different tidal creeks. Binary IDs were assigned in each segment in one tidal creek to identify flow-connected and flow-unconnected segments. The R package SSN was at last used to calculate hydrological distances between objective sites on flow-connected and flow-unconnected segments. Specifically, command importing was used to open the.ssn object, and command creatDisMat was used to generate the matrix of the hydrological distance between objective sites in each tidal creek network.

2.3.2 Quantifying values of resistance surfaces

Commute distances among the bifurcation sites in each tidal creek network could be calculated based on the resistance surfaces, according to random walk and resistance theory (Figure 2A). Commute distance, or resistance distance, was a graph-theoretic distance metric that was defined as the effective resistance between the nodes when each graph edge was replaced by conductance (McRae, 2006; Zeller et al., 2012). The commute distance was calculated based on the resistance surface. When comparing different commute distances from different resistance surfaces with the hydrological distance between the same objective sites,

10.3389/fmars.2023.1164065

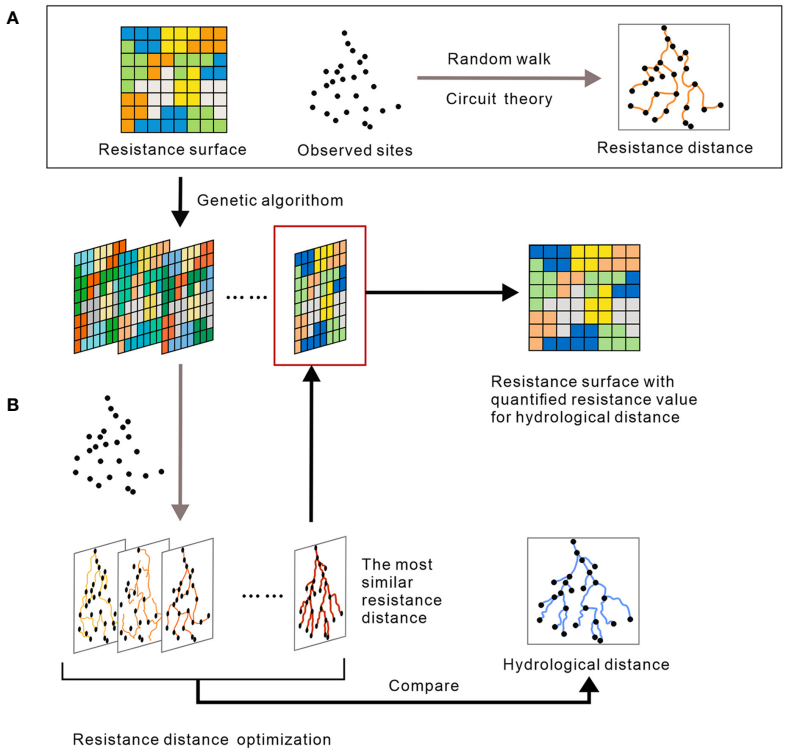

FIGURE 2
Framework for landscape resistance quantification. **(A)** Resistance distance calculation; **(B)** Resistance surface assignment based on observed hydrological distance.

the resistance surface with the most fitted commute distance (to hydrological distance) could reflect the influence of landscape features on the tidal creeks (Figure 2B). An R package, ResistanceGA v.4.0-14 was used to execute the calculation of commute distances and the comparison (Peterman, 2018).

The landscape features in the YRD that have the potential to influence tidal creek connectivity were classified into five categories (reclaimed land, sea enclosure activities, freshwater resource facilities, coastal wetland of saltwater, and engineering in oil fields) (details in Resistance surfaces generation). Each category that influenced tidal creek connectivity was considered one of the components of the resistance surface. To identify specific categories that have an influence on tidal creeks, all combinations of the five categories were generated (e.g., the Reclaim. Oil surface was composed of reclaimed land category and engineering in oil fields category). Each combination of categories formed a potential resistance surface. Each resistance surface was transformed into ASCII format to calculate commute distances. A series of random values were generated using genetic algorithms to assign landscape features to the category (Figure 2B). Commute distances between objective sites based on the assigned resistance surface were compared with hydrological distances between the same sites using a linear mixed-effect model named MLPE in the ResistanceGA. By comparing marginal R^2 (reflecting the influence of the fixed effect in the model, which is the landscape feature here) of the models, the most fitted commute distance could be selected, and the values on the resistance surface thus reflected the resistance degree. Apart from the comparison between models based on one resistance surface, models of resistance surfaces with all combinations of categories were also compared using the all_comb command in the ResistanceGA. By comparing the marginal R^2, or AIC, and running a bootstrap procedure, the most fitted model could be selected according to the rank. Resistance surface values in the corresponding resistance surface were regarded as the value that most closely resembled reality.

2.4 Tidal creek extraction

To understand the changes in the hydrological connectivity of tidal flats in the YRD, we extracted tidal creeks from Landsat images over the past 35 years at 5-year intervals. Level-1 Precision and Terrain (L1TP) data of Landsat-5 Thematic Mapper (TM) and Landsat-8 Operational Land Imager (OLI) were available from the United States Geological Survey (USGS) Earth Explorer (Survey, U.S. G., 2022). Images with a cloud cover of less than 10% were chosen. All images were pre-processed by ENVI 5.3. Radiometric calibration and Fast Line-of-Sight Atmospheric Analysis of Spectral Hypercubes (FLAASH) were used to eliminate the errors from sensors, solar radiation, and the atmosphere. (The information from the images, as well as the specific year chosen, are shown in Table 1).

To calculate the hydrological distance between specific sites, we focused on the center line of tidal creeks. Considering that the small creeks (e.g., first order according to the Horton–Strahler method) were difficult to extract from tidal flats using the

10.3389/fmars.2023.1164065

TABLE 1 Dates of satellite images used for tidal creek extraction with the corresponding Landsat sensor.

1985	1990	1995	2000	2005	2010	2015	2020
TM	TM	TM	TM	TM	TM	OLI	OLI
0314	0312	0206	0307	0305	0506	0213	0314
0501	0515	0310	0408	0422	0607	0301	0330
0805	0616	0326	0611	0524	0911	0504	0415
1,125		0918	1,017	1,015	1,013	0520	0501
		1,004	1,102	1,031	1,029	0,606	0517
		1,105	1,220	1,116	1,216	1,011	0906
		1,121				1,027	0922
		1,223					1,024

automatic methods, visual interpretation was employed for creek extraction. Considering the strong impact of tidal conditions on the appearance of tidal creeks in the images, we used the nonstandard false-color image to assist with the extraction. Because this combination of bands could better distinguish the boundaries between water bodies and land, it could help identify tidal creeks from tidal flats. Command of change RGB bands in ENVI 5.3 was used to execute the band combination of near-infrared bands, short-wave near-infrared bands, and red bands (453 and 564 for TM and OLI, respectively). The combination emphasizes water, which is often used to distinguish the boundaries between water and land in the coastline and tidal flat surveys.

2.5 Generation of resistance surfaces

The landscape features of sea reclamation activities in the YRD were obtained from the Northeast Institute of Geography and Agroecology, Chinese Academy of Sciences, to represent the resistance surface in the YRD. The sea reclamation activities in this dataset include categories of city construction land, port, industrial land, dry farmland, forest, bare land and tourism land, grass, salt pans, mariculture ponds, rivers, and reservoirs. On this basis, we reclassified these features into four categories, according to their similarities. City construction land, port, industrial land, dry farmland, forest, bare land, tourism land, and grass were classified as reclaimed land. Salt pans and mariculture ponds were classified as sea enclosure activities. Rivers, reservoirs, and offshore water were classified as freshwater resource facilities. Considering the high intensity and large temporal and spatial scale of oil exploration in the YRD, we also identified engineering in oil fields, including oil wells, roads leading to different oil wells, and oil fields that occupied large areas of land. In addition, coastal salt marshes and tidal flats were classified as coastal wetlands. All such surface data were processed into a raster stack to accommodate the requirements of the algorithm. The constructed resistance surface contains both a single and a combination of the sea reclamation activity categories (composite resistance surface).

3 Results

3.1 Identification of the key resistance surfaces for hydrological connectivity

The landscape resistance inversion results of tidal creeks with changes in 5-year intervals that were significantly related to landscape resistance revealed that resistance surfaces and the number of tidal creeks were different in different zones and at different times. Only resistance surfaces containing sea reclamation activity categories (with R^2 higher than 0.1) are shown as the leading resistance surface in the rank of all possible resistance surface combinations in each tidal creek (Table 2) (the model result with optimal resistance surfaces composed of only coastal wetland of saltwater, null model, and distance model is not listed in the table). In general, the period of 1990–1995 had the greatest number of tidal creeks influenced by resistance surfaces, followed by the period of 2000–2005. The creek ID in each zone demonstrates that the influence of resistance surfaces at different times can be seen in the same tidal creeks. The majority of resistance surfaces are composite resistance surfaces, with two surfaces of either human activity or natural elements. Based on the specific resistance surfaces identified in Table 2, we discovered that sea enclosure activity played a significant role in the formation of resistance surfaces in the majority of zones, as such activities were present in the majority of resistance surfaces in zones 1, 3, 4, 5, and 6. Freshwater resource facilities are the second surface resistance component since these facilities were involved in the majority of zone 2 and 6 resistance surfaces. Engineering in oil fields also contributed to zone 4 resistance surfaces.

3.2 Spatial–temporal variation of quantified resistance values

The result of the spatial-temporal distribution of resistance values in the YRD showed that high and low resistance values were distributed in different areas in different periods (Figures 3–5). According to the intensity of human activity and the invention time,

10.3389/fmars.2023.1164065

TABLE 2 Landscape resistance surface inversion results in period of 5-year interval in each zone.

Zone	Creek ID	Period	Resistance surface	R^2m
1	1	1990-1995	Salt.Enclose	0.74***
1	2	1990-1995	Reclaim.Oil	0.10**
1	3	1990-1995	Fresh.Oil	0.25***
1	4	2000-2005	Salt.Reclaim	0.89***
1	5	2005-2010	Fresh.Enclose	0.32***
1	6	2005-2010	Salt.Enclose	0.37***
1	6	2010-2015	Enclose	0.54***
2	1	1990-1995	Fresh.Salt.Enclose.Reclaim	0.10***
2	2	1990-1995	Fresh	0.19***
2	3	1990-1995	Salt.Reclaim	0.33**
2	4	1990-1995	Salt.Enclose	0.20***
2	2	1995-2000	Fresh	0.14***
3	1	1990-1995	Fresh.Enclose	0.49***
3	2	1990-1995	Enclose.Oil	0.36***
3	3	2000-2005	Enclose.Oil	0.65***
3	1	2005-2010	Fresh.Enclose.Oil	0.33***
3	4	2005-2010	Fresh.Salt.Reclaim	0.90***
4	1	1990-1995	Salt.Oil	0.83***
4	2	2000-2005	Salt.Enclose	0.17***
4	1	2005-2010	Salt.Oil	0.64***
4	2	2010-2015	Fresh.Enclose.Reclaim	0.11***
5	1	1990-1995	Enclose	0.42***
5	2	1990-1995	Enclose.Reclaim	0.34**
5	3	1995-2000	Fresh.Salt	0.95***
5	4	2000-2005	Enclose	0.33***
5	3	2005-2010	Salt.Enclose	0.46***
5	5	2005-2010	Salt.Reclaim	0.44***
6	1	1985-1990	Fresh.Reclaim	0.13***
6	2	1990-1995	Fresh.Enclose	0.25***
6	1	1990-1995	Fresh.Enclose	0.63***
6	1	1995-2000	Fresh.Enclose	0.17***
6	1	2005-2010	Salt.Reclaim	0.29***
6	2	2005-2010	Salt.Enclose	0.89***

CreekID represents each tidal creek number. Their names with dot separated are composite resistance surfaces. Fresh is short for freshwater resource facilities, Salt is short for coastal wetland of saltwater, Reclaim is short for reclaimed land, Enclose is short for sea enclosure activity. Oil is short for engineerings in oil field. R^2m=marginal R^2. Significant values are: *<0.05, **<0.01, ***<0.001.

the six zones were divided into three groups for analysis. Zones 1, 2, and 5 were grouped together because their human activities began at about the same time in the 1990s (Figure 3). Zones 3 and 6 were grouped together as their human activities began the earliest (and earlier than the time scale in this study) (Figure 4). Zone 4 was a single group with supposed minimal human intervention as the National Natural Reserve of the YRD is located within it (Figure 5). The findings revealed two types of connections between landscape elements and resistance values. One is that a single landscape feature had a single resistance value, such as mariculture in zone 1 with a resistance value of 0.12 in 1990–1995 in tidal creek 1 (Figure 3A). Another is in the form of component features (CF),

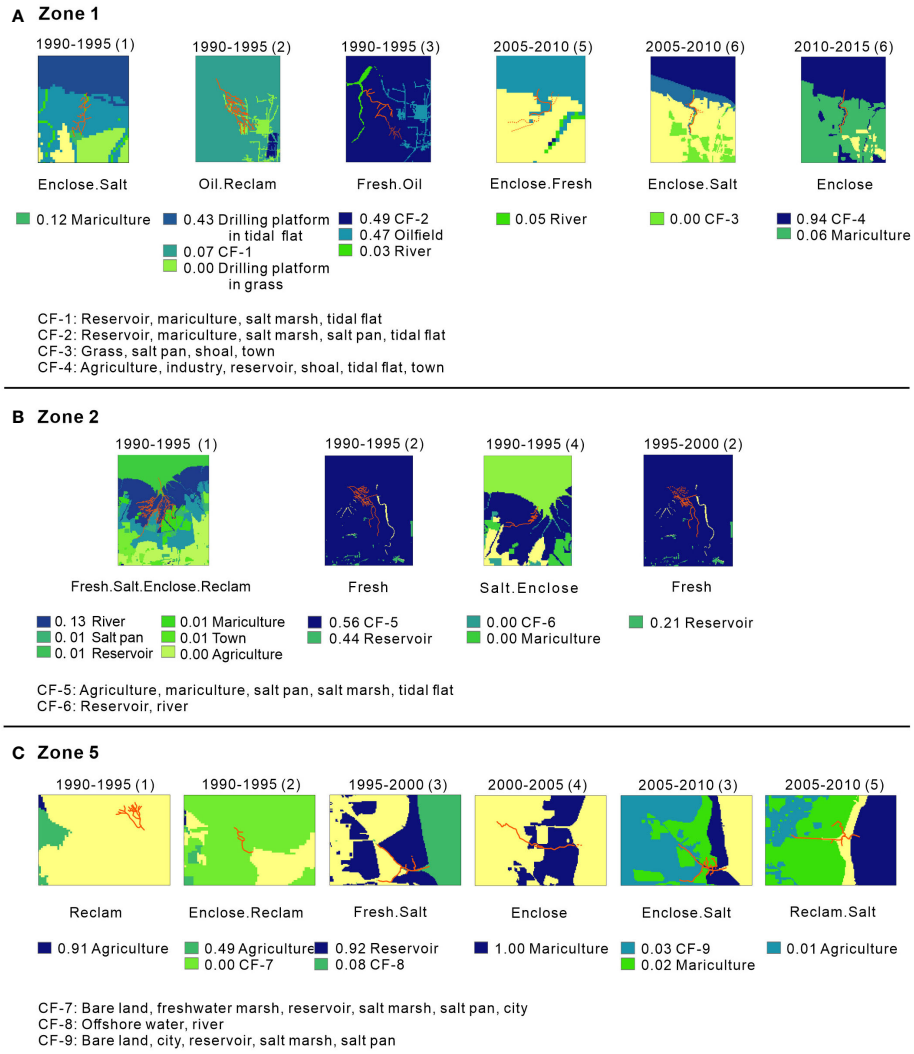

FIGURE 3
Spatial distribution of relative resistance values at resistance surfaces in zone 1**(A)**, 2**(B)**, and 5**(C)**. The number in parentheses represents the serial number of each influenced tidal creek (creek ID). CF, composite feature.

such as the CF-1 in zone 1 with a resistance value of 0.07 in tidal creek 2 in 1990–1995 (Figure 3A). CF-1 contained reservoir, mariculture, salt marsh, and tidal flat landscape features (Figure 3A). In the case of the former, each landscape feature had a single resistance value, therefore we referred to them as independent features. By comparison, for the latter, as multiple landscape features had a single resistance value, we termed them composite features. According to the circuit theory, higher resistance values might arise from attributes of landscape features or the distribution of the landscape features (McRae, 2006). From this point, independent features might be more likely to reflect the influence of landscape feature attributes than the same landscape features with the same resistance value. In addition, composite features might be more likely to reflect the influence of the distribution of the landscape features, as distinct landscape features in them did not make the resistance values different.

Agriculture (0.91), reservoir (0.92), and mariculture (1.00) in zone 5 were the independent feature types with the highest resistance values in zones 1, 2, and 5 (Figure 3, the initial stage of human activities) (Figure 3C). In zone 1, CF-4 (0.94) has the highest resistance value in composite features (Figure 3A). Other high values in resistance surface, both independent and composite features, are around or lower than 0.5. In zones 3 and 6 (Figure 4, the mature stage of human activities), the independent feature types with the greatest resistance values arise in the river (0.97) in zone 6 (Figure 4B) and mariculture (0.67) in zone 3. The highest resistance values in composite features were found in CF-3 (0.58) in zone 6 (Figure 4B) and CF-1 (0.50) in zone 3 (Figure 4A). Other high values in resistance surface, both independent and composite features, are around or less than 0.7. In zone 4 (Figure 5, reserve), the independent feature types with the highest resistance values appear in mariculture (0.78). Other high values on the resistance surface, primarily independent features, are less than 0.5. The results demonstrate that in regions with early phases of human activity, several specific features play key roles in the form of resistance, and they have an exceptionally high value. In

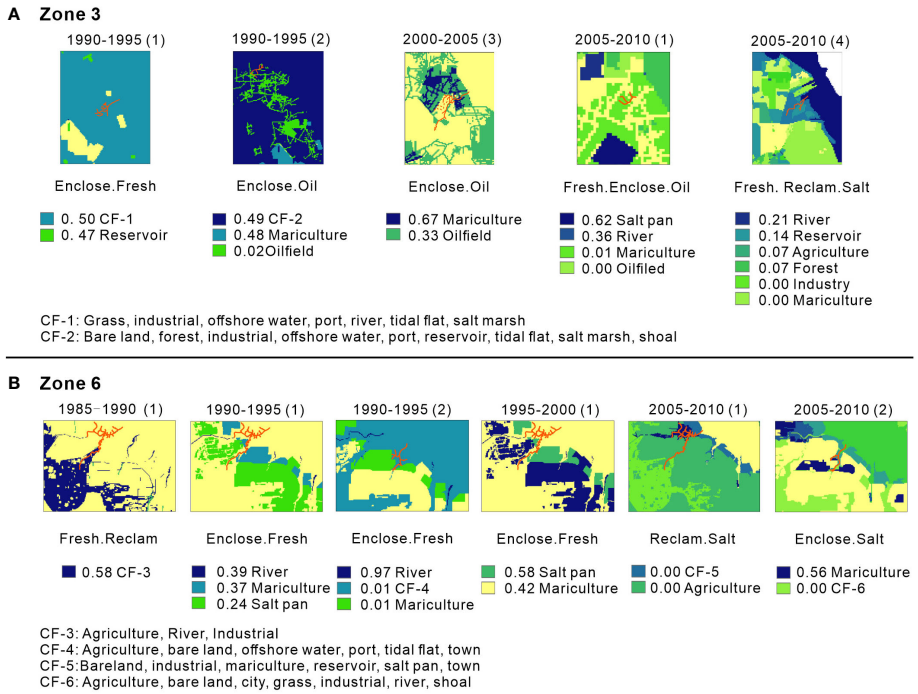

FIGURE 4
Spatial distribution of relative resistance values at resistance surfaces in zone 3**(A)** and 6**(B)**. The number in parentheses represents the serial number of each influenced tidal creek (creek ID). CF, composite feature.

comparison, the average value of landscape features was higher in places with mature stages of human activity than in areas with early stages of human activity.

3.3 Responses of tidal creek changes to resistance surface

The spatial distribution and their changes in the length of impacted tidal creeks by sea reclamation activities (influenced tidal creeks, for short) revealed that the tidal creeks in different zones had varied characteristics (Figure 6). Tidal creeks in zones 1 and 2 had the most lost edges, and their mean length was significantly longer than in other zones (Figure 6A). Tidal creeks in zone 4 had more edges that had changed length (increased or reduced) (Figure 6D). Tidal creeks in the other three zones all revealed a pattern of only one tidal creek changing significantly over a 5-year interval and other tidal creeks changing somewhat in edge number or edge length (Figures 6B, C, E, F).

Tidal creeks impacted by resistance surfaces (influenced tidal creeks, for short) were distributed across the Yellow River Delta near abandoned estuaries from the Yellow River's previous course. The Yellow River has changed its course thousands of times due to accumulative landform (due to significantly more sediment and less

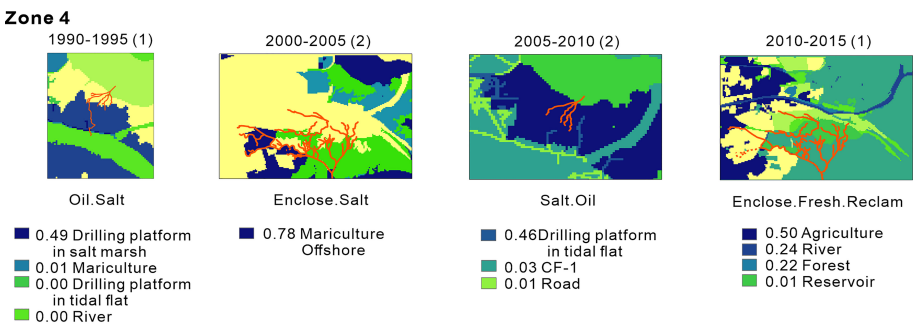

FIGURE 5
Spatial distribution of relative resistance values at resistance surfaces in zone 4. The number in parentheses represents the serial number of each influenced tidal creek (creek ID). CF, composite feature.

10.3389/fmars.2023.1164065

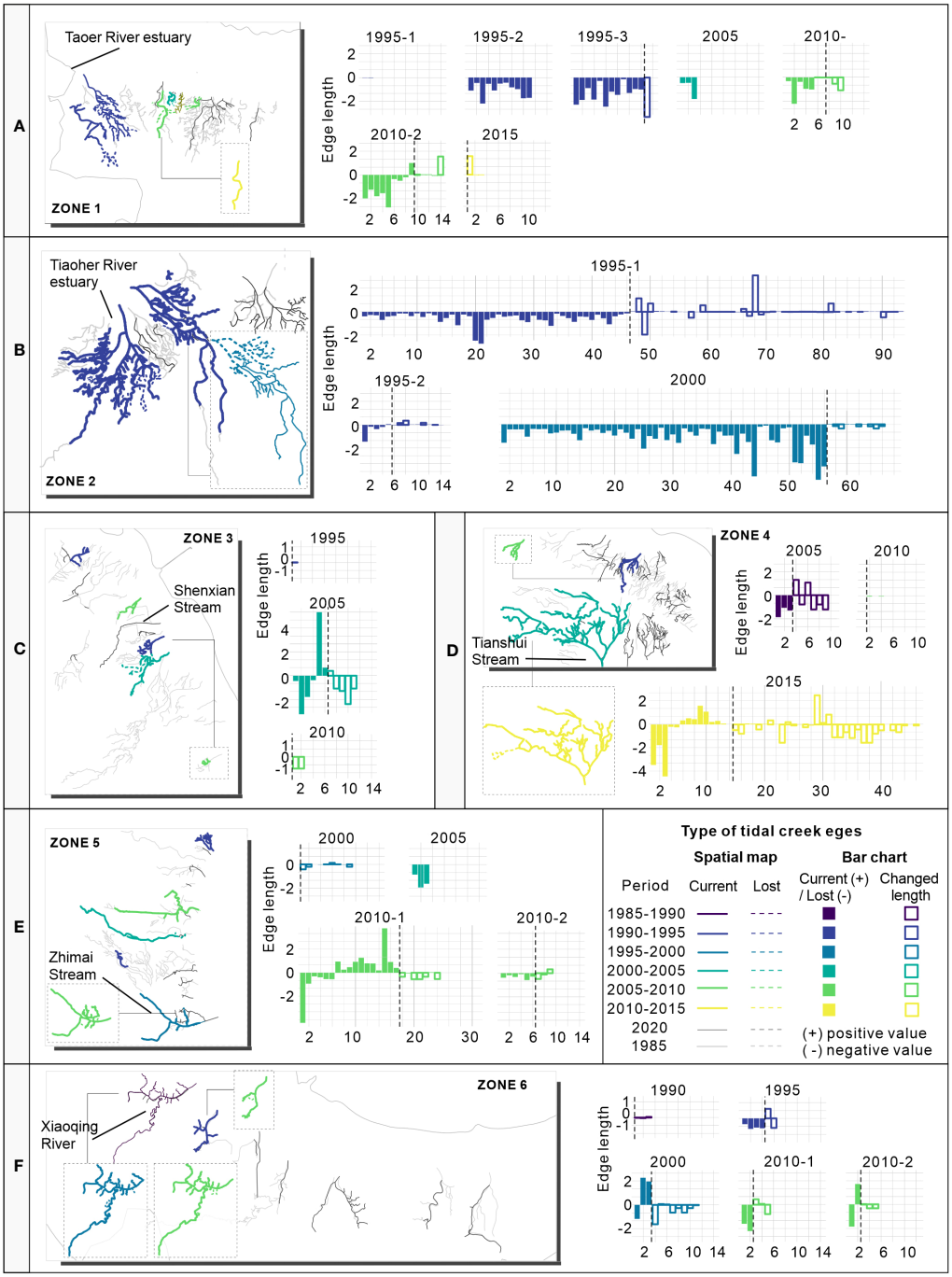

FIGURE 6
Spatial distribution of influenced tidal creeks in zone 1**(A)**, zone 2**(B)**, zone 3**(C)**, zone 4**(D)**, zone 5**(E)**, and zone 6**(F)**. Bar graphs of the edge length changes of the tidal creeks. The numbers in parentheses distinguish different tidal creeks of the same period.

water in the river), resulting in juxtaposed and imbricated deltaic lobes around the river mouths at different times (Zhang et al., 2018). The Taoer River estuary was the source of the most impacted tidal creeks in zone 1 from 1990 to 1995. Tidal creeks have formed in the Taoer River estuary since the Yellow River left. Because the Taoer River was one of the first routes that the Yellow River took to reach the sea (around 1904–1917), tidal creeks in the Taoer River estuary have developed for a long time. In zone 2, the Tiao River estuary had the greatest two impacted tidal creeks in the 1990–1995 and 1995–2000 periods (the Tiao River was the course that the Yellow River used to flow into the sea in 1917–1925). The three impacted tidal creeks in zone 3 were near the Stream Shenxian, which is the course that the Yellow River used to take into the sea in 1953–1960. The Stream Tianshui estuary in zone 4 had the most impacted tidal creek (the Stream Tianshui was the course that the Yellow River used to flow into the sea around 1934–1953). Another impacted tidal creek from the years 2000 to 2010 was in the

Stream Qingshui estuary (the Stream Qingshui was the route that the Yellow River took to reach the sea from 1976 to 1996). Tidal creeks of the Zhimai River estuary were impacted in zone 5 (the Zhimai River was the course that the Yellow River used to flow into the sea in 1929).

4 Discussion

4.1 Resistance as a result of human activity and tidal flat evolution

Resistance to movement values provided a quantitative estimate of how landscape features or environmental parameters affect movement. "resistance" refers to an organism's willingness, costs, or friction when traveling or moving on a surface (McRae, 2006; Zeller et al., 2012). Resistance is utilized in this study to represent the degree to which sea reclamation activities impede or promote water flow movement. The resistance surfaces of various tidal creeks with more than one impacted period varied at different periods. This finding was related to the rate of development of the YRD in the most recent 30 years. Specifically, mariculture activities in zones 1, 2, and 5 (in Zhanhua, Hekou District, and Dongying District) began in the mid-1980s, and generally obtained better yield and expanded the active area in the mid of 1990s after experiencing some technical difficulties and mariculture management measure adjustments (Committee, 2002; Committee, 2008; Committee, 2010). Consequently, mariculture has not yet become a resistance surface in these zones over the periods of 1985–1990 and 1990–1995. During that time, freshwater resource facilities served as resistance surfaces. Storm surges began to harm people and property more regularly as mariculture began to thrive in the tidal flats. When large-scale mariculture activities began after 1995, dikes and hydraulic engineering along the mainstream and near the estuaries of the rivers were built to higher engineering standards (Committee, 2010). As a result, alterations in tidal creeks may occur at the start of resource-use activities. In other words, resource utilization activities may serve as driving forces for the creation of resistance surfaces.

The spatial distribution of influenced tidal creeks exhibited a pattern related to tidal creek evolution. In the first five zones, the impacted tidal creeks, which were generally large-scale tidal creeks, were distributed near estuaries along previous courses of the Yellow River (Figure 6). Taking zone 1 as an example, as far from the Yellow River's current estuary (the Stream Qingshui estuary in zone 4), it has been affected only minimally by sediment from the recent course of the Yellow River, and the coastline in this area has changed slowly. As a relatively stable condition for tidal creek development, tidal creeks were thus extremely developed before 1985, when dike constructions began (Huang and Fan, 2004). Similarly, for zones 2 and 5, tidal creeks began developing when human activity began (Committee, 2002; Committee, 2008). The existence of increased and newly developed edges also revealed that many influenced tidal creeks were still developing. Thus, the formation of resistance was not only due to human activity but also the natural evolution of tidal creeks was an important aspect in the early stages of resistance formation.

4.2 Management implications

The results of different resistance values of human activities influencing hydrological connectivity revealed that the same type of human activity could have different influences at different times and spaces. The resistance value depended on the intensity of the human activity itself, for example, the area of sea reclamation activities. During approved sea reclamation activities in the YRD, strict classification has been made to regulate different human activities (Zhou, 2017; Liu, 2020). For example, in Shandong province, for reclamation projects that change the property of the sea completely, such as port and dike, projects with areas between 60 and 100 hm^2 should be applied to provincial government agencies (Administration, 2008). By comparison, projects that did not change the property of the sea with areas between 500 and 700 hm^2, such as bathing beaches, should be applied to the provincial government (Administration, 2008). However, the classification for each project was only based on the properties of each human activity. Although the impacts of sea reclamation activities on ecosystems have been assigned to environmental impact assessment the environmental impact assessments for reclamation activity projects have considered the impacts on the environment in aspects of hydrodynamic, water quality, landforms, oceanic sediment, and so on, it does not take hydrological connectivity of tidal creeks into consideration in the indexes. More comprehensive regulatory approval steps may be needed to take the impacts of the project on spatially explicit tidal creek connectivity into the evaluation system to classify projects, rather than the current criteria that only focused on project attributes. One of the suggested ways could be that resistance values related to tidal creek connectivity could first be calculated for each land use zone in the planning stage, which could make into a single resistance map. In the steps to check the location of the project in the planning map, the resistance zone of the project could be identified according to its location. Thus, the attributes to classify projects could include project types, area, as well as its resistance value.

The relationship between tidal flat evolution and resistance surface development revealed that there were several previous estuaries with the potential to develop large-scale tidal flats and become stopover hotspots along shorebirds' migratory routes. However, the government of these estuaries has not utilized the ecological value of tidal flats to both benefit local government and regional ecological safeguards. Instead, all the governments of the estuaries focused on resource development activities, for example, mariculture activities, to increase fiscal revenue. By comparison, in zone 4, as large-scale tidal flat and coastal salt marsh ecosystems are well preserved, developing tourism is chosen by the local government, which has also proved to be a good way to both increase fiscal revenue and maintain the ecosystem's benefits. Thus, a good understanding of the potential of resources within the jurisdictional zones is necessary for local governments in the YRD to choose the best way for sustainable development. This required systematic monitoring of the ecosystems and sufficient conservation awareness. Although human activity has caused the most tidal flat loss, except for that in the National Reserve of the Yellow River Delta (Shi et al., 2016; Chen et al., 2019), local areas with developing tidal creeks still exist, including, for example, the

Zhimai River estuary. Despite the fewer areas for conservation in regions such as the YRD, which has severe human activity, attention could also be paid to restoration, for example, returning mariculture to tidal flats (Zhang, 2022). According to the potential tidal and hydrodynamic conditions, further tidal flat development may also exist in some areas.

5 Conclusion

Sea reclamation activities have had strong impacts on tidal creeks. The method we used in this study provided a quantified analysis to assess the impacts of human activities on tidal creeks over a 5-year time scale. In the YRD, the periods of 1990–1995 and 2000–2005 had the greatest number of tidal creeks influenced by resistance surfaces. Most resistance surfaces were composite, the majority of which contained two surfaces. Resistance surfaces of sea enclosure activity, freshwater resource facilities, and engineering in oil fields played a major role in creating resistance surfaces. In areas at the initial development stage, the highest resistance values appeared in mariculture (1.00), reservoir (0.92), and agriculture (0.91). In areas at mature development stages, the highest resistance values appeared in the river (0.97) and mariculture (0.67). Therefore, in the natural resource governance in coastal zones, the plans for reclamation activity, particularly for mariculture, should make sure that their locations have no conflict with tidal creeks. As the formation of resistance was from both human activities and the natural evolution of tidal creeks, it is necessary to take the conditions of tidal creek development into consideration in the planning. Also, for the tidal creek that is in developing conditions, a resource utilization pattern that can benefit both economics and ecology is advised. To achieve this goal, a comprehensive understanding of resources in tidal flats is needed, which requires systematic monitoring and sufficient conservation awareness.

Data availability statement

The original contributions presented in the study are included in the article/supplementary material. Further inquiries can be directed to the corresponding authors.

Author contributions

YM and BC designed the research. YM and FZ collected the data. YM analyzed the data and drafted the manuscript. QW reviewed the manuscript. All authors contributed to the manuscript drafts. All authors contributed to the article and approved the submitted version

Funding

The study was supported financially by the Key Project of the National Natural Science Foundation of China (U2243208), the National Natural Science Foundation of China (52271256), the National Science Foundation for Young Scientists of China (42107057), and the National Postdoctoral Program for Innovative Talents (BX20220040).

Conflict of interest

Author FZ was employed by the company China Construction Eco-Environmental Group Co. Ltd.

The remaining authors declare that the research was conducted in the absence of any commercial or financial relationships that could be construed as a potential conflict of interest.

Publisher's note

References

Administration (2008). *Interim measures of shandong province for the administration of examination and approval of applications for the use of sea areas.* Jinan, Shandong Provincial People's Government.

Bilkovic, D. M. (2011). Response of tidal creek fish communities to dredging and coastal development pressures in a shallow-water estuary. *Estuar. Coast.* 34, 129–147. doi: 10.1007/s12237-010-9334-x

Boynton, W. R., Hodgkins, C., O Leary, C. A., Bailey, E. M., Bayard, A. R., and Wainger, L. A. (2014). Multi-decade responses of a tidal creek system to nutrient load reductions: mattawoman creek, Maryland USA. *Estuar. Coast.* 37, 111–127. doi: 10.1007/s12237-013-9690-4

Buzzelli, C. (2008). Development and application of tidal creek ecosystem models. *Ecol. Model.* 210, 127–143. doi: 10.1016/j.ecolmodel.2007.07.011

Chen, Y., Dong, J., Xiao, X., Ma, Z., Tan, K., Melville, D., et al. (2019). Effects of reclamation and natural changes on coastal wetlands bordering china's yellow Sea from 1984 to 2015. *Land Degrad. Dev.* 30, 1533–1544. doi: 10.1002/ldr.3322

Chen, Y., Fa, Z., Li, B., and Zhao, B. (2013a). Quantitative analysis of the development characteristics and influencing factors of tidal creeks in East chongming beach. *J. Jilin Univ. (Earth Sci. Edition)* 43, 212–219. doi: 10.13278/j.cnki.jjuese.2013.01.028

Chen, L., and Han, Z. (2015). Study of the influence of the deep-water channel project in the Yangtze river estuary on ecological landscape and fractal dimensions of jiuduan shoal tidal channels. *J. Coast. Res.* 73, 146–154. doi: 10.2112/SI73-026.1

Chen, Y., He, Z., Li, B., and Zhao, B. (2013b). Spatial distribution of tidal creeks and quantitative analysis of its driving factors in chongming dongtan,shanghai. *J. Jilin University. Earth Sci. Edition.* 43, 212–219. doi: 10.13278/j.cnki.jjuese.2013.01.028

Committee (2008). *Dongying district annuals* (Beijing: Local Records Publishing House).

Committee (2002). *Hekou district annuals* (Beijing: Local Records Publishing House).

Committee (2010). *Zhanhua county annuals* (Jinan: Qilu Publishing House).

Darrow, E. S., Carmichael, R. H., Calci, K. R., and Burkhardt, W.III (2017). Land-use related changes to sedimentary organic matter in tidal creeks of the northern gulf of Mexico. *Limnol. Oceanogr.* 62, 686–705. doi: 10.1002/lno.10453

DiDonato, G. T., Stewart, J. R., Sanger, D. M., Robinson, B. J., Thompson, B. C., Holland, A. F., et al. (2009). Effects of changing land use on the microbial water quality of tidal creeks. *Mar. pollut. Bull.* 58, 97–106. doi: 10.1016/j.marpolbul.2008.08.019

Fan, Y., Chen, S., Zhao, B., Yu, S., Ji, H., and Jiang, C. (2018). Monitoring tidal flat dynamics affected by human activities along an eroded coast in the yellow river delta, China. *Environ. Monit. Assess.* 190, 396. doi: 10.1007/s10661-018-6747-7

Fan, X., Huang, H., Zhang, Q., Sun, N., and Wang, Y. (2021). Response of tidal creek networks and tidal connectivity to coastal squeeze of saltmarshes in the southern bohai bay. *New Zeal. J. Mar. Fresh.* 56, 617–631. doi: 10.1080/00288330.2021.1917632

Ganio, L. M., Torgersen, C. E., and Gresswell, R. E. (2005). A geostatistical approach for describing spatial pattern in stream networks. *Front. Ecol. Environ.* 3, 138–144. doi: 10.1890/1540-9295(2005)003[0138:agafds]2.0.co;2

Holland, A. F., Sanger, D. M., Gawle, C. P., Lerberg, S. B., Santiago, M. S., Riekerk, G., et al. (2004). Linkages between tidal creek ecosystems and the landscape and demographic attributes of their watersheds. *J. Exp. Mar. Biol. Ecol.* 298, 151–178. doi: 10.1016/S0022-0981(03)00357-5

Huang, H., and Fan, H. (2004). Spatial-temporal changes of tidal flats in the huanghe river delta using landsat TM/ETM+ images. *J. Geogr. Sci.* 14, 365–374. doi: 10.11821/xb200405010

Lerberg, S. B., Holland, A. F., and Sanger, D. M. (2000). Responses of tidal creek macrobenthic communities to the effects of watershed development. *Estuaries* 23, 838–853. doi: 10.2307/1353001

Li, Q., Ma, C., Lu, W., Tian, W., and Zhao, Y. (2012). The effect of reclamation on community structure of macro-meso zooplankton in tidal creeks of the chongming dongtan. *J. Fudan University. Natural Sci.* 51, 515–522. doi: 10.15943/j.cnki.fdxb-jns.2012.04.018

Liu, F. (2020). *Study on the use and management of sea areas in zhanhua district of binzhou city* (Changsha (HN: Hunan Agricultural University).

McRae, B. H. (2006). Isolation by resistance. *Evolution* 60, 1551–1561. doi: 10.1111/j.0014-3820.2006.tb00500.x

Nelson, N. G., Munoz-Carpena, R., Neale, P. J., Tzortziou, M., and Megonigal, J. P. (2017). Temporal variability in the importance of hydrological, biotic, and climatic descriptors of dissolved oxygen dynamics in a shallow tidal-marsh creek. *Water Resour. Res.* 53, 7103–7120. doi: 10.1002/2016WR020196

Peterman, W. E. (2018). ResistanceGA: an r package for the optimization of resistance surfaces using genetic algorithms. *Methods Ecol. Evol.* 9, 1638–1647. doi: 10.1111/2041-210X.12984

Peterson, E., and Ver Hoef, J. (2014). STARS: an ArcGIS toolset used to calculate the spatial information needed to fit spatial statistical models to stream network data. *J. Stat. Software* 56, 1–17. doi: 10.18637/jss.v056.i02

Sanger, D., Blair, A., DiDonato, G., Washburn, T., Jones, S., Riekerk, G., et al. (2015). Impacts of coastal development on the ecology of tidal creek ecosystems of the US southeast including consequences to humans. *Estuar. Coast.* 38, 49–66. doi: 10.1007/s12237-013-9635-y

Sanger, D. M., Holland, A. F., and Hernandez, D. L. (2004). Evaluation of the impacts of dock structures and land use on tidal creek ecosystems in south Carolina estuarine environments. *Environ. Manage.* 33, 385–400. doi: 10.1007/s00267-003-0019-0

Shi, H., Shen, Y., and Kang, M. (2016). Rapid response of tidal creek network patterns to the reclamation on the central jiangsu coast. *Acta Oceanol. Sin.* 38, 106–115. doi: 10.3969/j.issn.0253-4193.2016.01.010

Song, H. (2015). *Influence of reclamation activities on ecosystem type and carbon sink function of the coastal wetland in the yellow river estuary. [Doctor of philosophy]* (Changchun (JL: Chinese Academy of Sciences).

Spear, S. F., Balkenhol, N., Fortin, M. E. E., McRae, B. H., and Scribner, K. (2010). Use of resistance surfaces for landscape genetic studies: considerations for parameterization and analysis. *Mol. Ecol.* 19, 3576–3591. doi: 10.1111/j.1365-294x.2010.04657.x

Tessler, Z. D., Voeroesmarty, C. J., Grossberg, M., Gladkova, I., Aizenman, H., Syvitski, J. P. M., et al. (2015). Profiling risk and sustainability in coastal deltas of the world. *Science* 349, 638–643. doi: 10.1126/science.aab3574

United States Geological Survey *Earth explorer*. Available at: https://earthexplorer.usgs.gov (Accessed March 23, 2022).

Ver Hoef, J., Peterson, E., Clifford, D., and Shah, R. (2014). SSN: an r package for spatial statistical modeling on stream networks. *J. Stat. Software* 56, 1–45. doi: 10.18637/jss.v056.i03

Ver Hoef, J. M., Peterson, E., and Theobald, D. (2006). Spatial statistical models that use flow and stream distance. *Environ. Ecol. Stat.* 13, 449–464. doi: 10.1007/s10651-006-0022-8

Wang, Q., Wang, X., Li, X., Wang, X., and Zhan, C. (2017). Grain size characteristics and coarsening phenomenon of inter-tidal flat surficial sediment along the abandoned southern yellow river Sub-delta. *Quaternary Sci.* 37, 353–367. doi: 10.11928/j.issn.1001-7410.2017.02.13

Wang, Q., Xie, T., Ning, Z., Chen, C., Man, Y., and Cui, B. (2021). Enhancement of lateral connectivity promotes the establishment of plants in saltmarshes. *Sci. Total Environ.* 767, 145484. doi: 10.1016/j.scitotenv.2021.145484

Washburn, T., and Sanger, D. (2011). Land use effects on macrobenthic communities in southeastern united states tidal creeks. *Environ. Monit. Assess.* 180, 177–188. doi: 10.1007/s10661-010-1780-1

Weikang, S., Xinghua, Z., Yikai, F., and Yanguang, F. (2018). Temporal and spatial characteristics of coastal tides in Shandong province. *J. Ocean Technol.* 37, 68–75. doi: 10.3969/j.issn.1003-2029.2018.04.011

Wessel, M. R., Leverone, J. R., Beck, M. W., Sherwood, E. T., Hecker, J., West, S., et al. (2021). Developing a water quality assessment framework for southwest florida tidal creeks. *Estuar. Coast.* 552, 1–21. doi: 10.1007/s12237-021-00974-7

Wu, Y., Liu, J., Yan, G., Zhai, J., Cong, L., Dai, L., et al. (2020). The size and distribution of tidal creeks affects salt marsh restoration. *J. Environ. Manage.* 259, 110070. doi: 10.1016/j.jenvman.2020.110070

Xie, C., Cui, B., Xie, T., Yu, S., Liu, Z., Wang, Q., et al. (2020). Reclamation shifts the evolutionary paradigms of tidal channel networks in the yellow river delta, China. *Sci. Total Environ.* 742, 140585. doi: 10.1016/j.scitotenv.2020.140585

Xie, W., He, Q., Wang, X., Guo, L., and Guo, C. (2017). Hydrodynamic process and sediment transport in a tidal creek system over the easten chongming Island,Yangtze estuary. *Acta Oceanol. Sin.* 39, 80–91. doi: 10.3969/j.issn.0253-4193.2017.07.008

Yang, Z., Shenliang, C., and Guochuan, G. (2015). Spatial extent and tidal characteristics of the diurnal tidal zone along the yellow river delta coast. *Chin. J. Hydrodynamics.* 30, 540–548. doi: 10.16076/j.cnki.cjhd.2015.05.008

Zeller, K. A., McGarigal, K., and Whiteley, A. R. (2012). Estimating landscape resistance to movement: a review. *Landscape Ecol.* 27, 777–797. doi: 10.1007/s10980-012-9737-0

Zhang, H. (2022). *Effects of wetland restoration on the spatial distribution of nests, nesting microhabitat and egg camouflage of shorebirds in liaohekou estuarine wetland* (Shenyang (LN: Liaoning University).

Zhang, X., Lu, Z., Jiang, S., Chi, W., Zhu, L., Wang, H., et al. (2018). The progradation and retrogradation of two newborn huanghe (Yellow river) delta lobes and its influencing factors. *Mar. Geol.* 400, 38–48. doi: 10.1016/j.margeo.2018.03.006

Zhou, C. (2017). *Sea Areas management problem study under the new situation —– illustrated by the case of wenzhou* (Nanchang (JX: Jiangxi Agricultural University).

Zhou, L., Wang, W., Gao, M., Bai, W., and Yue, B. (2016). Monitoring the tidal topography of the north yellow river delta with LIDAR data. *Geological Bull. China.* 35, 1661–1668. doi: 10.3969/j.issn.1671-2552.2016.10.014

frontiers | Frontiers in Marine Science

TYPE Original Research
PUBLISHED 10 August 2023
DOI 10.3389/fmars.2023.1226234

OPEN ACCESS

EDITED BY
Tian Xie,
Beijing Normal University, China

REVIEWED BY
Jingwen Zhang,
University of Illinois at Urbana-Champaign, United States
Fajin Chen,
Guangdong Ocean University, China
Yonggui Wang,
China University of Geosciences, China

*CORRESPONDENCE
Zhihao Xu
zhihaoxu@gdut.edu.cn

RECEIVED 21 May 2023
ACCEPTED 24 July 2023
PUBLISHED 10 August 2023

CITATION
Fan W, Xu Z, Dong Q, Chen W and Cai Y (2023) Remote sensing-based spatiotemporal variation and driving factor assessment of chlorophyll-*a* concentrations in China's Pearl River Estuary.
Front. Mar. Sci. 10:1226234.
doi: 10.3389/fmars.2023.1226234

Remote sensing-based spatiotemporal variation and driving factor assessment of chlorophyll-*a* concentrations in China's Pearl River Estuary

Wenjie Fan[1], Zhihao Xu[1,2]*, Qian Dong[1], Weiru Chen[1] and Yanpeng Cai[1,2]

[1]Guangdong Provincial Key Laboratory of Water Quality Improvement and Ecological Restoration for Watersheds, Institute of Environmental and Ecological Engineering, Guangdong University of Technology, Guangzhou, China, [2]Southern Marine Science and Engineering Guangdong Laboratory (Guangzhou), Guangzhou, China

Climate change and intensive anthropogenic activities have severely challenged the water quality of China's Pearl River Estuary (PRE). Further investigations into long-term water quality variation and associated driving mechanisms are therefore necessary to support the sustainable development of the PRE's Greater Bay Area (GBA). This study used remote sensing retrieval to address long-term spatiotemporal chlorophyll-*a* (Chl-*a*) variation characteristics in the PRE and the relationship between Chl-*a* concentrations and socioeconomic/environmental indicators. Three decades of Landsat satellite images and measured data were collected, and a two-band global algorithm was used to retrieve Chl-*a* concentration data. Results reveal significant spatiotemporal variability in Chl-*a* concentrations. The space-averaged Chl-*a* concentration exhibited a slight downward trend during the past three decades, and the multi-year mean value was 5.20 mg/L. Changes to environmental protection policies in recent years have improved overall PRE water quality. The western section of the PRE had the highest Chl-*a* concentration (i.e., 5.92 mg/L average) while the eastern section had the lowest (i.e., 3.98 mg/L average). This discrepancy was likely caused by the western section's more intensive industrial activities, resulting in a higher overall wastewater discharge volume. Affected by climatic conditions, winter Chl-*a* concentrations were evenly distributed while summer concentrations were significantly higher. Additionally, Chl-*a* concentrations significantly and positively correlated with total phosphorus (TP), total nitrogen (TN), ammonia nitrogen (NH_3-N), and the biotic oxygen demand (BOD_5). Chl-*a* concentrations also correlated with external factors (i.e., climate and anthropogenic activities). Among these factors, industrial wastewater discharge and the proportion of primary industries in coastal cities significantly and positively correlated with water quality. This study is intended to help direct water quality improvement management and urban sustainable development in the GBA.

KEYWORDS

estuary water quality, remote sensing, retrieval algorithm, chlorophyll-*a* concentration, spatiotemporal dynamics, driving factor

1 Introduction

Although Estuaries are among the most productive ecosystems in the world, they are vulnerable to climate change and anthropogenic activities (Scanes et al., 2020; Burford and Faggotter, 2021). Located at the land-ocean interface, estuaries are vulnerable to nutrient inputs from surrounding agricultural, industrial, and urban development (Jeffries et al., 2016). Meanwhile, the withdrawal of potable water from upstream catchments can significantly decrease freshwater inflow while facilitating nutrient accumulation in estuaries (Jiang et al., 2014). Additionally, estuarine eutrophication has become a global issue, causing multiple environmental issues, including harmful algal blooms, hypoxic "dead zones", and habitat degradation, which have affected species richness (Testa et al., 2018; Wurtsbaugh et al., 2019; Montefiore et al., 2023). On average, in China's coastal regions, there have been over 60 red tide events annually over the past two decades (Wang B et al., 2018). To improve estuary sustainability, it is important to clarify long-term water quality variation and associated driving factors in eutrophic estuaries.

Satellite-based remote sensing provides an efficient and cost-effective way to monitor environmental changes in aquatic systems (Gholizadeh et al., 2016; Jay et al., 2017; Chawla et al., 2020), which is becoming increasingly attractive because of its high monitoring frequency and spatiotemporal coverage (Tong et al., 2022). It has been widely used in retrieval of various water quality indicators, such as chlorophyll-*a* (Chl-*a*), total suspended solid (TSS), dissolved oxygen (DO), nutrients, and chromophoric dissolved organic matter (CDOM) (Ross et al., 2019; Kim et al., 2020). Specifically, Chl-*a* is a key indicator used to evaluate algal conditions and eutrophication status in freshwater and marine environments (Tong et al., 2022). Significant advancements have been made in Chl-*a* concentration research. For example, many relevant studies have used remote sensing algorithms to estimate Chl-*a* concentrations. These include fluorescence peak algorithms, artificial neural network algorithms, and blue-green band ratio and near-infrared-red band ratio (Gilerson et al., 2010; Ioannou et al., 2013; Beck et al., 2016; O'Reilly and Werdell, 2019). The application of these algorithms improves the accuracy and universality of Chl-*a* estimates through remote sensing. Much attention has been paid to long-term spatiotemporal variation in Chl-*a* concentrations and associated driving factors. Researchers have employed various remote sensing techniques and water quality monitoring methods to comprehensively analyze the spatiotemporal evolution of Chl-*a* concentrations (Zhang et al., 2013; Moradi and Kabiri, 2015; Wang et al., 2015). External driving factors, such as climate, anthropogenic activities (Conley et al., 2009; Paerl and Huisman, 2009), ENSO effects (i.e., climatic oscillations), and water mass transportation (Durack, 2015; Guo et al., 2017; Lao et al., 2022; Lao et al., 2023) have all been found to be extremely important factors that affect Chl-*a* variation. Changes in temperature, precipitation, and water pollution have a particularly impactful influence on Chl-*a* concentrations in estuarine zones (Ding et al., 2015; Shrestha et al., 2018; Li et al., 2022).

The Pearl River Estuary (PRE) is one of China's regions where anthropogenic activities and natural factors converge and conflict, particularly over the past three decades (Cao C et al., 2022). Therefore, it is vital that we investigate long-term spatiotemporal variation and associative driving factors in PRE water quality (Chen et al., 2021). Extensive relevant research has focused on the methods used to retrieve PRE water quality data (Zheng and DiGiacomo, 2017), including the three-band model (Chen et al., 2011), red-peak algorithms (Liu and Tang, 2019), and deep learning (Ye et al., 2021). Other studies have focused on analyzing spatiotemporal water quality variation in the PRE, such as spatiotemporal variation in Chl-*a* concentrations (Gao et al., 2020), total phosphorus (TP) (Lu et al., 2020), total nitrogen (TN) (Guo et al., 2022), dissolved organic carbon (DOC) (Liu et al., 2015), TSS (Wang C et al., 2018), and CDOM (Chen et al., 2004). Some studies have even explored the combined impact of natural factors and anthropogenic activities on PRE water quality. These studies have examined various factors, including air temperature, precipitation, reclamation initiatives, and industrial and agricultural activity development within the vicinity of water (Wang et al., 2019; Cao B et al., 2022; Shen et al., 2022). The aim of these studies was to understand the complex interactions that occur between natural processes and human interventions that subsequently influence estuarine water quality. Chl-*a* research has been especially extensive. This is due to its influencing factors, such as seasonality, tides, estuarine mixing, and seasonal changes in terrestrial nutrient inputs (Qiu et al., 2010; Ye et al., 2016; Tao et al., 2020; Liang et al., 2021). Moreover, Chl-*a* concentrations in the PRE exhibit distinct seasonal and interannual variation as well as significant spatial heterogeneity across different sections. Collectively, this pattern closely correlates to natural factors and anthropogenic activities (Sigman and Hain, 2012; Xu et al., 2022). However, there is a lack of comprehensive research on long-term spatiotemporal dynamics in the PRE prior to 2000, while relationships between Chl-*a* concentrations and internal and external factors remain unclear. Therefore, it is critical that we investigate long-term spatiotemporal dynamics and associative driving mechanisms of PRE water quality.

The aim of this study was to analyze the spatiotemporal evolution of PRE water quality over the past 30 years and explore its associative driving factors. For this study the PRE was divided into four regions where we collected water quality data, meteorological data, socio-economic development data, and satellite imagery products. Moreover, we built a Chl-*a* concentration retrieval model to analyze spatiotemporal variability within the PRE. Both statistical analysis and correlation analysis were used to investigate the relationship between Chl-*a* concentrations and associative driving factors in conjunction with spatial and temporal variability.

2 Methods

2.1 Study area

The Guangdong-Hong Kong-Macao Greater Bay Area (GBA), more commonly referred to as the GBA, is one region in China with

the highest urbanization and industrialization rates (Zhou et al., 2018). Along with the GBA's rapid economic development, a large amount of nitrogen (N) and phosphorus (P) pollutants from industrial and agricultural wastewater and domestic sewage is discharged into the PRE (Huang et al., 2003; Tao et al., 2021). The PRE's water surface area, which the GBA surrounds, is approximately 1700 km^2. Its longitudinal and latitudinal coordinates are 113°44′43.1″ E and 22°34′38.25″ N, respectively (Yuan et al., 2022). The PRE's complex hydrological network and diverse environmental conditions have made it a prominent research focus within the scientific community (Wu et al., 2016). Under the influence of its subtropical monsoon climate, river flow and wind speed are manifested by pronounced seasonal variation (Lu and Gan, 2015). Most annual discharge from the Pearl River (approx. 80%) occurs during the rainy season (Ye et al., 2017). This causes considerable disparity in river flow between the dry season (October to April) and the rainy season (May to September), with average values of approximately 1500 m^3/s and 20000 m^3/s, respectively (Liu et al., 2012). In the PRE, weak southwesterly winds predominant during the summer, whereas strong northeastern winds dominate during the winter (Zhang et al., 2019). Seasonal variations in hydrodynamic conditions have a considerable influence on seasonal water quality dynamics in the PRE. In brief, climate change and rapid urbanization exert a heavy strain on PRE water quality, posing significant challenges to its ecological well-being. The PRE is a large aquatic region. Anthropogenic activities in many of its cities throughout its different sections cause varying degrees of pollution and nutrient inputs, which significantly impact Chl-*a* concentrations. In this study, we divided the PRE into four sections based on its coastal cities to analyze spatiotemporal evolutionary features (Figure 1). These four sections were specifically divided into the northern section (adjacent to Guangzhou and Dongguan), the eastern section (adjacent to Shenzhen), the western section (adjacent to Zhuhai and Zhongshan), and the southern section (adjacent to the open sea).

2.2 Data sources

Since 1986, the Environmental Protection Department (EPD) of Hong Kong has measured water quality monthly within its coastal waters. This study uses water quality indicators, including Chl-*a*, TP, TN, ammonia nitrogen (NH_3-N), and biotic oxygen demand (BOD_5). Long-term data on these water quality indicators were collected between 1989–2019, which we sourced from 9 EPD meteorological stations (Figure 1). For detailed information on water quality, please refer to the EPD website. (https://www.epd.gov.hk).

Precipitation and temperature fluctuations can give rise to alterations in the physical and chemical attributes of aquatic environments. Anthropogenic activities, including the discharge of industrial wastewater and the agricultural development of urban areas, exert a considerable influence on water quality, which are as significant as external factors (Liu et al., 2022). A higher proportion of primary industries is indicative of a developed agricultural sector within urban areas. Therefore, this study selected temperature, precipitation, industrial wastewater discharge, and the proportion of primary industries as driving factors. Given the

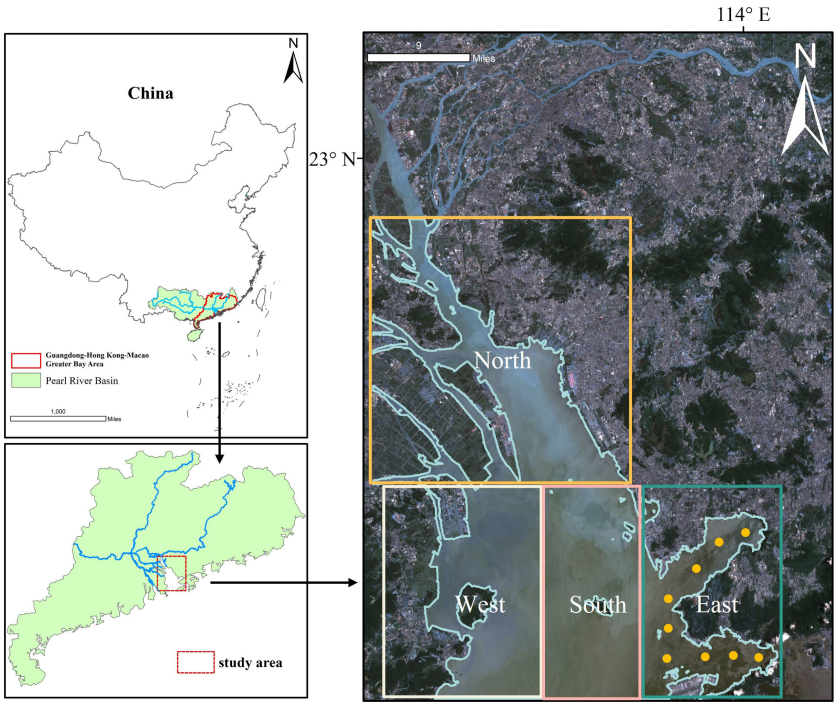

FIGURE 1
Location and sectional divisions of the study area. The locations where data were measured are marked with points.

limited availability of historical water temperature data within the study area, we used temperature data from cities near the PRE between 1989–2019, which we obtained from meteorological websites (http://data.cma.cn/). The precipitation data used in this study derive between 1989–2019, which we obtained from the daily global precipitation measurement dataset provided by the National Aeronautics and Space Administration (NASA) (https://disc.gsfc.nasa.gov). Socio-economic development factors considered in this study include the industrial wastewater discharge, and the proportion of the primary industry in the cities neighboring the PRE between 1989–2019. Urbanization data used in this study primarily derive from statistical yearbooks, which were obtained from various regions.

This study uses satellite imagery products, including digital products from the Landsat 5 and Landsat 7 satellites. The Landsat series satellites are jointly developed by NASA and the United States Geological Survey (USGS) which were launched in 1972. These satellites have a revisit period of 16 days and a spatial resolution of 30 m. Considering sampling time and cloud cover on satellite acquisition dates, we collected approximately 100 surface reflectance images of the PRE between 1989–2019. Satellite imagery products are obtained from USGS (https://earthexplorer.usgs.gov).

2.3 Retrieval model and model evaluation

The satellite images used in this study included both water and land information. However, only water information was used during the retrieval process. It was necessary to extract water information and remove land information. Google Earth Engine (GEE) platform offers a geospatial processing service. Users can perform large-scale geospatial processing provided by Google Cloud Platform support. Landsat 5 Collection 2 Tier 1 calibrated top-of-atmosphere reflectance (TOA) reflectance images were directly downloaded from the GEE platform (Mutanga and Kumar, 2019). Because the GEE platform eliminates the need for radiometric calibration and atmospheric correction, we used it to preprocess Landsat 5 images between 1989–2011, including cropping, cloud removal, and band manipulation.

To ensure research analysis accuracy and improve the extraction precision of satellite image information, it was necessary to use atmospheric correction to remove interference caused by atmospheric scattering and other factors on land features. In this study, ENVI 5.3 software was used to preprocess Landsat 7 images between 2012–2019, including cropping, striping removal, radiometric calibration, atmospheric correction, and band calculations. The FLAASH atmospheric correction tool was used for atmospheric correction, which ENVI 5.3 provides. It offers high multispectral data accuracy correction, and it has widely been used in atmospheric correction models. Additionally, digital numbers recorded by the sensor must be converted to radiance values. The radiometric calibration tool in ENVI 5.3 was used for conversions, applying the following formula:

$$L = \frac{DN}{a} + L_0 \tag{1}$$

where L is radiance; DN is the recorded sensor grayscale values; a represents gain; L_0 represents the offset value.

Chl-*a* concentration remote sensing retrieval is a process of estimating Chl-*a* concentrations from satellite images by utilizing its spectral reflectance characteristics. Chl-*a* exhibits strong absorption and reflection in the blue wavelength range(450-495nm) and green wavelength range(495-570nm) (O'Reilly et al., 1998). Both bands strongly correlate with Chl-*a*. Most empirical algorithms use them to establish models for Chl-*a* concentration retrieval.

Two-band (OC2v4) and four-band (OC4v4) global algorithms were developed by NASA; however, they tend to systematically overestimate Chl-*a* concentrations (D'Ortenzio et al., 2002). The OC2_D'Ortenzio algorithm is an improved version of OC2v4. It performs well when applied to biogeochemical measurements or satellite data (Pan et al., 2010). Considering the dynamic nature of the study area, we used the OC2_D'Ortenzio algorithm to construct a Chl-*a* concentration retrieval model. This algorithm is based on a nonlinear relationship, improved by a cubic polynomial function, between ocean reflectance and *in-situ* Chl-*a* concentrations measurements.

$$C = 10^{(a_0 + a_1 \times B + a_2 \times B^2 + a_3 \times B^3)} + a_4 \tag{2}$$

$$B = \frac{R_{rs}490}{R_{rs}555} \tag{3}$$

where C is the Chl-*a* concentration; B is the land-surface reflectance ratio; $R_{rs}490$ and $R_{rs}555$ were obtained from 490 nm and 555 nm land surface reflectance; a = 0.217, −2.728, 0.704, 0.297, and −0.035, which are algorithm constants.

To evaluate model accuracy, the statistical metrics used for validation were the coefficient of determination (R^2), the root-mean-square error (RMSE), and biases. The following equations show the formulae used:

$$R^2 = 1 - \frac{\sum_{i=1}^{n}(S_{est,i} - X_{obs,i})^2}{\sum_{i=1}^{n}(\bar{X}_{obs,i} - X_{obs,i})^2} \tag{4}$$

$$RMSE = \sqrt{\sum_{i=1}^{n}(X_{obs,i} - X_{est,i})^2 / n} \tag{5}$$

$$bias = \frac{1}{n}\sum_{i=1}^{n}(X_{obs,i} - X_{est,i}) \tag{6}$$

where n is the sample size; $S_{est,i}$ is the value fitting curve obtained; $X_{obs,i}$ is the *in-situ* data obtained; $\bar{X}_{obs,i}$ is the average of $X_{obs,i}$; $X_{est,i}$ is the estimated data obtained.

2.4 Driving factor analysis

Relationships among water quality factors (TP, TN, NH_3-N, and BOD_5) and external driving factors are examined through Pearson correlation analysis and regression analysis. Pearson

correlation coefficient is used to measure the correlation between various variables and Chl-*a* concentrations in the PRE. Pearson correlation coefficient ranges from −1 to +1, where −1 denotes no negative correlation, +1 denotes a positive correlation, and 0 denotes no correlation. A significance level<0.05 ($P< 0.05$) was considered statistically significant. Data preparation for Pearson correlation analysis was conducted using IBM SPSS Statistics 27 software.

Partial least squares regression (PLS regression) models were used to analyze driving factors. PLS regression is a statistical modeling method used to establish predictive models between input variables and output variables. Its advantage is its ability to manage highly correlated input variables. By constructing latent variables, it decouples relationships between input variables and output variables. Additionally, PLS regression can effectively manage small sample sizes. PLS regression effectiveness can be evaluated using Variable Importance in Projection (VIP) scores. VIP scores indicate the importance of each predictor variable in explaining the response variable. If the VIP score of a predictor variable is >1.0, the variable has a significant impact on explaining the response variable. On the other hand, if the VIP score is<0.5, the variable does not contribute significantly to explaining the response variable. Values between 0.5 and 1.0 indicate a moderate level of importance. PLS regression was constructed using IBM SPSS Statistics 27 software.

3 Results and discussion

3.1 Model validation

This study validates the performance of a remote sensing retrieval model used to estimate Chl-*a* concentrations by comparing simulated values with a dataset of measured data. The measured data spans from 1989 to 2019, with a total of 113 observations. Measured data were obtained from the EPD of Hong Kong and is considered highly reliable. Simulated Chl-*a* concentration values derived from satellite images. Simulated values and measured data correspond closely in time and geographical coordinates. The RMSE of the model was 2.55 mg/L, with a bias of −1.39 mg/L. A scatter plot (Figure 2) was generated using measured values as the independent variable and the simulated values as the dependent variable. Outliers that deviate significantly from other data points were removed, resulting in a total of 110 data points. The data points are relatively clustered, and the R^2 values between the linear regression line (i.e., the blue solid line) and the data points was 0.7155. Difference among verification results and that from other relevant PRE studies were within an acceptable range (Ma et al., 2022). This strongly indicates that this model used in this study can estimate PRE Chl-*a* concentrations.

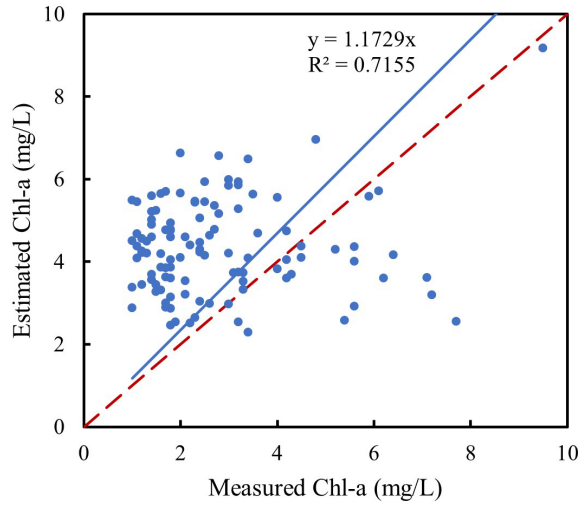

FIGURE 2
Comparison of estimated and measured Chl-*a* concentrations.

3.2 Spatial distribution

This study analyzed annual spatial distribution characteristics in PRE Chl-*a* concentrations using images taken in the spring (March to May), summer (June to August), autumn (September to November), and winter (December to February) of 2010 (Figure 3). The spatial distribution of PRE Chl-*a* concentrations exhibited distinct patterns across the various seasons. Average Chl-*a* concentrations in spring, summer, autumn, and winter were 5.07 mg/L, 6.15 mg/L, 4.29 mg/L, and 3.11 mg/L, respectively. Standard deviations were 2.59 mg/L, 1.52 mg/L, 2.25 mg/L, and 0.68 mg/L. In spring and autumn, the western and eastern sections exhibited high Chl-*a* concentrations while the northern and southern regions exhibited lower Chl-*a* concentrations. Elevated Chl-*a* concentrations were found near the coastline but gradually decreased the further inland they were. During winter, due to lower water temperatures and slower phytoplankton growth, Chl-*a* concentrations in the water column was relatively low. Furthermore, the mixing of water masses within the PRE was influenced by strong northeasterly monsoons and tidal currents, resulting in a relatively uniform Chl-*a* concentration phytoplankton in the water column. In summer, areas with high Chl-*a* concentrations were mainly within the northern and western sections, which exhibited a decreasing trend from north to south. Additionally, we simulated summer phytoplankton growth using influencing factors (i.e., temperature and rainfall), which resulted in significantly higher Chl-*a* concentrations and distinct spatial distribution patterns. Accordingly, we focused on investigating the spatiotemporal Chl-*a* concentration variations in the PRE during summer, accounting for the distinct characteristics and relevance to ecological processes and environmental management in the region.

Additionally, the eastern region had higher Chl-*a* concentrations during all four seasons, where areas with high concentrations were mainly distributed within the Shenzhen Bay area. This phenomenon is due to enclosed bays that typically have smaller openings or inlets, subsequently resulting in less water exchange compared to the surrounding open sea. This leads to nutrient accumulation via organic and inorganic substances within

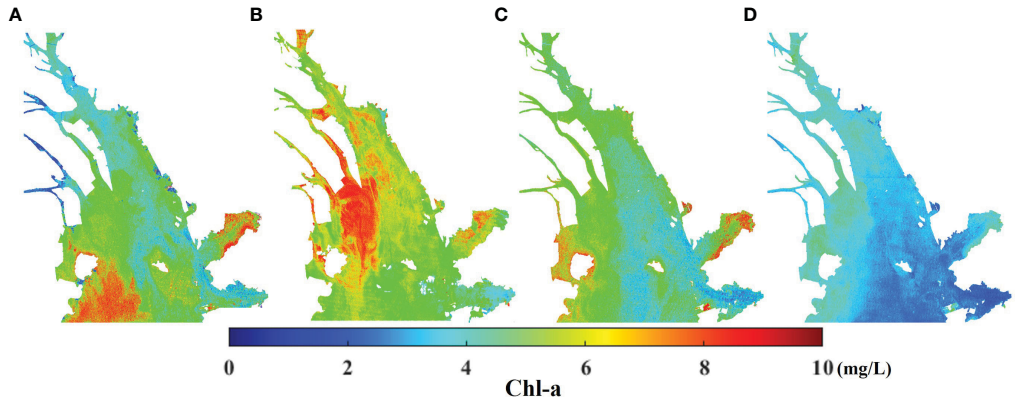

FIGURE 3
Distribution of Chl-*a* concentrations in 2010: **(A)** spring; **(B)** summer; **(C)** autumn; **(D)** winter.

enclosed bay areas. These substances provide ample nutrients for phytoplankton growth. Moreover, they can contribute to an increase in phytoplankton growth within enclosed bays, resulting in higher Chl-*a* concentrations.

In this study, remotely sensed images taken in the summer of 1999, 2009, and 2019 were used to analyze interannual variations in spatial distribution characteristics of Chl-*a* concentrations in the PRE (Figure 4). The overall distribution of Chl-*a* concentrations in the PRE was uneven and exhibited significant spatial differences. Specifically, in the northern section, Chl-*a* concentrations in 1999, 2009, and 2019 were 6.48 mg/L, 5.92 mg/L, and 6.75 mg/L, respectively. In the western section, Chl-*a* concentrations were 5.95 mg/L, 9.48 mg/L, and 6.01 mg/L, respectively. In the eastern section, the Chl-*a* concentrations were 3.69 mg/L, 4.52 mg/L, and 3.88 mg/L, respectively. In the southern section, Chl-*a* concentrations were 4.96 mg/L, 6.38 mg/L, and 5.07 mg/L, respectively.

The northern and western sections had higher Chl-*a* concentrations, which were significantly higher compared to the other two sections. The Chl-*a* concentration diffusion pattern exhibited a spread from west to east and from north to south. Additionally, interannual variations in Chl-*a* concentrations differed among the four sections. The northern section exhibited relatively low Chl-*a* concentration fluctuations, with an approximate range of 0.7 mg/L. The western section exhibited greater fluctuation, where the average Chl-*a* concentration reached 9.48 mg/L in 2009, surpassing the other section by a large margin. The eastern and southern sections exhibited a similar magnitude of variation (i.e., approximately 1.5 mg/L). Such significant interannual differences can be explained by urbanization near the PRE, including industrial wastewater and domestic sewage. Factors such as water temperature, rainfall, and light conditions during different years can also have influenced phytoplankton growth and eutrophication over the past 30 years.

3.3 Interannual variation

To obtain a better understanding of temporal water quality variation in the PRE, this study focused on changes in Chl-*a*

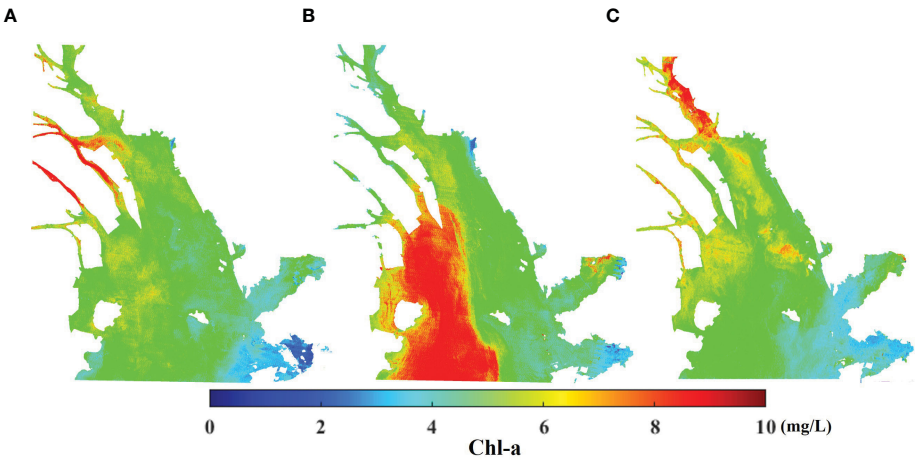

FIGURE 4
Distribution of mean Chl-*a* concentrations in summer: **(A)** 1999; **(B)** 2009; **(C)** 2019.

concentrations between 1989–2019 (Figure 5). Between 1989–2019, Chl-*a* concentration on average exhibited significant fluctuations over time, exhibiting a slight overall decreasing trend. Over the past 30 years, the average Chl-*a* concentration was 5.20 mg/L. The Chl-*a* concentration decreased from 6.74 mg/L in 1989 to 5.56 mg/L in 2019. The highest value was measured in 1989 (i.e., 6.74 mg/L), while the lowest was measured in 2005 (i.e., 3.66 mg/L). In 2009, a sudden jump in Chl-*a* concentration occurred, increasing from 4.26 mg/L to 6.73 mg/L. In this study, long-term (i.e., 30 year) Chl-*a* concentrations variation was divided into three distinct periods. Between 1989–1999, Chl-*a* concentrations only exhibited small fluctuations (i.e., 5.96 mg/L average). However, compared to the other two periods, this period exhibited significantly higher Chl-*a* concentrations. Between 2000–2009, Chl-*a* concentrations exhibited higher fluctuations (i.e., 5.02 mg/L average). On the other hand, there was a notable upward trend between 2004–2009, indicating water quality degradation during this period. Between 2010–2019, the average Chl-*a* concentration was 4.80 mg/L, which was the lowest among the three periods and exhibited a clear downward trend, indicating a significant improvement in water quality during this period.

In the different sections, Chl-*a* concentrations differed in spatial and temporal variation characteristics. This study divided the PRE into four sections to analyze each section's specific Chl-*a* concentration over time (Figure 6). The western section had the highest Chl-*a* concentration (i.e., 5.92 mg/L average). Additionally, the Chl-*a* concentration in the western section fluctuated the most, reaching 9.48 mg/L in 2009, indicating a more stable water quality environment. The Chl-*a* concentration in the eastern section was the lowest (i.e., 3.98 mg/L average) while more stable than the other sections over the past 30 years. This indicated that the eastern section's water quality environment was relatively good. This discrepancy was likely caused by the western section's more intensive industrial activities than the eastern section, resulting in a higher overall wastewater discharge volume. The average Chl-*a* concentrations in the northern and southern sections were 5.51 mg/L and 4.98 mg/L, respectively. Additionally, changes to Chl-*a* concentrations in these two sections were similar, both exhibiting a significant downward trend, indicating that water quality conditions have generally improved over the past 30 years.

Considering the geographical proximity of the four sections, several factors may have contributed to variations in Chl-*a* concentrations and the eutrophication phenomena. Natural factors can influence phytoplankton growth and eutrophication. Generally, high temperatures and rainfall can stimulate phytoplankton growth, resulting in higher concentrations. Conversely, lower water temperatures and rainfall limit phytoplankton growth. These factors can cause significant distribution variation in Chl-*a* concentrations during different seasons while also significantly impacting interannual variation. Agricultural and industrial activities, as well as densely populated urban areas near the PRE, can cause significant pollutant inputs into water, such as agricultural fertilizers, industrial wastewater, and domestic sewage. Over the past 30 years, the overall water quality of the PRE has improved. This improvement may be attributed to environmental protection policies that have led to a reduction of pollutants from entering its coastal areas, including industrial wastewater and domestic sewage discharge.

3.4 Relationship with water quality indicators

This study analyzed data from PRE monitoring stations over a 30-year period, using the average Chl-*a* concentration as the independent variable and water quality indicators as the dependent variable. Polynomial regression analysis and significance tests indicated a significant relationship between Chl-*a* and water quality (Figure 7). Additionally, TP and TN highly correlated with Chl-*a* concentrations. The R^2 value for TP was >0.6, indicating a positive correlation with Chl-*a* concentrations ($P< 0.05$), whose correlation coefficient was 0.64. Similarly, Chl-*a* concentrations positively

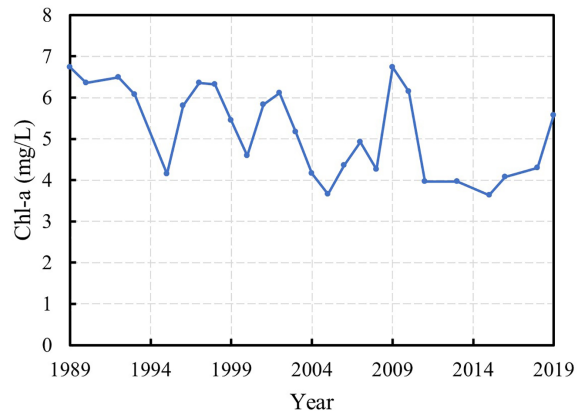

FIGURE 5
Changes of the mean Chl-*a* concentration in the PRE between 1989–2019.

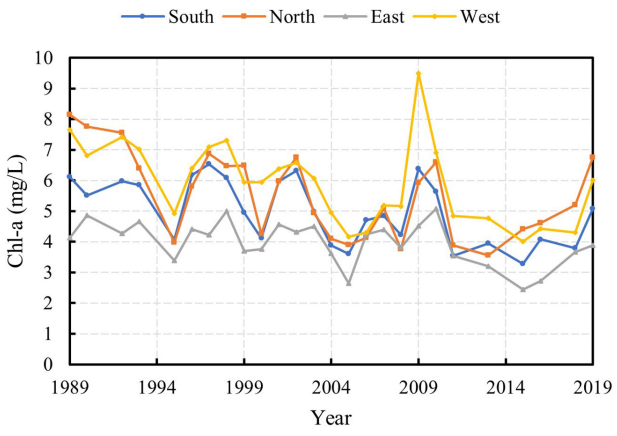

FIGURE 6
Seasonal Chl-*a* concentration changes in the PRE between 1989–2019.

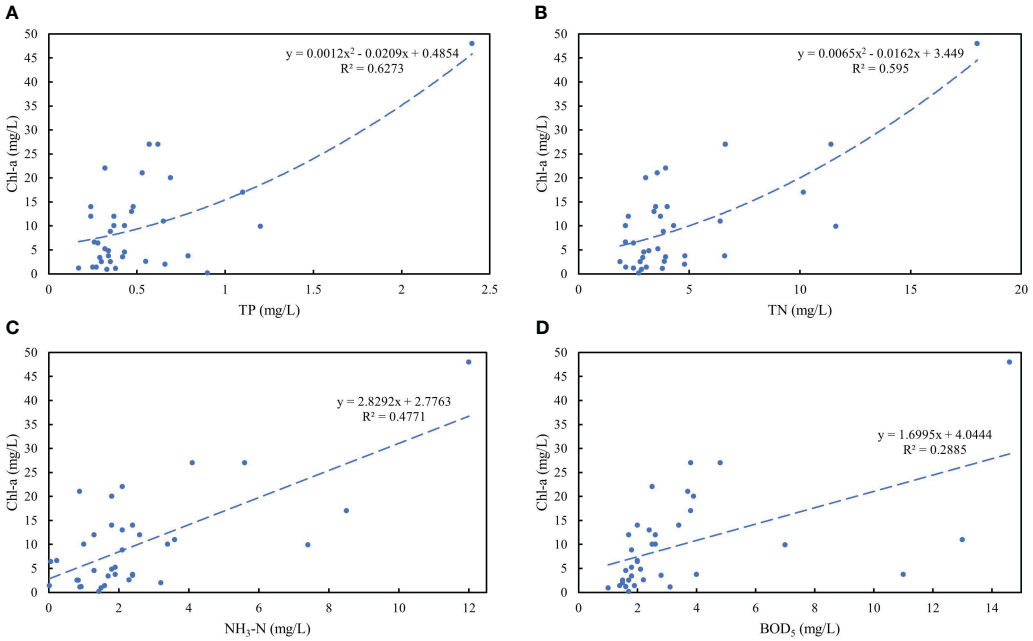

FIGURE 7
Relationship between Chl-a concentrations and water quality indicators: **(A)** TP; **(B)** TN; **(C)** NH_3-N; **(D)** BOD_5.

correlated with TN ($P< 0.05$), with a correlation coefficient of 0.71. Although TP and TN are important nutrients, they are often present in excessive amounts due to agricultural runoff and wastewater discharge. These nutrients can stimulate the growth of algae and aquatic plants, leading to increased Chl-*a* concentrations. Furthermore, Chl-*a* concentrations positively correlated with NH_3-N ($P< 0.05$), with a correlation coefficient of 0.69. High levels of NH_3-N can promote the growth of algae and aquatic plants, resulting in elevated Chl-*a* concentrations. Chl-*a* concentrations also positively correlated with BOD_5 ($P< 0.05$), with a correlation coefficient of 0.54. High Chl-*a* concentrations in water is generally indicative of increased algal growth. More algae will consume more oxygen, resulting in decreased DO levels and elevated BOD_5 in water. Therefore, a high Chl-*a* concentration is associated with elevated BOD_5 levels in water.

3.5 External driving factors

Suitable temperatures promote phytoplankton photosynthesis, resulting in increased phytoplankton biomass (Li et al., 2018). Between 1999–2008, Chl-*a* concentrations and temperatures in the northern section of the PRE significantly and positively correlated ($P< 0.05$), with a correlation coefficient of 0.51 (Figure 8A). Between 2009–2019, reduced rainfall in the vicinity of the PRE may have resulted in decreased nutrient absorption and a weakened water circulation, subsequently leading to an improvement in water quality. During this period, there was a significant positive correlation ($P< 0.05$) between Chl-*a* concentrations and rainfall in the northern section of the PRE, with a correlation coefficient of 0.43 (Figure 8B). Results from this study indicated that a reduction in rainfall would result in a decrease in nutrient flux into the PRE, subsequently enhancing its overall water quality. Additionally, Chl-*a* concentrations in the PRE exhibited a lag effect in response to climate factors (i.e., temperature and rainfall).

Due to oceanic currents, the industrial wastewater discharged from urban areas accumulates in the PRE, leading to changes in water quality (Li et al., 2020). Between 1989–2004, a positive correlation ($P< 0.05$) was observed between Chl-*a* concentrations in the northern section of the PRE and the volume of industrial wastewater discharged from coastal cities, with a correlation coefficient of 0.53 (Figure 9A). Both variables showed a consistent downward trend on a sweeping scale, while industrial wastewater discharge had a lag effect on Chl-*a* concentrations. Non-point source pollution from agriculture is widely recognized as one of the main causes of water quality degradation (Evans et al., 2019). A higher proportion of primary industries results in a greater increase in agricultural land area and fertilizer usage in urban areas. Since the beginning of China's economic reforms, the industrial structure of cities within the GBA has been optimized and adjusted, with a consecutive proportional decrease in primary industries. Between 1989–2019, there was a significant positive correlation ($P< 0.05$) between Chl-*a* concentrations in the northern section of the PRE and the proportion of primary industries in its coastal cities, with a correlation coefficient of 0.55 (Figure 9B). A general decrease in both variables was observed over the study period. Overall, the trend in PRE Chl-*a* concentrations is in decline, which may be attributed to a reduction in industrial wastewater discharge and a decrease in the proportion of primary industries in surrounding cities. In this study, PLS regression was constructed to assess how external driving factors influence Chl-*a* concentrations. The PLS

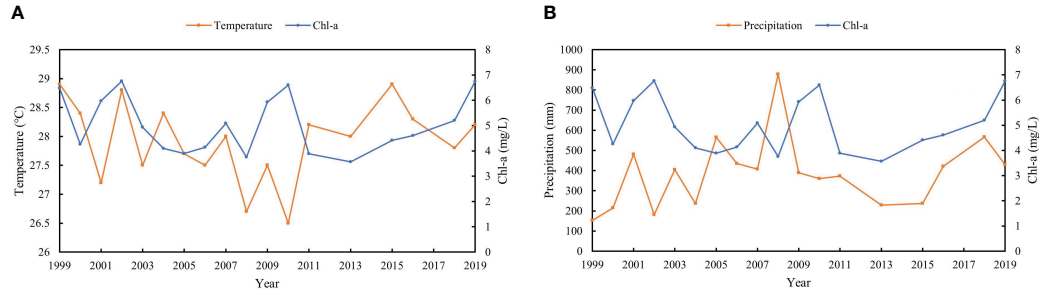

FIGURE 8
Correlation between Chl-*a* concentrations with **(A)** air temperature and **(B)** precipitation in the northern section of the PRE between 1999–2019.

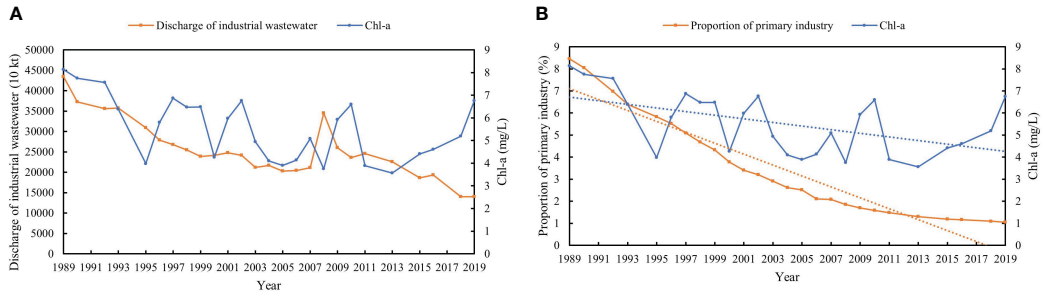

FIGURE 9
Correlation between Chl-*a* concentrations with **(A)** industrial wastewater discharge and **(B)** the proportion of primary industries in coastal cities of the PRE between 1989–2019.

factor weight and the loadings confirmed that all three PLS factors can effectively explain data variance while also demonstrating the good explanatory power of latent variables for observed variables. The contribution of the proportion of the primary industry factor within the three PLS factors was relatively high, indicating its important role in predicting Chl-*a* concentrations. From Table 1, it can be observed that temperature, rainfall, and the proportion of primary industries are commonly considered strong driving factors for changes in Chl-*a* concentrations (VIP > 1).

3.6 Implications and limitations

Regular collection and analysis of water samples while monitoring key water quality indicators (i.e., NH_3-N, TP, and Chl-*a* concentrations), are conducted. This aided in the establishment of a comprehensive water quality monitoring system, helped in the assessment of water quality conditions, and allowed for the prompt implementation of necessary management measures. Non-point source pollution from industrial and agricultural activities is one of the main causes for water quality degradation, so strengthening wastewater discharge management and improving the capacity and efficiency of wastewater treatment plants are critical. To address the poor water quality of the PRE's northern and western sections, the Government should strengthen supervision and reduce pollutant emissions. Measures should also be taken to reduce pollution, such as ecological restoration and wetland construction, subsequently enhancing its water purification capacities. Water quality is closely linked to factors such as temperature, rainfall, and other environmental conditions. Attention should also be paid to climate change impacts within the PRE region, while adaptive measures should be taken to address extreme weather events.

Because of its subtropical monsoon climate, the PRE region experiences a high frequency of cloud cover, and data gaps resulting from such frequent cloud cover events and the limited available samples present significant challenges for satellite monitoring. However, amassing field data and using other satellites (i.e., MODIS and Sentinel) to fill satellite-based data gaps may help to resolve this issue. Additionally, the PRE is an optically complex water system, and the potential to overestimate Chl-*a* concentrations under conditions of water turbidity should not be ignored. Therefore, it may not be appropriate to solely rely on band

TABLE 1 Variable Importance in Projection (VIP). A higher VIP value indicates that the variable has greater importance.

Variable	Latent Factors		
	1	2	3
Temperature	0.135	1.246	1.236
Precipitation	1.351	1.039	1.034
Wastewater discharge	0.893	0.910	0.925
Primary industry	1.166	1.071	1.075

ratio algorithms to estimate Chl-*a* concentrations in PRE water. It is necessary to consider other factors, such as seasonality and water characteristics, while establishing more complex retrieval models to analyze water quality changes in the PRE.

4 Conclusions

In this study, spatial and temporal Chl-*a* concentration variation was analyzed, showing distinct patterns across seasons and interannual fluctuations. Results showed a slight decreasing trend in PRE Chl-*a* concentrations over the study period. Compared to the other seasons, Chl-*a* concentrations were significantly higher in summer. The western section of the PRE consistently had higher Chl-*a* concentrations while the eastern section had lower concentrations. Correlation analysis between Chl-*a* concentrations and water quality indicators significantly correlated. Furthermore, external driving factors (i.e., climate and anthropogenic activities) influenced Chl-*a* concentration variation. Industrial wastewater discharge and the proportion of primary industries in coastal cities affected water quality, and results revealed a significant positive correlation. Findings from this study are intended to contribute to our understanding of Chl-*a* concentration dynamics in the PRE.

Data availability statement

The original contributions presented in the study are included in the article/supplementary material. Further inquiries can be directed to the corresponding author.

Author contributions

WF and ZX designed the research and drafted the manuscript. WF and QD collected and processed the data. WF and WC analyzed the data. YC reviewed the manuscript. All authors contributed to the article and approved the submitted version.

Funding

This study was financially supported by the Key Program of National Natural Science Foundation of China (No. 52239005), the Program for Guangdong Introducing Innovative and Entrepreneurial Teams (No. 2019ZT08L213), and the General Program of National Natural Science Foundation of China (No. 52279059).

Acknowledgments

The authors would like to acknowledge the support provided by the National Natural Science Foundation of China and the Program for Guangdong Introducing Innovative and Entrepreneurial Teams.

Conflict of interest

The authors declare that the research was conducted in the absence of any commercial or financial relationships that could be construed as a potential conflict of interest.

Publisher's note

References

Beck, R., Zhan, S., Liu, H., Tong, S., Yang, B., Xu, M., et al. (2016). Comparison of satellite reflectance algorithms for estimating chlorophyll-a in a temperate reservoir using coincident hyperspectral aircraft imagery and dense coincident surface observations. *Remote Sens. Environ.* 178, 15–30. doi: 10.1016/j.rse.2016.03.002

Burford, M. A., and Faggotter, S. J. (2021). Comparing the importance of freshwater flows driving primary production in three tropical estuaries. *Mar. pollut. Bull.* 169, 112565. doi: 10.1016/j.marpolbul.2021.112565

Cao, B., Qiu, J., Zhang, W., Xie, X., Lu, X., Yang, X., et al. (2022). Retrieval of suspended sediment concentrations in the pearl river estuary using multi-source satellite imagery. *Remote Sens.* 14 (16), 3896. doi: 10.3390/rs14163896

Cao, C., Zhu, K., Cai, F., Qi, H., Liu, J., Lei, G., et al. (2022). Vulnerability evolution of coastal erosion in the Pearl River estuary Great Bay area due to the influence of human activities in the past forty years. *Front. Mar. Sci.* 9. doi: 10.3389/fmars.2022.847655

Chawla, I., Karthikeyan, L., and Mishra, A. K. (2020). A review of remote sensing applications for water security: Quantity, quality, and extremes. *J. Hydrol.* 585, 124826. doi: 10.1016/j.jhydrol.2020.124826

Chen, S., Fang, L., Li, H., Chen, W., and Huang, W. (2011). Evaluation of a three-band model for estimating chlorophyll-a concentration in tidal reaches of the Pearl River Estuary, China. *ISPRS J. Photogrammet. Remote Sens.* 66 (3), 356–364. doi: 10.1016/j.isprsjprs.2011.01.004

Chen, X., Lee, R. M., Dwivedi, D., Son, K., Fang, Y., Zhang, X., et al. (2021). Integrating field observations and process-based modeling to predict watershed water quality under environmental perturbations. *J. Hydrol.* 602, 125762. doi: 10.1016/j.jhydrol.2020.125762

Chen, Z., Li, Y., and Pan, J. (2004). Distributions of colored dissolved organic matter and dissolved organic carbon in the Pearl River Estuary, China. *Continental Shelf Res.* 24 (16), 1845–1856. doi: 10.1016/j.csr.2004.06.011

Conley, D. J., Paerl, H. W., Howarth, R. W., Boesch, D. F., Seitzinger, S. P., Havens, K. E., et al. (2009). Controlling eutrophication: nitrogen and phosphorus. *Science* 323 (5917), 1014–1015. doi: 10.1126/science.1167755

D'Ortenzio, F., Marullo, S., Ragni, M., d'Alcalà, M. R., and Santoleri, R. (2002). Validation of empirical SeaWiFS algorithms for chlorophyll-a retrieval in the Mediterranean Sea: A case study for oligotrophic seas. *Remote Sens. Environ.* 82 (1), 79–94. doi: 10.1016/S0034-4257(02)00026-3

Ding, J., Jiang, Y., Fu, L., Liu, Q., Peng, Q., and Kang, M. (2015). Impacts of land use on surface water quality in a subtropical River Basin: a case study of the Dongjiang River Basin, Southeastern China. *Water* 7 (8), 4427–4445. doi: 10.3390/w7084427

Durack, P. J. (2015). Ocean salinity and the global water cycle. *Oceanography* 28 (1), 20–31. doi: 10.5670/oceanog.2015.03

Evans, A. E., Mateo-Sagasta, J., Qadir, M., Boelee, E., and Ippolito, A. (2019). Agricultural water pollution: key knowledge gaps and research needs. *Curr. Opin. Environ. sustainability* 36, 20–27. doi: 10.1016/j.cosust.2018.10.003

Gao, N., Ma, Y., Zhao, M., Zhang, L., Zhan, H., Cai, S., et al. (2020). Quantile analysis of long-term trends of near-surface chlorophyll-a in the Pearl River plume. *Water* 12 (6), 1662. doi: 10.3390/w12061662

Gholizadeh, M. H., Melesse, A. M., and Reddi, L. (2016). A comprehensive review on water quality parameters estimation using remote sensing techniques. *Sensors* 16 (8), 1298. doi: 10.3390/s16081298

Gilerson, A. A., Gitelson, A. A., Zhou, J., Gurlin, D., Moses, W., Ioannou, I., et al. (2010). Algorithms for remote estimation of chlorophyll-a in coastal and inland waters using red and near infrared bands. *Optics Express* 18 (23), 24109–24125. doi: 10.1364/OE.18.024109

Guo, Y., Deng, R., Li, J., Hua, Z., Wang, J., Zhang, R., et al. (2022). Remote sensing retrieval of total nitrogen in the pearl river delta based on landsat8. *Water* 14 (22), 3710. doi: 10.3390/w14223710

Guo, L., Xiu, P., Chai, F., Xue, H., Wang, D., and Sun, J. (2017). Enhanced chlorophyll concentrations induced by Kuroshio intrusion fronts in the northern South China Sea. *Geophys. Res. Lett.* 44 (22), 11–565. doi: 10.1002/2017GL075336

Huang, X. P., Huang, L. M., and Yue, W. Z. (2003). The characteristics of nutrients and eutrophication in the Pearl River estuary, South China. *Mar. pollut. Bull.* 47 (1-6), 30–36. doi: 10.1016/S0025-326X(02)00474-5

Ioannou, I., Gilerson, A., Gross, B., Moshary, F., and Ahmed, S. (2013). Deriving ocean color products using neural networks. *Remote Sens. Environ.* 134, 78–91. doi: 10.1016/j.rse.2013.02.015

Jay, S., Maupas, F., Bendoula, R., and Gorretta, N. (2017). Retrieving LAI, chlorophyll and nitrogen contents in sugar beet crops from multi-angular optical remote sensing: Comparison of vegetation indices and PROSAIL inversion for field phenotyping. *Field Crops Res.* 210, 33–46. doi: 10.1016/j.fcr.2017.05.005

Jeffries, T. C., Schmitz Fontes, M. L., Harrison, D. P., Van-Dongen-Vogels, V., Eyre, B. D., Ralph, P. J., et al. (2016). Bacterioplankton dynamics within a large anthropogenically impacted urban estuary. *Front. Microbiol.* 6. doi: 10.3389/fmicb.2015.01438

Jiang, Z., Liu, J., Chen, J., Chen, Q., Yan, X., Xuan, J., et al. (2014). Responses of summer phytoplankton community to drastic environmental changes in the Changjiang (Yangtze River) estuary during the past 50 years. *Water Res.* 54, 1–11. doi: 10.1016/j.watres.2014.01.032

Kim, Y. H., Son, S., Kim, H. C., Kim, B., Park, Y. G., Nam, J., et al. (2020). Application of satellite remote sensing in monitoring dissolved oxygen variabilities: A case study for coastal waters in Korea. *Environ. Int.* 134, 105301. doi: 10.1016/j.envint.2019.105301

Lao, Q., Liu, S., Ling, Z., Jin, G., Chen, F., Chen, C., et al. (2023). External dynamic mechanisms controlling the periodic offshore blooms in Beibu Gulf. *J. Geophys. Res.: Oceans*. 128(6), e2023JC019689. doi: 10.1029/2023JC019689

Lao, Q., Zhang, S., Li, Z., Chen, F., Zhou, X., Jin, G., et al. (2022). Quantification of the seasonal intrusion of water masses and their impact on nutrients in the Beibu Gulf using dual water isotopes. *J. Geophys. Res.: Oceans* 127 (7), e2021JC018065. doi: 10.1029/2021JC018065

Li, D., Gan, J., Hui, R., Liu, Z., Yu, L., Lu, Z., et al. (2020). Vortex and biogeochemical dynamics for the hypoxia formation within the coastal transition zone off the Pearl River Estuary. *J. Geophys. Res.: Oceans* 125 (8), e2020JC016178. doi: 10.1029/2020JC016178

Li, Y., Wang, H., Deng, Y., Liang, D., Li, Y., and Shen, Z. (2022). How climate change and land-use evolution relates to the non-point source pollution in a typical watershed of China. *Sci. Total Environ.* 839, 156375. doi: 10.1016/j.scitotenv.2022.156375

Li, Y., Zhang, Y., Shi, K., Zhou, Y., Zhang, Y., Liu, X., et al. (2018). Spatiotemporal dynamics of chlorophyll-a in a large reservoir as derived from Landsat 8 OLI data: understanding its driving and restrictive factors. *Environ. Sci. pollut. Res.* 25, 1359–1374. doi: 10.1007/s11356-017-0536-7

Liang, B., Xiu, P., Hu, J., and Li, S. (2021). Seasonal and spatial controls on the eutrophication-induced acidification in the Pearl River Estuary. *J. Geophys. Res.: Oceans* 126 (5), e2020JC017107. doi: 10.1029/2020JC017107

Liu, S., Fu, R., Liu, Y., and Suo, C. (2022). Spatiotemporal variations of water quality and their driving forces in the Yangtze River Basin, China, from 2008 to 2020 based on multi-statistical analyses. *Environ. Sci. pollut. Res.* 29 (46), 69388–69401. doi: 10.1007/s11356-022-20667-3

Liu, D., Fu, D., Xu, B., and Shen, C. (2012). Estimation of total suspended matter in the Zhujiang (Pearl) River estuary from Hyperion imagery. *Chin. J. Oceanol. Limnol.* 30 (1), 16–21. doi: 10.1007/s00343-012-0148-5

Liu, D., Pan, D., Bai, Y., He, X., Wang, D., Wei, J. A., et al. (2015). Remote sensing observation of particulate organic carbon in the Pearl River Estuary. *Remote Sens.* 7 (7), 8683–8704. doi: 10.3390/rs70708683

Liu, F., and Tang, S. (2019). Evaluation of red-peak algorithms for chlorophyll measurement in the Pearl River Estuary. *IEEE Trans. Geosci. Remote Sens.* 57 (11), 8928–8936. doi: 10.1109/TGRS.2019.2923754

Lu, S., Deng, R., Liang, Y., Xiong, L., Ai, X., and Qin, Y. (2020). Remote sensing retrieval of total phosphorus in the pearl river channels based on the GF-1 remote sensing data. *Remote Sens.* 12 (9), 1420. doi: 10.3390/rs12091420

Lu, Z., and Gan, J. (2015). Controls of seasonal variability of phytoplankton blooms in the Pearl River Estuary. *Deep Sea Res. Part II: Topical Stud. Oceanog.* 117, 86–96. doi: 10.1016/j.dsr2.2013.12.011

Ma, C., Zhao, J., Ai, B., Sun, S., and Yang, Z. (2022). Machine learning based long-term water quality in the turbid pearl river estuary, China. *J. Geophys. Res.: Oceans* 127 (1), e2021JC018017. doi: 10.1029/2021JC018017

Montefiore, L. R., Nelson, N. G., Staudinger, M. D., and Terando, A. (2023). Vulnerability of estuarine systems in the contiguous United States to water quality change under future climate and land-use. *Earth's Future* 11 (3), e2022EF002884. doi: 10.1029/2022EF002884

Moradi, M., and Kabiri, K. (2015). Spatio-temporal variability of SST and Chlorophyll-a from MODIS data in the Persian Gulf. *Mar. pollut. Bull.* 98 (1-2), 14–25. doi: 10.1016/j.marpolbul.2015.07.018

Mutanga, O., and Kumar, L. (2019). Google earth engine applications. *Remote Sens.* 11 (5), 591. doi: 10.3390/rs11050591

O'Reilly, J. E., Maritorena, S., Mitchell, B. G., Siegel, D. A., Carder, K. L., Garver, S. A., et al. (1998). Ocean color chlorophyll algorithms for SeaWiFS. *J. Geophys. Res.: Oceans* 103 (C11), 24937–24953. doi: 10.1029/98JC02160

O'Reilly, J. E., and Werdell, P. J. (2019). Chlorophyll algorithms for ocean color sensors-OC4, OC5 & OC6. *Remote Sens. Environ.* 229, 32–47. doi: 10.1016/j.rse.2019.04.021

Paerl, H. W., and Huisman, J. (2009). Climate change: a catalyst for global expansion of harmful cyanobacterial blooms. *Environ. Microbiol. Rep.* 1 (1), 27–37. doi: 10.1111/j.1758-2229.2008.00004.x

Pan, Y., Tang, D., and Weng, D. (2010). Evaluation of the SeaWiFS and MODIS chlorophyll a algorithms used for the Northern South China Sea during the summer season. *TAO: Terrestrial Atmospheric Oceanic Sci.* 21 (6), 9. doi: 10.3319/TAO.2010.02.11.01(Oc

Qiu, D., Huang, L., Zhang, J., and Lin, S. (2010). Phytoplankton dynamics in and near the highly eutrophic Pearl River Estuary, South China Sea. *Continental Shelf Res.* 30 (2), 177–186. doi: 10.1016/j.csr.2009.10.015

Ross, M. R., Topp, S. N., Appling, A. P., Yang, X., Kuhn, C., Butman, D., et al. (2019). AquaSat: A data set to enable remote sensing of water quality for inland waters. *Water Resour. Res.* 55 (11), 10012–10025. doi: 10.1029/2019WR024883

Scanes, E., Scanes, P. R., and Ross, P. M. (2020). Climate change rapidly warms and acidifies Australian estuaries. *Nat. Commun.* 11 (1), 1803. doi: 10.1038/s41467-020-15550-z

Shen, Y., Zhang, H., and Tang, J. (2022). Hydrodynamics and water quality impacts of large-scale reclamation projects in the Pearl River Estuary. *Ocean Eng.* 257, 111432. doi: 10.1016/j.oceaneng.2022.111432

Shrestha, S., Bhatta, B., Shrestha, M., and Shrestha, P. K. (2018). Integrated assessment of the climate and landuse change impact on hydrology and water quality in the Songkhram River Basin, Thailand. *Sci. Total Environ.* 643, 1610–1622. doi: 10.1016/j.scitotenv.2018.06.306

Sigman, D. M., and Hain, M. P. (2012). The biological productivity of the ocean. *Nat. Educ. Knowledge* 3 (10), 21. Available at: https://www.nature.com/scitable/knowledge/

Tao, W., Niu, L., Dong, Y., Fu, T., and Lou, Q. (2021). Nutrient pollution and its dynamic source-sink pattern in the pearl river estuary (South China). *Front. Mar. Sci.* 8. doi: 10.3389/fmars.2021.713907

Tao, W., Niu, L., Liu, F., Cai, H., Ou, S., Zeng, D., et al. (2020). Influence of river-tide dynamics on phytoplankton variability and their ecological implications in two Chinese tropical estuaries. *Ecol. Indic.* 115, 106458. doi: 10.1016/j.ecolind.2020.106458

Testa, J. M., Murphy, R. R., Brady, D. C., and Kemp, W. M. (2018). Nutrient-and climate-induced shifts in the phenology of linked biogeochemical cycles in a temperate estuary. *Front. Mar. Sci.* 5. doi: 10.3389/fmars.2018.00114

Tong, Y., Feng, L., Zhao, D., Xu, W., and Zheng, C. (2022). Remote sensing of chlorophyll-a concentrations in coastal oceans of the Greater Bay Area in China: Algorithm development and long-term changes. *Int. J. Appl. Earth Observat. Geoinformat.* 112, 102922. doi: 10.1016/j.jag.2022.102922

Wang, C., Li, W., Chen, S., Li, D., Wang, D., and Liu, J. (2018). The spatial and temporal variation of total suspended solid concentration in Pearl River Estuary during 1987–2015 based on remote sensing. *Sci. Total Environ.* 618, 1125–1138. doi: 10.1016/j.scitotenv.2017.09.196

Wang, M. X., Liang, L. N., Siu, W. S., Fan, D., Sun, H. R., Zhao, H. H., et al. (2019). Loss accounting of environmental pollution within Pearl River Delta region, South China. *Environ. pollut.* 249, 676–685. doi: 10.1016/j.envpol.2019.03.081

Wang, B., Xin, M., Wei, Q., and Xie, L. (2018). A historical overview of coastal eutrophication in the China Seas. *Mar. pollut. Bull.* 136, 394–400. doi: 10.1016/j.marpolbul.2018.09.044

Wang, J., Zhang, Y., Yang, F., Cao, X., Bai, Z., Zhu, J., et al. (2015). Spatial and temporal variations of chlorophyll-a concentration from 2009 to 2012 in Poyang Lake, China. *Environ. Earth Sci.* 73, 4063–4075. doi: 10.1007/s12665-014-3691-x

Wu, C. S., Yang, S., Huang, S., and Mu, J. (2016). Delta changes in the Pearl River estuary and its response to human activities, (1954–2008). *Quaternary Int.* 392, 147–154. doi: 10.1016/j.quaint.2015.04.009

Wurtsbaugh, W. A., Paerl, H. W., and Dodds, W. K. (2019). Nutrients, eutrophication and harmful algal blooms along the freshwater to marine continuum. *Wiley Interdiscip. Reviews: Water* 6 (5), e1373. doi: 10.1002/wat2.1373

Xu, S., Liu, Y., Fan, J., Xiao, Y., Qi, Z., and Lakshmikandan, M. (2022). Impact of salinity variation and silicate distribution on phytoplankton community composition in Pearl River estuary, China. *Ecohydrol. Hydrobiol.* 22 (3), 466–475. doi: 10.1016/j.ecohyd.2022.01.004

Ye, F., Guo, W., Shi, Z., Jia, G., and Wei, G. (2017). Seasonal dynamics of particulate organic matter and its response to flooding in the P earl River Estuary, China, revealed by stable isotope (δ13 C and δ15 N) analyses. *J. Geophys. Res.: Oceans* 122 (8), 6835–6856. doi: 10.1002/2017JC012931

Ye, F., Jia, G., Xie, L., Wei, G., and Xu, J. (2016). Isotope constraints on seasonal dynamics of dissolved and particulate N in the P earl R iver E stuary, south China. *J. Geophys. Res.: Oceans* 121 (12), 8689–8705. doi: 10.1002/2016JC012066

Ye, H., Tang, S., and Yang, C. (2021). Deep learning for Chlorophyll-a concentration retrieval: A case study for the Pearl River Estuary. *Remote Sens.* 13 (18), 3717. doi: 10.3390/rs13183717

Yuan, X., Wang, S., Fan, F., Dong, Y., Li, Y., Lin, W., et al. (2022). Spatiotemporal dynamics and anthropologically dominated drivers of chlorophyll-a, TN and TP concentrations in the Pearl River Estuary based on retrieval algorithm and random forest regression. *Environ. Res.* 215, 114380. doi: 10.1016/j.envres.2022.114380

Zhang, G., Cheng, W., Chen, L., Zhang, H., and Gong, W. (2019). Transport of riverine sediment from different outlets in the Pearl River Estuary during the wet season. *Mar. Geol.* 415, 105957. doi: 10.1016/j.margeo.2019.06.002

Zhang, X., Shi, Z., Liu, Q., Ye, F., Tian, L., and Huang, X. (2013). Spatial and temporal variations of picoplankton in three contrasting periods in the Pearl River Estuary, South China. *Continental Shelf Res.* 56, 1–12. doi: 10.1016/j.csr.2013.01.015

Zheng, G., and DiGiacomo, P. M. (2017). Remote sensing of chlorophyll-a in coastal waters based on the light absorption coefficient of phytoplankton. *Remote Sens. Environ.* 201, 331–341. doi: 10.1016/j.rse.2017.09.008

Zhou, Y., Shan, Y., Liu, G., and Guan, D. (2018). Emissions and low-carbon development in Guangdong-Hong Kong-Macao Greater Bay Area cities and their surroundings. *Appl. Energy* 228, 1683–1692. doi: 10.1016/j.apenergy.2018.07.038

frontiers | Frontiers in Marine Science

TYPE Original Research
PUBLISHED 22 August 2023
DOI 10.3389/fmars.2023.1231928

OPEN ACCESS

EDITED BY
Laibin Huang,
University of California, Davis, United States

REVIEWED BY
Peng Zhao,
Hainan University, China
Guan Bo,
Ludong University, China
Wen Xing Long,
Hainan University, China
Jiang Bao Xia,
Binzhou University, China

*CORRESPONDENCE
Banghua Cao
caobanghua@126.com

†These authors have contributed equally to this work and share first authorship

RECEIVED 31 May 2023
ACCEPTED 08 August 2023
PUBLISHED 22 August 2023

CITATION
Mao P, Lin Q, Pang Y, Wang K, Ni R, Han X and Cao B (2023) Eco-physiological response mechanism of *Tamarix chinensis* to soil water changes in coastal wetlands of the Yellow River Delta. *Front. Mar. Sci.* 10:1231928. doi: 10.3389/fmars.2023.1231928

Eco-physiological response mechanism of *Tamarix chinensis* to soil water changes in coastal wetlands of the Yellow River Delta

Peili Mao†, Qingzhi Lin†, Yuanxiang Pang†, Kexin Wang, Ruiqiang Ni, Xin Han and Banghua Cao*

State Forestry and Grassland Administration Key Laboratory of Silviculture in downstream areas of the Yellow River, Shandong Agricultural University, Tai'an, China

Elucidating the effect of soil moisture on the adaptation of dominant plants in coastal wetlands is important for predicting the evolution of vegetation in the region. In this paper, *Tamarix chinensis*, a dominant species in the Yellow River Delta, was used as the object to study the changes of its growth and physiological parameters with increasing soil salinity under different moisture conditions (normal watering, persistent drought and persistent waterlogging). Different salt stress (2‰, 5‰, 8‰, 12‰, 16‰, and 20‰) using pot experiments was also used to reveal the mechanism of soil moisture on its salt tolerance. The results showed that the relative growth rate between 5‰-8‰ soil salinity was the largest, and growth was significantly inhibited above 20‰. Among different moisture conditions, the difference in relative growth rate under normal watering and persistent drought were nonsignificant, while both were significantly lower than those under persistent waterlogging. With increasing soil salinity, relative water content and total chlorophyll content significantly decreased, and cell membrane permeability (malondialdehyde), sodium ion, osmoregulatory substances (proline, soluble protein), and protective enzyme activity (SOD) significantly increased, while changes in non-structural carbohydrates (NSC) were not significant. Compared with normal watering and persistent waterlogging, persistent drought had the lowest leaf relative water content, total chlorophyll content, and sodium ions, and the highest cell membrane permeability, osmoregulatory substances and protective enzyme activity. With increasing treatment time, the relative leaf water content and total chlorophyll content significantly decreased, and cell membrane permeability, osmoregulatory substances and protective enzyme activity increased more significantly than normal watering and persistent waterlogging. NSC increased under normal watering and persistent waterlogging, while significantly decreased under persistent drought. Correlation analysis showed that the relationships between sodium ions, total chlorophyll content and malondialdehyde were various under different moisture conditions. Under persistent drough, malondialdehyde was significantly positively correlated with relative conductivity, superoxide dismutase, proline, soluble protein and soluble sugar. Total chlorophyll content was the key indicator reflecting the salt and waterlogging tolerance of *T. chinensis* under normal watering and persistent

waterlogging, while cell membrane damage was under persistent drought. In summary, *T. chinensis* has strong salt and waterlogging tolerance, but persistent drought with salt stress can have serious impacts on its growth and survival.

KEYWORDS

dominant species, relative growth rate, chlorophyll, malondialdehyde, nonstructural carbohydrates

1 Introduction

Along with the frequent occurrence of extreme climate events from global warming, the increase in temperature leads to more evaporation of water and exacerbates drought in wetlands (Middleton and Kleinebecker, 2012). Water availability and variability will have a significant impact on the evolution of global vegetation (Smith and Boers, 2023). Climate warming has increased the probability of coastal flooding by melting iceberg and permafrost, and thus rising sea levels (Taherkhani et al., 2020), which severely impact on coastal wetland ecosystems (Schuerch et al., 2018). Jiang et al. (2013) found that climate features play a dominant role in seasonal variation in vegetation cover in the coastal wetland. Lu et al. (2016) reported that the increasing in annual average temperature, annual precipitation, and humidity index of the Yellow River Delta from 1986 to 2005 led to a significant decrease in river runoff and reduced the water supply to the marshes. The inflow of freshwater has a significant impact on the water-salt status of coastal wetlands, which in turn affects the plant community and vegetation dynamics (Cui et al., 2009). Therefore, it is important to reveal the adaptation of plants to water and salt changes to predict the dynamic of vegetation in the coastal wetland (Sun et al., 2022).

Climate change is predicted to lead soil moisture and salinity particularly in the coastal regions through sea level rise and salt water intrusion (Rahmstorf, 2007; Dasgupta et al., 2009). Soil moisture has an important influence on the adaptation of plants in coastal saline lands (Souid et al., 2018). During the rainy season in this region, soil water content increases and soil salinity decreases, but in the dry season the changes are reversed (Souid et al., 2018; Guo et al., 2021). Studies on the halophyte *Limonium delicatulum* have found that the salt ion content and protective enzyme activity in its aboveground parts were significantly higher in the dry season than in the rainy season (Souid et al., 2018), and osmoregulatory substances had similar changes (Maaloul et al., 2021). Severe drought can cause extensive vegetation mortality in coastal wetlands (Watson et al., 2016; Liu et al., 2020a). In a restoration of vegetation in an estuarine wetland of the Liao River in China, it was found that *Suaeda salsa* mortality significantly increased during the dry season, which was closely related to the synergistic effects of drought and high salinity (Liu et al., 2020b). Seedling height and seedling biomass of *S. salsa* increased under light salt and drought co-stress treatments, but significantly decreased under heavy salt and drought stress, much more severely than single salt stress (Jia et al., 2018). Waterlogging is one of the key factors determining the distribution of vegetation in coastal wetlands (Hou et al., 2020). Flooding significantly reduced the biomass of the halophyte *Triglochin maritima* and *Argentina pacifica*, and the aboveground biomass of *Carex lyngbyei* and *A. pacifica* was significantly affected by a combination of salt and flooding (Buffington et al., 2020). In the Yellow River Delta, the growth of *Phragmites australis* (Guan et al., 2017) and *S. salsa* (Guan et al., 2011) has also been inhibited by flooding. Smith and Lee (2015) found that prolonged flooding for a few months can eradicate *Spartina alterniflora*. Thus, salinity and waterlogging are key factors in determining distribution of vegetation in coastal wetlands (Hou et al., 2020).

The growth and development of plants were inhibited under salt stress. With increasing salt concentration, Na^+ accumulation caused a decrease in chlorophyll content and decomposition (Borzouei et al., 2020; Irshad et al., 2021; Mushtaq et al., 2021), leading to a decrease in photosynthetic capacity (Muchate et al., 2016). Salt stress leads to the accumulation of reactive oxygen in plants, and the excess of reactive oxygen peroxidizes cell membrane lipids, disrupting the intra-membrane environment and affecting all physiological metabolism (Nxele et al., 2017; Kiarash et al., 2020). Excessive salinity in the soil makes the soil water potential usually lower than the plant cells, and plants have difficulty in water uptake and water retention reduction (Mao et al., 2016; Nxele et al., 2017). Salt stress increases Na^+ content in plants, inhibiting the uptake and transport of nutrients such as Ca^{2+} and K^+ and disrupting ionic balance (Muchate et al., 2016). Osmoregulation and antioxidant regulation are important mechanisms by which plants adapt to salt stress (Rangani et al., 2018). Under salt stress, osmoregulatory substances significantly increase, reducing the osmotic potential and increasing the ability to absorb water (Benjamin et al., 2019; Borzouei et al., 2020). These nitrogenous compounds significantly enhance the antioxidant effect of plants as well as acting as osmoregulatory substances (Khoshbakht et al., 2018; Arbelet-Bonnin et al., 2020). To avoid cell membrane damage resulting from the massive accumulation of reactive oxygen under salt stress, plants synthesize and accumulate antioxidant enzymes and antioxidants to protect cell membranes (Muchate et al., 2016; Irshad et al., 2021; Mushtaq et al., 2021). However, at high salt concentrations, osmoregulatory substances such as soluble sugars, soluble proteins, and proline content are significantly reduced, and

osmoregulatory capacity is significantly reduced (Ghaderi et al., 2018; Mushtaq et al., 2021), and protective enzyme activity is also reduced (Ghaderi et al., 2018).

Non-structural carbohydrates (NSC) are substrates for plant growth and metabolism, consist mainly of soluble sugars and starch (Hoch et al., 2003). NSC are products of photosynthesis, a temporary storage material between photosynthesis and utilization. When photosynthesis is insufficient, plants consume NSC to provide energy (O'Brien et al., 2014). NSC also has important roles in osmoregulation and defense against diseases and insects under stressful conditions (Sala et al., 2012; Dietze et al., 2014). Soluble sugars are an important osmoregulatory substance and provide direct available substrates and energy for physiological activities such as plant growth and respiration (Hartmann and Trumbore, 2016), while starch is stably stored in organs as a storage carbon source (Macneill et al., 2017). It was found that plants actively increase the concentration of nonstructural carbohydrates in their bodies under adversity (Gao et al., 2021). When plants are subjected to stress condition, starch and sugar can be converted to each other in response to the external environment (Kozlowski, 1992; da Silva et al., 2019). Under stress, the consumption of photosynthesis, respiration, and osmoregulation in plants determines the amount of NSC (Guo et al., 2020). A comparative study revealed that plant NSC changes under drought stress and salt stress are not the same (Cui et al., 2019). And how water conditions affect the accumulation of NSC under salt stress is still not clear.

The Yellow River Delta is the most extensive and youngest coastal wetland in the primary stage of succession in the temperate zone of China (Cong et al., 2019). Previous study (Li et al., 2019) has shown that soil salinity as a key environmental factor direactly and hydrological factors by altering soil salinity indirectly affect the spatial differentiation pattern of plant communities. *T. chinensis*, one of the dominant species in this area, is mainly distributed in supratidal wetlands on higher terrain or far from the sea and inland saline areas generally below 4 m in elevation, which are characterized by seasonal waterlogging and heavy salinization. Seasonal waterlogging occurs in summer, when a shallow water is connected to surface waterlogging, creating a highly saline and waterlogged environment. In spring, late autumn, and winter, precipitation is often scarce, and *T. chinensis* faces the combined effects of salinity and drought. Moisture and salinity are key factors affecting the growth of *T. chinensis* forests in this region, leading to low quality and inefficiency of the stands (Xia et al., 2013). Current studies on *T. chinensis* mainly focused on soil nutrient characteristics at the community level (Yang et al., 2021), distribution patterns at the population level (Jiao et al., 2021), and physiological and biochemical characteristics under salt and drought stress conditions (Liu et al., 2014). Also, the effects of soil moisture (Gao et al., 2017) and groundwater level (Xia et al., 2017) on the photosynthetic physiology of *T. chinensis* had been systematically studied. However, studies on the effect of soil moisture on the salt acclimation of *T. chinensis* are still insufficient. Precipitation in the Yellow River Delta gradually increased in recent decades (Lu et al., 2016). Thus, the study on physiological and ecological responses of *T. chinensis* seedlings under different soil salinity and soil moisture conditions (normal watering, persistent drought and persistent waterlogging) using pot experiments will contribute to systematically reveal the mechanisms of moisture conditions on its salt acclimatization. The aim is to provide theoretical and technical support for vegetation restoration and ecological construction in coastal wetland ecosystems.

2 Materials and methods

2.1 Study area

The study was conducted in Dongying City (36°55′~38°10′ N, 118°07′~119°10′ E) in the Yellow River Delta of China. It has a warm temperate monsoon continental climate, where the annual average temperature is 12.3°C, the annual average frost-free period is 210 d, and the annual average precipitation is 559 mm, 70% of which is distributed in summer. Due to the influence of the Yellow River flooding sediment, the soil is mainly coastal tidal salt soil, the soil salt content is high, depending on the salt content of the growth of various types of salt vegetation. The main vegetation types in this area are scrub and saline meadows, and the common ones are *S. salsa*, *Miscanthus sacchariflorus*, *P. australis*, *T. chinensis*.

2.2 Experimental design

The experiment was conducted in the greenhouse of Shengda Eco-Forestry, Shengda Branch of Shengli Oilfield (37°20'53" N, 118° 37'10" E), which is located in Hekou District, Dongying City, Shandong Province (Figure 1). The soil in the forest farm has a salinity of about 2‰, a soil pH of 8.21, a total nitrogen content of 0.54 g/kg, a hydrolytic nitrogen content of 50.79 mg/kg, an effective phosphorus content of 4.42 mg/kg, a fast-acting potassium content

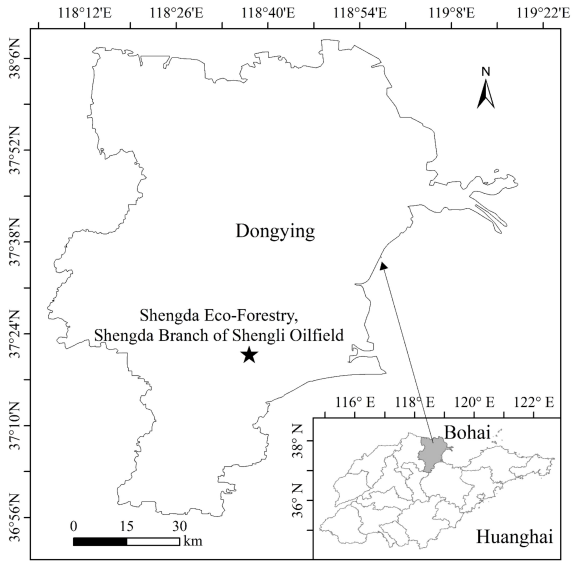

FIGURE 1
Geographical location of the study area and experiment site (Shengda Eco-Forestry, Shengda Branch of Shengli Oilfield).

of 140.55 mg/kg, and organic matter content of 10.58 g/kg. The soil from this forest farm was used for potted test of *T. chinensis* seedlings. The *T. chinensis* seedlings used for the pot test were annual cuttings with an average height of 20 cm and an average ground diameter of 15 mm. The cuttings were transplanted into 15.5 cm × 22.8 cm × 19 cm (bottom diameter × diameter × height) pots on April 30, 2021, and one plant individual in each pot.

After transplanting, the *T. chinensis* annual cuttings were placed in a refinement shed for growth, during which regular watering and weeding were carried out. Seedlings of uniform growth were selected for the experiment on June 19th, and the soil salinity (soil salinity/soil dry weight) was controlled by configuring different concentration gradients of NaCl solution in multiple waterings, with salt concentrations of 5‰, 8‰, 12‰, 16‰, and 20‰, and the soil salinity of 2‰ in the woodland was used as the control. The bottom of the pots were equipped with trays. To prevent salt loss, the leaking water from the trays was poured back into the pots and the trays were cleaned, and the cleaning water was also poured into the pots. The whole experiment was divided into three groups based on water treatment, each group including two factors of salinity and treatment time, and arranged in a randomized group design with 15 replicates for each treatment. The soil salinity in the pots reached the design level on 0d. The three moisture treatments on the same day were normal watering, persistent drought and persistent waterlogging.

Normal watering test: the normal watering amount was 80% of the soil field water holding capacity, using the weighing method and regular water supplementation. Mature leaves of *T. chinensis* with the same growing parts and normal growth were collected at 1d, 11d, 21d and 31d, respectively, for index determination. The normal watering lasted for 31 days.

Persistent waterlogging test: the double set pot method was used so that the bottom of the pots did not leak and watered heavily until the level was parallel with the sides of the pots, after which water was replenished daily. Similar to the normal watering experiment, mature leaves with the same growth site and normal growth were collected on days 1, 11, 21, and 31 for indicator measurement. The persistent waterlogging test lasted for 31 days.

Persistent drought test: watering was done by small and repeated watering until the water seeped out from the bottom of the pot, and then no watering was needed. Leaves were collected at 1d, 11d, and 21d of stress and soil was taken at 10 cm from the bottom of the pot using the perforation method to determine the water and salinity content of the soil. Due to the death of all the aboveground parts of *T. chinensis* on the 31st day, no sampling was conducted. The average soil moisture content was 13.21%, 9.49%, and 3.77% on days 1, 11, and 21, respectively. The soil moisture content gradually decreases with the duration of stress, and the soil salt content gradually increased (Table 1). The persistent drought test lasted for 21 days.

TABLE 1 Variation of soil salt content under persistent drought (‰).

Salt content (‰)	1 d	11 d	21 d
2	2.89	3.67	4.67
5	5.93	7.28	7.28
8	8.55	9.36	9.36
12	12.9	14.32	15.32
16	17.1	17.67	18.93
20	20.88	22.38	23.72

At the beginning and end of the test, the height and ground diameter of *T. chinensis* seedlings were measured, the seedling height was measured using a meter ruler, and the ground diameter was measured using a vernier caliper. At the end of the experiments, all seedlings were dug out and the whole root system was obtained, and the root system was slowly rinsed with running water. The above-ground parts and roots were placed in an oven at 75°C for 48 h and then weighed for dry weight using a one-thousandth electronic balance.

2.3 Indicator measurement and methods

2.3.1 Soil indicators

Soil moisture content (SMC, %) was measured by the drying method; soil salt content (SSC, ‰) was determined using the conductivity method, and the standard curve of soil salt concentration was measured using the drying residue method and the conductivity meter.

2.3.2 Leaf physiological indicators

Total chlorophyll content (Chl, mg/g) was determined by acetone extraction; leaf cell membrane permeability was determined by relative conductivity (RC, %) method; Malondialdehyde (MDA, μmol/g) content was determined by the thiobarbituric acid method; superoxide dismutase (SOD, U/g) activity was determined by the nitrogen blue tetrazolium photoreduction method, and 50% of the nitrogen blue tetrazolium photoreduction was used as one enzyme activity unit (U); Proline (Pro, μg/g) content was determined by acidic ninhydrin colorimetric method; soluble sugar (SS, mg/g) and starch (ST, mg/g) content were determined by anthrone colorimetric method; soluble protein (SP, mg/g) content was determined by coomassie blue staining (Wu, 2018). The contents of Na^+ (%) were determined by the water bath extraction method using a mixture of perchloric acid and concentrated nitric acid (Ou et al., 2019).

2.3.3 Related indicators calculation

Relative height growth rate (RGR_H, cm/(cm.d)):

$$\boldsymbol{RGR_H} = (lnH2 - lnH1)/(T2 - T1)$$

Relative ground diameter growth rate (RGR_D, mm/(mm.d)):

$$\boldsymbol{RGR_D} = (lnD2 - lnD1)/(T2 - T1)$$

Where: H_1 is the seedling height at the beginning of the trial, H_2 is the seedling height at the end of the trial, D_1 is the seedling ground diameter at the beginning of the trial, D_2 is the seedling ground diameter at the end of the trial, T_1 represents the start time of the trial, and T_2 represents the end time of the trial.

FIGO, International Federation of Gynecology and Obstetrics; NOS, Newcastle-Ottawa Scale; PD-1, programmed death-1.

$$\text{Leaf relative water content (RWC, \%)} = (\text{fresh weight} - \text{dry weight})/(\text{saturated fresh weight} - \text{dry weight}) \times 100\,\%$$

$$\text{Non-structural carbohydrate(NSC, mg/g)} = \text{soluble sugar content} + \text{starch content}$$

2.4 Data processing

Excel 2010 was used to organize and calculate the data and draw graphs, and SPSS 17.0 was used for all experimental data analysis. A two-way ANOVA was performed on the relative growth rates of *T. chinensis* seedlings for water treatment and salt gradient, and a three-factor ANOVA was performed on the physiological indicators (Chl, RC, MDA, SOD, Pro, SP,RWC, ST, SS, NSC and Na^+) for water treatment, salt gradient, and stress time. If the differences were significant, multiple comparisons were then performed using the least significant difference (LSD) method with a significance difference test level of $P< 0.05$. Correlation analyses and principal component analysis were conducted separately for the physiological indicators (Chl, RC, MDA, SOD, Pro, SP,RWC, ST, SS, NSC and Na^+) under different moisture treatments.

3 Results

3.1 Effect of soil moisture conditions and salinity on the growth of *T. chinensis* seedlings

Soil salt treatment had a significant effect on RGR_H ($F=2.62$, $P<0.05$) and RGR_D ($F=4.63$, $P<0.01$), moisture conditions had a highly significant effect on RGR_H ($F=6.48$, $P<0.01$) and RGR_D ($F=19.81$, $P<0.01$), and the interactions between the two factors had insignificant effects on RGR_H ($F=0.16$, $P>0.05$) and RGR_D ($F=0.66$, $P>0.05$). With increasing soil treatment, both RGR_H and RGR_D increased and then decreased, with RGR_H being maximum at 5‰ (Figure 2A), while RGR_D was maximum at 5‰ under normal watering and maximum at 8‰ under persistent drought and persistent waterlogging (Figure 2B). Among moisture conditions, both RGR_H and RGR_D were not significantly different between normal watering and persistent drought ($P>0.05$), and both were highly significantly lower than persistent waterlogging ($P<0.01$).

3.2 Effect of soil moisture conditions and salinity on the physiology of *T. chinensis* seedlings

3.2.1 Leaf relative water content

Soil salt treatment, moisture conditions and treatment time and the interactions among these three factors all had highly significant effects on leaf relative water content (Table 2). The leaf relative water content decreased significantly with increasing soil salt concentration (Figure 3). Under moisture conditions, the relative water content showed as persistent drought< normal watering< persistent waterlogging ($P<0.01$). The pattern of variation of leaf relative water content with the duration of treatment was different among moisture conditions. As the treatment time increased, the leaf relative water content decreased slowly under normal watering (Figure 3A), rapidly under persistent drought (Figure 3B), and not significantly under persistent waterlogging (Figure 3C). Under normal watering and persistent drought, the higher the soil treatment and the longer the treatment time, the lower the leaf relative water content.

3.2.2 Chlorophyll content

Total chlorophyll content was highly significantly affected by soil salt treatment, water conditions and time of treatment, and the effect of interactions among the three factors were also significant (Table 2). Total chlorophyll content significantly decreased with increasing soil salt content (Figure 4). Among different water conditions, the ranking of total chlorophyll content was persistent drought< normal watering< persistent waterlogging ($P<0.01$). With increasing treatment time, total chlorophyll content gradually increased under normal watering (Figure 4A) and persistent waterlogging (Figure 4C),

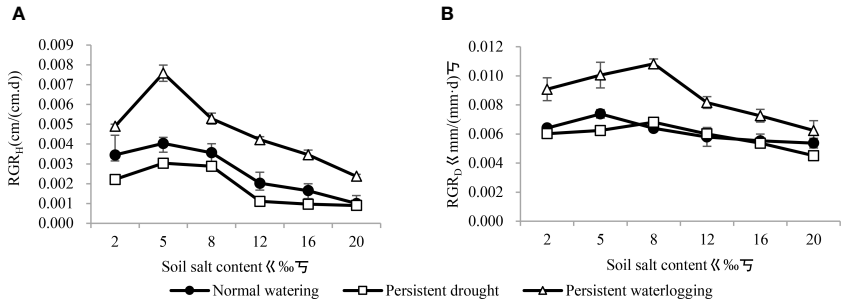

FIGURE 2
Changes in relative growth rates of *Tamarix chinensis* seedling height **(A)** and ground diameter **(B)** under different water conditions with increasing soil salinity.

TABLE 2 Three-way ANOVA of the effects of water conditions, stress time and soil salinity on physiological indicators of *Tamarix chinensis* seedlings.

Indicators	Moisture conditions (A)		Time of coercion (B)		Soil salinity (C)		A×B		A×C		B×C		A×B×C	
	F	P	F	P	F	P	F	P	F	P	F	P	F	P
Chl	56.10	<0.01	101.34	<0.01	26.07	<0.01	28.12	<0.01	6.90	<0.01	4.97	<0.01	2.21	<0.01
RC	0.04	0.96	61.64	<0.01	30.24	<0.01	10.89	<0.01	2.95	<0.01	5.00	<0.01	1.85	<0.05
MDA	446.04	<0.01	116.17	<0.01	3.34	<0.01	203.11	<0.01	2.17	<0.01	1.46	0.13	1.66	<0.05
SOD	42.54	<0.01	85.64	<0.01	3.18	<0.05	31.20	<0.01	5.08	<0.01	1.34	0.19	1.79	<0.05
Pro	234.21	<0.01	119.61	<0.01	105.52	<0.01	59.48	<0.01	12.81	<0.01	3.34	<0.01	1.56	0.06
SP	55.10	<0.01	72.03	<0.01	83.03	<0.01	35.80	<0.01	1.39	0.19	1.73	0.05	2.43	<0.01
RWC	256.80	<0.01	126.24	<0.01	6.15	<0.01	124.87	<0.01	4.26	<0.01	5.74	<0.01	3.86	<0.01
SS	7.58	<0.01	88.30	<0.01	2.47	<0.05	10.84	<0.01	2.81	<0.01	4.69	<0.01	1.35	0.14
ST	0.37	0.70	244.21	<0.01	1.80	0.12	46.28	<0.01	5.37	<0.01	7.41	<0.01	3.01	<0.01
NSC	4.24	<0.05	55.13	<0.01	1.74	0.13	43.89	<0.01	4.11	<0.01	9.00	<0.01	2.42	<0.01
Na^+	16.41	<0.01	1191.82	<0.01	46.15	<0.01	43.72	<0.01	5.58	<0.01	5.15	<0.01	2.41	<0.01

Chl, chlorophyll content; RC, relative conductivity; MDA, malondialdehyde; SOD, superoxide dismutase; Pro, proline; SP, soluble protein; RWC, relative water content; SS, soluble sugar; ST, starch; NSC, non-structural carbohydrate.

while it increased and then decreased under persistent drought (Figure 4B). Overall, the poorer the water conditions, the higher the soil treatment and the lower the total chlorophyll content.

3.2.3 Cell membrane permeability

Soil salt treatment and treatment time had significant effects on relative conductivity, moisture conditions had insignificant effect, and the interactions of all three factors were significant (Table 2). As the soil salt content increased, the relative conductivity decreased and then increased, with 12‰ being the lowest and 20‰ being the highest (Figure 5). The relative conductivity gradually increased with increasing treatment time (Figure 5). Overall, the relative conductivity increased less under normal watering and persistent impregnation, and the relative conductivity increased the most under each soil salt content and the most under persistent drought.

Malondialdehyde was significantly affected by soil salt treatment, soil conditions and time of treatment, and the interactions of the three factors (except time and salt) also had a significant effect (Table 2). The malondialdehyde content fluctuated and increased with increasing soil salt content, with the highest at 20‰ (Figure 5). The difference in malondialdehyde content between moisture conditions was not significant between normal watering and persistent water logging and was significantly lower than that of persistent drought. Malondialdehyde content fluctuated with increasing treatment time under normal watering (Figure 5) and persistent waterlogging for each soil salt content (Figure 5C), but significantly increased under persistent drought (Figure 5B).

3.2.4 Leaf Na^+ content

Na^+ content was significantly affected by soil treatment, water conditions and treatment time, and the interactions among the three factors were also significant (Table 2). The Na^+ content increased significantly with increasing soil treatment (Figure 6). Under moisture conditions, the Na^+ content were ranked as persistent drought< normal watering< persistent water logging. The Na^+ content also increased significantly with the increasing duration of treatment. Overall, the better the moisture conditions, the higher the soil treatment and the longer the duration of treatment, the higher the Na^+ content (Figure 6).

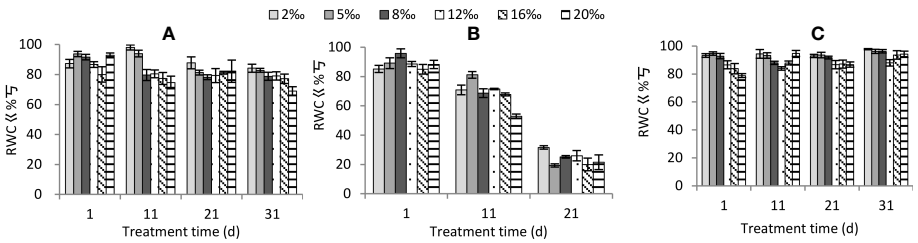

FIGURE 3
Changes in relative water content of *Tamarix chinensis* seedlings under different soil moisture conditions and soil salt content with increasing treatment time. **(A)** normal watering; **(B)** persistent drought; **(C)** persistent waterlogging.

10.3389/fmars.2023.1231928

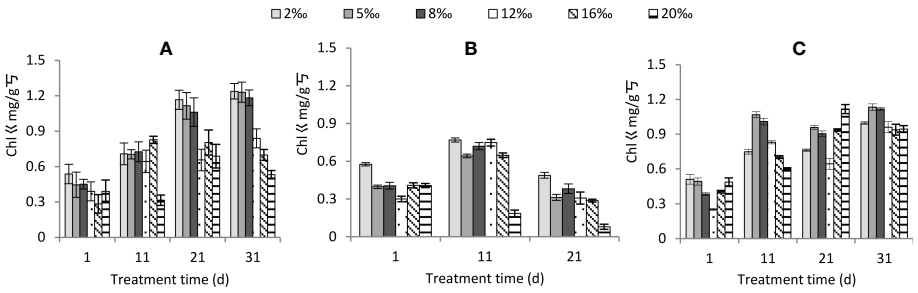

FIGURE 4
Changes in total chlorophyll content of *Tamarix chinensis* seedlings under different soil moisture conditions and soil salt content with increasing treatment time. **(A)** normal watering; **(B)** persistent drought; **(C)** persistent waterlogging.

3.2.5 Osmoregulatory substances

Soil treatment gradient, moisture conditions and time of treatment all had significant effects on proline and soluble protein content (Table 2). Both proline and soluble protein content significantly increased with increasing soil treatment (Figure 7). Among water conditions, proline was ranked as persistent waterlogging< normal watering< persistent drought, and soluble protein was ranked as normally watering< persistent waterlogging< persistent drought. Both proline and soluble protein content significantly increased with increasing treatment time. In terms of interaction of three factors, except for soil treatment gradient × moisture condition × stress time, the other interaction of three factors had significant effects on proline. And for soluble protein, except for soil treatment gradient × moisture condition and soil treatment gradient × treatment time, the other interaction of three factors had significant effects (Table 2). Overall, the higher the soil treatment and the longer the treatment time, the higher the proline and soluble protein content under persistent drought, while the normal watering and persistent waterlogging did not vary much in the stress time (Figure 7).

3.2.6 SOD activity

SOD activity was significantly affected by salt treatment, moisture conditions and treatment time (Table 2). The interactions of the three factors, except soil salt gradient × treatment time, also had a significant effect on it (Table 2). Among the soil salt treatments, SOD activity was greatest at 20‰ ($P<0.01$), while the differences between the other treatments were not significant ($P>0.05$). The differences between normal watering and persistent waterlogging were not significant

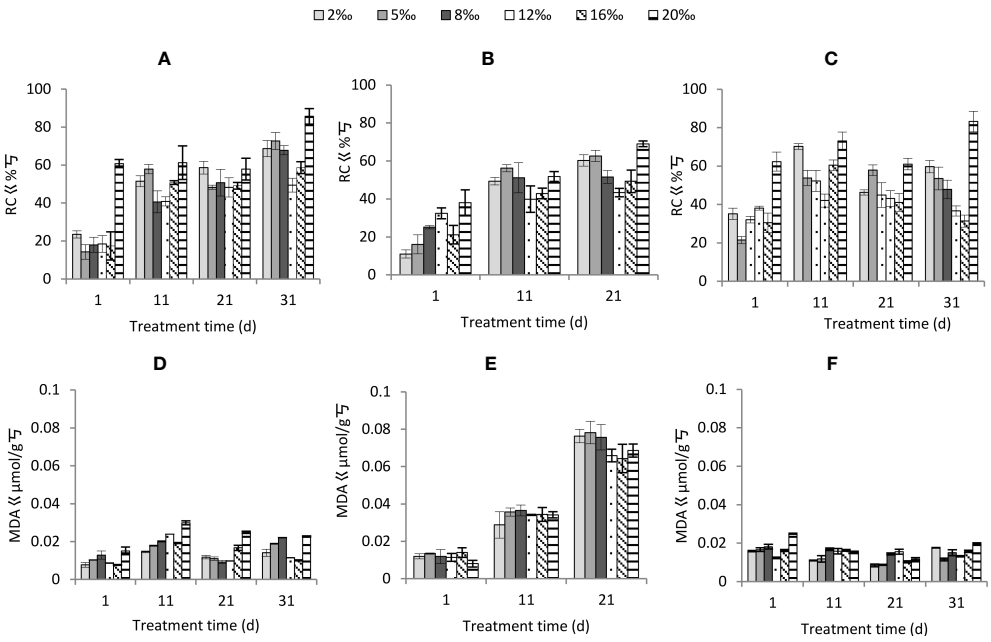

FIGURE 5
Changes in cell membrane permeability of *Tamarix chinensis* seedlings under different soil moisture conditions and soil salt content with increasing treatment time. **(A)** Relative conductivity under normal watering; **(B)** Relative conductivity under persistent drought; **(C)** Relative conductivity under persistent waterlogging; **(D)** Relative conductivity under normal watering; **(E)** Relative conductivity under persistent drought; **(F)** Relative conductivity under persistent impregnated water.

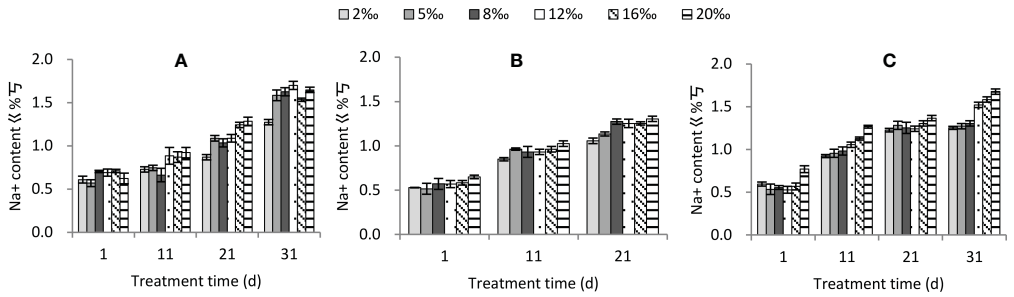

FIGURE 6
Changes in Na^+ content of *Tamarix chinensis* seedlings with increasing treatment time under different soil moisture conditions and soil salt content. **(A)** normal watering; **(B)** persistent drought; **(C)** persistent waterlogging.

(P>0.05), and both were significantly lower (P<0.01) than persistent drought. The SOD activity increased significantly with increasing treatment time (Figure 8). Under persistent drought, the increase in SOD activity with increasing treatment time was significantly higher than that of normal watering and persistent waterlogging.

3.2.7 NSC

Soil salt gradient, moisture conditions and treatment time had significant effects on soluble sugars. Soil salt gradient and moisture conditions did not have significant effects on starch, while treatment time had significant effects on starch (Table 2). The soil salt gradient had no significant effect on NSC, and moisture conditions and treatment time had significant effects on it. Among moisture conditions, soluble sugars were ranked as normal watering > persistent waterlogging > persistent drought; NSC content was significantly greater in normal watering than in persistent drought and persistent waterlogging (P<0.05), and the difference between persistent drought and persistent waterlogging was not significant (P>0.05).

The interaction of the three factors significantly affected soluble sugars, starch and NSC (except for soil treatment gradient × moisture condition and soil treatment gradient × treatment time which did not significantly affect soluble sugars) (Table 2). Soluble sugars, starch and NSC increased gradually with stress time under both normal watering (Figures 9A, D, G) and persistent waterlogging (Figures 9C, F, I), whereas they all decreased gradually under persistent drought (Figures 9B, E, H).

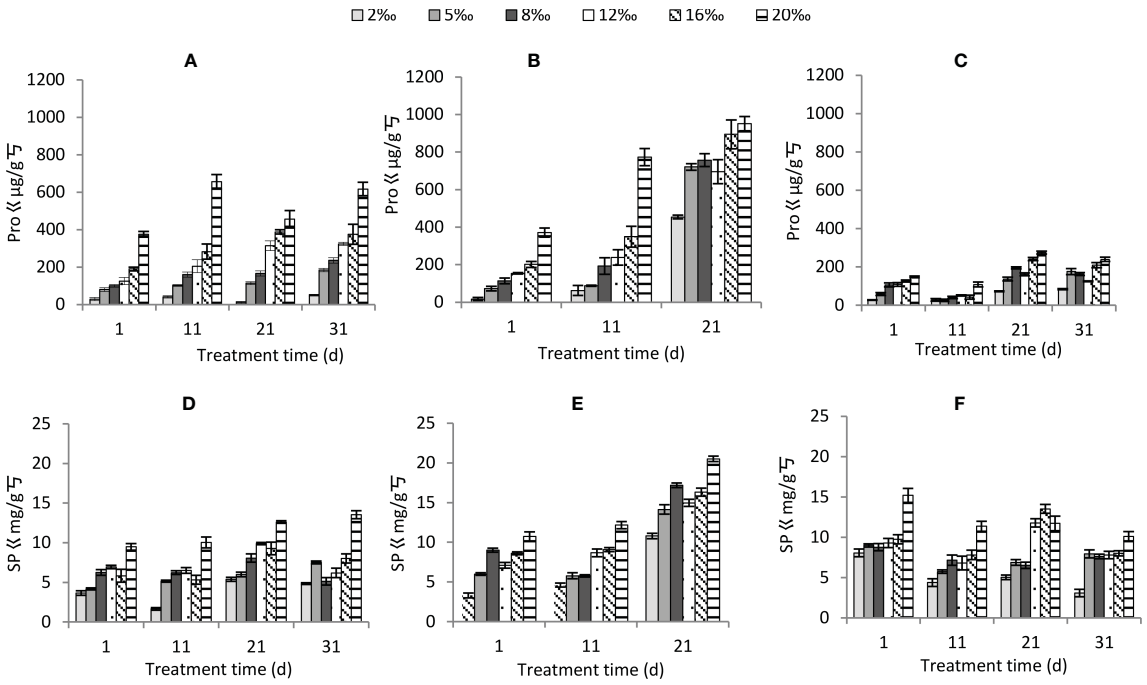

FIGURE 7
Changes in osmoregulatory substances of *Tamarix chinensis* seedlings under different soil moisture conditions and soil salt content with increasing treatment time **(A)** proline under normal watering; **(B)** proline under persistent drought; **(C)** proline under persistent waterlogging **(D)** soluble protein under normal watering; **(E)** soluble protein under persistent drought; **(F)** soluble protein under persistent waterlogging.

10.3389/fmars.2023.1231928

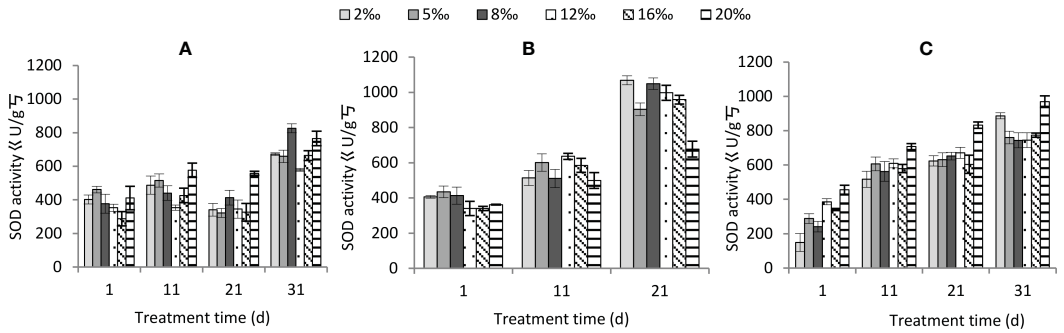

FIGURE 8
Changes in SOD enzyme activity of *Tamarix chinensis* seedlings under different soil moisture conditions and soil salt content with increasing treatment time. **(A)** normal watering; **(B)** persistent drought; **(C)** persistent waterlogging.

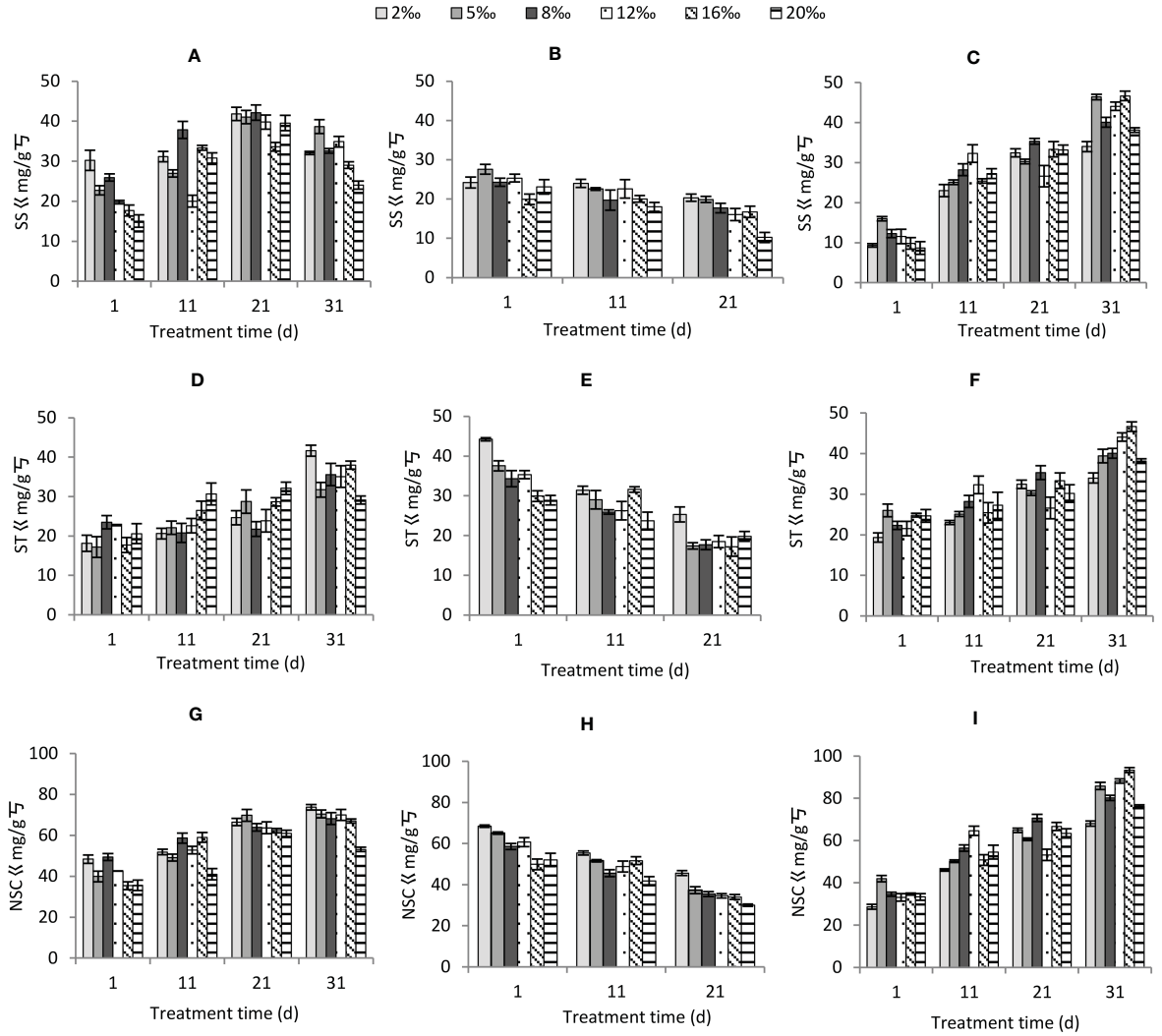

FIGURE 9
Changes in non-structural carbohydrates of *Tamarix chinensis* seedlings under different soil moisture conditions and soil salt content with increasing treatment time **(A)** soluble sugars under normal watering; **(B)** soluble sugars under persistent drought; **(C)** soluble sugars under persistent waterlogging **(D)** starch under normal watering; **(E)** starch under persistent drought; **(F)** starch under persistent waterlogging **(G)** Non-structural carbohydrates under normal watering; **(H)** Non-structural carbohydrates under persistent drought; **(I)** Non-structural carbohydrates under persistent waterlogging.

3.3 Correlation between physiological indicators under different watering conditions

3.3.1 Normal watering

Under normal watering (Table 3), Na^+ was significantly and positively correlated with total chlorophyll content, relative conductivity, SOD activity, proline and soluble sugar content ($P< 0.01$), while had highly significantly negative correlations ($P< 0.01$) with relative leaf water content and soluble starch. MDA was highly significantly and positively correlated with SOD ($P< 0.01$), and highly and negatively correlated with ST ($P< 0.01$) and NSC ($P< 0.01$). ST was highly significantly and negatively correlated with RC ($P< 0.01$), Pro ($P< 0.01$) and SS ($P< 0.01$), and SS was positively correlated with RC ($P< 0.01$).

Four principal components were obtained under normal watering conditions, with contributions of 24.64%, 21.16%, 15.01%, and 14.57% in the order, with a cumulative contribution of 75.38% (Table 4). The first principal component consisted of chlorophyll, soluble sugars, sodium ions, relative conductivity, and proline, reflecting the changes in chlorophyll. The second principal component consisted mainly of NSC and starch, reflecting the changes in nonstructural carbon.

3.3.2 Persistent drought

As shown in Table 5, under persistent drought, Na^+ was significantly and positively correlated with malondialdehyde ($P< 0.01$), SOD activity ($P< 0.01$), proline ($P< 0.01$), soluble protein ($P< 0.01$), relative conductivity ($P< 0.01$), soluble sugar ($P< 0.01$), and negatively correlated with leaf relative water content ($P< 0.01$) and soluble starch ($P< 0.01$). MDA was significantly and positively correlated with RC ($P< 0.01$), SOD ($P< 0.01$), Pro ($P< 0.01$), SP ($P< 0.01$), SS ($P< 0.01$), and negatively correlated with RWC ($P< 0.01$), ST ($P< 0.01$) and NSC ($P< 0.01$). ST was significantly and negatively correlated with RC ($P< 0.01$), SOD ($P< 0.01$), Pro ($P< 0.01$), SP ($P< 0.01$) and SS ($P< 0.01$); SS was positively correlated with SOD ($P< 0.05$) and negatively correlated with RWC ($P< 0.01$).

Three principal components were obtained under persistent drought stress, with contributions of 35.58%, 28.75%, and 16.49% in the order, and the cumulative contribution was 80.82% (Table 6). The first principal component consisted of NSC, starch, relative conductivity, malondialdehyde, and SOD, reflecting the integrity of the cell membrane structure. The second principal component consisted of soluble protein, chlorophyll, proline, and relative water content, reflecting the changes in chlorophyll.

3.3.3 Persistent waterlogging

Under persistent waterlogging (Table 7), sodium ions were significantly and positively correlated with total chlorophyll ($P< 0.01$), relative conductivity ($P< 0.01$), SOD activity ($P< 0.01$), proline ($P< 0.01$), soluble sugars ($P< 0.01$) and NSC content ($P< 0.01$), and negatively correlated with MDA ($P< 0.05$). MDA was negatively correlated with Pro ($P< 0.05$) and SS ($P< 0.05$), and positively correlated with SP ($P< 0.05$) and ST ($P< 0.01$). SS was positively correlated with Pro ($P< 0.01$) and RWC ($P< 0.05$), and negatively correlated with SP ($P< 0.05$).

Four principal components were obtained under persistent waterlogging, with contributions of 27.96%, 18.19%, 16.98%, and 14.58% in the order, with a cumulative contribution of 77.70% (Table 8). The first principal component consisted of sodium ions, soluble sugars, proline, chlorophyll, and malondialdehyde, which reflected the changes in chlorophyll. The second principal component consisted of relative conductivity and SOD, reflecting the integrity of the cell membrane structure.

4 Discussion

In coastal wetland ecosystems, plants are combinedly affected by soil moisture and salinity. Soil water change regulating the soil salt content obviously influence the plant adaptability. In the present study, we found that the physiological adaptability of *T. chinensis* siginificantly changed along the soil moisture. The

TABLE 3 Correlation analysis of physiological indices of *Tamarix chinensis* seedlings response to salinity under normal watering.

	Chl	RC	MDA	SOD	Pro	SP	RWC	ST	SS	NSC	Na^+
Chl	1										
RC	0.56**	1									
MDA	0.03	0.32*	1								
SOD	0.24	0.39**	0.40**	1							
Pro	0.42**	0.31*	-0.00	0.11	1						
SP	0.06	-0.01	-0.06	-0.18	0.27*	1					
RWC	-0.29*	-0.26*	-0.16	-0.15	-0.35**	-0.35**	1				
ST	-0.53**	-0.63**	-0.36**	-0.11	-0.44**	-0.23	0.22	1			
SS	0.50**	0.34**	-0.05	0.07	0.26*	0.21	-0.25*	-0.35**	1		
NSC	-0.29*	-0.47**	-0.40**	-0.07	-0.33*	-0.13	0.09	0.86**	0.18	1	
Na^+	0.62**	0.56**	0.10	0.38**	0.63**	0.19	-0.44**	-0.42**	0.43**	-0.21	1

*, indicates significance at 0.05; **, indicates significance at 0.01.
Chl, chlorophyll content; RC, relative conductivity; MDA, malondialdehyde; SOD, superoxide dismutase; Pro, proline; SP, soluble protein; RWC, relative water content; SS, soluble sugar; ST, starch; NSC, non-structural carbohydrate.

10.3389/fmars.2023.1231928

TABLE 4 Principal component analysis of physiological indexes of *Tamarix chinensis* seedlings under normal watering.

Indexes	Principal component			
	F1	F2	F3	F4
Chl	0.82	-0.28	0.08	0.02
SS	0.77	0.11	-0.09	0.14
Na^+	0.74	-0.14	0.29	0.34
RC	0.58	-0.49	0.39	-0.04
Pro	0.49	-0.30	-0.02	0.47
NSC	0.01	0.97	-0.10	-0.08
ST	-0.39	0.87	-0.05	-0.15
SOD	0.25	0.05	0.84	-0.08
MDA	-0.20	-0.42	0.72	0.08
SP	0.01	-0.13	-0.27	0.81
RWC	-0.25	-0.03	-0.30	-0.75
Eigenvalue	2.71	2.33	1.62	1.60
Contribution rate (%)	24.64	21.16	15.01	14.57
Cumulative contribution rate (%)	24.64	45.80	60.81	75.38

Chl, chlorophyll content; RC, relative conductivity; MDA, malondialdehyde; SOD, superoxide dismutase; Pro, proline; SP, soluble protein; RWC, relative water content; SS, soluble sugar; ST, starch; NSC, non-structural carbohydrate.

combined roles of persistent drought and soil salinity further intensified the inhibition of *T. chinensis* growth.

4.1 Effect of soil moisture conditions on salt tolerance of *T. chinensis* seedlings

The relative seedling height and ground diameter growth rates of *T. chinensis* seedlings first increased and then decreased with increasing salt concentration. Studies on *S. salsa* also found that low salt promoted their growth while high salt significantly inhibited it (Jia et al., 2018). The relative seedling height, ground diameter growth rate and chlorophyll content of seedlings were the highest under persistent waterlogging, indicating that *T. chinensis* is highly tolerant to flooding. Chlorophyll is an extremely important pigment affecting photosynthesis, and the level of content reflects the photosynthetic capacity of the plant (Muchate et al., 2016). The changes in chlorophyll were the first principal component under normal watering and persistent waterlogging and the second

TABLE 5 Correlation analysis of physiological indexes of *Tamarix chinensis* seedlings in response to salt under persistent drought. .

	Chl	RC	MDA	SOD	Pro	SP	RWC	ST	SS	NSC	Na^+
Chl	1										
RC	0.02	1									
MDA	-0.16	0.42**	1								
SOD	-0.11	0.34*	0.86**	1							
Pro	-0.28*	0.17	0.70**	0.60**	1						
SP	-0.48**	0.24	0.72**	0.62**	0.70**	1					
RWC	0.24	-0.35*	-0.88**	-0.79**	-0.73**	-0.78**	1				
ST	-0.14	-0.52**	-0.76**	-0.65**	-0.55**	-0.53**	0.64**	1			
SS	0.01	0.10	0.41**	0.29*	0.24	0.19	-0.38**	-0.33*	1		
NSC	-0.14	-0.51**	-0.65**	-0.58**	-0.49**	-0.49**	0.54**	0.94**	0.02	1	
Na^+	-0.11	0.34*	0.86**	0.75**	0.64**	0.72**	-0.77**	-0.84**	0.43**	-0.73**	1

*, indicates significance at 0.05; **, indicates significance at 0.01.
Chl, chlorophyll content; RC, relative conductivity; MDA, malondialdehyde; SOD, superoxide dismutase; Pro, proline; SP, soluble protein; RWC, relative water content; SS, soluble sugar; ST, starch; NSC, non-structural carbohydrate.

10.3389/fmars.2023.1231928

TABLE 6 Principal component analysis of physiological indicators of *Tamarix chinensis* seedlings under persistent drought conditions.

Indexes	Principal component		
	F1	F2	F3
NSC	-0.95	-0.18	0.02
ST	-0.89	-0.19	-0.31
RC	0.68	0.02	-0.06
Na^+	0.66	0.48	0.45
MDA	0.62	0.56	0.45
SOD	0.58	0.51	0.37
SP	0.36	0.84	0.14
Chl	0.32	-0.81	0.18
Pro	0.37	0.70	0.24
RWC	-0.49	-0.66	-0.41
SS	-0.02	0.07	0.95
Eigenvalue	3.91	3.16	1.81
Contribution rate (%)	35.58	28.75	16.49
Cumulative contribution rate (%)	35.58	64.33	80.82

Chl, chlorophyll content; RC, relative conductivity; MDA, malondialdehyde; SOD, superoxide dismutase; Pro, proline; SP, soluble protein; RWC, relative water content; SS, soluble sugar; ST, starch; NSC, non-structural carbohydrate.

principal component under persistent drought, suggesting that the maintenance of chlorophyll is an important physiological basis for its adaptation to coastal saline sites, in agreement with the results of the study on *Cakile maritima* (Farhat et al., 2021). Under persistent drought stress, the higher the salt concentration and longer the treatment time, the lower the chlorophyll content, with the lowest chlorophyll content of only 0.08 mg/g at the 21st d salt concentration of 20‰, and almost all of the *T. chinensis* leaves lost their green color. In dry seasons, soil salinity increases in coastal saline sites (Souid et al., 2018). We similarly found that soil treatment gradually increased with the increase of persistent stress time in our study, which was an important reason for the aboveground mortality of *T. chinensis* seedlings in the experiment. With global climate change, *T. chinensis* natural forests may experience prolonged drought, which will threaten the maintenance of their populations in coastal wetlands.

TABLE 7 Correlation analysis of physiological indexes of *Tamarix chinensis* seedlings in response to salt under persistent waterlogging.

	Chl	RC	MDA	SOD	Pro	SP	RWC	ST	SS	NSC	Na^+
Chl	1										
RC	0.31*	1									
MDA	-0.24*	0.01	1								
SOD	0.51**	0.44**	0.02	1							
Pro	0.28*	0.07	-0.29*	0.12	1						
SP	-0.22	-0.12	0.27*	-0.10	-0.11	1					
RWC	0.19	0.10	-0.22	0.08	0.15	-0.41**	1				
ST	-0.21	-0.22	0.33**	0.13	0.11	0.04	0.03	1			
SS	0.70**	0.23	-0.30*	0.50**	0.53**	-0.29*	0.28*	0.05	1		
NSC	0.38**	0.02	0.00	0.50**	0.45**	-0.18	0.22	0.69**	0.76**	1	
Na^+	0.75**	0.35**	-0.27*	0.49**	0.62**	-0.09	0.10	-0.09	0.83**	0.55**	1

*, indicates significance at 0.05; **, indicates significance at 0.01.
Chl, chlorophyll content; RC, relative conductivity; MDA, malondialdehyde; SOD, superoxide dismutase; Pro, proline; SP, soluble protein; RWC, relative water content; SS, soluble sugar; ST, starch; NSC, non-structural carbohydrate.

TABLE 8 Principal component analysis of physiological indicators of *Tamarix chinensis* seedlings under persistent waterlogging conditions.

Indexes	Principal component			
	F1	F2	F3	
Na^+	0.85	0.44	-0.01	-0.03
SS	0.81	0.37	0.17	0.24
Pro	0.81	-0.12	0.09	0.03
Chl	0.61	0.56	-0.13	0.15
MDA	-0.50	0.21	0.50	-0.37
RC	0.00	0.80	-0.18	0.07
SOD	0.25	0.78	0.27	0.03
ST	-0.00	-0.15	0.95	0.01
NSC	0.59	0.17	0.75	0.19
SP	-0.07	-0.10	0.03	-0.83
RWC	0.08	0.04	0.07	0.81
Eigenvalue	3.08	2.00	1.87	1.60
Contribution rate (%)	27.96	18.19	16.98	14.58
Cumulative contribution rate (%)	27.96	46.15	63.12	77.70

Chl, chlorophyll content; RC, relative conductivity; MDA, malondialdehyde; SOD, superoxide dismutase; Pro, proline; SP, soluble protein; RWC, relative water content; SS, soluble sugar; ST, starch; NSC, non-structural carbohydrate.

4.2 Effects of soil moisture conditions on the physiological adaptation of *T. chinensis* seedlings under salt stress

4.2.1 Osmotic stress and regulation

The salt treatment caused osmotic stress to *T. chinensis* seedlings, and the leaf relative water content under high salt treatment was lower than that of low salt treatment, which was related to the difficulty of water uptake by the soil due to low osmotic potential caused by high salt concentration in the soil. A decrease in leaf relative water content with increasing salt concentration was also found in *Robinia pseudoacacia* (Mao et al., 2016) and *Lonicera japonica* (He et al., 2021). The decrease in leaf relative water content indicates that an increase in water deficit occurs in them (Mao et al, 2016). Increased proline (Nxele et al., 2017; Per et al., 2017) and soluble protein content (Arbelet-Bonnin et al., 2020) are important ways to increase the osmoregulatory capacity of plants under salt stress. Proline and soluble protein content in *T. chinensis* in this study gradually increased with increasing salt concentration, which suggested that both were involved in osmoregulation. In this paper, we found that the relative water content of *T. chinensis* leaves under three moisture conditions was lowest under persistent drought and highest under persistent waterlogging. A regular leaf water content could ensure normal physiological metabolism (Mao et al., 2016), which is an important reason for the highest relative growth rate under persistent waterlogging. Under the three different water conditions, the content of proline and soluble protein increased with increasing treatment time, but they were the highest under persistent drought stress. It wad suggested that although proline increased significantly under drought and salt stress, the osmoregulatory capacity was limited (Nxele et al., 2017). Arbelet-Bonnin et al. (2020) concluded that the increase in proline was related to the tolerant ability of halophyte *C. maritima* to salt stress. Benjamin et al. (2019), on the other hand, concluded that there were differences in osmoregulatory substances in different saline plants. Correlation analysis showed that the relative leaf water content was significantly negatively correlated with proline and soluble protein. This suggested that osmoregulatory substances, although significantly increased under persistent drought, were not sufficient to counteract water deficit due to stress, which indicated that there might be other substances involved in the process.

4.2.2 Cell membrane damage and protection

The relative conductivity and malondialdehyde content of salt concentration 20‰ in this study was higher than other salt treatments, indicating that heavy salt stress severely damaged cell membranes (Muchate et al., 2016). Malondialdehyde content was highest under persistent drought and increased rapidly with increasing treatment time, while it did not change much under normal watering and persistent waterlogging. The MDA content of halophyte *L. delicatulum* was also highest in the dry season (Souid et al., 2018). Studies on *S. salsa* have shown that cell membrane persecution is more severe under combined salt-drought effects (Jia et al., 2018). The full use of sodium ions to adapt to salt environments is a common performance of saline plants (Muchate et al., 2016; He et al., 2021). In this paper, it was found that *T. chinensis* absorbed large amounts of sodium ions under all moisture conditions. However, correlation analysis showed that malondialdehyde and sodium ions were significantly and positively

correlated with malondialdehyde under persistent drought, but not under normal watering and persistent waterlogging, suggesting that increased sodium ions under drought stress was an important factor contributing to cell membrane disruption in *T. chinensis*. Cell membrane disruption under persistent drought was the first principal component and was the main mode leading to severe stress in *T. chinensis*. Studies on *Sorghum bicolor* have also identified cell membrane disruption as an important cause of its cell death under drought and salt stress (Nxele et al., 2017). In response to oxidative stress damage to cell membranes, *T. chinensis* SOD activity increased with increasing soil salt content. Under persistent drought, SOD activity was significantly higher than that under normal watering and persistent waterlogging, indicating that SOD is an important way to eliminate superoxide ions under drought stress (Souid et al., 2018). It has been shown that proline (Per et al., 2017) and other osmoregulatory substances are also important ways to eliminate oxygen radicals (Khoshbakht et al., 2018; Arbelet-Bonnin et al., 2020). Correlation analysis showed that under persistent drought MDA was significantly and positively correlated with Pro, SP, and SS, in addition to SOD. Thus, protective enzymes and osmoregulatory substances together protected cell membranes under persistent drought. As a whole, MDA was an important indicator in response to the stress suffered by *T. chinensis*.

4.2.3 NSC regulation

Soluble sugars, starch and NSC increased first and then decreased with increasing salt concentration under normal water and persistent waterlogging, and gradually decreased under persistent drought. Arbelet-Bonnin et al. (2020) suggested that sugar content decreased under high salt stress due to the inhibition of photosynthesis. It has been shown that NSC increases under adversity suggesting plants with strong resilience (Gao et al., 2021). The second principal component of the highest soluble sugars and NSC under normal watering was correlated with NSC changes, suggesting that NSC accumulation was an important way of its adaptation to salt stress. The persistent increase in NSC of *T. chinensis* under persistent waterlogging also indicated its strong adaptation to waterlogging. In this paper, we found that the total chlorophyll content decreased under persistent drought. Therefore, the decrease in photosynthesis is an important reason for the decrease in NSC under persistent drought. The significantly negative correlation between SS and ST under normal watering and persistent drought indicated that there was a conversion between them. This further supported the founding that the interconversion between soluble sugars and starches was an important way to cope with the external environment (McDowell, 2011). ST was significantly negatively correlated with Pro and SS under normal watering and with SOD, Pro and SS under persistent drought. These suggested that the breakdown of starch to soluble sugars under stress, which provided a carbon shelf for nitrogenous compounds, was an important way to adapt to adversity (Hartmann and Trumbore, 2016). The reduction in soluble sugar content of *T. chinensis* under persistent drought indicated that depletion was much greater than photosynthetic production, which maybe one of important reasons for the decrese in NSC. After drought stress was eliminated, NSC content was significantly reduced in trees that did not die and was used for tissue repair (Tomasella et al., 2019). Therefore, the high depletion of NSC under persistent drought was detrimental to the survival of *T. chinensis* in coastal saline sites.

5 Conclusion

This study found that the seedling growth of *T. chinensis* is significantly inhibited with a soil salinity above 20‰. Soil moisture conditions significantly influenced the physiological processes of tolerance of *T. chinensis* in different soil salinity. Under normal watering and persistent waterlogging, the physiology of *T. chinensis* was less affected under different soil salinity, especially the highest relative growth rate under persistent waterlogging. These results illustrated that *T. chinensis* in persistent waterlogging conditions could tolerate different salt stress. Under persistent drought stress, with the decrease of soil water content and the significant increase of soil salinity, *T. chinensis* suffered from both drought and salt stress, the relative water content in the body was significantly reduced, chlorophyll and cell membrane suffered serious damage, and although osmoregulation and protective enzyme activities were significantly increased, they were not sufficient to offset the damage caused by water deficit, which eventually led to aboveground death. Under the regular water condition of normal and persistent waterlogging, sodium ion was an important osmoregulatory substance, while under persistent drought it is a key factor leading to cell membrane disruption. NSC significantly increased under normal and persistent waterlogging while significantly decreased under persistent drought. In this process, starch played an important role in carbon storage function and was an important carbon source for various physiological maintenance. Malondialdehyde correlated well with various indicators under persistent drought and was a good indicator to reflect the tolerance under drought stress. With the intensification of global climate change, the change of temperature and precipitation will intensify the hydrological changes of coastal wetlands. It is of great significance to strengthen the research on the dynamic monitoring of precipitation and water-salt and their impacts on dominant plants in the Yellow River Delta in the future, which is meaningful for predicting the dynamic evolution of vegetation and improving the management level.

Data availability statement

The raw data supporting the conclusions of this article will be made available by the authors, without undue reservation.

Author contributions

PM and BC designed and reviewed the manuscript. QL, YP and KW collected the data. QL drafted the manuscript. YP analyzed the date. RN and XH reviewed and improved the manuscript. All authors contributed to the article and approved the submitted version.

Conflict of interest

The authors declare that the research was conducted in the absence of any commercial or financial relationships that could be construed as a potential conflict of interest.

Funding

This research was funded by Major Scientific Technological Innovation Projects of Shandong Province (2017CXGC0316), China Natural Science Foundation (31770668), Central Finance Forestry Reform and Development Fund (2020TG08) and Germplasm resources nursery project of saline alkali tolerant tree species in the Yellow River Delta (2019-370505-05-03-035206).

Publisher's note

References

Arbelet-Bonnin, D., Blasselle, C., Palm, E. R., Redwan, M., and Bouteau, F. (2020). Metabolism regulation during salt exposure in the halophyte cakile maritima. *Environ. Exp. Bot.* 177, 104075. doi: 10.1016/j.envexpbot.2020.104075

Benjamin, J. J., Lucini, L., Jothiramshekar, S., and Parida, A. (2019). Metabolomic insights into the mechanisms underlying tolerance to salinity in different halophytes. *Plant Physiol. Bioch.* 135, 528–545. doi: 10.1016/j.plaphy.2018.11.006

Borzouei, A., Shalmani, M. A. M., and Eskandari, A. (2020). Effects of salt and nitrogen on physiological indices and carbon isotope discrimination of wheat cultivars in the northeast of Iran. *J. Integr. Agr.* 19 (3), 656–667. doi: 10.1016/S2095-3119(19)62629-8

Buffington, K. J., Goodman, A. C., Freeman, C. M., and Thorne, K. M. (2020). Testing the interactive effects of flooding and salinity on tidal marsh plant productivity. *Aquat. Bot.* 164, 103231. doi: 10.1016/j.aquabot.2020.103231

Cong, P., Chen, K., Qu, L., and Han, J. (2019). Dynamic changes in the wetland landscape pattern of the Yellow River Delta from 1976 to 2016 based on satellite data. *Chin. Geogra. Sci.* 29 (3), 372–381. doi: 10.1007/s11769-019-1039-x

Cui, B., Yang, Q., Yang, Z., and Zhang, K. (2009). Evaluating the ecological performance of wetland restoration in the Yellow River Delta, China. *Ecol. Eng.* 35, 1090–1103. doi: 10.1016/j.ecoleng.2009.03.022

Cui, G., Zhang, Y., Zhang, W., Lang, D., Lang, D., Zhang, X., and Li, Z. (2019). Response of carbon and nitrogen metabolism and secondary metabolites to drought stress and salt stress in plants. *J. Plant Biol.* 62, 387–399. doi: 10.1007/s12374-019-0257-1

Dasgupta, S., Laplante, B., Meisner, C., Wheeler, D., and Yan, J. (2009). The impact of sealevel rise on developing countries: a comparative analysis. *Clim. Change.* 93, 379–388. doi: 10.1007/s10584-008-9499-5

da Silva, H. A., , de Oliveira, D. F. A., Avelino, A. P., de Macêdo, C. E. C., Barros-Galvão, T., and Voigt, E.L. (2019). Salt stress differentially regulates mobilisation of carbon and nitrogen reserves during seedling establishment of Pityrocarpa moniliformis. *Plant Biol. J.* 21, 1110–1118. doi: 10.1111/plb.13017

Dietze, M. C., Sala, A., Carbone, M. S., Czimczik, C. I., Mantooth, J. A., Richardson, A. D., et al. (2014). Nonstructural carbon in woody plants. *Annu. Rev. Plant Biol.* 65, 667–687. doi: 10.1146/annurev-arplant-050213-040054

Farhat, N., Kouas, W., Braun, H. P., and Debez, A. (2021). Stability of thylakoid protein complexes and preserving photosynthetic efficiency are crucial for the successful recovery of the halophyte *Cakile maritima* to high salinity. *Plant Physiol. Bioch.* 166, 177–190. doi: 10.1016/j.plaphy.2021.05.044

Gao, Y., Sun, Y., Ou, Y., Zheng, X., Feng, Q., Zhang, H., et al. (2021). Pretreating poplar cuttings with low nitrogen ameliorates salt stress responses by increasing stored carbohydrates and priming stress signaling pathways. *Ecotox. Environ. Safe.* 225, 112801. doi: 10.1016/j.ecoenv.2021.112801

Gao, Y., Xia, J., Chen, Y., Zhao, Y., Kong, Q., and Lang, Y. (2017). Effects of extreme soil water stress on photosynthetic efficiency and water consumption characteristics of *Tamarix chinensis* in China's Yellow River Delta. *J. For. Res.* 28 (3), 491–501. doi: 10.1007/s11676-016-0339-6

Ghaderi, N., Hatami, M., Mozafari, A., and Siosehmardeh, A. (2018). Change in antioxidant enzymes activity and some morpho-physiological characteristics of strawberry under long-term salt stress. *Physiol. Mol. Biol. Plants* 24 (5), 833–843. doi: 10.1007/s12298-018-0535-2

Guan, B., Yu, J., Hou, A., Han, G., Wang, G., Qu, F., et al. (2017). The ecological adaptability of *Phragmites australis* to interactive effects of water level and salt stress in the Yellow River Delta. *Aquat. Ecol.* 51, 107–116. doi: 10.1007/s10452-016-9602-3

Guan, B., Yu, J., Wang, X., Fu, Y., Kan, X., Lin, Q., et al. (2011). Physiological responses of halophyte suaeda salsa to water table and salt stresses in coastal wetland of yellow river delta. *Clean. – Soil. Air. Water* 39 (12), 1029–1035. doi: 10.1002/clen.201000557

Guo, L., Cao, B., Mao, P., Li, Z., Hao, M., Wang, T., et al. (2021). Fine root vertical-seasonal distribution of *Robinia pseudoacacia* in relation to abiotic factors in a chronosequence in coastal saline alkali land of the Yellow River Delta, China. *Turk. J. Agric. For.* 45, 750–765. doi: 10.3906/tar-2105-100

Guo, Q. X., Wu, X. Y., Korpelainen, H., and Li, C. Y. (2020). Stronger intraspecific competition aggravates negative effects of drought on the growth of *Cunninghamia lanceolata*. *Environ. Exp. Bot.* 175, 104042. doi: 10.1016/j.envexpbot.2020.104042

Hartmann, H., and Trumbore, S. (2016). Understanding the roles of nonstructural carbohydrates in forest trees-From what we can measure to what we want to know. *New Phytol.* 211, 386–403. doi: 10.1111/nph.13955

He, W., Yan, K., Zhang, Y., Bian, L., Mei, H., and Han, G. (2021). Contrasting photosynthesis, photoinhibition and oxidative damage in honeysuckle (*Lonicera japonica* Thunb.) under iso-osmotic salt and drought stresses. *Environ. Exp. Bot.* 182, 104313. doi: 10.1016/j.envexpbot.2020.104313

Hoch, G., Richter, A., and Korner, C. (2003). Non-structural carbon compounds in temperate forest trees. *Plant Cell Environ.* 26 (7), 1067–1081. doi: 10.1046/j.0016-8025.2003.01032.x

Hou, W., Zhang, R., Xi, Y., Liang, S., and Sun, Z. (2020). The role of waterlogging stress on the distribution of salt marsh plants in the Liao River estuary wetland. *Glob. Ecol. Conserv.* 23, e01100. doi: 10.1016/j.gecco.2020.e01100

Irshad, A., Rehman, R. N. U., Abrar, M. M., Saeed, Q., Sharif, R., and Hu, T. (2021). Contribution of rhizobium-legume symbiosis in salt stress tolerance in *Medicago truncatula* evaluated through photosynthesis, antioxidant enzymes, and compatible solutes accumulation. *Sustainability* 13, 3369. doi: 10.3390/su13063369

Jia, J., Huang, C., Bai, J., Zhang, G., Zhao, Q., and Wen, X. (2018). Effects of drought and salt stresses on growth characteristics of euhalophyte *Suaeda salsa* in coastal wetlands. *Phys. Chem. Earth* 103, 68–74. doi: 10.1016/j.pce.2017.01.002

Jiang, D., Fu, X., and Wang, K. (2013). Vegetation dynamics and their response to freshwater inflow and climate variables in the Yellow River Delta, China. *Quat. Int.* 304, 75–84. doi: 10.1016/j.quaint.2012.10.059

Jiao, L., Zhang, Y., Sun, T., Yang, W., Shao, D., Zhang, P., et al. (2021). Spatial analysis as a tool for plant population conservation: a case study of *Tamarix chinensis* in the Yellow River Delta, China. *Sustainability* 13, 8291. doi: 10.3390/su13158291

Khoshbakht, D., Asghari, M. R., and Haghighi, M. (2018). Influence of foliar application of polyamines on growth, gas-exchange characteristics, and chlorophyll fluorescence in *Bakraii citrus* under saline conditions. *Photosynthetica* 56 (2), 731–742. doi: 10.1007/s11099-017-0723-2

Kiarash, J. G., Amin, B., Mansour, K., and Foad, F. (2020). Combined effects of salinity and drought on physiological and biochemical characteristics of pistachio rootstocks. *Sci. Hortic-amsterdam.* 261, 108970. doi: 10.1016/j.scienta.2019.108970

Kozlowski, T. T. (1992). Carbohydrate sources and sinks in woody plants. *Bot. Rev.* 58 (2), 107–222. doi: 10.1007/BF02858600

Li, X., Xia, J., Zhao, X., and Chen, Y. (2019). Effects of planting *Tamarix chinensis* on shallow soil water and salt content under different groundwater depths in the Yellow River Delta. *Geoderma* 335, 104–111. doi: 10.1016/j.geoderma.2018.08.017

Liu, Z., Fagherazzi, S., Ma, X., Xie, C., and Cui, B. (2020a). Efficient tidal channel networks alleviate the drought-induced die-off of salt marshes: Implications for coastal restoration and management. *Sci. Total. Environ.* 749, 141493. doi: 10.1016/j.scitotenv.2020.141493

Liu, Z., Fagherazzi, S., Ma, X., Xie, C., Li, J., and Cui, B. (2020b). Consumer control and abiotic stresses constrain coastal saltmarsh restoration. *J. Environ. Manage.* 274, 111110. doi: 10.1016/j.jenvman.2020.111110

Liu, J., Xia, J., Fang, Y., Li, T., and Liu, J. T. (2014). Effects of salt-drought stress on growth and physiobiochemical characteristics of *Tamarix chinensis* seedlings. *Sci. World J.* 6, 765–840. doi: 10.1155/2014/765840

Lu, Q., Kang, L., Shao, H., Zhao, Z., Chen, Q., Bi, X., et al. (2016). Investigating marsh sediment dynamics and its driving factorsin Yellow River delta for wetland restoration. *Ecol. Eng.* 90, 307–313. doi: 10.1016/j.ecoleng.2016.01.059

Maaloul, S., Abdellaoui, R., Mahmoudi, M., Bouhamda, T., Bakhshandeh, E., and Boughalleb, F. (2021). Seasonal environmental changes affect differently the physiological and biochemical responses of two limonium species in sabkha biotope. *Physiol. Plantarum.* 172, 2112–2128. doi: 10.1111/ppl.13446

Macneill, G. J., Mehrpouyan, S., Minow, M. A. A., Patterson, J. A., Tetlow, I. J., and Emes, M. J. (2017). Starch as a source, starch as a sink: the bifunctional role of starch in carbon allocation. *J. Exp. Bot.* 68, 4433–4453. doi: 10.1093/jxb/erx291

Mao, P., Zhang, Y., Cao, B., Guo, L., Shao, H., Cao, Z., et al. (2016). Effects of salt stress on eco-physiological characteristics in *Robinia pseudoacacia* based on salt-soil rhizosphere. *Sci. Total. Environ.* 568, 118–123. doi: 10.1016/j.scitotenv.2016.06.012

McDowell, N. G. (2011). Mechanisms linking drought, hydraulics, carbon metabolism, and vegetation mortality. *Plant Physiol.* 155, 1051–1059. doi: 10.1104/pp.110.170704

Middleton, B. A., and Kleinebecker, T. (2012). "The effects of climate-change-induced drought and freshwater wetlands," in *Global change and the function and distribution of wetlands. Global change ecology and wetlands*, vol. 1 . Ed. B. Middleton (Dordrecht: Springer).

Muchate, N. S., Nikalje, G. C., Rajurkar, N. S., Suprasanna, P., and Nikam, T. D. (2016). Physiological responses of the halophyte sesuvium portulacastrum to salt stress and their relevance for saline soil bio-reclamation. *Flora* 224, 96–105. doi: 10.1016/j.flora.2016.07.009

Mushtaq, Z., Faizan, S., and Gulzar, B. (2021). Inoculation of rhizobium alleviates salinity stress through modulation of growth characteristics, physiological and biochemical attributes, stomatal activities and antioxidant defence in *Cicer arietinum* L. *J. Plant Growth Regul.* 40, 2148–2163. doi: 10.1007/s00344-020-10267-1

Nxele, X., Klein, A., and Ndimba, B. K. (2017). Drought and salinity stress alters ROS accumulation, water retention, and osmolyte content in sorghum plants. *S. Afr. J. Bot.* 108, 261–266. doi: 10.1016/j.sajb.2016.11.003

O'Brien, M., Leuzinger, , S., Philipson, C., Tay, J., and Hector, A. (2014). Drought survival of tropical tree seedlings enhanced by non-structural carbohydrate levels. *Nature Clim. Change* 4, 710–714. doi: 10.1038/nclimate2281

Ou, C., Zhang, M., Yao, X., Yang, L., Liu, Y., and Qu, C. (2019). Effects of melatonin on growth, ion absorption and photosynthesis of *Toona sinensis* seedlings under salt stress. *Acta Bot. Boreal.–Occident. Sin.* 39 (12), 2226–2234. doi: 10.7606/j.issn.1000-4025.2019.12.2226

Per, T. S., Khan, N. A., Reddy, P. S., Masood, A., Hasanuzzaman, M., Khan, M., et al. (2017). Approaches in modulating proline metabolism in plants for salt and drought stress tolerance: phytohormones, mineral nutrients and transgenics. *Plant Physiol. Bioch.* 115, 126–140. doi: 10.1016/j.plaphy.2017.03.018

Rahmstorf, S. (2007). A semi-empirical approach to projecting future sea-level rise. *Science* 315, 368–370. doi: 10.1126/science.1135456

Rangani, J., Panda, A., Patel, M., and Parida, A. K. (2018). Regulation of ros through proficient modulations of antioxidative defense system maintains the structural and functional integrity of photosynthetic apparatus and confers drought tolerance in the facultative halophyte *Salvadora persica* L. *J. Photoch. Photobio. B.* 189, 214–233. doi: 10.1016/j.jphotobiol.2018.10.021

Sala, A., Woodruff, D. R., and Meinzer, F. C. (2012). Carbon dynamics in trees: feast or famine. *Tree Physiol.* 32 (6), 764–775. doi: 10.1093/treephys/tpr143

Schuerch, M., Spencer, T., Temmerman, S., Kirwan, M. L., Wolff, C., Lincke, D., et al. (2018). Future response of global coastal wetlands to sea-level rise. *Nature* 561, 231–234. doi: 10.1038/s41586-018-0476-5

Smith, T., and Boers, N. (2023). Global vegetation resilience linked to water availability and variability. *Nat. Commun.* 14, 498. doi: 10.1038/s41467-023-36207-7

Smith, S. M., and Lee, K. D. (2015). The influence of prolonged flooding on the growth of *Spartina alterniflora* in Cape Cod (Massachusetts, USA). *Aquat. Bot.* 127, 53–56. doi: 10.1016/j.aquabot.2015.08.002

Souid, A., Bellani, L., Magné, C., Zorrig, W., Smaoui, A., Abdelly, C., et al. (2018). Physiological and antioxidant responses of the sabkha biotope halophyte *Limonium delicatulum* to seasonal changes in environmental conditions. *Plant Physiol. Bioch.* 123, 180–191. doi: 10.1016/j.plaphy.2017.12.008

Sun, B. Y., Jiang, M., Han, G., Zhang, L., Zhou, J., Bian, C., et al. (2022). Experimental warming reduces ecosystem resistance and resilience to severe flooding in a wetland. *Sci. Adv.* 8 (4), eabl9526. doi: 10.1126/sciadv.abl9526

Taherkhani, M., Vitousek, S., Barnard, P. L., Frazer, N., Anderson, T. R., and Fletcher, C. H. (2020). Sea-level rise exponentially increases coastal flood frequency. *Sci. Rep.* 10, 6466. doi: 10.1038/s41598-020-62188-4

Tomasella, M., Casolo, V., Aichner, N., Petruzzellis, F., Savi, T., Trifilò, P., et al. (2019). Non-structural carbohydrate and hydraulic dynamics during drought and recovery in *Fraxinus ornus* and *Ostrya carpinifolia* saplings. *Plant Physiol. Bioch.* 145, 1–9. doi: 10.1016/j.plaphy.2019.10.024

Watson, E. B., Szura, K., Wigand, C., Raposa, K. B., Blount, K., and Cencer, M. (2016). Sea level rise, drought and the decline of *Spartina patens* in New England marshes. *Biol. Conserv.* 196, 173–181. doi: 10.1016/j.biocon.2016.02.011

Wu, Q. (2018). *Experimental guidelines in plant physiology* (Beijing: China Agriculture Press).

Xia, J., Zhang, S. Y., Zhang, G. C., Xu, J. W., Liu, J. T., and Li, C. R. (2013). Growth dynamics and soil water ecological characteristics of *Tamarix Chinensis* Lour. forests with two site types in coastal wetland of Bohai golf. *J. Food Agric. Environ.* 11, 1492–1498.

Xia, J., Zhao, X., Ren, J., Lang, Y., Qu, F., and Xu, H. (2017). Photosynthetic and water physiological characteristics of *Tamarix chinensis* under different groundwater salinity conditions. *Environ. Exp. Bot.* 138, 173–183. doi: 10.1016/j.envexpbot.2017.03.015

Yang, H., Xia, J., Cui, Q., Liu, J., Wei, S., Feng, L., et al. (2021). Effects of different Tamarix chinensis-grass patterns on the soil quality of coastal saline soil in the Yellow River Delta, China. *Sci. Total. Environ.* 772, 145501. doi: 10.1016/j.scitotenv.2021.145501

frontiers | Frontiers in Marine Science

TYPE Original Research
PUBLISHED 08 September 2023
DOI 10.3389/fmars.2023.1245513

OPEN ACCESS

EDITED BY
Milko Alberto Jorquera,
University of La Frontera, Chile

REVIEWED BY
Shiyuan Ding,
Tianjin University, China
Ying Yang,
Dongguan University of Technology, China

*CORRESPONDENCE
Yan Xu
grawain007@163.com

RECEIVED 23 June 2023
ACCEPTED 22 August 2023
PUBLISHED 08 September 2023

CITATION
Xu Y, Huo X, Jordán F, Zhou M, Cai Y and Sun J (2023) Identifying marine food web homogenization patterns. *Front. Mar. Sci.* 10:1245513. doi: 10.3389/fmars.2023.1245513

Identifying marine food web homogenization patterns

Yan Xu[1,2]*, Xumeng Huo[1], Ferenc Jordán[3], Mingliang Zhou[1], Yanpeng Cai[4] and Jun Sun[1]

[1]College of Marine Science and Technology, China University of Geosciences, Wuhan, China, [2]John von Neumann Faculty of Informatics, Biomatics and Applied Artificial Institution, Óbuda University, Budapest, Hungary, [3]Department of Chemistry, Life Sciences and Environmental Sustainability, University of Parma, Parma, Italy, [4]Guangdong Provincial Key Laboratory of Water Quality Improvement and Ecological Restoration for Watersheds, Institute of Environmental and Ecological Engineering, Guangdong University of Technology, Guangzhou, China

Ecosystems become increasingly similar to each other, based on species composition. Despite the inevitability of homogenized ecosystems due to global change, few studies have specifically addressed the identification of homogeneous systems in food webs. This study focuses on identifying different patterns of marine food web homogenization by selecting 41 marine food webs and establishing an indicator system. The research classifies the food webs into seven main types based on three different homogenization processes (I, II, III, IV, V, VI, and VII), with approximately 60.1%, 46.3%, and 61% of the homogenization being structural, functional, and resource homogenization, respectively. It highlights the importance of homogenization processes in marine ecosystems, which are mainly driven by interactions between structural and resource homogenization. The research found that Type V exhibited universality in both temporal and spatial dimensions, while Type III also showed universality when the food webs were dominated by resource homogenization. On the other hand, Type I, which was associated with human activities, showed locality when the food web only manifested structural homogenization. Functional homogenization often occurred alongside structural homogenization, as seen in Type IV and Type VII. Yet, when the food web exhibited functional homogenization (Type II), it was directly linked to human activities over the past 20 years. The research aimed to improve the methodology in terms of (a) identifying different food web homogenization patterns; (b) establishing indicators system to quantify food web homogenization; and (c) clarifying the ecological significance of food web homogenization. The study provided a comprehensive understanding of food web homogenization and its associated risks, which could inform nature-based ecosystem management strategies to mitigate the impacts of future climate change.

KEYWORDS

food web, homogenization, indicators, structure and function, resources, marine ecosystem

1 Introduction

Ongoing climate change the behavior, reproduction and phenology of many species (Descamps et al., 2019). Some need to change their area and invade new habitats. Together with human-generated introductions, seriously reshuffle species distributions, resulting in homogenization (Lövei, 1997). Altered species composition results in changes in interspecific interactions and, ultimately, the structure and functioning of ecosystems worldwide. Invading species and novel interactions rewire food webs (Bartley et al., 2019). Evidence suggests that this rewiring is creating a novel heterogeneity, resulting in asymmetries and mismatches to physical and abiotic properties (Lehikoinen et al., 2019; Rathore et al., 2020). This heterogeneity is causing structural variations in ecosystems, which in turn affects the link configuration and node features of food web networks (Gonzalez et al., 2020; Schell et al., 2020). Kortsch et al. (2015) detects that the expansion of the sub-network module size dominated by generalist species has increased network connectance and reduced modularity in the Barents Sea (Kortsch et al., 2015). A few generalist and often cosmopolitan species may be involved in a large number of inter-specific interaction, either as prey or predator, host or parasite (Scott and Helfman, 2001). These ubiquitous changes made to networks may result in novel topologies, for example, make them more similar to scale-free networks, with characteristics such as preferential attachment and high clustering coefficient. It will result in both high vulnerability and robustness in a food web (Barabási and Bonabeau, 2003). This process is known as food web homogenization (in terms of topology, beyond homogenization in terms of species composition) and simplifies the interrelationships within the network (Dunne et al., 2004). This reflects the ecological homogenization problem at the food web level, which has been the subject of increasing reports in recent decades. Magurran has proposed that the biotic homogenization phenomenon of fish communities in the North Atlantic reflects community feedback to ocean temperature changes (Magurran et al., 2015). The issue of biotic homogeneity is not limited to one aspect of ecosystems, but rather is widespread throughout various stages. It can be seen in various instances such as the occasional mixing of taxa through paleontological records, breakdown of biogeographic fauna, and genetic similarities in freshwater and terrestrial ecosystems (Olden et al., 2004; Olden, 2006). Biotic homogenization can be classified into three types: genetic, taxonomic, and functional, which explain how homogenization occurs at the molecular, individual, and population levels (Clavel et al., 2011). While homogenized ecosystems are believed to be an inevitable result of global change (Lövei, 1997; Hobbs et al., 2009; Groffman et al., 2014), there has been little research on how homogenization is expressed in food webs and the identification of different types of homogenization processes.

Food web homogenization (FwH) is a phenomenon that reflects several state characteristics of an ecosystem (Rooney and McCann, 2012). One of these characteristics is topological simplification, which occurs when the complexity of the network decreases due to species loss (reduced number of nodes). But beyond the size of the network (in terms of the number of nodes), topology can be simplified in other ways, including connectivity density and network diameter reduction. Several mechanisms may lead to an increased similarity in link structure and reduced network modularity. This structural dynamic is mainly caused by a biotic homogenization process and can result in alterations in interspecific interactions (Cazelles et al., 2019). It is probably presented as a series of network topology problems, such as network sparsification, network path length reduction, network hierarchy flattening and reduced average mutual information in the network (Ulanowicz, 2004). Functional non-redundancy is one of the manifestations of FwH (see also Heymans et al., 2014), where multiple species have similar ecological roles and functions in the food web, leading to increased competition in the ecosystem. Additionally, FwH can also lead to resource centralization, where middle and low-level species occupy core importance, resulting in the formation of hub resource nodes and making the system more vulnerable to directional disturbances (somewhat similarly to an agro-ecological monoculture, in an extreme case, where disturbing the crop species may result in the collapse of the whole system). Phenotypic differences in state characteristics can lead to various ecosystem risks, including biodiversity decline, nutrient cycling imbalances, and eutrophication (Schiettekatte et al., 2020; Obura et al., 2021; Geng et al., 2022). Therefore, it is important to identify the types of food web homogeneity in order to explore systematic risks.

Combined with previous research, biotic homogenization can be characterized by several indicators in the literature (Wang et al., 2021). β-biodiversity can indicate the spatial heterogeneity of the community (Willig et al., 2023), and the Sørensen dissimilarity index (β_{SOR}) is commonly used in ecological research to compare the spatial differentiation between communities (Musseau et al., 2022). The Jaccard index is typically used to calculate compositional similarity excludes joint absence (Fraser et al., 2022), while the Bray-Curtis Similarity index or Morisita's index is applied to measure relative abundance data (Olden and Rooney, 2006; Knop, 2016). Food web homogenization, on the other hand, is different from biotic homogenization in the general sense, as it includes the connotation of biotic homogenization, but is considered a more detailed elaboration of the complexity of the network object.

Due to the relatively narrow range of demands on primary producers in marine food webs, there is a higher risk of food web homogenization. In this research, we aimed to identify various patterns of homogenization in marine food webs. We selected 41 marine food webs and established an indicator system to classify them into 7 main types (I, II, III, IV, V, VI, and VII) based on 3 different homogenization processes (structural, functional, and resource homogenization). We recorded specific information for each food web, such as latitude, sampling time, and the total number of nodes and links. We used complex network methods to calculate relevant network indicators and established thresholds for these indicators. Finally, we calculated correlations between indicators. This study aims to enhance the methodology in terms of (a) identifying different food web homogenization patterns; (b) establishing an indicator system to quantify food web homogenization; and (c) clarifying the ecological significance of food web homogenization. The work will provide a comprehensive concept of food web homogenization and improve our

understanding of the risks associated with homogenizing systems, which will contribute to the development of nature-based ecosystem management countermeasures against future climate change.

2 Methods

2.1 Classification of food web homogenization

Based on the state characteristics of food webs depicted in Figure 1, we categorized food web homogenization into three types. (a) Structural Homogenization (SH), which refers to a topological simplification process in food webs resulting in a decrease in complexity. From the perspective of complex networks, apart from a reduction in the number of nodes or links, this process is predominantly reflected in the issue of decreased modularity. The degree of network modularity is directly proportional to the structural complexity of a network. Therefore, if a network has a high number of nodes and links but few aggregated sub-net modules, it implies that the network structure follows a simple cascading relationship and lacks complex network characteristics such as small-worldness, self-organization, or scale-free properties.

(b) Functional homogenization (FH). It represents ecological functional non-redundancy in food webs, which includes a decline of niche overlap or functional diversity. Each species and predator-prey linkages in a food web perform different ecological functions. For example, top predators can directly affect connected prey and indirectly impact basal-species, leading to a trophic cascade (Soler et al., 2015). The functional diversity of species interactions is significantly and positively related to ecosystem stability (Gonzalez et al., 2020). Numerous functionalized redundancy groups can enhance the system's resistance against random disturbances.

(c) Resources homogenization (RH) refers to a process of resource centralization in food webs. The primary producers in aquatic ecosystems have a relatively unitary composition pattern. In the ocean, phytoplankton is the sole source of primary productivity in oligotrophic regions. In some freshwater lakes affected by human activities, the decline in biomass of benthic organisms and zooplankton, which are prey resources for higher trophic-level species, has resulted in a food web that depends solely on a monodominant resource group for material and energy supply (it referred to a special case of FH).

2.2 Quantifying the food web homogenization

In section 2.1, we used various indicators to quantify FwH. To measure network complexity, we relied on modularity, a key index for structural homogenization. The modularity of a food web is determined by the degree of clustering between nodes. A higher degree of modularity indicates that nodes in the food web tend to form closely connected modules or functional blocks, with relatively fewer connections between modules. Research has demonstrated that modularity is strongly linked to food web complexity (Montoya et al., 2015). For directed networks, we used the Newman-Girvan modularity approach (Newman, 2004), considered a density-based modularity approach (Guimerà et al., 2010). It is a network aggregation method within the complex networks field (Giacomuzzo and Jordán, 2021). To determine the total number of modules, we applied an extension of the Leiden algorithm (Traag et al., 2019). It solved the problem of arbitrarily connected and disconnected communities, which is expressed by the following equation:

$$Q = \frac{1}{L}\sum_{ij}(A_{ij} - \frac{k_i^{in}k_j^{out}}{L})\delta_{m_i m_j} \quad (1)$$

where Q represents the network modularity; L is referred to the total number of links; A_{ij} is the adjacency matrix of the food web; k_i^{in} represents the in-degree of node i; k_j^{out} is the out-degree of node j; δ_{mimj} represents the Kronecker delta for module i and j, which provides a succinct encoding of the graph information (Kozen and Timme, 2007). We utilized the R package igraph to calculate food web modularity (https://r.igraph.org/).

In addition, for functional homogenization, we treated interaction profile diversity (IPD) as an indicator to quantify functional diversity or redundancy, reflected heterogeneity in ecosystem traits. We used a network-based measure of functional

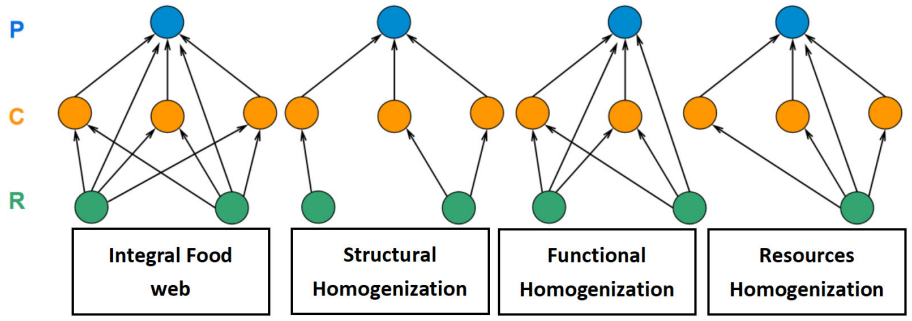

FIGURE 1
The diagrammatic sketch of food web homogenization. Blue nodes referred to the predator; orange nodes referred to the consumer; green nodes referred to the resource.

diversity, based on the positive and negative effects of species *i* and *j* up on *n* steps (i.e. $E_{ij,n}^{+}$, $E_{ij,n}^{-}$) and applied the complementary Marczewski-Steinhaus index to quantify the dissimilarity of species interactions (Lin et al., 2022). Apart from Rao's quadratic entropy method (Botta-Dukát, 2005), the IPD method, which is a network-based approach, calculates the average dissimilarity between two interaction profiles, and the IPD value increases with the higher functional diversity in the food web. The related equations are listed below:

$$E_{ij,n}^{+} = \frac{1}{n}(a_{ij,1}^{+} + a_{ij,2}^{+} + \ldots + a_{ij,n}^{+}) \tag{2}$$

$$E_{ij,n}^{-} = \frac{1}{n}(a_{ij,1}^{-} + a_{ij,2}^{-} + \ldots + a_{ij,n}^{-}) \tag{3}$$

$$d_{ij} = \frac{\sum_{k=1}^{N}\left|E_{ik}^{+} - E_{jk}^{+}\right| + \sum_{k=1}^{N}\left|E_{ik}^{-} - E_{jk}^{-}\right|}{\sum_{k=1}^{N}\max\left\{E_{ik}^{+}, E_{jk}^{+}\right\} + \sum_{k=1}^{N}\max\left\{E_{ik}^{-}, E_{jk}^{-}\right\}} \tag{4}$$

$$IPD = \frac{\sum_{i=1}^{N}\sum_{j>i}^{N} d_{ij}}{(S^2 - S)/2} \tag{5}$$

where $a_{ij,n}$ represents the n-step effect of species i on species j, in this research, n is assigned 3. d_{ij} represents dissimilarity of interaction profiles for species *i* and *j*, which ranges from 0 to 1, and large d_{ij} referred to high dissimilarity. *S* represents the total number of species nodes. When the IPD is small, it indicates fewer interactions in the network, resulting in lower functional diversity within the system, thereby potentially giving rise to functional homogenization issues.

To ensure consistency in identifying resource nodes, it is important to recognize that in a food web, not only the basal species with a k_i^{in} value of 0 are considered as resources. Primary or secondary consumers such as Antarctic krill (*Euphausia superba*) are also included. Therefore, for the purpose of this research, we define resource nodes as those with an out-degree significantly greater than their in-degree ($k_i^{out} > k_i^{in}$). To achieve this, we propose using the parameter *dk*.

$$dk = \frac{k_i^{in}}{k_i^{out}} \quad 0 \le dk < 1,\ k_i^{out} \neq 0 \tag{6}$$

where *dk* represents the ratio of out-degree and in-degree with species *i*. When *dk* equals 0, it referred to the node as basal species. When a node in a food web has an in-degree smaller than the out-degree, i.e., *dk* is less than 0.5, it indicates that the node is more often utilized as a food resource by other nodes, while it shows relatively lower preferences in selecting other nodes as food resources. In the ecological context, this suggests that the node plays a prominent role as a prey, being more frequently preyed upon by other nodes, thus qualifying it as a resource node. Correspondingly, when *dk* is below 0.25, to be specific, over 75% of the links are associated with predation relationships involving the node, positioning it in the upper quartile of the total link count. This considerable number implies that the majority of predators preferentially choose this node as a food resource. Therefore, we defined a resource node when *dk* is below 0.5 and a core resource node when *dk* is below 0.25.

The importance of resource nodes increases significantly during the homogenization process, which determines by resource dependence. However, calculating metrics like node importance or centrality alone cannot fully capture the phenomenon of resource homogenization. Resource homogenization is best reflected when a small number of nodes with high keystoneness and importance are targeted by multiple predators in the network (Gouveia et al., 2021). It results in a concentrated being-preyed relationship in the minority nodes. A power law distribution in the out-degree of a network can indicate a resource homogenization process (Stivala et al., 2020). In our study, we utilized the Kolmogorov–Smirnov (KS) test to verify the power law distribution for a food web (Kovalev and Utkin, 2020). We obtained the R-squared, *pk(out)*, value through the maximum likelihood estimation (MLE) approach (supplementary material). The igraph R package (https://r.igraph.org/) was used for the relevant analyses. If the fitting value *pk(out)* of the output degree distribution of the network is greater than 0.9, it indicates that the network is experiencing a serious issue with resource homogenization.

2.3 Identifying food web homogenization patterns

In real food webs, certain changes may lead to the occurrence of all three types of food web homogenization processes simultaneously. In order to better assess the vulnerability of the ecosystem, it is important to identify homogenization patterns. We propose the following equation:

$$FwH = f(SH, FH, RH) \tag{7}$$

In a real ecosystem, the function f here is difficult to fit, which may require more related work to seek to find the appropriate function. Our hypothesis is that food web homogenization can be viewed as a superposition of these three processes, and relevant indicators can be used to comprehensively identify homogenization patterns in real food webs.

$$FwH = SH + FH + RH \tag{8}$$

where *FwH* represents the comprehensive effects of food web homogenization; *SH* represents the effects of structural homogenization; *FH* represents the effects of functional homogenization; *RH* represents the effects of resource homogenization. According to different permutations and combinations of the three homogenization types, the FwH consists of 7 types. Each type includes 3 levels of FwH intensity by assigning values to three different indicators, such as serious (S), intermediate (I), and ordinary (O). The thresholds for each indicator are calculated based on the food web data in the database we are building, which is determined using percentiles according to the data distribution type and data characteristics. Our

database has collected 115 marine food web data sets from around the world, all of which have complete data. For this paper, we randomly selected 41 food webs from this database. Thus, we established the methods to identify food web homogenization processes integrally, as shown in Table 1.

2.4 Real food web data

We investigated several databases (e.g., EcoBase, http://ecobase.ecopath.org/) and literature (http://www.isiknowledge.com), and randomly acquired 41 marine food webs to identify food web homogenization patterns. These food webs cover different types of marine ecosystems (including estuaries, coastal zone, coral reefs, etc.). Detailed information is listed in the supplementary material. We collected the timeframe during which the authors mentioned in the published articles were actively collecting data, specifically, the time when these food web data were sampled in their natural habitat. As the publication time of literature frequently differs from the actual sampling time, we adopt the latter as a representation of the food web's state at that specific moment. Ideally, we would need long time series of food webs to follow the temporal dynamics within local ecosystems, but data are quite scarce for this.

3 Results

3.1 Network modularity (Q)

In our study, we calculated the network density-based modularity (Q) of 41 marine food webs using equation (1). We then used the Spearman coefficient to analyze the correlation between Q and related network parameters, such as S, L, time, and module. We found that 60.9% of marine food webs had low network modularity (Q<0.1). Our analysis, as shown in Figures 2A, B, revealed that there was no strong correlation between network modularity and network size (Q~S: cor=-0.103; Q~L: cor=-0.164), but a weak negative correlation existed. It supports our hypothesis that there is no direct relationship between network size and the formation of structural homogenization. According to Figures 2A, B, food webs with smaller network sizes generally appear to be more susceptible to severe SH. However, in the case of small size but highly modular food webs, the risks of SH can be effectively mitigated. Furthermore, in larger-scale food webs, although there still exists a certain level of risk (close to the red line), the formation of severe SH becomes more challenging. In comparison to the time of food web data acquisition, approximately 66.7% of marine food webs recorded low modularity after the year 2008, as seen in Figure 2C. It represents an increase of around 31.8% compared to

TABLE 1 The main indicators to identify different food web homogenization patterns.

Types	*Q*	*IPD*	*pk(out)*	Levels	FwH patterns
I	≤0.01	>0.6	<0.6	Serious (S)	*SH*
	≤0.05	>0.6	<0.6	Intermediate (I)	
	≤0.1	>0.6	<0.6	Ordinary (O)	
II	>0.1	≤0.2	<0.6	Serious (S)	*FH*
	>0.1	≤0.4	<0.6	Intermediate (I)	
	>0.1	≤0.6	<0.6	Ordinary (O)	
III	>0.1	>0.6	≥0.9	Serious (S)	*RH*
	>0.1	>0.6	≥0.8	Intermediate (I)	
	>0.1	>0.6	≥0.6	Ordinary (O)	
IV	≤0.01	≤0.2	<0.6	Serious (S)	*SH+FH*
	≤0.05	≤0.4	<0.6	Intermediate (I)	
	≤0.1	≤0.6	<0.6	Ordinary (O)	
V	≤0.01	>0.6	≥0.9	Serious (S)	*SH+RH*
	≤0.05	>0.6	≥0.8	Intermediate (I)	
	≤0.1	>0.6	≥0.6	Ordinary (O)	
VI	>0.1	≤0.2	≥0.9	Serious (S)	*FH+RH*
	>0.1	≤0.4	≥0.8	Intermediate (I)	
	>0.1	≤0.6	≥0.6	Ordinary (O)	
VII	≤0.01	≤0.2	≥0.9	Serious (S)	*SH+FH+RH*
	≤0.05	≤0.4	≥0.8	Intermediate (I)	
	≤0.1	≤0.6	≥0.6	Ordinary (O)	

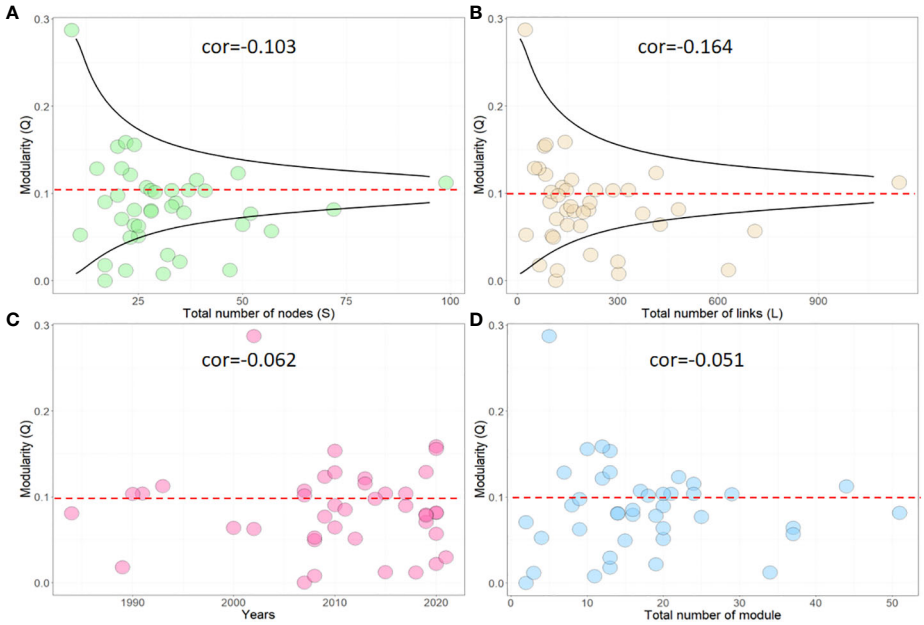

FIGURE 2
Correlation between network modularity (*Q*) and other network parameters, including **(A)** total nodes (*S*), **(B)** total links(*L*), **(C)** time, and **(D)** modules. cor represents the Spearman correlation coefficient.

the proportion of low-*Q* food webs recorded before 2008, indicating the widespread nature of SH issues. It is worth noting that network modularity does not appear to have a significant correlation with the number of modules (*Q*~modules: cor=-0.051). However, about 80% of food webs with a high number of modules (modules number>30) have been identified as having a low-*Q* value, as shown in Figure 2D.

3.2 Interaction profile diversity

We calculated the IPD index of 41 food webs to assess their functional redundancy. We used the Spearman coefficient to determine the correlation between IPD and related network parameters, including *S*, *L*, time, and network diversity (Supplementary material). Our results showed that approximately 46.3% of marine food webs had low functional diversity (IPD<0.6). As illustrated in Figures 3A, B, IPD demonstrated a moderate and weak positive correlation with network size (IPD~*S*: cor=0.402; IPD~*L*: cor=-0.131). These findings are consistent with the correlation analysis results of Jordán et al. (Lin et al., 2022), and suggest that large-scale networks are more likely to form redundant functional modules, which can significantly reduce the risk of functional homogenization. For food webs with smaller network sizes, the risk of FH is higher (below the red line). It implies that there may be an inherent link between the factors driving FH formation and the decline in biodiversity. Based on the findings presented in Figure 3C, it can be observed that the temporal evolution pattern of IPD displays a certain degree of randomness. It should be noted that this variability does not exhibit a consistent trend across global marine ecosystems. Additionally, when the food web is considered as an undirected network, the network diversity was found to have a slightly positive correlation with IPD, as shown in Figure 3D.

3.3 Distinguishing resources node and calculating pk(out) value

We also analyzed 41 food webs and calculated their *pk(out)* values, as well as identified the resource nodes in each web. To explore the relationship between *pk(out)* and other network parameters, such as *S*, *L*, time, and the total number of core resource nodes (when *dk*<0.25), we used the Spearman coefficient. We found that approximately 61.1% of marine food webs had a high *pk(out)* value (*pk(out)*>0.6), indicating a common issue of resource centralization in marine ecosystems. Our analysis also revealed that *pk(out)* had a moderate positive correlation with network size (*pk(out)*~*S*: cor=0.352; *pk(out)*~*L*: cor=0.212), but only a weak correlation with temporal dynamics (cor=-0.137), Figures 4A-C. Interestingly, we observed that about 53.3% of food webs had high *pk(out)* values after the year 2008. However, this figure was 81.8% before 2008, representing a decrease of approximately 34.6%, Figure 4C. Finally, core resource nodes (dk<0.25) express a weak positive correlation with the goodness of fit between the out-degree distribution and the power-law distribution (cor=0.282), Figure 4D. These findings suggest that resource centralization is a widespread phenomenon in marine food webs, and that network size and time may play important roles in shaping network structure.

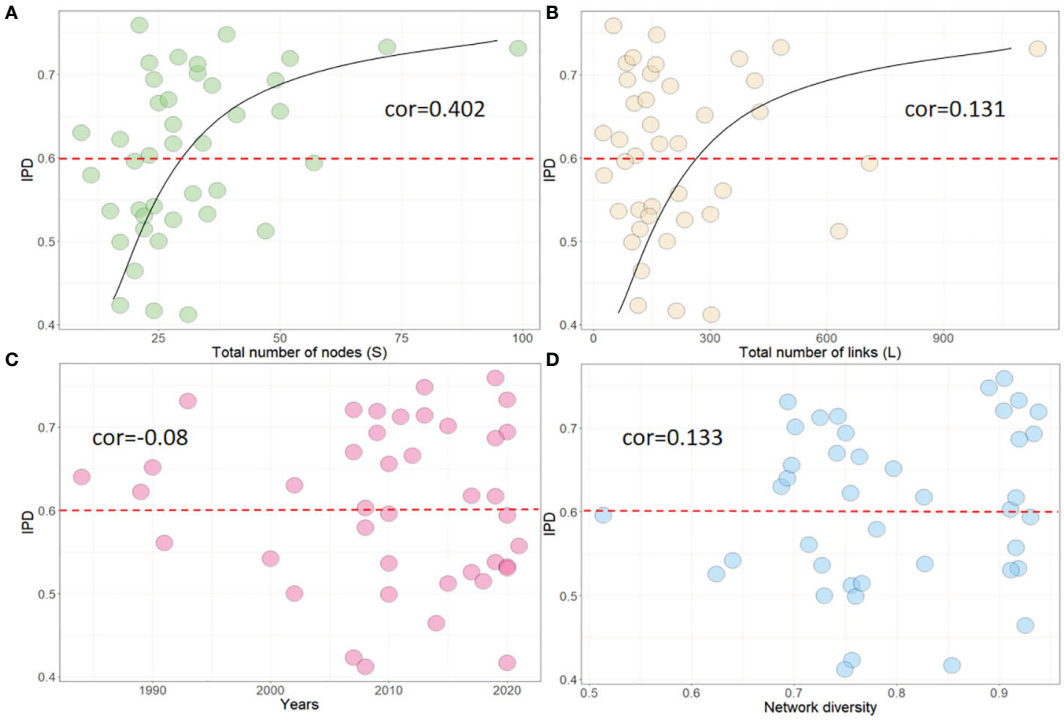

FIGURE 3
Correlation between IPD and other network parameters, including **(A)** total nodes (*S*), **(B)** total links(*L*), **(C)** time, and **(D)** Network diversity. cor represents the Spearman correlation coefficient.

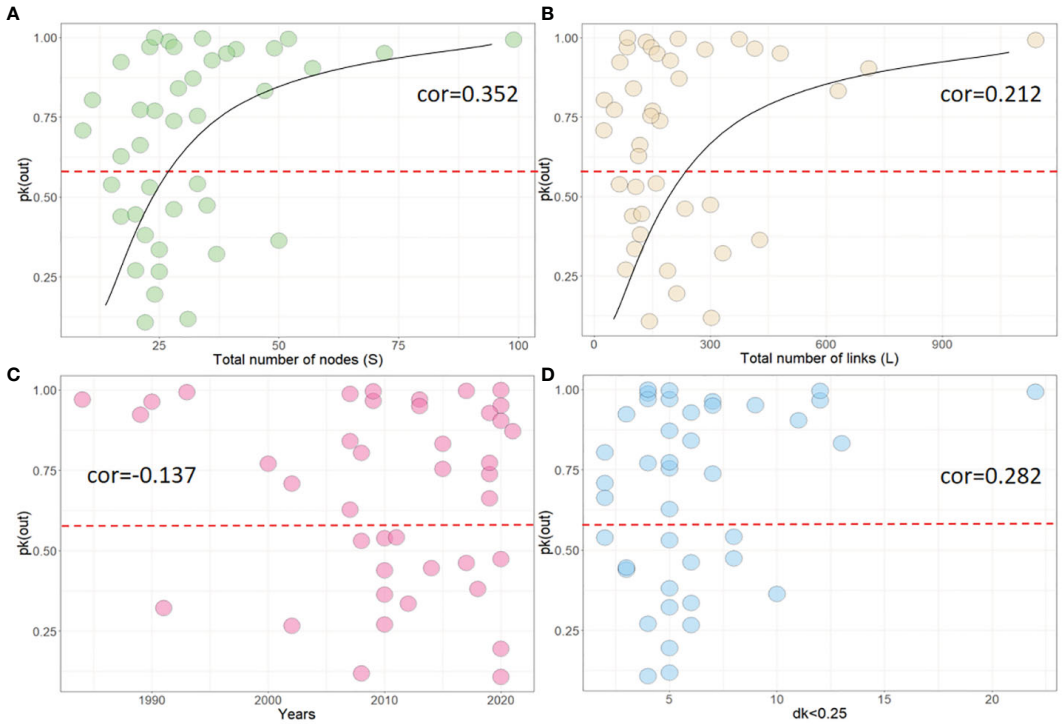

FIGURE 4
Correlation between pk(out) and other network parameters, including **(A)** total nodes (*S*), **(B)** total links(*L*), **(C)** time, and **(D)** total number of nodes which *dk*<0.25. cor represents the Spearman correlation coefficient.

3.4 Identifying food web homogenization patterns

According to section 2.3, we were able to identify FwH patterns in 41 marine food webs. Our analysis revealed that 9.56% of food webs fell under type I, showing only SH; 12.1% were classified as type II, showing only FH; 26.8% were categorized as type III, showing only RH; and approximately 17.1% of food webs were classified as type IV (SH+FH), V (SH+RH) and VII (SH+FH+RH), as shown in Figure 5A. We also found that only 7.3% of food webs were in the process of intermediate food web homogenization (I), with types I, III, and V being the most common. Furthermore, we found that all food webs that exhibited serious homogeneity problems were classified as type III. In summary, the proportion of FwH related to SH, FH, and RH are approximately 60.1%, 46.3%, and 61% relatively. It believes that marine ecosystems have a higher probability of undergoing food web homogenization processes involving SH and RH.

Additionally, we also calculated the correlation among *Q*, IPD, and *pk(out)*, as shown in Figures 5B-D. Our findings suggest that IPD has a moderate and strong positive correlation with *Q* and *pk (out)*, respectively (*pk(out)*~IPD: cor=0.646; *Q*~IPD: cor=0.382). However, *Q* shows a weak positive correlation with *pk(out)* (cor=0.098). By using different colored scatter points, we were able to distinguish the different types of FwH, which were located in different graphic orientations. Among these, Figure 5D was the most intuitive. Type III was consistently located in the upper-right of the graph. Therefore, one can roughly differentiate the food web homogenization pattern of a specific study area by calculating the food web IPD and *pk(out)* values, especially for type I and VII. Yet, to accurately identify FwH patterns, it is still necessary to use the methods provided in this research.

Finally, we examined the distribution of FwH patterns over time and space. We classified marine ecosystems into two categories based on the degree of human impact: significantly human-impacted (S-HI) and insignificantly human-impacted (I-HI). Ecosystems such as nearshore seas, coastal zones, estuaries, and coral reefs were classified as S-HI, while pelagic regions and polar areas were classified as I-HI. Our findings, as shown in Figure 6A, indicate that Types III and V of FwH patterns are present in every latitude belt globally, indicating their ubiquity in marine ecosystems. Type I ecosystems are exclusively found in mid-low latitude regions of the Earth and are only composed of ecosystems belonging to the S-HI category. It suggests that human activities are responsible for the formation of type I ecosystems and they exhibit localized characteristics. In contrast, FwH is more likely to occur in mid-low latitudes while FwH in high latitudes is consistently associated with RH, supporting the high-latitude dominance hypothesis of food webs (Unpublished paper). Types III and V are observed to occur over longer periods than other types, emphasizing their ubiquity in marine ecosystems. Coincidentally, the timeline shows similarities between Type I and Type II ecosystems. Since 2008, Type II ecosystems have consistently been composed of the S-HI category, indicating significant human impact on both types. Overall, the frequency of FwH occurrences has increased in recent decades, potentially due to global climate change and human activities.

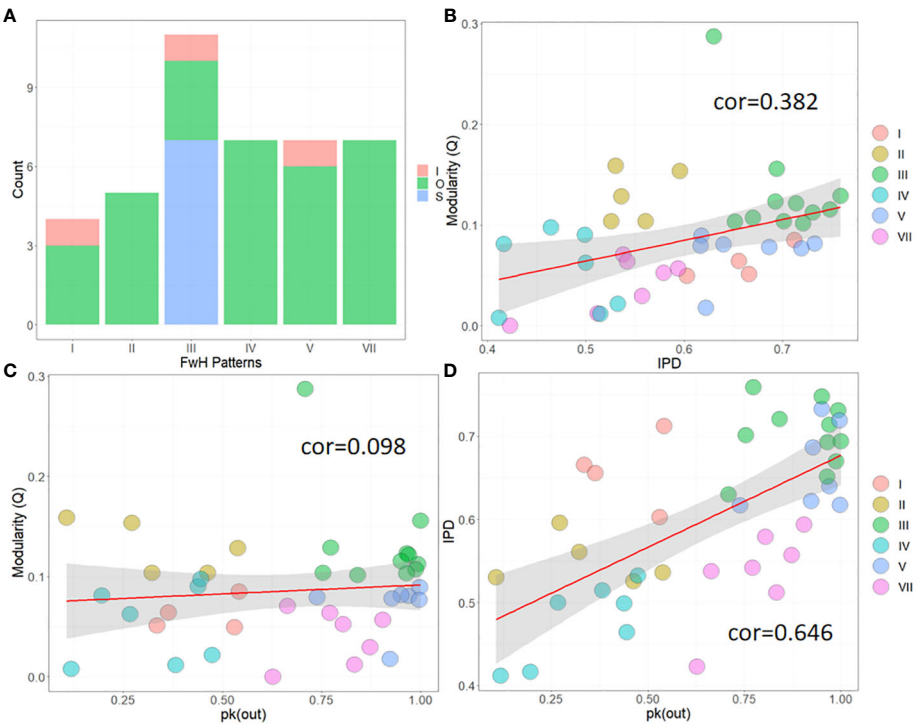

FIGURE 5
Statistical graph of FwH patterns. **(A)** the number of different FwH types; **(B)** Correlation between *Q* and IPD; **(C)** Correlation between *Q* and *pk(out)*; **(D)** Correlation between IPD and *pk(out)*. Scatter points of different colors represent different FwH types.

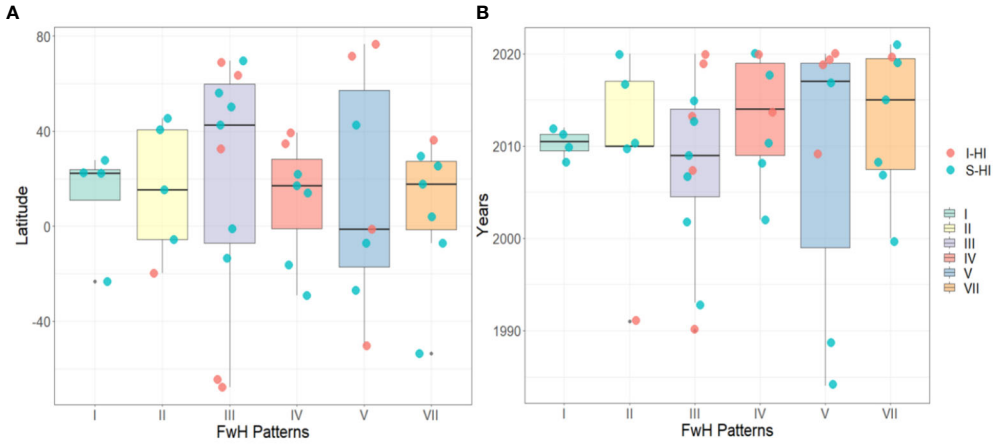

FIGURE 6
(A) Spatial and **(B)** temporal distribution of FwH patterns. Scatter points represent the two categories of marine ecosystems based on the degree of human impact: significantly human-impacted (S-HI) and insignificantly human-impacted (I-HI).

4 Discussion

This study aimed to identify different patterns of marine food web homogenization by analyzing 41 marine food webs and developing an indicator system to quantify the different patterns of FwH. The research classified the FwH into three main types, which are structural homogenization (SH), functional homogenization (FH), and resource homogenization (RH). The network indicators, including *Q*, IPD, and *pk(out)*, were calculated, and different thresholds were assigned to determine 7 types of FwH. Each type contained 3 levels (i.e., S, I, O). The study found that SH has a relationship with the network size of a food web, whereas the formation of FH is not a common occurrence in marine ecosystems and accounts for only 46.3%. In contrast, RH is present on both temporal and spatial scales universally. In conclusion, the frequency of FwH occurrences had increased in the past decades, which could be strongly linked to global climate change and human activities.

In real food webs, these three types of homogenization processes often occur simultaneously. Especially for SH and RH, a higher number of network nodes and links tend to form more sub-networks than others, where the interactions between these sub-networks are typically weakly connected, which enhances the modularity. Thus, increasing the overall stability of the food web (Grilli et al., 2016), as depicted by the upper half of the red dashed line in Figures 2A, B. On the other hand, when there is an excessive number of network nodes and links, because of resource dependence, a large number of upper-level nodes require more resources to sustain their life activities (Barton et al., 2019). These interactions with the core resource nodes (dk<0.25) often lead to the formation of large modules centered around core resource nodes, where numerous connections link to these core resource nodes, resembling a scale-free network structure, as shown by the upper half of the red dashed line in Figures 4A, B. Such networks are often characterized by ecological vulnerability, where perturbations in these networks are likely to result in irreversible ecological risks (Di Mauro et al., 2022). Therefore, as revealed by this study, the homogenization processes of food webs driven by the interactions between SH and RH play a significant role in the natural evolution of marine ecosystems. This might have implications related to the adaptability of these marine ecosystems to global change.

When biodiversity increases to a certain extent, it hinders the formation of SH, as illustrated by the lower half of the red dashed line in Figures 2A, B. However, when biodiversity surpasses a certain ecological threshold, it will lead to the emergence of core resource nodes and the occurrence of the RH issue within the food web. These processes may alternately occur during the ecosystem evolution, which explained why type V, predominantly influenced by both SH and RH, exhibits universality in both temporal and spatial dimensions (Figure 6). Furthermore, the FwH is driven by a single factor of RH, also exhibits universality (Type III), and some food webs even show a serious tendency (S) towards FwH. It is mainly due to the unique characteristics of marine ecosystems. In marine ecosystems, primary producers are relatively uniform and primarily composed of photoautotrophic phytoplankton (Casabianca et al., 2021). In oligotrophic marine areas across the globe, acquiring and sustaining the necessary nutrients for the survival of phytoplankton poses a challenge (Rodríguez-Gómez et al., 2022). Thus, resources become the primary competitive factor, shaping high out-degree nodes, as shown in Figure 4D. When the network size is larger, this phenomenon is more significant. On the other hand, the FwH driven by a single factor of SH shows locality conversely (Type I) and is associated with human activities (Figure 6). Unlike the natural evolution of ecosystems, human activities often lead to instantaneous disruptions in food webs (Wilkinson et al., 2021). If a food web itself has not developed strong stability (highly modular functional groups characterized by weak interactions), it is highly susceptible to module disintegration effects. In such cases, the system has not fully evolved adaptive strategies or redundant functional

groups for self-restoration, resulting in structural adjustments (Brose et al., 2019). Severe disturbances can cause the ecosystem to regress to its early evolutionary stage, characterized by the proliferation of generalist species and the formation of SH.

The process of functional homogenization (FH) often accompanies the occurrence of structural homogenization (SH), such as type IV and type VII. It is because the functional overlap is typically positively correlated with the degree of structural modularity, as shown in Figure 5B. When the FwH is driven by a single factor of RH (Type II), which basically consists of ecosystems sensitive to human activities (S-HI) and has been recorded concentratedly in the last 20 years, as depicted in Figure 6. Biologically, it should be related to the interaction of gradient and functional features (Stuart-Smith et al., 2013). Without altering the network structure, the decrease in IPD is directly associated with the sparsification of network interactions. Since IPD is trait-based, this sparsification of functional groups enhances network robustness, which also explains the significant positive correlation between IPD and *pk(out)*, as shown in Figure 5D. In general, the sparsification of functional groups is temporary, but human activities often maintain this stage in a stable manner (e.g., the vulnerability of agricultural and urban ecosystems) (Cannistraci et al., 2013). Changes in human decision-making and management concepts regarding nature may produce different effects. It can be concluded that Type III is more amenable to restoration through human attention to natural sustainability than others. We think that these results may support decision-making in future fisheries management, following better tests on these proposed indicators.

Although Type VI was not observed in the randomly sampled real food web data, it could not be concluded that it does not occur in real networks. Future research will address this issue. It is important to note that the method used in this study is a static computational approach, and more investigation is needed to determine if dynamic models can effectively identify homogenization in food webs. Additionally, long time series data is necessary to support food web data. The findings of this study can contribute to a greater focus on food web homogenization and enhance the theoretical foundation for systematic ecological conservation.

5 Conclusion

Based on the research findings, it can be concluded that the proportion of FwH related to SH, FH, and RH were approximately 60.1%, 46.3%, and 61% respectively. It implies that marine ecosystems have a higher probability of undergoing food web homogenization processes involving SH and RH. The research found that Type V, which was mainly influenced by both SH and RH, exhibited universality in both temporal and spatial dimensions, while Type III also showed universality when the food webs were dominated by RH. Conversely, Type I, which was associated with human activities, showed locality when the food web only manifested SH. The study also found a moderate positive correlation (cor=0.382) between IPD and *Q*, indicating that FH often occurred alongside SH like type IV and type VII. When the FwH is driven by a single factor of RH (Type II), which basically consists of ecosystems sensitive to human activities (S-HI) and has been recorded concentratedly in the last 20 years. In summary, FwH is more likely to occur in mid-low latitudes, while FwH in high latitudes is consistently associated with RH, which indirectly supports the high-latitude dominance hypothesis of food webs. The frequency of FwH occurrences has increased in the past decades, which is possibly linked to global climate change and human activities. Our work provided a comprehensive concept of food web homogenization and improved the understanding of homogenized system risks, which contributed to the development of nature-based ecosystem management countermeasures against future climate change.

Data availability statement

The original contributions presented in the study are included in the article/Supplementary Material. Further inquiries can be directed to the corresponding author.

Author contributions

YX conceived the ideas, designed methodology, and led the writing of the manuscript. XH collected and analyzed the data. FJ led the revision of the manuscript. MZ visualized data. YC performed validation. JS contributed to the discussion. All authors contributed critically to the drafts and gave final approval for publication.

Funding

This research was supported by: National Natural Science Foundation of China (No. 42277470), Open fund of Key Laboratory of Ecological Prewarning, Protection and Restoration of Bohai Sea, Ministry of Natural Resources (No. 2022106), Foundation of State Environmental Protection Key Laboratory of Coastal Ecological Environment, National Marine Environmental Monitoring Center of China (202310), Knowledge Innovation Program of Wuhan-Shuguang Project (No. 2022020801020210), and was supported by John von Neumann Faculty of Informatics, Óbuda University, Budapest, Hungary. The research of FJ was made by a contract co-financed by the European Union - PON Research and Innovation 2014-2020 based on art. 24, paragraph 3, letter a) of the Law of 30 December 2010, Nr. 240 and subsequent amendments of Ministerial Decree of 10 August 2021 Nr. 1062.

Conflict of interest

The authors declare that the research was conducted in the absence of any commercial or financial relationships that could be construed as a potential conflict of interest.

Publisher's note

All claims expressed in this article are solely those of the authors and do not necessarily represent those of their affiliated organizations, or those of the publisher, the editors and the reviewers. Any product that may be evaluated in this article, or claim that may be made by its manufacturer, is not guaranteed or endorsed by the publisher.

Supplementary material

The Supplementary Material for this article can be found online at: https://www.frontiersin.org/articles/10.3389/fmars.2023.1245513/full#supplementary-material

References

Barabási, A. L., and Bonabeau, E. (2003). Scale-free networks. *Sci. Am.* 288 (5), 60–69. doi: 10.1038/scientificamerican0503-60

Bartley, T. J., McCann, K. S., Bieg, C., Cazelles, K., Granados, M., Guzzo, M. M., et al. (2019). Food web rewiring in a changing world. *Nat. Ecol. Evol.* 3 (3), 345–354. doi: 10.1038/s41559-018-0772-3

Barton, M. B., Litvin, S. Y., Vollenweider, J. J., Heintz, R. A., Norcross, B. L., and Boswell, K. M. (2019). Implications of trophic discrimination factor selection for stable isotope food web models of low trophic levels in the Arctic nearshore. *Mar. Ecol. Prog. Ser.* 613, 211–216. doi: 10.3354/meps12893

Botta-Dukát, Z. (2005). Rao's quadratic entropy as a measure of functional diversity based on multiple traits. *J. Veg. Sci.* 16 (5), 533–540. doi: 10.1111/j.1654-1103.2005.tb02393.x

Brose, U., Archambault, P., Barnes, A. D., Bersier, L. F., Boy, T., Canning-Clode, J., et al. (2019). Predator traits determine food-web architecture across ecosystems. *Nat. Ecol. Evol.* 3 (6), 919–927. doi: 10.1038/s41559-019-0899-x

Cannistraci, C. V., Alanis-Lobato, G., and Ravasi, T. (2013). From link-prediction in brain connectomes and protein interactomes to the local-community-paradigm in complex networks. *Sci. Rep.* 3 (1), 1613. doi: 10.1038/srep01613

Casabianca, S., Bellingeri, A., Capellacci, S., Sbrana, A., Russo, T., Corsi, I., et al. (2021). Ecological implications beyond the ecotoxicity of plastic debris on marine phytoplankton assemblage structure and functioning. *Environ. pollut.* 290, 118101. doi: 10.1016/j.envpol.2021.118101

Cazelles, K., Bartley, T., Guzzo, M. M., Brice, M. H., MacDougall, A. S., Bennett, J. R., et al. (2019). Homogenization of freshwater lakes: Recent compositional shifts in fish communities are explained by gamefish movement and not climate change. *Glob. Change Biol.* 25 (12), 4222–4233. doi: 10.1111/gcb.14829

Clavel, J., Julliard, R., and Devictor, V. (2011). Worldwide decline of specialist species: toward a global functional homogenization? *Front. Ecol. Environ.* 9 (4), 222–228. doi: 10.1890/080216

Descamps, S., Ramírez, F., Benjaminsen, S., Anker-Nilssen, T., Barrett, R. T., Burr, Z., et al. (2019). Diverging phenological responses of Arctic seabirds to an earlier spring. *Glob. Change Biol.* 25 (12), 4081–4091. doi: 10.1111/gcb.14780

Di Mauro, L. S., Pluchino, A., Conti, E., and Mulder, C. (2022). Ecological validation of soil food-web robustness for managed grasslands. *Ecol. Indic.* 141, 109079. doi: 10.1016/j.ecolind.2022.109079

Dunne, J. A., Williams, R. J., and Martinez, N. D. (2004). Network structure and robustness of marine food webs. *Mar. Ecol. Prog. Ser.* 273, 291–302. doi: 10.3354/meps273291

Fraser, D., Villaseñor, A., Tóth, A. B., Balk, M. A., Eronen, J. T., Andrew Barr, W., et al. (2022). Late quaternary biotic homogenization of North American mamMalian faunas. *Nat. Commun.* 13 (1), 3940. doi: 10.1038/s41467-022-31595-8

Geng, M., Zhang, W., Hu, T., Wang, R., Cheng, X., and Wang, J. (2022). Eutrophication causes microbial community homogenization via modulating generalist species. *Water Res.* 210, 118003. doi: 10.1016/j.watres.2021.118003

Giacomuzzo, E., and Jordán, F. (2021). Food web aggregation: effects on key positions. *Oikos* 130 (12), 2170–2181. doi: 10.1111/oik.08541

Gonzalez, A., Germain, R. M., Srivastava, D. S., Filotas, E., Dee, L. E., Gravel, D., et al. (2020). Scaling-up biodiversity-ecosystem functioning research. *Ecol. Lett.* 23 (4), 757–776. doi: 10.1111/ele.13456

Gouveia, C., Móréh, Á., and Jordán, F. (2021). Combining centrality indices: maximizing the predictability of keystone species in food webs. *Ecol. Indic.* 126, 107617. doi: 10.1016/j.ecolind.2021.107617

Grilli, J., Rogers, T., and Allesina, S. (2016). Modularity and stability in ecological communities. *Nat. Commun.* 7 (1), 12031. doi: 10.1890/120374

Groffman, P. M., Cavender-Bares, J., Bettez, N. D., Grove, J. M., Hall, S. J., Heffernan, J. B., et al. (2014). Ecological homogenization of urban USA. *Front. Ecol. Environ.* 12 (1), 74–81. doi: 10.1890/120374

Guimerà, R., Stouffer, D. B., Sales-Pardo, M., Leicht, E. A., Newman, M. E. J., and Amaral, L. A. (2010). Origin of compartmentalization in food webs. *Ecology* 91 (10), 2941–2951. doi: 10.1890/09-1175.1

Heymans, J. J., Coll, M., Libralato, S., Morissette, L., and Christensen, V. (2014). Global patterns in ecological indicators of marine food webs: a modelling approach. *PloS One* 9 (4), e95845. doi: 10.1371/journal.pone.0095845

Hobbs, R. J., Higgs, E., and Harris, J. A. (2009). Novel ecosystems: implications for conservation and restoration. *Trends Ecol. Evol.* 24 (11), 599–605. doi: 10.1016/j.tree.2009.05.012

Knop, E. (2016). Biotic homogenization of three insect groups due to urbanization. *Glob. Change Biol.* 22 (1), 228–236. doi: 10.1111/gcb.13091

Kortsch, S., Primicerio, R., Fossheim, M., Dolgov, A. V., and Aschan, M. (2015). Climate change alters the structure of arctic marine food webs due to poleward shifts of boreal generalists. *P. R. Soc B-Biol. Sci.* 282 (1814), 20151546. doi: 10.1098/rspb.2015.1546

Kovalev, M. S., and Utkin, L. V. (2020).). A robust algorithm for explaining unreliable machine learning survival models using the Kolmogorov-Smirnov bounds. *Neural Netw.* 132, 1–18. doi: 10.1016/j.neunet.2020.08.007

Kozen, D., and Timme, M. (2007). Indefinite summation and the Kronecker delta.-Ecommons. *Cornell. Edu*. https://ecommons.cornell.edu/handle/1813/8352

Lehikoinen, A., Lindén, A., Karlsson, M., Andersson, A., Crewe, T. L., Dunn, E. H., et al. (2019). Phenology of the avian spring migratory passage in Europe and North America: Asymmetric advancement in time and increase in duration. *Ecol. Indic.* 101, 985–991. doi: 10.1016/j.ecolind.2019.01.083

Lin, W. H., Lai, S. M., Davis, A. J., Liu, W. C., and Jordán, F. (2022). A network-based measure of functional diversity in food webs. *Biol. Lett.* 18 (6), 20220183. doi: 10.1098/rsbl.2022.0183

Lövei, G. (1997). Global change through invasion. *Nature* 388, 627–628. doi: 10.1038/41665

Magurran, A. E., Dornelas, M., Moyes, F., Gotelli, N. J., and McGill, B. (2015). Rapid biotic homogenization of marine fish assemblages. *Nat. Commun.* 6 (1), 8405. doi: 10.1038/ncomms9405

Montoya, D., Yallop, M. L., and Memmott, J. (2015). Functional group diversity increases with modularity in complex food webs. *Nat. Commun.* 6 (1), 7379. doi: 10.1038/ncomms8379

Musseau, C. L., Onandia, G., Petermann, J. S., Sagouis, A., Lischeid, G., and Jeschke, J. M. (2022). Nonlinear effects of environmental drivers shape macroinvertebrate biodiversity in an agricultural pondscape. *Ecol. Evol.* 12 (11), e9458. doi: 10.1002/ece3.9458

Newman, M. E. (2004). Fast algorithm for detecting community structure in networks. *Phys. Rev. E.* 69 (6), 66133. doi: 10.1103/PhysRevE.69.066133

Obura, D. O., Katerere, Y., Mayet, M., Kaelo, D., Msweli, S., Mather, K., et al. (2021). Integrate biodiversity targets from local to global levels. *Science* 373 (6556), 746–748. doi: 10.1126/science.abh2234

Olden, J. D. (2006). Biotic homogenization: a new research agenda for conservation biogeography. *J. Biogeogr.* 33 (12), 2027–2039. doi: 10.1111/j.1365-2699.2006.01572.x

Olden, J. D., Poff, N. L., Douglas, M. R., Douglas, M. E., and Fausch, K. D. (2004). Ecological and evolutionary consequences of biotic homogenization. *Trends Ecol. Evol.* 19 (1), 18–24. doi: 10.1016/j.tree.2003.09.010

Olden, J. D., and Rooney, T. P. (2006). On defining and quantifying biotic homogenization. *Glob. Ecol. Biogeogr.* 15 (2), 113–120. doi: 10.1111/j.1466-822X.2006.00214.x

Rathore, S., Bindoff, N. L., Phillips, H. E., and Feng, M. (2020). Recent hemispheric asymmetry in global ocean warming induced by climate change and internal variability. *Nat. Commun.* 11 (1), 2008. doi: 10.1038/s41467-020-15754-3

Rodríguez-Gómez, C. F., Vázquez, G., Papiol, V., Marino-Tapia, I., and Enriquez, C. (2022). Phytoplankton distribution and its ecological and hydrographic controls in two contrasting areas of a stratified oligotrophic system. *Hydrobiologia* 849 (14), 3175–3195. doi: 10.1007/s10750-022-04924-7

Rooney, N., and McCann, K. S. (2012). Integrating food web diversity, structure and stability. *Trends Ecol. Evol.* 27 (1), 40–46. doi: 10.1016/j.tree.2011.09.001

Schell, C. J., Dyson, K., Fuentes, T. L., Des Roches, S., Harris, N. C., Miller, D. S., et al. (2020). The ecological and evolutionary consequences of systemic racism in urban environments. *Science* 369 (6510), eaay4497. doi: 10.1126/science.aay4497

Schiettekatte, N. M., Barneche, D. R., Villéger, S., Allgeier, J. E., Burkepile, D. E., Brandl, S. J., et al. (2020). Nutrient limitation, bioenergetics and stoichiometry: A new model to predict elemental fluxes mediated by fishes. *Funct. Ecol.* 34 (9), 1857–1869. doi: 10.1111/1365-2435.13618

Scott, M. C., and Helfman, G. S. (2001). Native invasions, homogenization, and the mismeasure of integrity of fish assemblages. *Fisheries* 26 (11), 6–15. doi: 10.1577/1548-8446(2001)026<0006:NIHATM>2.0.CO;2

Soler, G. A., Edgar, G. J., Thomson, R. J., Kininmonth, S., Campbell, S. J., Dawson, T. P., et al. (2015). Reef fishes at all trophic levels respond positively to effective marine protected areas. *PloS One* 10 (10), e0140270. doi: 10.1371/journal.pone.0140270

Stivala, A., Robins, G., and Lomi, A. (2020). Exponential random graph model parameter estimation for very large directed networks. *PloS One* 15 (1), e0227804. doi: 10.1371/journal.pone.0227804

Stuart-Smith, R. D., Bates, A. E., Lefcheck, J. S., Duffy, J. E., Baker, S. C., Thomson, R. J., et al. (2013). Integrating abundance and functional traits reveals new global hotspots of fish diversity. *Nature* 501 (7468), 539–542. doi: 10.1038/nature12529

Traag, V. A., Waltman, L., and Van Eck, N. J. (2019). From Louvain to Leiden: guaranteeing well-connected communities. *Sci. Rep.* 9 (1), 5233. doi: 10.1038/s41598-019-41695-z

Ulanowicz, R. E. (2004). Quantitative methods for ecological network analysis. *Comput. Biol. Chem.* 28, 5–6, 321-339. doi: 10.1016/j.compbiolchem.2004.09.001

Wang, S., Loreau, M., De Mazancourt, C., Isbell, F., Beierkuhnlein, C., Connolly, J., et al. (2021). Biotic homogenization destabilizes ecosystem functioning by decreasing spatial asynchrony. *Ecology* 102 (6), e03332. doi: 10.1002/ecy.3332

Wilkinson, C. L., Chua, K. W., Fiala, R., Liew, J. H., Kemp, V., Hadi Fikri, A., et al. (2021). Forest conversion to oil palm compresses food chain length in tropical streams. *Ecology* 102 (1), e03199. doi: 10.1002/ecy.3199

Willig, M. R., Presley, S. J., Klingbeil, B. T., Kosman, E., Zhang, T., and Scheiner, S. M. (2023). Protecting biodiversity via conservation networks: Taxonomic, functional, and phylogenetic considerations. *Biol. Conserv.* 278, 109876. doi: 10.1016/j.biocon.2022.109876

frontiers | Frontiers in Marine Science

TYPE Original Research
PUBLISHED 18 October 2023
DOI 10.3389/fmars.2023.1202300

OPEN ACCESS

EDITED BY
Laibin Huang,
University of California, Davis, United States

REVIEWED BY
John W. Day,
Louisiana State University, United States
Binbin Wang,
Saint Louis University, United States

*CORRESPONDENCE
Wei Wu
wei.wu@usm.edu

RECEIVED 08 April 2023
ACCEPTED 25 September 2023
PUBLISHED 18 October 2023

CITATION
Wu W, Grimes E and Suir G (2023) Impact of freshwater diversions on vegetation in coastal wetlands based on remote sensing derived vegetation index. *Front. Mar. Sci.* 10:1202300. doi: 10.3389/fmars.2023.1202300

Impact of freshwater diversions on vegetation in coastal wetlands based on remote sensing derived vegetation index

Wei Wu[1]*, Evan Grimes[1] and Glenn Suir[2,3]

[1]School of Ocean Science and Engineering, The University of Southern Mississippi, Ocean Springs, MS, United States, [2]Environmental Laboratory, US Army Engineer Research and Development Center, Lafayette, LA, United States, [3]School of Geosciences, University of Louisiana at Lafayette, Lafayette, LA, United States

There exist contrasting results on the impact of large-scale freshwater and sediment diversions on land gain/loss. To improve understanding on the efficacy of diversion projects in restoring coastal wetlands, we aim to evaluate the long-term impacts of diversion-altered salinity and water level on vegetation productivity in coastal wetlands. Two freshwater diversion projects Caernarvon and Davis Pond in Louisiana, U.S. and associated reference sites were selected for inclusion in this study. We implemented multi-level Bayesian models to evaluate 1) how vegetation productivity approximated by Landsat-derived Normalized Difference Vegetation Index (NDVI) in peak biomass season changed over time (pre- and post-construction and operation of the freshwater diversions), and 2) how peak-season NDVI responded to mean and variability of water level and salinity among a suite of factors that could affect vegetation productivity. Analysis showed difference in temporal trends of NDVI between the reference and diversion site for the Caernarvon project with a significant increase at the diversion site although NDVI negatively responded to diversion at the beginning. Diversion did not seem to negatively affect NDVI for the Davis Pond project and NDVI only marginally increased at the diversion site. For both projects, NDVI negatively responded to water level, while salinity negatively affected NDVI or showed quadratic relation with NDVI. At the Caernarvon diversion project, the negative impact of water level on NDVI was greater at the diversion site than at the reference site. At the Davis Pond project, it was the salinity that showed different impact between the diversion and reference site. The temporal increase of NDVI at the Caernarvon diversion site can be explained by the lower salinity driven by diversion. The quadratic relation between salinity and NDVI at the Davis Pond diversion project led to only marginal increase at the diversion site. This study provided uncertainty estimates in temporal trend of NDVI and the impact of two key abiotic drivers on NDVI. The improved understanding on vegetation productivity will help predict landscape change in response to freshwater diversions.

KEYWORDS

normalized difference vegetation index (NDVI), inundation, salinity, variability, Bayesian models, freshwater diversions

Introduction

Coastal wetlands provide a wide variety of important ecosystem services, such as carbon sequestration, nursery habitats, protection from coastal storms, improved water quality, cultural values, and recreational opportunities (Costanza et al., 1997; Engle, 2011). However, coastal wetlands are disappearing rapidly in many parts of the world. Therefore, extensive efforts have been undertaken to restore coastal wetlands as an important aspect of wetland ecosystem management.

Wetland management decisions have historically been guided by target functions and/or restoration goals, such as the reduction of salinity or the amount of habitat or wetlands restored, but less considered has been the management or restoration of hydrologic cycles (Forbes et al., 2008). However, water level is a primary driver in wetland ecosystem structure and function. Water regime variation is increasingly recognized as important in maintaining wetland functionality and diversity, so better understanding of water regime effects and abiotic controls on plant communities can improve future modeling and management of wetlands resources (Brock and Britton, 1995; Zedler, 2001; Snedden et al., 2015). Previous emphasis of water level research has been on relative sea level rise and the gradual inundation of marshes, where plants have some capabilities to adapt and respond (Morris et al., 2002; Kirwan et al., 2010; Wu et al., 2020). However, some hydrologic alterations and water management actions induce intermittent, instantaneous changes in inundation that fall outside of typical ranges. The large variability of water level can impose entirely different vegetation and soil stresses and responses. Currently, there are data and knowledge gaps associated with the impact of atypical changes in water levels on wetland plants and soils (Baustian et al., 2018).

In addition to accelerating sea level rise, climate change will intensify variability of each component of hydrological cycle (i.e., precipitation, surface-water flow, and evapotranspiration), which will likely lead to more frequent droughts and floods (Lavers et al., 2015; Lane and Kay, 2021). As a result, hydrologic management is an increasingly vital component of wetland ecosystem restoration and management. Recently, long-term and large-scale coastal ecosystem restoration and management efforts have focused on hydrologic alterations as a way of enhancing and/or creating wetlands while promoting beneficial ecological processes (Allison and Meselhe, 2010; Kearney et al., 2011; Couvillion et al., 2013; Kenney et al., 2013). The 2017 Coastal Master Plan developed by the Coastal Protection and Restoration Authority (CPRA) (CPRA, 2017) proposes seven large-scale freshwater/sediment diversion projects over the next 50 years (Pahl et al., 2020). This approach to wetland creation is relatively slow, when compared to traditional measures (i.e., placement of dredged material or vegetation planting), but can provide nourishment and sediment benefits over longer timeframes.

In addition to changing water levels, diverting freshwater from a river channel can alter salinity, nutrient concentrations, and sediment loading in wetland outfall areas. All of these factors simultaneously affect vegetation composition, vegetation growth, and soil organic matter decomposition, which can directly and indirectly affect wetland accretion and elevation change (Day et al., 2007; Day et al., 2009; Elsey-Quirk et al., 2019). There is currently a lack of data and understanding of how these environmental factors additively and/or interactively affect wetland vegetation as well as short- and long-term impacts of freshwater diversions on wetland restoration, including effectiveness, potential damages, and economic impacts.

Previous studies exhibit large variability on the efficacy of freshwater diversions on wetland restoration. Some studies have noted significant wetland gain that is related to the volume of water and sediment diverted, particularly increased deposition of inorganic river sediment or enhanced vertical accretion (DeLaune et al., 2003; Lane et al., 2006; Day et al., 2009; CPRA, 2012; Day et al., 2014; DeLaune et al., 2013; Day et al., 2016a; Rutherford et al., 2018; White et al., 2023). Other studies observed deleterious effects of long-term freshwater diversion onto the marshes due to elevated nutrients (Kearney et al., 2011), lack of wetland gains (Metzger, 2007), land gains near the diversion outlets but loss further away (Brown et al., 2019), or failing to reduce wetland loss (Hardy and Wu, 2021).

Considering the high levels of uncertainty and cost, there is an immediate need to evaluate the influence of freshwater diversions and subsequent changes in environmental factors on wetland plant dynamics. Therefore, the goal of this study was to fill gaps of data and information that are required to adequately model and predict the impacts of freshwater diversions that are proposed for ecosystem restoration and management. The objectives of this study are: 1) to evaluate long-term remote sensing-based vegetation productivity across pre- and post-diversion condition, and 2) to predict the impact of key abiotic factors (i.e., water level and salinity) on vegetation productivity in diversion outfall areas and their corresponding reference areas. Ultimately, this study will evaluate the impact of atypical changes in water level (i.e., increased depths and durations of flooding) and salinity (i.e., introduction of freshwater inputs) on vegetation condition in wetlands with natural and altered hydrologic regimes. We have two hypotheses: 1) vegetation productivity decreased initially after the freshwater diversion began, but eventually increased after adapting to the novel hydrological regimes, and 2) water level and salinity significantly affected vegetation productivity and the effect varied between diversion and reference sites.

Methods

We applied a combination of tools, including remote sensing and Bayesian models to provide enhanced and efficient scientific measures for evaluating impacts of changing water regimes. These tools are especially useful in altered or complex ecosystems with varied interactions of biotic and abiotic factors (Lai et al., 2013). We took advantage of long-term remote sensing data and applied a remote sensing derived vegetation index to approximate peak vegetation biomass that represents vegetation productivity in coastal wetlands. The hydrology and salinity data came from the existing coast-wide reference monitoring system (CRMS). We applied Bayesian multi-level models that assimilated multi-source data to make predictions that account for uncertainties from

parameters and model structures. The uncertainties were generally lacking in previous studies, however, they are important to inform future use of freshwater diversions for wetland restoration.

Study sites

We selected two representative freshwater diversion projects: Davis Pond and Caernarvon, and their respective reference sites in Louisiana, U.S. (Figure 1). The Caenarvon and Davis Pond diversion projects, which utilize pulsed operations (brief increases in flow through the diversion structure) with maximum flows of 255 cubic meters per second (cms) (Caernarvon) and 302 cms (Davis Pond), were primarily designed to mitigate saltwater intrusion from the Gulf of Mexico, reduce wetland loss, and enhance emergent vegetation growth (Jenkins et al., 2011; Plitsch, 2014; Peyronnin et al., 2017; White et al., 2023). The references sites used in this study were selected based on two primary factors: 1) geographic zone (i.e., same watershed basin as associated diversion site) and 2) environmental conditions (e.g., consist of similar vegetation to the pre-diversion study site). These environmental characteristics are supported in historic wetland surveys within each of the study and reference areas (Chabreck et al., 1968; Chabreck and Linscombe, 1997; Linscombe and Chabreck, 2001).

Davis Pond

The Davis Pond study site consists of 2,770 hectares (ha) of marsh and associated shallow water bodies and is located in Barataria Basin, Louisiana (29.88° N, 90.28° W, Figure 1) (Kral et al., 2012; Keogh et al., 2019). The Davis Pond study site has historically been a fresh Maidencane community dominated by *Panicum hemitomon* (maidencane), *Sagittaria lancifolia* (bulltongue arrowhead), Eleocharis macrostachy (pale spikerush), and *Alternanthera philoxeroides* (alligatorweed) (Chabreck et al., 1968; Chabreck and Linscombe, 1997; Linscombe and Chabreck, 2001). This study site comprises the direct outfall area of the Davis Pond freshwater diversion of the Mississippi River.

The Davis Pond freshwater diversion structure is a restoration project that began operations in July 2002 (USACE, 2002). Four 4.27-meter culverts were installed and designed to release more than 280 cms of water when necessary (Plitsch, 2018). Since construction and operation of the Davis Pond Diversion, the study site has transitioned to a Bulltongue community dominated by *Sagittaria lancifolia* and *Zizaniopsis miliacea* (giant cutgrass) (Sasser et al., 2008; Sasser et al., 2014; Coastal Protection and Restoration Authority (CPRA) of Louisiana, 2019). The project anticipates protecting 13,355 ha of wetlands and 314,440 ha of estuaries during its lifespan, and annual economic benefits are estimated to be over $15 million (USACE, 2002).

The Davis Pond reference site consists of 4,508 ha of wetlands in the Barataria Basin and is located south of Lac des Allemands, approximately 17 km west of the Davis Pond study site (29.84° N, 90.52° W, Figure 1). Since the 1960s, the Davis Pond reference site has maintained a fresh Maidencane vegetation community dominated by *Panicum hemitomon* and *Sagittaria lancifolia* (Chabreck et al., 1968; Chabreck and Linscombe, 1997;

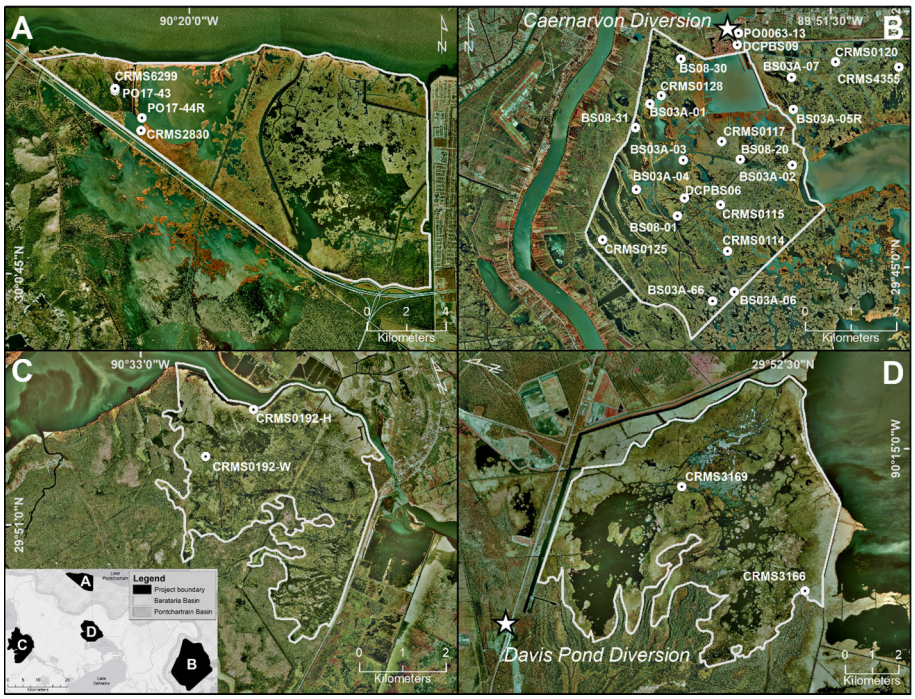

FIGURE 1
The study area (boundaries in white lines) demonstrating diversion [Caernarvon, **(B)** and Davis Pond, **(D)**] and reference sites [Caernarvon Reference, **(A)** and Davis Pond Reference, **(C)**], and Coastwide Reference Monitoring System (CRMS) stations where salinity and water level data were obtained, in southeastern Louisiana, U.S.

Linscombe and Chabreck, 2001; Sasser et al., 2008; Sasser et al., 2014; CPRA, 2019), similar to the Davis Pond freshwater diversion outfall area prior to the diversion operations. In addition to the prominent attached emergent vegetation, the Davis Pond and Davis Pond reference sites consist of some floating marsh mats (Sasser, 1994), which may be more resilient to changes in water regime.

Caernarvon

The Caernarvon diversion project outfall study site, which consists of 10,912 ha of marsh and associated shallow water bodies, is located in the Pontchartrain Basin, Louisiana (29.78°N, 89.93° W, Figure 1). From 1949 to 2001 the Caernarvon study site fluctuated between a brackish and intermediate system (O'Neil, 1951; Visser et al., 2002). Historically the area consisted of a Wiregrass vegetation community dominated by *Spartina patens* (saltmeadow cordgrass), *Schoenoplectus americanus* (chairmaker's bulrush), *Eleocharis* spp. (spikerush), and *Vigna luteola* (hairypod cowpea) (Chabreck et al., 1968; Chabreck and Linscombe, 1997; Linscombe and Chabreck, 2001). Since 2001, the Caernarvon site has transitioned to a fresher system, with a Bulltongue community to the north (dominated by *Polygunum punctatum* and *Alternanthera philoxeroides*) and a Wiregrass community in the south (dominated by *Spartina patens*) (CPRA, 2019; Sasser et al., 2008; Sasser et al., 2014).

Caernarvon Diversion was completed in 1991 and is designed to release up to 255 cms of freshwater through five 4.57 m culverts, but has been operated at an average of 62.3 cms from 1993 to 2001 (USACE, 2013; Lopez et al., 2014). The diverted water flows directly into Big Mar Pond and disperses throughout Breton Sound, providing numerous habitat and ecosystem benefits (Villarrubia, 2002).

The Caernarvon Reference Site consists of 1,907 ha of wetlands and is located approximately 23 km west-northwest of New Orleans in the Pontchartrain Basin, Louisiana (30.03° N, 90.32° W, Figure 1). Since the 1960s, the Caernarvon Reference site has been a Wiregrass community dominated by *Spartina patens*, with considerable amounts of *Eleocharis* spp., *Schoenoplectus americanus*, *Spartina alterniflora* (smooth cordgrass), and *Ipomoea sagittata* (saltmarsh morning-glory) (Chabreck et al., 1968; Chabreck and Linscombe, 1997; Linscombe and Chabreck, 2001; Sasser et al., 2008; Sasser et al., 2014; CPRA, 2019), similar to the historical vegetation community in the Caernarvon diversion outfall area before the diversion started.

Remote sensing

Data acquisition and processing

Peak-season green biomass that represents vegetation productivity within the study areas was evaluated using space-borne imagery. Remote sensing assessments were performed using Landsat 5 Thematic Mapper [TM], Landsat 7 Enhanced Thematic Mapper Plus [ETM+], and Landsat 8 Operational Land Imager [OLI] for all diversion and reference sites. The Landsat constellation of sensors, which span the period of analysis from 1984 to 2018, provide moderate spatial (30 meter) and temporal (16 day return) resolution imagery (Suir et al., 2018). Landsat data are useful for evaluating long-term landscape trends, and estimating short-term variations linked to disturbance events and/or prevailing environmental conditions (Suir et al., 2011). Raw and processed Landsat data are available through the Google Earth Engine (GEE) image service. GEE provides Tier 1 surface reflectance imagery, which meets geometric, radiometric, and atmospheric quality requirements (Kalnay et al., 1996; Chander et al., 2009; Schmidt et al., 2013). Additionally, since cloud cover can be a significant limitation to Landsat imagery usage, the GEE uses aggregation functions (i.e., use of outlier values to remove cloud cover from neighboring scenes) to create monthly image composites. All cloud free scenes and composites of Landsat images used in this study, from 1984 to 2018, were acquired using the GEE.

Normalized Difference Vegetation Index

The Normalized Difference Vegetation Index (NDVI) utilizes a band ratio of image-derived reflectance between a near-infrared (NIR) and red band ($\frac{NIR-Red}{NIR+Red}$, Rouse et al., 1974) to measure an ecosystem's ability to capture solar energy and convert it to organic carbon or biomass (An et al., 2013). Since healthy green vegetation absorbs light in the red portion of the electromagnetic spectrum and reflects light in the NIR portion of the spectrum, the NDVI provides a useful relative measure for assessing vegetation biomass/vigor, and its changes over time (Carle, 2013; Suir and Sasser, 2019a; Suir and Sasser, 2019b). As such, this index was used with data collected within the vegetation peak biomass season to assess changes in green biomass and vegetation productivity in the diversion and reference areas.

Optical inspections were performed on all scenes and composites to identify and remove satellite images of poor quality. ESRI ArcGIS version 10.5 (Redlands, CA: Environmental Systems Research Institute) was used to process all Landsat-derived NDVI images for each site. All water and cloud features within the diversion and reference sites were initially excluded from each satellite image using the density slicing method (Frazier and Page, 2000; Wang et al., 2002). Since NDVI values less than zero (< 0) are typical of non-vegetation features (e.g., mud flats and bare earth) (Reif et al., 2011; Carle, 2013), those were also excluded from each image. Given the large number of Landsat image pixels per site, and the spatial variability within site not being the focus of this study, median NDVI values (from peak biomass season, August to October) across pixels of each site were used as model response variables to better evaluate temporal patterns of vegetation condition and change. In addition, the lack of well distributed water and salinity spatial data, described below, limited development of spatial model of NDVI. We applied paired t-test and Mann-Kendall non-parametric test to compare NDVI between diversion and reference site for each diversion project, and detect the temporal trend of NDVI at each site respectively.

Environmental variables

The distribution, abundance, growth potential, and productivity of wetland plants are influenced by a variety of environmental factors (Lacoul and Freedman, 2006a), related to geomorphology

(geology and topography), sediment, climate, hydrology, water quality constituents, episodic events, and competition (Lacoul and Freedman, 2006b; Allen and Suir, 2014; Suir et al., 2018; He et al., 2023). Since water level and salinity are key abiotic factors to vegetation productivity, are directly impacted by freshwater diversions, and their data is abundant and available in coastal Louisiana, we focus on them as environmental variables in this study. The Louisiana Coastwide Reference Monitoring Station (CRMS) system and data were used to identify ranges of natural and managed hydrology and salinity in the project and reference areas (Figure 1). We calculated the average and standard deviation of daily water level and salinity within growing season (March to October) for each year and used them as the covariates in the Bayesian model. We applied paired t-test to compare water level and salinity between diversion and reference site for each diversion project.

Bayesian models

Limited data, limited understanding, and natural variability only lead to large uncertainties in prediction of vegetation response to environmental and wetland stressors. These responses are knowledge gaps that have recently limited the modeling and efficient implementation of wetland restoration through freshwater diversion measures. Bayesian inference has the advantage of quantifying uncertainties related to parameters and predictions through credible intervals (CI) of posteriors (Clark, 2004; Wu et al., 2012). Therefore, we implemented multi-level (or multi-scale) Bayesian models (Figure 2) to investigate temporal trends of peak-season NDVI and how salinity and water level affected it in the Caernarvon and Davis Pond diversion project areas. For this study, two distinct spatial scales were evaluated: 1) project scale (includes both diversion and reference sites), and 2) finer site scale (diversion or reference site).

For each diversion project, we developed two types of models. The first type of models analyzed temporal trends of peak-season NDVI with year (in reference to initiation of freshwater diversion) and its quadratic term as the covariates to capture nonlinear trends, especially the potential minimum NDVI around or after the initiations of the freshwater diversions. The second type of models analyzed the impact of water level and salinity on peak-season NDVI. Limited availability of water level and salinity data temporally compared to NDVI data, especially at the reference sites, reduced temporal coverage in the second type of models. The data of the first type of models ranged from 1984 to 2018, while the data of the second type of models ranged from 1996 to 2018 for the Carnarvon project and from 1998 to 2018 for the Davis Pond project.

For each type of models, we developed a variety of model candidates to explore whether the effect of a particular covariate should be included or its effect differed between diversion and reference sites (see Supplementary Materials Tables S1–S3). We compared these models based on deviance information criterion (DIC) and predictive posterior loss (PPL) (Hooten and Hobbs, 2015). The lower the DIC or PPL, the better the model predicts. We ranked the models mainly based on DIC, but we compared PPL when the models had different hierarchies (for example, the models that accounted for site-specific parameters vs. the models that had parameters that did not vary by site).

The posteriors of the coefficients for the covariates, particularly, summarized in the medians and credible intervals (95% CIs, from 2.5% quantile to 97.5% quantile, and 50% CIs, from the first quartile to the third quartile), facilitated the inference on the long-term trends of NDVI and abiotic factors' impact on NDVI. The 95% or 50% CIs of a coefficient represent that there is a 95% probability or

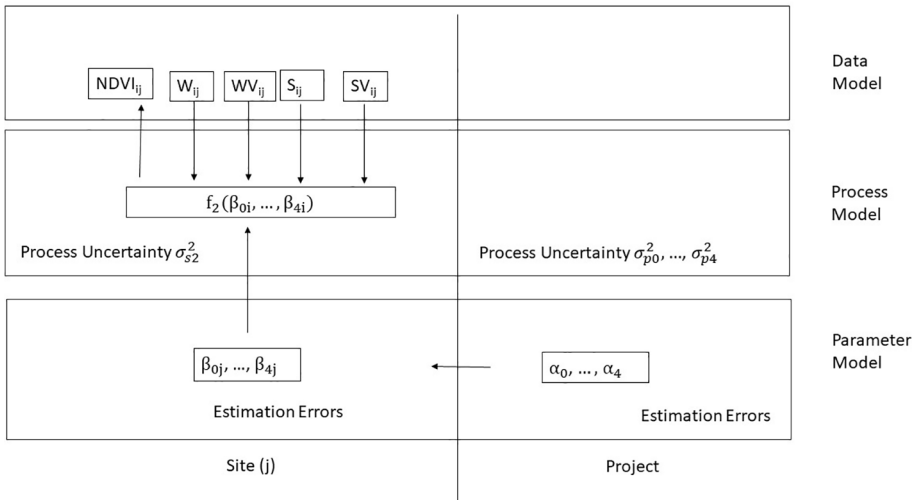

FIGURE 2
Structure of the full Bayesian multi-level model used to identify the effect of water level and salinity on NDVI. The complexity of the model was decomposed into stages of data, process and parameters (vertical direction) and the association of different spatial scales (horizontal direction). (Adapted from Wu et al., 2012). The symbols correspond to those in Eq. 5 – Eq. 8. W- mean daily water level, WV – standard deviation of daily water level, S – mean daily salinity, and SV – standard deviation of daily salinity, σ^2 – variance, αs and βs denote model parameters, and subscript i denotes year. The project scale includes both diversion and reference site.

50% probability that this coefficient lies within the intervals. If a 95% CI does not overlap zero, then there is a significant effect of the corresponding covariate on NDVI. From the posteriors, we can also summarize the probability of a particular coefficient or prediction being positive or negative.

Temporal trend models

To represent the peak-season NDVI at Site j (diversion or reference) in Year i (D_{ij}), let $D_{ij}.\mu_1$ represent the mean of D_{ij}, and σ_{s1}^2 represent the variance of D at the site scale. D_{ij} was modeled by assuming it followed (denoted by ~) a normal distribution (N) (Equation 1).

$$D_{ij} \sim N(D_{ij}.\mu_1, \sigma_{s1}^2) \tag{1}$$

To account for nonlinear trends, we included the years passed (Y) in reference to the diversion initiation years (1991 for Caernarvon diversion and 2002 for Davis Pond diversion) and its quadratic term (Y^2) as the covariates (Equation 2).

$$D_{ij}.\mu_1 = f_1(\gamma_{0j}, \gamma_{1j}, \gamma_{2j}) = \gamma_{0j} + \gamma_{1j}Y_{ij} + \gamma_{2j}Y_{ij}^2 \tag{2}$$

Where γ_{0j}, γ_{1j}, and γ_{2j} represent intercept and coefficients for Y and Y^2 respectively, and j=1 (diversion site) or 2 (reference site). For some models we compared (not shown here), there was no subscript j, therefore, γ_{0j}, γ_{1j}, or γ_{2j} became lumped parameters γ_0, γ_1, or γ_2 that did not vary between the diversion and reference sites.

Therefore, the D at two sites was modeled as in Equation 3.

$$p(D_i|\gamma_{0j}, \gamma_{1j}, \gamma_{2j}, \sigma_{s1}^2) \propto \prod_{j=1}^{2} N(D_{ij}| f_1(\gamma_{0j}, \gamma_{1j}, \gamma_{2j}), \sigma_{s1}^2) \tag{3}$$

Where $\propto$ denotes "is proportional to". The parameters γs at the site scale were all modeled by assuming they were distributed as (~) normal distributions (N) with the mean (θ_0, θ_1, θ_2) and variance (σ_0^2, σ_1^2, σ_2^2) at the project scale (including both reference and diversion sites) (Equation 4). A lumped parameter that did not account for site-specific difference skipped this step.

$$\begin{aligned} \gamma_{0j} &\sim N(\theta_0, \sigma_0^2) \\ \gamma_{1j} &\sim N(\theta_1, \sigma_1^2) \\ \gamma_{2j} &\sim N(\theta_2, \sigma_2^2) \end{aligned} \tag{4}$$

Models to evaluate the impact of water level and salinity on NDVI

Mean of the NDVI at Site j (diversion or reference) in Year i ($D_{ij}.\mu_2$) was modeled as a linear function of water level and salinity. The covariates did not only include mean daily water level (W_{ij}) and salinity (S_{ij}) from March to October, but also their standard deviations (WV_{ij}, SV_{ij}) to represent variability (Equation 5, Figure 2). The variability is important in dynamic systems but has been rarely accounted for previously. We also explored the nonlinear response of NDVI to mean water level and mean salinity by including their quadratic terms in the models (not described in the equations). We did not detect multicollinearity based on inflation variance factor using "car" package in R for the Caernarvon diversion project (Fox and Weisberg, 2019). Equation 5 represents the full model for this project. However, there existed multicollinearity if we included both mean and standard deviation of salinity for the Davis Pond diversion project, therefore we removed standard deviation of salinity to eliminate multicollinearity in the models for the Davis Pond diversion project.

$$\begin{aligned} D_{ij}.\mu_2 &= f_2(\beta_{0j}, \beta_{1j}, \beta_{2j}, \beta_{3j}, \beta_{4j}) \\ &= \beta_{0j} + \beta_{1j}W_{ij} + \beta_{2j}WV_{ij} + \beta_{3j}S_{ij} + \beta_{4j}SV_{ij} \end{aligned} \tag{5}$$

Where β_{0j}, β_{1j}, β_{2j}, β_{3j}, β_{4j} represent intercept, coefficients for mean water level, variability of water level, mean salinity, and variability of salinity respectively with j=1 (diversion site) or 2 (reference site).

Therefore, the D at two sites for a particular diversion project was modeled as in Equation 6.

$$\begin{aligned} &p(D_i|\beta_{0j}, \beta_{1j}, \beta_{2j}, \beta_{4j}, \sigma_{s2}^2) \\ &\propto \prod_{j=1}^{2} N(D_{ij}| f_2(\beta_{0j}, \beta_{1j}, \beta_{2j}, \beta_{3j}, \beta_{4j}), \sigma_{s2}^2) \end{aligned} \tag{6}$$

The site-scale parameters βs (β_{0j}, … β_{4j}) were all modeled by assuming they were distributed as (~) a normal distribution (N) with the means (α_0, … α_4) and variances (σ_{p0}^2, … σ_{p5}^2) at the project scale (Equation 7).

$$\begin{aligned} \beta_{0j} &\sim N(\alpha_0, \sigma_{p0}^2) \\ \beta_{1j} &\sim N(\alpha_1, \sigma_{p1}^2) \\ &\dots \\ \beta_{4j} &\sim N(\alpha_4, \sigma_{p4}^2) \end{aligned} \tag{7}$$

Bayesian models require prior distributions for unknown parameters (αs, θs, $\sigma^2 s$). For computation efficiency, we used conjugated priors, i.e., the priors and posteriors have the same probability distribution forms (Calder et al., 2003). As such, the priors for αs, θs, were normally distributed and the priors for $\sigma^2 s$ followed inverse gamma distributions. As we had limited knowledge on the parameters, we also defined the priors distributions flat to only weakly influence the posteriors (Lambert et al., 2005).

We derived the joint distribution of unknowns in Eq. 8 using the second type of models as an example by combining the parameter (priors), process, and data models.

$$\begin{aligned} &p(D|W, S, WV, SV, \beta, \alpha, \sigma^2) \\ &\propto p(D|\beta_{0j}, \dots, \beta_{4j}, \sigma_{s2}^2) \times p(\beta_{0j}|\alpha_0, \sigma_{p0}^2) \times \dots \times p(\beta_{4j}|\alpha_4, \sigma_{p4}^2) \\ &\times p(\alpha_0) \times \dots \times p(\alpha_4) \\ &\times p(\sigma_{s2}^2) \times p(\sigma_{p0}^2) \dots \times p(\sigma_{p4}^2) \end{aligned} \tag{8}$$

We computed the posterior distributions using Markov Chain Monte Carlo Simulation (MCMC) (Robert and Casella, 2004) in the software JAGS 4.3.0 (Plummer, 2017). We summarized quantiles,

95% and 50% credible intervals, and the probability of a particular parameter being positive or negative based on the posteriors.

We normalized the covariates to increase the speed of convergence of MCMC for the second type of models (Hooten and Hobbs, 2015). In addition, we could directly compare the covariates' effects based on the magnitudes of their parameters with these covariates being normalized to the similar ranges (Hardy and Wu, 2021).

Results

Temporal trends of water level and salinity

Water level at the diversion and reference sites was not significantly different from each other for both projects (p-value of paired t-test = 0.060 for Caernarvon project, and p-value = 0.86 for Davis Pond project) (Figures 3, 4). Meanwhile, salinity at the

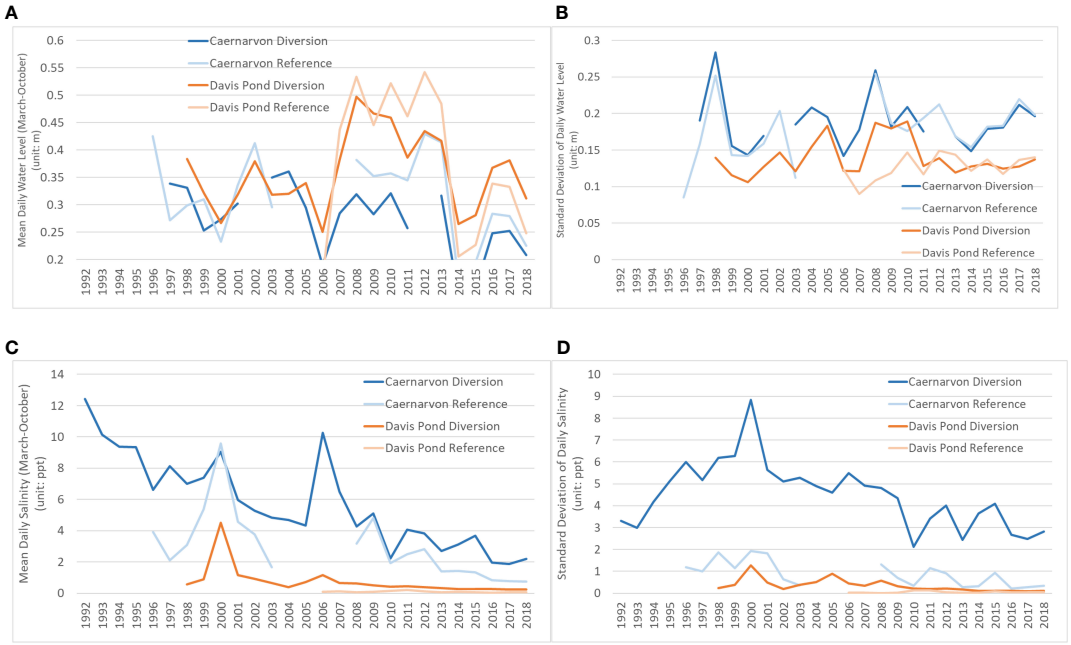

FIGURE 3
Time series of water level and salinity and their standard deviations. **(A)** Mean daily water level from March to October (unit: m), **(B)** Standard deviation of daily water level from March to October (unit: m), **(C)** Mean daily salinity from March to October (unit: ppt), and **(D)** Standard deviation of daily salinity from March to October (unit: ppt).

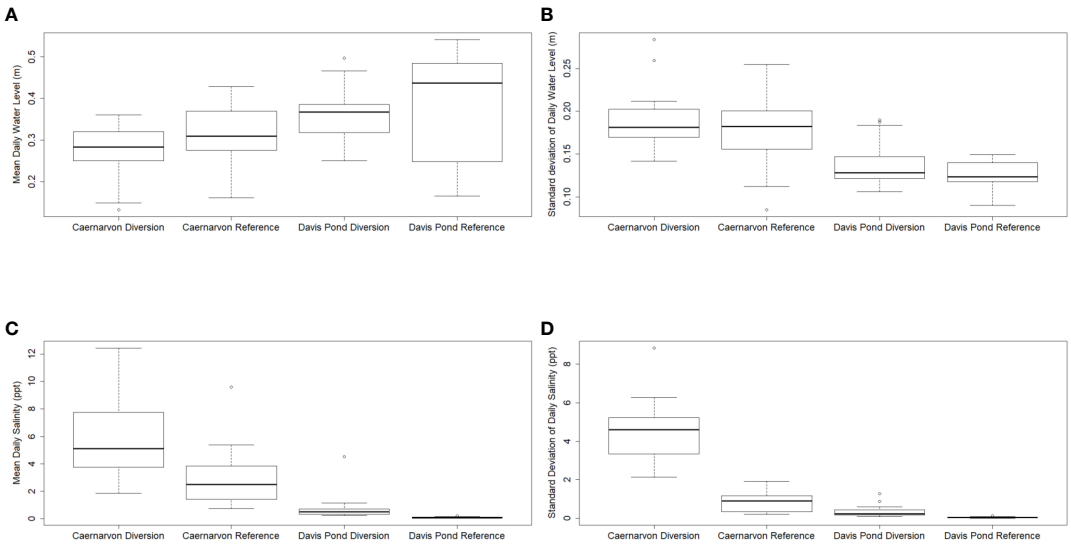

FIGURE 4
Box plots of water level and salinity and their standard deviations. **(A)** Mean daily water level from March to October (unit: m), **(B)** Standard deviation of daily water level from March to October (unit: m), **(C)** Mean daily salinity from March to October (unit: ppt), and **(D)** Standard deviation of daily salinity from March to October (unit: ppt).

diversion sites was significantly higher than at the reference sites for both projects (p-value = 5.0×10^{-5} for Caernarvon project, and p-value = 2.5×10^{-4} for Davis Pond project) and it decreased over time. Variability of water level at the diversion sites was not significantly different from the reference sites for both diversion projects (p-value = 0.11 for Caernarvon project, and p-value = 0.12 for Davis Pond project), however the variability of salinity was significantly larger at the diversion sites than at the reference sites (p-value = 4.2×10^{-10} for Caernarvon project, and p-value = 0.0024 for Davis Pond project).

Temporal trends of NDVI

NDVI values were greater at the Davis Pond diversion and reference sites with lower salinity than at the Caernarvon diversion and references sites with higher salinity (Figure 5). Comparing between the diversion and reference sites, NDVI values were significantly greater at the Davis Pond diversion site than at the reference site (p-value = 3.1×10^{-6}), while there did not exist significant difference between the diversion and reference site for the Caernarvon diversion project (p-value = 0.34). From the Mann-Kendall trend test, NDVI increased significantly at the Caernarvon diversion site (p= 0.00073), but not at the reference site (p=0.73). NDVI increased marginally at the Davis Pond diversion site (p=0.085), and stayed similar at the reference site (p=0.54). The higher the NDVI, the higher the productivity and the more healthy the plants. Though increased NDVI does not indicate land gains, healthy plants will likely contribute to increased accretion and land gains in the long run.

From the modeling results, we did not find a consistent response of NDVI to diversion between the Caernarvon diversion project and Davis Pond project. The best temporal model for Caernarvon diversion project included site variant intercept (γ_{0j}) and site variant coefficient of years passed since diversion initiation (lapse of years) (γ_{1j}) (Table S1; Figures 6A1, 6B1). The coefficient of squared lapse of year was a lumped parameter that did not differentiate between reference and diversion site (γ_2) (Table S1; Figure 6C1). The best temporal model for Davis Pond project included site variant intercept (γ_{0j}) (Table S1; Figure 6A2) while the coefficients for both lapse of years (γ_1) and quadratic term (γ_2) were lumped parameters (Table S1; Figures 6B2, 6C2). It is important to include the quadratic term to indicate nonlinear trend as the models that did not include it yielded higher DIC and PPL (Table S1). Since the parameters (γ_2) for the quadratic term of lapse of years were positive (inferred by the positive 95% credible intervals of γ_2 in Figure 6C) for both diversion projects, the general temporal trends of NDVI showed a nonlinear form with the existence of minimum NDVIs in time (Figure 6D).

For the Caernarvon diversion project, the lapse of years for the minimum NDVI was not different from zero as both 95% and 50% credible intervals for it overlapped zero at the diversion site, while it was positive based on its positive 95% credible interval at the reference site (Figure 6D1). This indicated that the NDVI values dropped to the minimum when the diversion initiated at the diversion site but not at the reference site, therefore, diversion negatively affected vegetation at the very beginning of diversion. In more detail, the lapse of years with a minimum NDVI at the diversion site had a median of 0.7 year and 95% credible interval of -10.6 to 5.1 years, showing NDVI started the recovery trajectory up to 5 years since the diversion started. The lapse of years with a minimum NDVI at the reference site had a median of 9.2 years and 95% credible interval of 4.7 to 13.2 years. When we compared the lapse of years for the minimum NDVIs between diversion and reference site, there existed about 99.9% of probability that it was earlier at the diversion site than at the reference site.

For the Davis Pond diversion project, there was about 99.4% of probability that the minimum NDVI occurred before the diversion started at both diversion and reference sites (Figure 6D2). As such, freshwater diversion did not seem to negatively affect peak season vegetation biomass even at the beginning. As there was no difference of the coefficients for year and squared year in the best model, diversion did not seem to affect the temporal trends of NDVI for the Davis Pond project.

The impact of water level and salinity on NDVI

Both mean water level and mean salinity were included in the best models to predict NDVI for the two diversion projects (Tables S2, S3). For the Carnarvon diversion project, the impact of water level on NDVI differed between the diversion and reference site, while salinity's impact did not show difference between the two

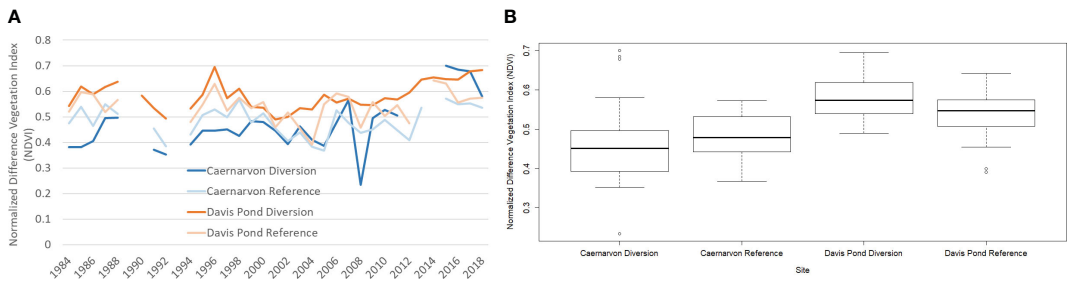

FIGURE 5
Landsat derived normalized difference vegetation index from 1984 to 2018 at Caernarvon diversion, reference sites and Davis Pond diversion and reference sites. **(A)** Time series of medians, and **(B)** Box plots of the time series of medians.

sites. Both mean water level and mean salinity showed negative effect on NDVI. There was an about 95% probability that the effect of mean water level was more negative at the diversion site compared to the reference site (Figure 7). Focusing on the median impacts on NDVI at the diversion site, water level showed larger impact than salinity. At the reference site, water level and salinity showed similar impact.

Similarly, both mean daily water level and mean daily salinity were important to predict NDVI for the Davis Pond diversion project (Figure 8). Mean water level's effect on NDVI did not differ between the diversion and reference site and it was negative. In contrast, mean salinity's effect differed between the diversion and reference site. Different from the Caernarvon diversion project, salinity's impact on NDVI showed parabolic relation, indicating a minimum NDVI at a certain salinity (median of 2.8 ppt and up to 4.7 ppt at the diversion site, and median of 0.15 ppt and up to 3.0 ppt at the reference site). The parabolic relation was not detected for water level as the inclusion of the quadratic term of water level did not improve model predictions (Table S3). Salinity's impact was larger than the water level's impact for the diversion site.

Discussion

We developed a multi-level modeling framework to integrate existing data to evaluate the impact of freshwater diversion on vegetation productivity approximated by NDVI in peak biomass season (August to October) with a focus on NDVI's temporal trend and NDVI's response to salinity and water level. The study was not about wetland areal gains or losses, instead we focused on gaining some insights on the mechanisms of vegetation dynamics, which can help improve understanding on land dynamics. Wetland restoration involves many other aspects and functions that cannot easily be detected using remote sensing images, such as soil processes, belowground biomass, biogeochemical cycle, and microbial composition. However, in terms of wetland restoration, vegetation productivity can serve as indicators of other wetland functions, which generally occur at a more lagged time scale (Suir and Sasser, 2017).

The varying results for different diversion projects pinpoint both the need to evaluate these projects separately, and the difficulty in generalizing the efficacy of diversion projects. Both water level and salinity were important to predict NDVI, however, water level's impact for the Caernarvon project differed between the diversion and reference site with the larger negative impact at the diversion site (based on the medians of the posteriors), while it did not vary between the two sites for the Davis Pond project. The opposite is the case for the salinity's impact. Water level and salinity's impacts differed in magnitude, driven by diversion attributes, biogeophysical conditions, and vegetation of the sites. Higher water level decreased NDVI, consistent with lower end-of-season biomass of *Spartina alterniflora* and *Spartina patens* with increased inundation

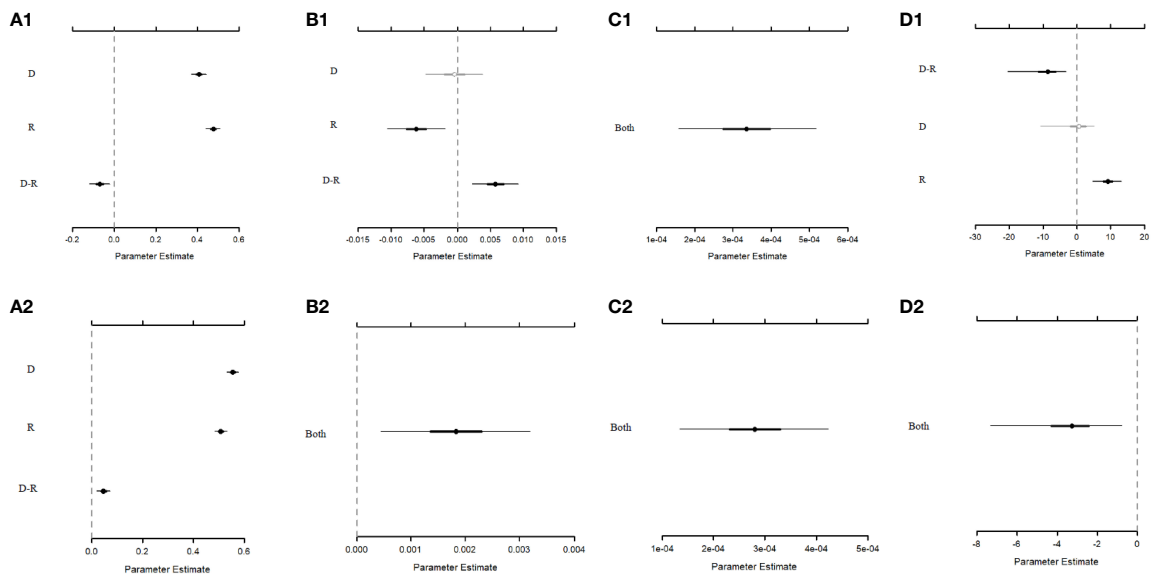

FIGURE 6
Credible intervals for the parameters **(A)** Intercept (γ_0), **(B)** Coefficient for Y (γ_1), **(C)** Coefficient for Y^2 (γ_2), and **(D)** Years passed since diversion initiated when minimum normalized difference vegetation index (NDVI) occurred (there existed minimum NDVI as the coefficient for Y^2 was positive, calculated as $-\frac{\gamma_1}{2\gamma_2}$), in the best temporal trend models for Caernarvon diversion project (top), and Davis Pond diversion project (bottom). The labels for Y-axis: "D" denotes diversion site, "R" denotes reference site, "D-R" denotes difference of diversion and reference sites, and "Both" denotes the coefficient is a lumped variable that does not vary between reference site and diversion site. The thin line shows the 95% credible interval and the thick line shows the 50% credible interval. The dot represents median. The grey line with open dot indicates that both 50% and 95% credible intervals overlap zero, the grey line with grey dot indicates that 50% credible interval does not overlap zero while 95% credible interval does, and the black line with black dot indicates that both 50% and 95% credible intervals do not overlap zero and the parameter shows statistical significance. The dashed vertical line represents estimate of 0. Lines to its right represent positive estimates and lines to its left represent negative estimates. Plot generated using MCMCvis package in R (Youngflesh, 2018).

(Snedden et al., 2015). The impact of salinity on vegetation was greater than that of water level at the lower salinity location (Davis pond sites), consistent with the previous research that shows salinity is the most important abiotic factor in determining coastal wetland habitat types (White and Kaplan, 2017; Lin et al., 2018). On the other hand, the impact of water level was greater at the higher salinity location (e.g. Caernarvon diversion site). Furthermore, salinity's impact on NDVI showed different functional forms. NDVI monotonically declined with salinity for the Caernarvon diversion project, while the relation between NDVI and salinity was parabolic for the Davis Pond diversion project. The different functional forms either represent a declining (improving) vegetation condition with higher (lower) salinity (DeLaune et al., 2005; Snedden et al., 2015) or vegetation community shift driven by salinity (White and Kaplan, 2017). This was observed at the Caernarvon Site which experienced a shift from brackish and intermediate vegetation types between the 1940s and the early 2000s (O'Neil, 1951; Chabreck et al., 1968; Chabreck and Linscombe, 1997; Linscombe and Chabreck, 2001) to freshwater vegetation in 2007 and 2013 (Sasser et al., 2008; Sasser et al., 2014).

Lower salinity and higher water levels are generally accompanied by freshwater diversions. Though salinity was higher at the diversion sites than at the reference sites for both projects (Figures 2, 3), due to their proximity to the ocean, the reduced salinity due to diversion can benefit vegetation. The freshwater flow into these areas is expected to nourish and enhance the marsh vegetation that is going through salinity-induced stress (Metzger, 2007). Lower salinity could also lead to shifts in vegetation communities from salt tolerant communities to freshwater marshes. One study showed vegetation production increased as salinity decreased within coastal wetlands (Stagg et al., 2016). On the other hand, higher water levels had negative impacts on vegetation. In our study, the temporal increase of NDVI at the Caernarvon diversion site can be explained by the lower salinity driven by diversion. The quadratic relation between salinity and NDVI at the Davis Pond diversion project led to only marginal increase at the diversion site.

The combined effects of inundation and salinity involved large uncertainties, as evident in the posteriors (Figures 6–8), and noticed in the previous studies (e.g. Snedden et al., 2015; Brown et al., 2019; Elsey-Quirk et al., 2019). The large uncertainties summarized in our Bayesian analysis, lacking in many other studies that mainly focus on mean response, may partially explain the mixed results on the previous evaluation of freshwater diversion projects (Metzger, 2007;

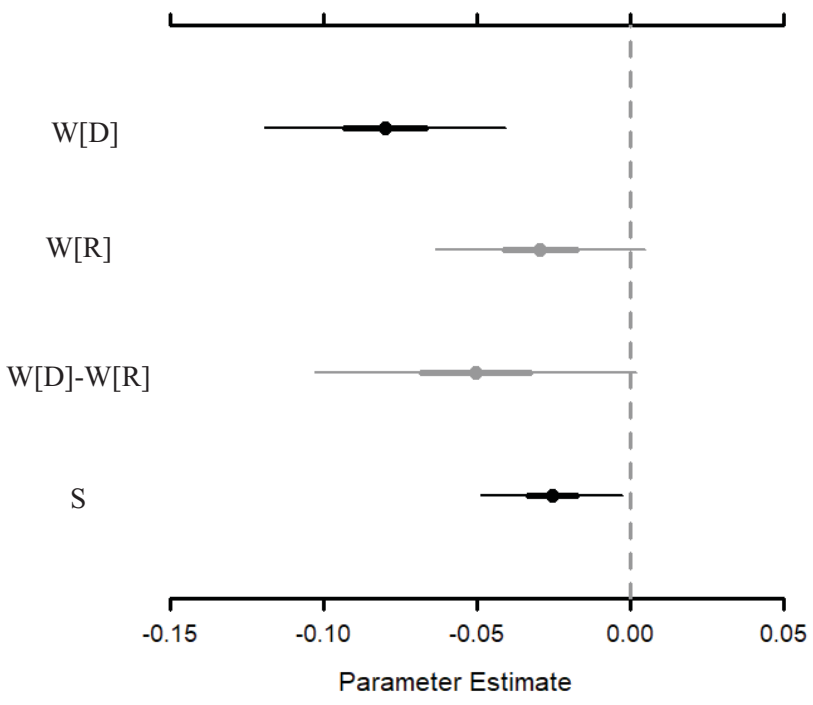

FIGURE 7
Credible intervals of the parameters for water level and salinity in the final model to evaluate the impact of environmental variables on NDVI for Caernarvon diversion project. [D] denotes diversion site, and [R] denotes reference site. S denotes mean of daily salinity, and W denotes mean of daily water level. If a particular parameter does not have brackets, this parameter does not differ between diversion and reference site. W[D]-W[R] denotes difference of the parameters for mean daily water level between diversion and reference site. The dot represents median. The thin line shows the 95% credible interval and the thick line shows the 50% credible interval. The grey line with open dot indicates that both 50% and 95% credible intervals overlap 0, the grey line with grey dot indicates that 50% credible interval does not overlap zero while 95% credible interval does, and the black line with black dot indicates that both 50% and 95% credible intervals do not overlap 0. Plot generated using MCMCvis package in R (Youngflesh, 2018).

Kearney et al., 2011; CPRA, 2012; Day et al., 2014; Day et al., 2016a; Rutherford et al., 2018; Brown et al., 2019; Turner et al., 2019; Hardy and Wu, 2021; White et al., 2023). The different results are potentially due to differences in assessment methods, data, and data quality (remote sensing, field measurements, permanent change data), differences in receiving areas and conditions (e.g., proximity to river source, fetch, depth), and differences in diversion operation methods (i.e., diversion volume, timing, frequency) (Snedden et al., 2007; Day et al., 2009). Day et al. (2016b) showed that large and infrequent river diversions were more effective to restore Mississippi Delta and limit displacement of fisheries, water quality problems and wetland deterioration due to overloading of nutrients, compared to small and frequent river diversions. Our study is consistent with this finding. Caernarvon and Davis Pond diversion projects fall into the infrequent river diversions. Due to the infrequent diversions, water levels got controlled (not different from the reference sites), and therefore the potential negative impact due to higher water level was small. Other ecosystem models exist to predict vegetation productivity related to coastal wetland restoration. The primary productivity model in SEDLIB only accounts for local water depth (Brown et al., 2019), while Louisiana vegetation biomass model (LAVegMod) accounts for the effect of inundation, salinity, nutrients, and temperature (Visser et al., 2017; Baustian et al., 2018). However, none of the previous models predicted the uncertainties of the functions between vegetation productivity and abiotic factors, as done in this study. The uncertainty information derived from this study can be factored into these ecosystem models to improve the predictions of land gains/losses with uncertainties accounted for.

Nutrient and sediment change related to freshwater diversions are important to impact vegetation productivity and land gains/loss (Day et al., 2013; White et al., 2023), however, our study did not account for them due to lack of available data. Hollis and Turner (2019) and Turner (2011) showed significant decline in root strength or soil strength after small increases in nutrient availability. High nutrient did not necessarily lead to decreased belowground production though (Anisfeld and Hill, 2012; Fox et al., 2012; Day et al., 2013). Based on the review by Elsey-Quirk et al. (2019), larger sediment availability is necessary to offset the negative impact from the larger variability of environmental factors or excessive nutrients driven by freshwater diversions. On the other hand, greenhouse studies showed that biomass production of *Spartina patens* increased with nitrogen addition, with more increase in lower salinity than in higher salinity (DeLaune et al.,

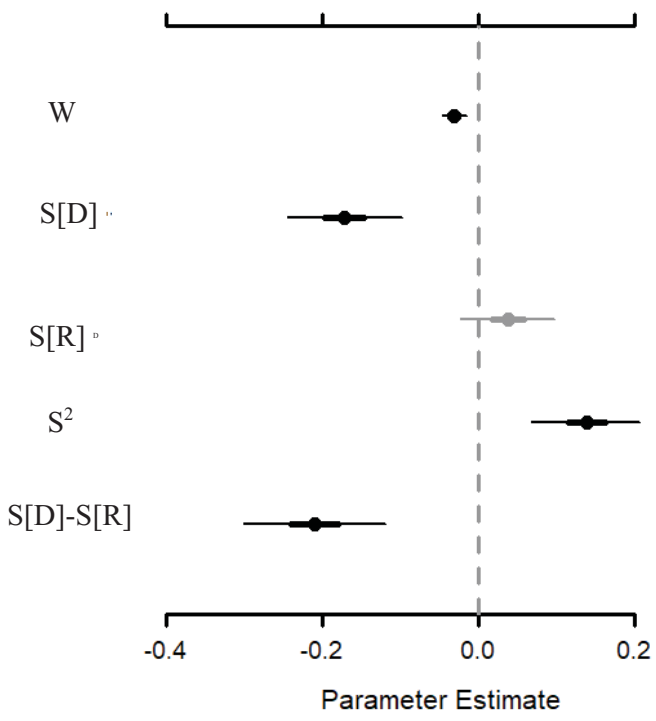

FIGURE 8
Credible intervals of the parameters for water level and salinity in the final model to evaluate the impact of environmental variables on NDVI for Davis Pond diversion project. S denotes mean daily salinity, and W denotes mean daily water level. [D] denotes diversion site, and [R] denotes reference site. If a particular parameter does not have brackets, this parameter does not differ between diversion and reference site. S[D]-S[R] denotes difference of the parameters for mean daily salinity between diversion and reference site. The dot represents median. The thin line shows the 95% credible interval and the thick line shows the 50% credible interval. The grey line with open dot indicates that both 50% and 95% credible intervals overlap 0, the grey line with grey dot indicates that 50% credible interval does not overlap 0 while 95% credible interval does, and the black line with black dot indicates that both 50% and 95% credible intervals do not overlap 0. Plot generated using MCMCvis package in R (Youngflesh, 2018).

2005). A greenhouse study conducted at Breton Sound influenced by river water from the Caernarvon diversion showed that 36% of added nitrate was assimilated in the above- and belowground macrophytes, while the majority was removed from gaseous loss by denitrification (VanZomeren et al., 2012; White et al., 2019).

Adding sediment could raise marsh surface, increase aboveground biomass and number of regenerating shoots of *Spartina alterniflora* (DeLaune et al., 1990). The actual freshwater or sediment diverted for both Davis Pond and Carnarvon projects was less than the capacity designed. How and where the sediment will settle related to freshwater diversion will affect wetland gain or loss spatially. Our model does not only lack data, but also lacks the spatial scales needed to address that question. Other research has shown freshwater diversions are more effective if fine sediment transport in the system (many rivers have experienced long-term reductions) is restored (Kemp et al., 2016; Day et al., 2019). Thus, nutrients and sediment loading data should be collected and accounted for in future evaluations of the impacts of diversion projects on coastal wetlands. Other potential abiotic factors that need to be accounted for include redox potential and sulfide concentration that can affect vegetation growth (DeLaune et al., 1983; Twilley et al., 2019).

This study is not the first one to utilize remote sensing data to evaluate the impact of freshwater diversions on coastal wetlands in Louisiana. Metzger (2007) applied Landsat images to evaluate wetland gains and loss until 2005 for the Caernarvon project. Our study expanded temporal and spatial coverages by including two diversion projects and the analysis was conducted until 2018. As the impact of freshwater diversions tends to be long term, the inclusion of longer-term data is necessary. Another remote sensing-based study (White et al., 2023) showed land gains in the Davis Pond diversion outfall area but not at the Caernarvon diversion outfall area. Our study showed a significant increase of NDVI at the Caernarvon diversion site and a marginal increase at the Davis Pond diversion site. Meanwhile, NDVI at the reference sites of the diversion projects did not change significantly. The increase of NDVI, approximating increased primary productivity, will likely contribute to increased sediment accretion that can lead to land gains.

There are many vegetation indices in the remote sensing literature. Potentially we can compare them to select the one that best indicated vegetation productivity as in Wu et al. (2018). However, lack of spatial data of vegetation productivity presents a barrier for this comparison and analysis of multiple vegetation indices is beyond the scope of this study that focused on evaluating how Bayesian models can facilitate the evaluation of freshwater diversions on wetland vegetation temporally by accounting for the drivers of salinity and inundation.

Conclusion

There existed differences between the two diversion projects in NDVI's temporal trends and how water levels and salinity impacted NDVI. Based on the NDVI alone, they increased or marginally increased over time at the diversion sites but not at the reference sites for both diversion projects. These indicated that freshwater diversions helped increase vegetation productivity. Both mean salinity and mean water level were consistently included in the NDVI models as important predictors.

This study provides a Bayesian modeling framework that can help evaluate freshwater diversion projects with uncertainty accounted for with a focus on the impact to vegetation. It also shows the importance of investigating the impact of both water level and salinity on vegetation in addition to the temporal trend analysis. The inclusion of these abiotic factors aids in gaining a better understanding of vegetative response to freshwater diversions, and therefore contributes to improved prediction on land change and more-informed coastal wetland restoration decisions in the future.

Data availability statement

The original contributions presented in the study are included in the article/Supplementary Material. Further inquiries can be directed to the corresponding author.

Author contributions

Material preparation, data collection and analysis were performed by WW (Bayesian models), EG (preliminary Bayesian models and abiotic data compilation), and GS (remote sensing image analysis). The first draft of the manuscript was written by WW, and all authors commented on previous versions of the manuscript. All authors contributed to the article and approved the submitted version.

Funding

This work was supported by the fund from the U.S. Army Engineer Research and Development Center through the agreement of Gulf Coast Cooperative Ecosystem Studies Unit with the award number of W912HZ-19-2-0012.

Acknowledgments

We are grateful for the valuable review comments provided by Molly Reif at the U.S. Army Engineer Research and Development Center and two reviewers. We would like to thank Coastwide Reference Monitoring System funded by Coastal Wetlands Planning, Protection, and Restoration Act, The National Aeronautics and Space Administration, and Google Earth Engine, which made environmental data and remote sensing images available for this study.

Conflict of interest

The authors declare that the research was conducted in the absence of any commercial or financial relationships that could be construed as a potential conflict of interest.

Publisher's note

All claims expressed in this article are solely those of the authors and do not necessarily represent those of their affiliated organizations, or those of the publisher, the editors and the reviewers. Any product that may be evaluated in this article, or claim that may be made by its manufacturer, is not guaranteed or endorsed by the publisher.

Supplementary material

The Supplementary Material for this article can be found online at: https://www.frontiersin.org/articles/10.3389/fmars.2023.1202300/full#supplementary-material

References

Allen, Y. C., and Suir, G. M. (2014). *Using high-resolution, regional-scale data to characterize floating aquatic nuisance vegetation in coastal Louisiana navigation channels* (Vicksburg, MS, US: Army Corps of Engineers Engineer Research and Development Center).

Allison, M. A., and Meselhe, E. A. (2010). The use of large water and sediment diversions in the lower Mississippi River (Louisiana) for coastal restoration. *J. Hydrol.* 387 (3–4), 346–360. doi: 10.1016/j.jhydrol.2010.04.001

An, N., Price, K. P., and Blair, J. M. (2013). Estimating above-ground net primary productivity of the tallgrass prairie ecosystem of the Central Great Plains using AVHRR NDVI. *Int. J. Remote Sens.* 34 (11), 3717–3735. doi: 10.1080/01431161.2012.757376

Anisfeld, S. C., and Hill, T. D. (2012). Fertilization effects on elevation change and belowground carbon balance in a long Island sound tidal marsh. *Estuaries Coasts*. 35, 201–211. doi: 10.1007/s12237-011-9440-4

Baustian, M. M., Meselhe, E., Jung, H., Sadid, K., Duke-Sylvester, S. M., Visser, J. M., et al. (2018). Development of an Integrated Biophysical Model to represent morphological and ecological processes in a changing deltaic and coastal ecosystem. *Environ. Model. Softw.* 109, 402–419. doi: 10.1016/j.envsoft.2018.05.019

Brock, M. A., and Britton, D. L. (1995). The role of seed banks in the revegetation of Australian temporary wetlands. In B. Wheeler, S. Shaw, W. Fojt and A. Robertson (eds), *The Restoration of Temperate Wetlands*. Wiley, Chichester, 183–188.

Brown, G. L., McAlpin, J. N., Pevey, K. C., Luong, P. V., Price, C. R., and Kleiss, B. A. (2019). *Mississippi River hydrodynamic and delta management study: Delta management modeling. AdH/SEDLIB multi-dimensional model validation and scenario analysis report* (Vicksburg, MS, US: Engineer Research and Development Center).

Calder, C., Lavine, M., Müller, P., and Clark, J. S. (2003). Incorporating multiple sources of stochasticity into dynamic population models. *Ecology* 84 (6), 1395–1402. doi: 10.1890/0012-9658(2003)084[1395:IMSOSI]2.0.CO;2

Carle, M. (2013). *Spatial structure and dynamics of the plant communities in a prograding river delta: Wax Lake Delta, Atchafalaya Bay, Louisiana*. (Baton Rouge, LA, US: PhD dissertation, Louisiana State University).

Chabreck, R. H., and Linscombe, G. (1997). *Vegetative type map of the Louisiana coastal marshes* (Baton Rouge: Louisiana Department of Wildlife and Fisheries).

Chabreck, R. H., Palmisano, A. W., and Joan, T. (1968). *Vegetative type map of the Louisiana coastal marshes* (Baton Rouge: Louisiana Department of Wildlife and Fisheries).

Chander, G., Markham, B. L., and Helder, D. L. (2009). Summary of current radiometric calibration coefficients for Landsat MSS, TM, ETM+, and EO-1 ALI sensors. *Remote Sens. Environ.* 113 (5), 893–903. doi: 10.1016/j.rse.2009.01.007

Clark, J. S. (2004). Why environmental scientists are becoming Bayesians: Modelling with Bayes. *Ecol. Lett.* 8 (1), 2–14. doi: 10.1111/j.1461-0248.2004.00702.x

Costanza, R., d'Arge, R., de Groot, R., Farber, S., Grasso, M., Hannon, B., et al. (1997). The value of the world's ecosystem services and natural capital. *Nature* 387 (6630), 253–260. doi: 10.1038/387253a0

Couvillion, B. R., Steyer, G. D., Wang, H., Beck, H. J., and Rybczyk, J. M. (2013). Forecasting the effects of coastal protection and restoration projects on wetland morphology in coastal Louisiana under multiple environmental uncertainty scenarios. *J. Coast. Res.* 67, 29–50. doi: 10.2112/SI_67_3

CPRA (2012). *Louisiana's comprehensive master plan for a sustainable coast*. Available at: https://issuu.com/coastalmasterplan/docs/coastal_master_plan-v2?e=3722998/2447530.

CPRA (2017) *Louisiana's Comprehensive Master Plan for a Sustainable Coast*. Available at: https://coastal.la.gov/wp-content/uploads/2017/04/2017-Coastal-Master-Plan_Web-Single-Page_CFinal-with-Effective-Date-06092017.pdf.

CPRA (Coastal Protection and Restoration Authority of Louisiana) (2019) *Coastwide reference monitoring system-wetlands monitoring data. Retrieved from coastal information management system (CIMS) database*. Available at: https://lacoast.gov/crms/.

Day, J. W., Boesch, D. F., Clairain, E. J., Kemp, G. P., Laska, S. B., Mitsch, W. J., et al. (2007). Restoration of the Mississippi Delta: lessons from hurricanes Katrina and Rita. *Science* 315, 1679–1684. doi: 10.1126/science.1137030

Day, J. W., Cable, J. E., Cowan, J. H., Delaune, R., De Mutsert, K., Fry, B., et al. (2009). The impacts of pulsed reintroduction of river water on a Mississippi delta coastal basin. *J. Coast. Res.* (54), 225–243. doi: 10.2112/SI54-015.1

Day, J. W., Cable, J. E., Lane, R. R., and Kemp, G. P. (2016a). Sediment deposition at the Caernarvon Crevasse during the Great Mississippi Flood of 1927: Implications for coastal restoration. *Water* 8 (2), 38. doi: 10.3390/w8020038

Day, J. W., Hunter, R. G., Lane, R. R., Shaffer, G. P., and Day, J. N. (2019). Long-term assimilation wetlands in coastal Louisiana: Review of monitoring data and management. *Ecol. Eng.* 137, 7–20. doi: 10.1016/j.ecoleng.2018.09.019

Day, J. W., Kemp, G. P., Freeman, A. M., and Muth, D. P. (2014). "Introduction: Perspectives on the Restoration of the Mississippi Delta," in *Perspectives on the Restoration of the Mississippi Delta: The Once and Future Delta*. Eds. J. W. Day, G. P. Kemp, A. M. Freeman and D. P. Muth (Springer Science+Business Media Dordrecht), 1–7. doi: 10.1007/978-94-017-8733-8_1

Day, J. W., Lane, R. R., D'Elia, C. F., Wiegman, A. R. H., Rutherford, J. S., Shaffer, G. P., et al. (2016b). Large infrequently operated river diversions for Mississippi delta restoration. *Estuar. Coast. Shelf Sci.* 183, 292–303. doi: 10.1016/j.ecss.2016.05.001

Day, J. W., Lane, R., Moerschbaecher, M., DeLaune, R., Mendelssohn, I., Baustian, J., et al. (2013). Vegetation and soil dynamics of a Louisiana estuary receiving pulsed Mississippi River water following Hurricane Katrina. *Estuaries Coasts* 36, 1–18. doi: 10.1007/s12237-012-9581-0

DeLaune, R. D., Jugsujinda, A., Peterson, G. W., and Patrick, W. H. (2003). Impact of Mississippi River freshwater reintroduction on enhancing marsh accretionary processes in a Louisiana estuary. *Estuar. Coast. Shelf Sci.* 58, 653–662. doi: 10.1016/S0272-7714(03)00177-X

DeLaune, R. D., Kongchum, M., White, J. R., and Jugsujinda, A. (2013). Freshwater diversions as an ecosystem management tool for maintaining soil organic matter accretion in coastal marshes. *Catena* 107, 139–144. doi: 10.1016/j.catena.2013.02.012

DeLaune, R. D., Pezeshki, S. R., and Jugsujinda, A. (2005). Impact of Mississippi River freshwater reintroduction on Spartina patens marshes: Responses to nutrient input and lowering of salinity. *Wetlands* 25, 155–161. doi: 10.1672/0277-5212(2005)025[0155:IOMRFR]2.0.CO;2

DeLaune, R. D., Pezeshki, S. R., Pardue, J. H., Whitcomb, J. H., and Patrick, W. H. (1990). Some influences of sediment addition to a deteriorating salt marsh in the Mississippi river deltaic plain: a pilot study. *J. Coast. Res.* 6, 181–188.

DeLaune, R. D., Smith, C. J., and Patrick, J. W.H. (1983). Relationship of marsh elevation, redox potential and sulfide to Spartina alterniflora productivity. *Soil Sci. Soc Am. J.* 47, 930–935. doi: 10.2136/sssaj1983.03615995004700050018x

Elsey-Quirk, T., Graham, S. A., Mendelssohn, I. A., Snedden, G., Day, J. W., Twilley, R. R., et al. (2019). Mississippi river sediment diversions and coastal wetland sustainability: Synthesis of responses to freshwater, sediment, and nutrient inputs. *Estuarine Coast. Shelf Sci.* 221, 170–183. doi: 10.1016/j.ecss.2019.03.002

Engle, V. D. (2011). Estimating the provision of ecosystem services by Gulf of Mexico coastal wetlands. *Wetlands* 31 (1), 179–193. doi: 10.1007/s13157-010-0132-9

Forbes, M. G., Alexander, H. D., and Dunton, K. H. (2008). Effects of pulsed riverine versus non-pulsed wastewater inputs of freshwater on plant community structure in a semi-arid salt marsh. *Wetlands* 28 (4), 984–994. doi: 10.1672/07-127.1

Fox, L., Valiela, I., and Kinney, E. L. (2012). Vegetation cover and elevation in long-term experimental nutrient-enrichment plots in great sippewissett salt marsh, cape cod, massachusetts: implications for eutrophication and sea level rise. *Estuaries Coasts* 35, 445–458. doi: 10.1007/s12237-012-9479-x

Fox, J., and Weisberg, S. (2019). *An R Companion to Applied Regression. 3rd ed* (Thousand Oaks, CA: SAGE). Available at: https://socialsciences.mcmaster.ca/jfox/Books/Companion/.

Frazier, P. S., and Page, K. J. (2000). Water body detection and delineation with Landsat TM data. *Photogram. Eng. Remote Sens.* 66 (12), 1461–1468.

Hardy, T., and Wu, W. (2021). Impact of different restoration methods on coastal wetland loss in Louisiana: Bayesian analysis. *Environ. Monit. Assess.* 193 (1), 1. doi: 10.1007/s10661-020-08746-9

He, K., Li, W., Zhang, Y., Sun, G., McNulty, S. G., Flanagan, N. E., et al. (2023). Identifying driving hydrogeomorphic factors of coastal wetland downgrading using random forest classification models. *Sci. Total Environ.* 894, 164995. doi: 10.1016/j.scitotenv.2023.164995

Hollis, L. O., and Turner, R. E. (2019). The tensile root strength ofSpartina patens: response to atrazine exposure and nutrient addition. *Wetlands*. doi: 10.1007/s13157-019-01126-1

Hooten, M. B., and Hobbs, N. T. (2015). A guide to Bayesian model selection for ecologists. *Ecol. Monogr.* 85 (1), 3–28. doi: 10.1890/14-0661.1

Jenkins, J. A., Olivier, H. M., Draugelis-Dale, R. O., and Kaller, M. D. (2011). *Davis Pond freshwater diversion biomonitoring—prediversion and postdiversion freshwater fish data: U.S. Geological Survey Data Series 604*. Revised 2012. (Reston, Virginia).

Kalnay, E., Kanamitsu, M., Kistler, R., Collins, W., Deaven, D., Gandin, L., et al. (1996). The NCEP/NCAR 40-year reanalysis project. *Bull. Am. Meteorol. Soc.* 77 (3), 437–472. doi: 10.1175/1520-0477(1996)077<0437:TNYRP>2.0.CO;2

Kearney, M. S., Riter, J. C. A., and Turner, R. E. (2011). Freshwater river diversions for marsh restoration in Louisiana: Twenty-six years of changing vegetative cover and marsh area. *Geophys. Res. Lett.* 38 (16), L16405. doi: 10.1029/2011GL047847

Kemp, G. P., Day, J. W., Rogers, J. D., Giosan, L., and Peyronnin, N. (2016). Enhancing mud supply from the Lower Missouri River to the Mississippi River Delta USA: Dam bypassing and coastal restoration. *Estuarine Coast. Shelf Sci.* 183, 304–313. doi: 10.1016/j.ecss.2016.07.008

Kenney, M. A., Hobbs, B. F., Mohrig, D., Huang, H., Nittrouer, J. A., Kim, W., et al. (2013). Cost analysis of water and sediment diversions to optimize land building in the Mississippi River delta: Cost analysis to optimize Mississippi Delta land building. *Water Resour. Res.* 49 (6), 3388–3405. doi: 10.1002/wrcr.20139

Keogh, M. E., Kolker, A. S., Snedden, G. A., and Renfro, A. A. (2019). Hydrodynamic controls on sediment retention in an emerging diversion-fed delta. *Geomorphology* 332, 100–111. doi: 10.1016/j.geomorph.2019.02.008

Kirwan, M. L., Guntenspergen, G. R., D'Alpaos, A., Morris, J. T., Mudd, S. M., and Temmerman, S. (2010). Limits on the adaptability of coastal marshes to rising sea level. *Geophys. Res. Lett.* 37 (23), L23401. doi: 10.1029/2010GL045489

Kral, F., Corstanje, R., White, J. R., and Veronesi, F. (2012). A geostatistical analysis of soil properties in the Davis Pond Mississippi freshwater diversion. *Soil Sci. Soc. America J.* 76 (3), 1107–1118. doi: 10.2136/sssaj2011.0206

Lacoul, P., and Freedman, B. (2006a). Environmental influences on aquatic plants in freshwater ecosystems. *Environ. Rev.* 14 (2), 89–136. doi: 10.1139/a06-001

Lacoul, P., and Freedman, B. (2006b). Relationships between aquatic plants and environmental factors along a steep Himalayan altitudinal gradient. *Aquat. Bot.* 84 (1), 3–16. doi: 10.1016/j.aquabot.2005.06.011

Lai, X., Jiang, J., and Huang, Q. (2013). Effects of the normal operation of the Three Gorges Reservoir on wetland inundation in Dongting Lake, China: A modelling study. *Hydrol. Sci. J.* 58 (7), 1467–1477. doi: 10.1080/02626667.2013.831418

Lambert, P. C., Sutton, A. J., Burton, P. R., Abrams, K. R., and Jones, D. R. (2005). How vague is vague? A simulation study of the impact of the use of vague prior distributions in MCMC using WinBUGS. *Stat Med.* 24 (15), 2401–2428. doi: 10.1002/sim.2112

Lane, R. R., Day, J. W., and Day, J. N. (2006). Wetland surface elevation, vertical accretion, and subsidence at three Louisiana estuaries receiving diverted Mississippi River water. *Wetlands* 26, 1130–1142. doi: 10.1672/0277-5212(2006)26[1130:WSEVAA]2.0.CO;2

Lane, R. A., and Kay, A. L. (2021). Climate change impact on the magnitude and timing of hydrological extremes across great britain. *Front. Water* 3. doi: 10.3389/frwa.2021.684982

Lavers, D. A., Ralph, F. M., Waliser, D. E., Gershunov, A., and Dettinger, M. D. (2015). Climate change intensification of horizontal water vapor transport in CMIP5. *Geophys. Res. Lett.* 42, 5617–5625. doi: 10.1002/2015GL064672

Lin, Y., Yu, J., Cai, J., Sneeuw, N., and Li, F. (2018). Spatio-temporal analysis of wetland changes using a kernel extreme learning machine approach. *Remote Sens.* 10 (7), 1129. doi: 10.3390/rs10071129

Linscombe, R., and Chabreck, R. (2001). *Coastwide aerial survey, brown marsh 2001 assessment: Salt marsh dieback in Louisiana-Brown marsh data information management system*, Vol. 8, Task III. Available at: https://lacoast.gov/new/ed/articles/brownmarsh.aspx.

Lopez, J., Henkel, T., Moshogianis, A., Baker, A., Boyd, E., Hillmann, E., et al. (2014). Examination of deltaic processes of Mississippi River outlets-Caernarvon Delta and Bohemia Spillway in Southeast Louisiana. *GCAGS J.* (3), p. 79–93.

Metzger, M. G. (2007). Assessing the Effectiveness of Louisiana' s Freshwater Diversion Projects Using Remote Sensing (New Orleans, LA, US: Thesis, University of New Orleans). Available at: https://scholarworks.uno.edu/td/633/.

Morris, J. T., Sundareshwar, P. V., Nietch, C. T., Kjerfve, B., and Cahoon, R. ,. D. (2002). Responses of coastal wetlands to rising sea level. *Ecology* 10, 2869–2877). doi: 10.1890/0012-9658(2002)083[2869:ROCWTR]2.0.CO;2

O'Neil, T. (1951). *The muskrat in the Louisiana coastal marshes: A study of the ecological, geological, biological, tidal and climatic factors governing the production and management of the muskrat industry in Louisiana* (New Orleans, LA, US: Federal Aid Section, Fish and Game Division, Louisiana Department of Wild Life and Fisheries).

Pahl, J. W., Freeman, A. M., Raynie, R. C., and Day, J. (2020). Response of the coastal systems to freshwater input with emphasis on Mississippi River deltaic plain river diversions: Synthesis of the state of the science. *Estuar. Coast. Shelf Sci.* 243, 106866. doi: 10.1016/j.ecss.2020.106866

Peyronnin, N. S., Caffey, R. H., Cowan, J. H., Justic, D., Kolker, A. S., Laska, S. B., et al. (2017). Optimizing sediment diversion operations: Working group recommendations for integrating complex ecological and social landscape interactions. *Water (Switzerland)* 9 (6), 368. doi: 10.3390/w9060368

Plitsch, E. M. (2014). *2013 operations, maintenance and monitoring report* (Coastal Protection and Restoration Authority of Louisiana).

Plitsch, E. M. (2018). *2017 operations, maintenance, and monitoring report for Davis Pond freshwater diversion (BA-01)* (Baton Rouge, LA, US: Coastal Protection and Restoration Authority of Louisiana).

Plummer, M. (2017). *JAGS version 4.3. 0 user manual*, [Computer software manual]. Retrieved from Sourceforge. Net/Projects/Mcmc-Jags/Files/Manuals/4. x, 2.

Reif, M. K., Macon, C. L., and Wozencraft, J. M. (2011). Post-Katrina land-cover, elevation, and volume change assessment along the south shore of Lake Pontchartrain, Louisiana, USA. *J. Coast. Res.* 62, 30–39. doi: 10.2112/SI_62_4

Robert, C. P., and Casella, G. (2004). *Monte Carlo statistical methods. 2. ed* (Springer Science+Business Media New York). doi: 10.1007/978-1-4757-4145-2

Rouse, J. W., Haas, R. H., Schell, J. A., and Deering, D. W. (1974). "Monitoring vegetation systems in the Great Plains with ERTS," in *Proceedings of the Third Earth Resources Technology Satellite-1 Symposium*, Greenbelt, MD: NASA SP-351. 309–317.

Rutherford, J. S., Day, J. W., D'Elia, C. F., Wiegman, A. R., Willson, C. S., Caffey, R. H., et al. (2018). Evaluating trade-offs of a large, infrequent sediment diversion for restoration of a forested wetland in the Mississippi delta. *Estuarine Coast. Shelf Sci.* 203, 80–89. doi: 10.1016/j.ecss.2018.01.016

Sasser, C. E. (1994). *Vegetation dynamics in relation to nutrients in floating marshes in Louisiana, USA*. (Baton Rouge, LA, US: Coastal Ecology Institute, Louisiana State University).

Sasser, C. E., Visser, J. M., Mouton, E., Linscombe, G. ,. J., and Hartley, S. (2008). *Vegetation types in coastal Louisiana in 2007: U.S. Geological Survey open file report 2008-1224*, 1 sheet, scale 1:550,000 (Open-File Report) [Open-File Report].

Sasser, C. E., Visser, J. M., Mouton, E., Linscombe, J., and Hartley, S. B. (2014). *Vegetation types in coastal Louisiana in 2013: U.S. Geological Survey Scientific Investigations Map 3290*, 1 sheet, scale 1:550,000 (Scientific Investigations Map) [Scientific Investigations Map]. doi: 10.3133/sim3290

Schmidt, G. L., Jenkerson, C., Masek, J. G., Vermote, E., and Gao, F. (2013). Landsat ecosystem disturbance adaptive processing system (LEDAPS) algorithm description: U.S. Geological Survey Open-File Report 2013–1057, 17 p. (Reston, Virginia, US). doi: 10.3133/ofr20131057

Snedden, G. A., Cable, J. E., Swarzenski, C., and Swenson, E. (2007). Sediment discharge into a subsiding Louisiana deltaic estuary through a Mississippi River diversion. *Estuar. Coast. Shelf Sci.* 71, 181–193. doi: 10.1016/j.ecss.2006.06.035

Snedden, G. A., Cretini, K., and Patton, B. (2015). Inundation and salinity impacts to above- and belowground productivity in Spartina patens and Spartina alterniflora in the Mississippi River deltaic plain: Implications for using river diversions as restoration tools. *Ecol. Eng.* 81, 133–139. doi: 10.1016/j.ecoleng.2015.04.035

Stagg, C. L., Krauss, K. W., Cahoon, D. R., Cormier, N., Conner, W. H., and Swarzenski, C. M. (2016). Processes contributing to resilience of coastal wetlands to sea-level rise. *Ecosystems* 19 (8), 1445–1459. doi: 10.1007/s10021-016-0015-x

Suir, G., Saltus, C., Johnston, J., and Barras, J. (2011). *Development of methodology to classify historical panchromatic aerial photography. Analysis of landscape features on Point au Fer Island, Louisiana-from 1956 to 2009: A case study*. (Baton Rouge, LA, US: Engineer Research and Development Center).

Suir, G. M., and Sasser, C. E. (2017). *Floristic quality index of restored wetlands in coastal Louisiana* (Vicksburg, MS, US: Engineer Research and Development Center).

Suir, G. M., and Sasser, C. E. (2019a). Use of NDVI and landscape metrics to assess effects of riverine inputs on wetland productivity and stability. *Wetlands* 39 (4), 815–830. doi: 10.1007/s13157-019-01132-3

Suir, G., and Sasser, C. E. (2019b). Redistribution and impacts of nearshore berm sediments: Chandeleur Barrier Islands, Louisiana, United States. *Ocean Coast. Manage.* 168, 103–116. doi: 10.1016/j.ocecoaman.2018.10.029

Suir, G., Suir, K., and Sapkota, S. (2018). *Use of remote sensing to detect and predict aquatic nuisance vegetation growth in coastal Louisiana: Summary of findings* (Environmental Laboratory (U.S). doi: 10.21079/11681/26649

Turner, R. E. (2011). Beneath the salt marsh canopy: Loss of soil strength with increasing nutrient loads. *Estuaries Coasts* 34 (5), 1084–1093. doi: 10.1007/s12237-010-9341-y

Turner, R. E., Layne, M., Mo, Y., and Swenson, E. M. (2019). Net land gain or loss for two Mississippi River diversions: Caernarvon and Davis Pond. *Restor. Ecol.* 27 (6), 1231–1240. doi: 10.1111/rec.13024

Twilley, R. R., Day, J. W., Bevington, A. E., Castañeda-Moya, E., Christensen, A., Holm, G., et al. (2019). Ecogeomorphology of coastal deltaic floodplains and estuaries in an active delta: Insights from the Atchafalaya Coastal Basin. *Estuar. Coast. Shelf Sci.* 227, 106341. doi: 10.1016/j.ecss.2019.106341

USACE (2002) *Davis Pond Freshwater Diversion*. Available at: https://www.mvn.usace.army.mil/About/Projects/Davis-Pond-Freshwater-Diversion/.

USACE (2013) *Modification of Caernarvon Diversion*. Available at: https://www.mvn.usace.army.mil/Portals/56/docs/environmental/LCA/Near-Term%20Projects/ModofCaernarvonFactSheetJanuary2013PAO.pdf.

VanZomeren, C. M., White, J. R., and DeLaune, R. D. (2012). Fate of nitrate in vegetated brackish coastal marsh. *Soil Sci. Soc Am. J.* 76, 1919–1927. doi: 10.2136/sssaj2011.0385

Villarrubia, C. (2002). *Caernarvon Freshwater Diversion Project* (Louisiana, US: Louisiana Department of Natural Resources), 30. Available at: https://lacoast.gov/reports/project/3890870~1.pdf.

Visser, J., Duke-Sylvester, S., Shaffer, G., Hester, M., Couvillion, B., Broussard, W.III, et al. (2017). *Coastal Master Plan: Attachment C3-5: Vegetation* (Baton Rouge, Louisiana: Coastal Protection and Restoration Authority), 1–128.

Visser, J. M., Sasser, C. E., Chabreck, R. H., and Linscombe, R. G. (2002). The impact of a severe drought on the vegetation of a subtropical estuary. *Estuaries* 25 (6), 1184–1195. doi: 10.1007/BF02692215

Wang, Y., Colby, J. D., and Mulcahy, K. A. (2002). An efficient method for mapping flood extent in a coastal floodplain using Landsat TM and DEM data. *Int. J. Remote Sens.* 23 (18), 3681–3696. doi: 10.1080/01431160110114484

White, J. R., Couvillion, B., and Day, J. W. (2023). Coastal wetland area change for two freshwater diversions in the Mississippi River Delta. *Ecol. Eng.* 186, 106819. doi: 10.1016/j.ecoleng.2022.106819

White, J. R., DeLaune, R. D., Justic, D., Day, J. W., Pahl, J., Lane, R. R., et al. (2019). Consequences of Mississippi River diversions on nutrient dynamics of coastal wetland soils and estuarine sediments: A review. *Estuar. Coast. Shelf Sci.* 224, 209–216. doi: 10.1016/j.ecss.2019.04.027

White, E., and Kaplan, D. (2017). Restore or retreat? Saltwater intrusion and water management in coastal wetlands. *Ecosys. Health Sustain.* 3 (1), e01258. doi: 10.1002/ehs2.1258

Wu, W., Bethel, M., Mishra, D. R., and Hardy, T. (2018). Model selection in Bayesian framework to identify the best WorldView-2 based vegetation index in predicting green biomass of salt marshes in the northern Gulf of Mexico. *GIScience Remote Sens.* 55 (6), 880–904. doi: 10.1080/15481603.2018.1460934

Wu, W., Biber, P., Mishra, D. R., and Ghosh, S. (2020). Sea-level rise thresholds for stability of salt marshes in a riverine versus a marine dominated estuary. *Sci. Total Environ.* 718, 137181. doi: 10.1016/j.scitotenv.2020.137181

Wu, W., Biber, P. D., Peterson, M. S., and Gong, C. (2012). Modeling photosynthesis of Spartina alterniflora (smooth cordgrass) impacted by the Deepwater Horizon oil spill using Bayesian inference. *Environ. Res. Lett.* 7 (4), 45302. doi: 10.1088/1748-9326/7/4/045302

Youngflesh, C. (2018). MCMCvis: Tools to visualize, manipulate, and summarize MCMC output. *J. Open Source Software* 3, 640. doi: 10.21105/joss.00640

Zedler, J. B. (2001). *Handbook for Restoring Tidal Wetlands* (Boca Raton, Florida, US: CRC Press). Available at: http://www.crcnetbase.com/isbn/9780849390630.

frontiers | Frontiers in Marine Science

TYPE Original Research
PUBLISHED 29 November 2023
DOI 10.3389/fmars.2023.1280373

OPEN ACCESS

EDITED BY
Tian Xie,
Beijing Normal University, China

REVIEWED BY
Surya Prakash Tiwari,
King Fahd University of Petroleum and Minerals, Saudi Arabia
Dixon Gevaña,
University of the Philippines Los Baños, Philippines

*CORRESPONDENCE
Demin Zhou
zhoudemin@cnu.edu.cn
Yinghai Ke
yke@cnu.edu.cn

RECEIVED 20 August 2023
ACCEPTED 14 November 2023
PUBLISHED 29 November 2023

CITATION
Wang Y, Wang X, Khan S, Zhou D and Ke Y (2023) Evaluation of mangrove restoration effectiveness using remote sensing indices - a case study in Guangxi Shankou Mangrove National Natural Reserve, China. *Front. Mar. Sci.* 10:1280373.
doi: 10.3389/fmars.2023.1280373

Evaluation of mangrove restoration effectiveness using remote sensing indices - a case study in Guangxi Shankou Mangrove National Natural Reserve, China

Yuhang Wang[1], Xifei Wang[2], Shahbaz Khan[3], Demin Zhou[1*] and Yinghai Ke[1*]

[1]College of Resource Environment and Tourism, Capital Normal University, Beijing, China, [2]Faculty of Geo-Information Science and Earth Observation (ITC), University of Twente, Enschede, Netherlands, [3]United Nations Educational, Scientific and Cultural Organization (UNESCO) Beijing Cluster Office, Beijing, China

As one of the most productive marine ecosystems in the coastal wetlands, mangrove forests have been severely threatened by intensive human activities. Many countries and regions have carried out mangrove restoration projects. The evaluation of mangrove restoration effectiveness is of great significance for scientific decision-making for restoration engineering and wetland management. In this study, we presented a remote-sensing-based Mangrove Restoration Effectiveness Index (MREI) to evaluate mangrove restoration effectiveness. We took the Guangxi Shankou Mangrove National Natural Reserve (GSMNNR) in China, a UNESCO Biosphere Reserve, as our study area, where four phases of afforestation were implemented during 1990-2022. The MREI was developed based on Landsat-series images by considering the change in mangrove area and the Normalized Difference Vegetation Index (NDVI) from the start year to the end year of each afforestation phase (evaluation period). We further evaluated the Persistence of Restoration Effectiveness (PRE) based on the MREI change trajectory during the whole evaluation period, and the Process-based Restoration Effectiveness Index (PREI) was developed to evaluate the restoration effectiveness at village scale. The results showed that MREI can effectively represent the trajectory of mangrove restoration and showed consistent pattern with high-spatial-resolution imagery. From 1990 to 2022, the mangrove forest area increased from 235.26 ha in 1990 to 873.27 ha in 2022, and 84.59% of the mangrove forest was converted from tidal flats in the reserve. The average value of MREI in the five evaluation phases were 0.48, 0.24, 0.29, 0.17, and 0.72, respectively. The dynamic change of MREI showed that 5.24% of the zones had poor PRE, 44.17% of the zones had excellent PRE. From the perspective of spatial distribution, the Zones with PREI values ranging from high to low were follows: Zone A, E, J, G, C, H, I (D), F, B. Overall, the high value zones of PREI were mainly distributed in the central of the Dandou Sea and the northern part of the Yingluo Bay. The low value zones were distributed in the northwest of the Dandou Sea. We expect the MREI and PREI have great potential to be applied to other regions to evaluate mangrove restoration effectiveness.

KEYWORDS

afforestation, NCSSCP (National Coastal Shelterbelt System Construction Project), mangrove cover, MREI (Mangrove Restoration Effectiveness Index), PREI (Process-based Restoration Effectiveness Index), growth

1 Introduction

Mangroves have significant social, economic, and ecological values and play an important role in maintaining coastal ecological stability, reducing coastal erosion, and mitigating global warming (Carugati et al., 2018; Worthington et al., 2020). In the 1980s, mangroves were disappearing at about 1% per year, making them one of the most threatened ecosystems in the world (Friess et al., 2019). According to this trend, the global mangrove forests will disappear within 100 years (Duke et al., 2007; Polidoro et al., 2010). After the 21st century, many countries began to pay attention to mangrove restoration and management. The research on the mangrove wetlands restoration mainly focuses on four aspects: 1) selection of suitable afforestation site; 2) selection of tree species; 3) planting techniques; 4) management and monitoring after planting (Peng et al., 2008). With the recognition of the importance of mangroves and the implementation of mangrove restoration projects, the mangrove loss rate gradually slowed down compared to the previous period (Hamilton and Casey, 2016).

Although mangrove restoration strategies include natural and artificial restoration, most restoration focuses on direct mangrove planting (Kamali and Hashim, 2011). In 1988, China proposed the National Coastal Shelterbelt System Construction Project (NCSSCP), and mangrove planting and restoration is one of the important contents. The NCSSCP Phase I Plan (1990-2000) was implemented in 1990. In 2001, the State Forestry Administration launched the NCSSCP Phase II Plan (2001-2010). Subsequently, in order to further expand the scope of construction, the second phase planning period was extended to 2015. The NCSSCP Phase III Plan (2016-2015) was officially launched in 2016, and it is planned to restore 48,650 ha of mangrove by 2025 (Bao and Yang, 2022). Moreover, a number of mangrove nature reserves have been set up since the 1980s in China. At present, 38 mangrove reserves have been established, which cover more than 75% of the existing natural mangroves (Lu et al., 2022). Due to China's strict protection and large-scale planting restoration of mangrove forests, the mangrove area has grown at an average annual rate of 1.8% since 2001 (Wang et al., 2020; Jia et al., 2021; Huang et al., 2023). The restoration effectiveness of mangroves is often influenced by many factors, including natural factors like soil salinity, water level, and biological invasions, as well as human-related factors like afforestation technology, tree species selection, and post-planting management (Primavera and Esteban, 2008; Wodehouse and Rayment, 2019). However, in some regions the survival and preservation rates of mangrove cultivation are low, posing challenges for mangrove restoration. For example, the preservation rate of afforestation in Fangchenggang City, Guangxi, was only 9.28% from 2002 to 2007 (Fan and Mo, 2018). The mangrove planting cases in the Philippines from 1984 to 1995 showed that the survival rate of directly planting mangroves was less than 20% due to mismatched tree species and planting locations, as well as a lack of post planting management (Primavera and Esteban, 2008). Therefore, some regions have explored community-based mangrove restoration schemes that do not directly plant mangroves. For example, a study in the Mekong Delta shows that if local shrimp farmers are given sufficient economic incentives and legal rights, and assigned responsibility for mangroves, they can participate in the protection and sustainable management of mangroves (Ha et al., 2012). Ayeyarwady Delta in Myanmar planted mangroves under the framework of community-based integrated coastal zone management (ICZM), with a survival rate of over 60% (Veettil et al., 2018). It is important to conduct quantitative evaluations of the mangrove restoration effectiveness in order to guide the government in inspecting the results of restoration projects, adjusting subsequent restoration locations, and improving restoration techniques.

In order to evaluate the success of mangrove ecosystem restoration, indicators such as biodiversity, mangrove area, vegetation growth, and carbon sequestration can be used to characterize the recovery trajectory of mangrove growth over time. Traditional biodiversity monitoring methods such as transect and plot can be used to acquire these indices (Cadier et al., 2020; Gatt et al., 2022; Gerona-Daga and Salmo, 2022). These monitoring methods can finely evaluate the mangrove restoration effectiveness, however, the field measurement is difficult to carry out large-scale monitoring and reveal spatial heterogeneity. Remote sensing technology has the potential to obtain historical images of inaccessible areas, which has been widely used for large-scale and long-term mangrove monitoring efforts (Seto and Fragkias, 2007; Wang et al., 2019). At present, there are many publicly available mangrove mapping datasets which were generated using remote sensing techniques. These datasets include global or regional mangrove maps with spatial resolution of 30 m or 10 m, such as Global Mangrove Watch (Bunting et al., 2022), Global Mangrove Distribution USGS (Giri et al., 2011), LERIS_GLOBAL_MANGROVE (Xiao et al., 2021), Tidal Wetlands in East Asia (Zhang Z. et al., 2022), Mangrove Map of China for 2019 (Zhao and Qin, 2022), CAS_Mangrove (Jia et al., 2018), etc. In addition to global mangrove datasets, many studies carried out mangrove monitoring using land cover classification at regional scale

(Gevana et al., 2015). Although global datasets provide necessary baseline mangrove maps in a single year or multiple years, they did not provide other land cover types nearby the mangroves. Therefore, they did not support the analysis of conversion between mangroves and other land cover types. In addition, none of the datasets cover the entire phases of NCSSCP. It is necessary to classify mangroves and other land cover according to specific objectives.

Most studies used dynamic changes in land cover and landscape indices to reveal the effectiveness of mangrove restoration and protection. The commonly used landscape indices include patch area, patch density, boundary density, aggregation, etc., (Suyadi et al., 2018; Zhen, 2019; Du et al., 2023). Some researchers combined multiple landscape indices to build a composite index for evaluation of mangrove restoration effectiveness (Liu et al., 2022). Most of these indices are calculated based on the mangrove distribution maps. Note that the recovery of mangrove ecosystems is characterized by the increase of mangrove area and canopy density, which can be represented by the change in remote sensing spectral indexes, such as Normalized Difference Vegetation Index (NDVI). Zhu et al. (2021) used the method of time series analysis using mangrove NDVI and combined it with land cover data to study the changes in mangrove growth in Qinglan Port, China (Zhu et al., 2021). However, at present, few studies have integrated the mangrove area and the vegetation index to evaluate the restoration effectiveness (Wang et al., 2018; Gilani et al., 2021).

The Guangxi Shankou Mangrove National Natural Reserve (GSMNNR), located in Beihai City, Guangxi, was established in 1990 and is recognized as a UNESCO Biosphere Reserve. The NCSSCP project can be divided into four mangrove afforestation phases in GSMNNR: NCSSCP Phase I during 1990-2000 (Phase 1), the first half of NCSSCP Phase II during 2000-2008 (Phase 2), the second half of NCSSCP Phase II during 2008-2015 (Phase 3), NCSSCP Phase III during 2015-2022 (Phase 4). In this study, we aimed to present remote-sensing-based indices to evaluate the mangrove restoration effectiveness and the Persistence of Restoration Effectiveness (PRE). We took GSMNNR as our study area, and analyzed the conversion between mangroves and other land cover types during the NCSSCP project phases based on remote sensing classification results. Then, we developed Mangrove Restoration Effectiveness Index (MREI) to evaluate the effectiveness of mangrove restoration during each evaluation period by taking account of both mangrove area change and the change in NDVI. Based on the change trajectory of MREI, further developed a Process-based Restoration Effectiveness Index (PREI) to evaluate the persistence of the restoration effectiveness during the whole evaluation period. Note that "restoration" here indicates recovery of mangrove vegetation, and the restoration of the entire ecosystem function was not involved. The objectives of the study are to 1) propose a novel framework for evaluating the effectiveness of mangrove restoration and verify its feasibility; 2) take GSMNNR as a case study, explore the mangrove restoration effectiveness under the background of NCSSCP; 3) propose some suggestions for mangrove restoration.

2 Materials and methods

2.1 Study area

The GSMNNR(109°37′22″E~109°47′03″E, 21°28′21″N~21°36′59″N) is located on the Shatian peninsula, adjacent to the southern boundary of the Beibu Gulf (Figure 1). It includes Yingluo Bay as its eastern part and the Dandou Sea as its western part, covering an area of 800 km^2. The reserve joined the Chinese Man and the Biosphere (MAB) in 1993, joined the UNESCO World Network of Man and the Biosphere Reserves in January 2000, and was listed as a wetland of international importance in February 2002. Most of the mudflats in the reserve are submerged by water during the high tide period, and all of them are exposed when the tide ebbs. The soil is muddy saline-alkali, which is severely eroded by waves, tides, and erosion, resulting in severe collapse of the coastal edges. In the low tidal mudflat zone, pioneer tree species such as *Avicennia marina*, *Aegiceras corniculatum*, and *Sonneratia caseolaris* are planted; In the middle tidal beach area, species such as *Acanthus ilicifolius*, *Bruguiera gymnorrhiza*, *Ceriops tagal*, *Kandelia obovate*, and *Rhizophora stylosa* are planted; The high tide zone is mainly composed of semi-mangroves, such as *Excoecaria agallocha*, *Lumnitzera littorea*, *Hibiscus tiliaceus*, etc. The afforestation density of general tree species is about 120 plants per hectare, while the afforestation density of caseolaris and apetala is about 30 plants per hectare. *Spartina alterniflora* is a salt marsh plant native to the west coast of north America and was introduced in China in 1979 (Min et al., 2023). *S. alterniflora* spread from 167.0 ha in 2003 to 413.0 ha in 2015 due to its strong ability to adapt and reproduce, posing a threat to native mangrove species and biodiversity (Liu, 2018; Li et al., 2021). According to the boundaries of Beihai's administrative villages and the Google Earth images, the reserve was divided into ten zones.

2.2 Data source

2.2.1 Landsat imagery

Landsat 5 Thematic Mapper (TM) and Landsat 8 Operational Land Imager (OLI) images with a spatial resolution of 30m in 1990, 2000, 2008, 2015, and 2022 were obtained from Google Earth Engine (GEE), according to the timeline of NCSSCP (Supplementary, Table A). These images are used to acquire land use data in the reserve. Because mangroves are periodically inundated by tides and during the growing season, *S. alterniflora* has similar spectral characteristics to mangroves. In order to improve interpretation accuracy, all images were screened and the optimal images were downloaded annually for classification. The optimal images are considered to be those of low tide and non-growing seasons. (Xu et al., 2021). In addition, all available Landsat 5 TM and Landsat 8 OLI images in five years were obtained, respectively. After cloud removal, the maximum synthesis method was used to generate the annual maximum NDVI ($NDVI_{max}$) images in the corresponding years. The image filtering and pre-processing processes were based on GEE.

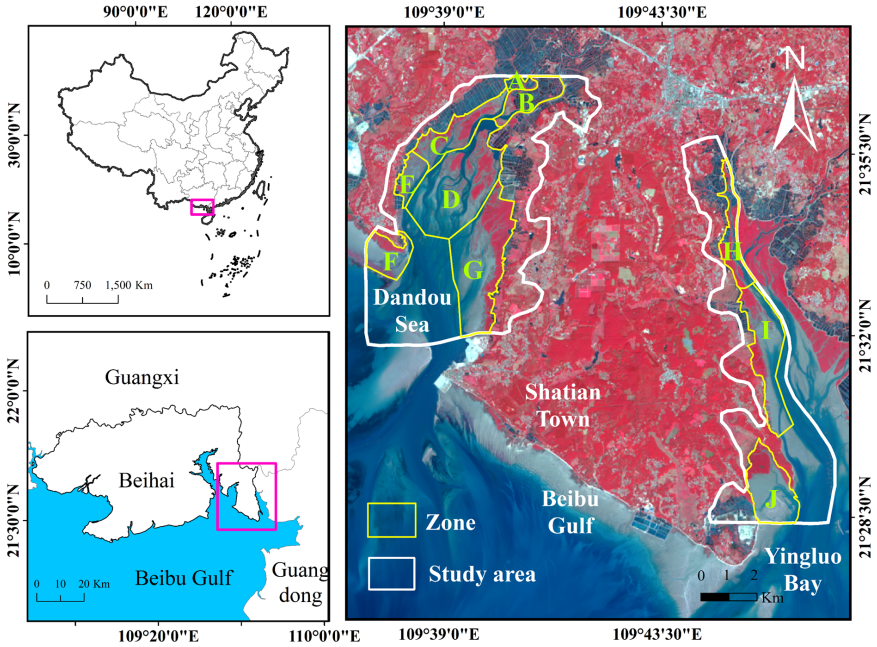

FIGURE 1
Location of the study area. A: Najiang village, B: Najiao village, C: Natan village, D: Dandou village, E: Herong village, F: Shawei village, G: Yongan village, H: Gaopo village, I: Beijie village, J: Yingluo village.

2.2.2 Ancillary data

Mangroves, *S. alterniflora*, and aquaculture ponds are typical wetland types in the study area, and their accurate mapping is an important part of mangrove wetland research. Scholars have published corresponding mapping products. We downloaded public mapping data of mangroves, *S. alterniflora*, and aquaculture ponds from the corresponding years close to our research period for accuracy verification. Data products with a resolution of 30 m were selected. The datasets include the mangrove dataset for 1990, 2000, 2010, and 2015; the *S. alterniflora* dataset for 2000, 2010, and 2015; and the aquaculture pond dataset for 1990, 2000, 2010, 2015, and 2020. These datasets were downloaded from the National Science and Technology Infrastructure Platform - National Earth System Science Data Center.

PlanetScope (PS) images are available in spectral bands: blue (455-515 nm), green (500-590 nm), red (590-670 nm), and near-infrared (NIR, 780-860 nm), with a spatial resolution of 3 m (Roy et al., 2021). In order to facilitate the accuracy validation, we downloaded two cloud-free, atmospherically corrected surface reflectance products (level-3B) for 2016 and 2022 through the education and research program of Planet Labs PBC (Planet Team, 2022).

2.3 Methods

The Landsat-series images were pre-processed and the land cover types in 1990, 2000, 2008, 2015 and 2022 were classified, at the same time, the maximum NDVI during each year was calculated to represent the growing condition of mangroves. Then, mangrove changes were divided into four categories, and the area of each class was estimated using a stratified random sampling method (section 2.3.1). Next, MREI was developed by taking account of both mangrove area change and NDVI change from the start year and the end year of a period (section 2.3.2). As MREI only evaluated the restoration effectiveness during a single period, we further developed a Process-based Restoration Effectiveness Index (PREI) based on the trajectory of MREI change to evaluate the persistence of the restoration effectiveness during the whole evaluation period (from 1990 to 2022) (section 2.3.3). We analyzed the spatial pattern of MREI and PREI at two different scales: grid and village. Section 3.1 describes the classification map of land cover and the dynamic changes between different land covers; Section 3.2 describes the distribution and changes of MREI in a single period; Section 3.3 shows the accuracy of MREI indication effect; Section 3.4 shows the dynamic changes of MREI over multiple periods. (Supplementary, Figure S1).

2.3.1 Land cover classification

In order to extract mangrove extents, spectral indices including Mangrove Vegetation Index (MVI), NDVI, Normalized Difference Built-up Index (NDBI), and Modified Normalized Difference Water Index (mNDWI) were calculated using the following functions (Table 1). ρ_{NIR} is the reflectance of the near-infrared band, ρ_{Red} is the reflectance of the red band, ρ_{Green} is the reflectance of the green band, and ρ_{SWIR} is the reflectance of a short-wave infrared band in Landsat 5 TM and Landsat 8 OLI images.

Then, the Support Vector Machine (SVM) supervised classification method was used to classify the images from 1990, 2000, 2008, 2015, and 2022 into eight land covers, including

TABLE 1 Spectral indices used in this study.

Indices	Abbrev-iation	Formulation	References
Nominalized Difference Vegetation Index	NDVI	$NDVI = \frac{\rho_{NIR} - \rho_{Red}}{\rho_{NIR} + \rho_{Red}}$	(Rouse et al., 1974)
Mangrove Vegetation Index	MVI	$MVI = \frac{\rho_{NIR} - \rho_{Green}}{\rho_{SWIR} - \rho_{Green}}$	(Baloloy et al., 2020)
Normalized Difference Built-up Index	NDBI	$NDBI = \frac{\rho_{SWIR} - \rho_{NIR}}{\rho_{SWIR} + \rho_{NIR}}$	(Zha et al., 2003)
Modified Normalized Difference Water Index	mNDWI	$mNDWI = \frac{\rho_{Green} - \rho_{SWIR}}{\rho_{Green} + \rho_{SWIR}}$	(Xu, 2005)

mangrove forest, tidal flat, *S. alterniflora*, water body, woodland, aquaculture pond, built-up land, and grassland. Around 5,000 samples were collected from Google Earth and PlanetScope images between 1990 and 2022, with around 1,000 samples collected each year within the study area. Overall Accuracy (OA), User's Accuracy (UA), Producer's Accuracy (PA), and F1 Score (F1) were used to evaluate the classification accuracy of mangroves and other land use types. The F1 combines precision and recall into a single value, providing a balanced measure of accuracy. The accuracy evaluation metrics were calculated using the following functions:

$$OA = \frac{\sum_{i=1}^{k} n_{ii}}{N} \quad (1)$$

$$UA_i = \frac{n_{ii}}{n_{i+}} \quad (2)$$

$$PA_i = \frac{n_{ii}}{n_{+i}} \quad (3)$$

$$F1\ \ score = 2 \times \frac{UA_i \times PA_i}{UA_i + PA_i} \quad (4)$$

where N is the total number of samples, n_{ii} represents the number of samples where both the data to be evaluated and the reference data are classified as class i, n_{+i} is the sum of samples classified as class i in the reference data, n_{i+} is the sum of samples classified as class i in the evaluated data (map data).To further evaluate our resultant map's reliability, we verified the mangrove, *S. alterniflora*, and aquaculture pond areas by comparing them to the results from other datasets.

The area of conversion between land cover is usually obtained from remote sensing data. However, the mapping results of remote sensing are rarely perfect, and any map made from remote sensing data may contain some errors. Therefore, there may also be deviations in the area of change calculated based on the mapping results (such as the number of pixels). We adopted the method by Olofsson et al. (2014) to estimate the area change of mangroves, which utilized stratified sampling and error matrices for change area estimation. In this study, we categorized the mangrove change into four classes: stable mangrove, stable non-mangrove, mangrove gain, mangrove loss. The confidence interval for area of change estimation is 95%.

2.3.2 Development of MREI

The restoration of mangroves was reflected by area gain, and the improvement of growth status, e.g., the increase in biomass, density of leaves or canopy cover, which can be represented by NDVI. The MREI was developed on a grid basis and considered both factors. First, the study area was divided into grid cells with size of 150 x 150 m (the area A_1=22,500 m^2). Then, five evaluation periods were established based on the NCSSCP and the time of the establishment of GSMNNR: 1990-2000 (afforestation phase 1), 2000-2008 (afforestation phase 2), 2008-2015 (afforestation phase 3), 2015-2022 (afforestation phase 4), and 1990-2022 (GSMNNR established - 2022, phase 5). For a certain evaluation period, the change in the mangrove area (U) within each grid cell was calculated and expressed as ΔU. Significant increase in the mangrove area indicated that mangrove has been well restored. However, classification errors are inherent in the remote-sensing-based mangrove maps. Therefore, we considered that ΔU should be no less than a tolerance threshold E_0 and $\Delta U \geq E_0$ was defined as the criterion to determine whether there has been any change in the mangrove area. The calculation of E_0 is listed in Eq. 5, which adjusts for the classification error.

$$E_0 = (1 - \overline{U_A}) * \frac{A_1}{A_2} \quad (5)$$

where $\overline{U_A}$ represents the average user accuracy of mangrove classification for the five evaluation phases, which was 0.93 in this study. A_1 is the area of the grid determined, which is 22,500 m^2 in this study, A_2 is the minimum area of the mangrove patch, which was 900 m^2 in this study.

For the grid cells with $0 < \Delta U < E_0$, we considered that the mangrove area has not experienced significant increase, and the change in canopy cover should be accounted for. We calculated the average $NDVI_{max}$ ($\overline{NDVI_{max}}$) within the grid cell in the start year and end year, respectively, and the difference in the $\overline{NDVI_{max}}$ ($\Delta\overline{NDVI}$) was used to represent the change of the canopy cover. Based on changes in mangrove area and vegetation cover (expressed as $\Delta\overline{NDVI}$), the mangrove restoration effectiveness was categorized into four groups and linked to the four intervals of MREI values (Table 2). The MREI formula is built as follows:

$$MREI = \begin{cases} rescale(\Delta U, \{0.5, 1\}), if\ \Delta U > E_0 \\ rescale(\Delta\overline{NDVI}, \{0, 0.5\}), if - E_0 \leq \Delta U \leq E_0\ and\ \Delta\overline{NDVI} \geq 0 \\ rescale(\Delta\overline{NDVI}, \{-0.5, 0\}), if - E_0 \leq \Delta U \leq E_0\ and\ \Delta\overline{NDVI} < 0 \\ rescale(\Delta U, \{-1, -0.5\}), if\ \Delta U < -E_0 \end{cases}, \quad (6)$$

$$rescale(x, \{a, b\}) = a + \frac{b-a}{x_{max} - x_{min}}(x - x_{min})$$

where $rescale\,(x,\ \{a\,,\ b\})$ operator rescaled the variable x to the range of $\{a\,,\ b\}$. The maximum and minimum values of ΔU in all grids in the five evaluation phases were expressed as ΔU_{max}, ΔU_{min}, and the maximum and minimum values of $\Delta\overline{NDVI}$ were expressed as $\Delta\overline{NDVI}_{max}$, $\Delta\overline{NDVI}_{min}$, respectively. Therefore, the four categories of MREI value range represents the four types of

TABLE 2 Four categories characterizing mangrove growth conditions modeled by MREI.

TYPE	MREI value range	Implications
Area increase	(0.5,1)	Mangrove area increase. The larger the value, the more the area increases
Area decrease	(-1,-0.5)	Mangrove area decrease. The smaller the value, the more the area decrease
Better growth	(0, 0.5)	Mangroves grow better, and insignificant changes in the area occur. The larger the value, the better the growth
Worse growth	(-0.5,0)	Mangroves grow worse, and insignificant changes in the area occur. The smaller the value, the worse the growth

restoration effectiveness (Table 2), and the values of MREI represent the degree of restoration effectiveness.

2.3.3 Development of PREI and evaluation of mangrove restoration effectiveness

MREI can be used to evaluate the mangrove recovery during a single period. In order to evaluate the Persistence of the Restoration Effectiveness (PRE) during the whole study period (from 1990 to 2022), we defined the four categories of the MREI change trajectory (Table 3). A grid with positive MREI during all the four evaluation periods is considered to have excellent PRE, while a grid with MREI< -0.5 during at least two periods is considered to have poor PRE.

The PRE category represents the process of restoration effectiveness during the whole period at grid scale. We further developed a Process-based Restoration Effectiveness Index (PREI) at village scale (Eq. 7-8).

$$VMREI = \frac{N_1 * 0.4 + N_2 * 0.3 + N_3 * 0.2 + N_4 * 0.1}{N_t} \quad (7)$$

$$PREI = \frac{VMREI - VMREI_{min}}{VMREI_{max} - VMREI_{min}} \quad (8)$$

where VMREI represents the restoration effectiveness of multiple afforestation phases at a village, N_1, N_2, N_3, N_4 represent the number of grids with excellent, good, average, and poor PRE, respectively within the village, N_t represents the total number of grids in which restoration activities have taken place in the village, PREI is the result of the normalization of the VMREI of all the villages, and the larger the value of PREI, the better restoration effectiveness persistence in the village.

TABLE 3 Four classes for classifying PRE based on MREI trajectory.

Trajectory of MREI	Persistence of restoration effectiveness
MREI > 0 during all four evaluation periods	Excellent
MREI > 0 during at least one evaluation period, while -0.5 ≤ MREI< 0 during one or more periods	Good
There is only one period with MREI< -0.5	Average
There are at least two periods with MREI< -0.5	Poor

3 Results

3.1 Land cover classification

3.1.1 Accuracy assessment

The land cover classification accuracies of GSMNNR in 1990, 2000, 2008, 2015, and 2022 are shown in Table 4. The OA of the corresponding years was 0.92, 0.95, 0.95, 0.92 and 0.94, respectively. The PA values of mangrove ranged from 0.78 to 0.95, and the UA values ranged from 0.91 to 0.98. The average F1 score of mangrove forests exceeded 0.92.

To further assess the accuracy of our resultant map, we compared the area of mangrove forests, aquaculture ponds, and *S. alterniflora* between our data with the publicly available data. We replaced the missing year data with the data set closest to the corresponding study period. Specifically, the aquaculture pond data from 2008 and 2022 were replaced with data from 2010 and 2020, respectively. The mangrove data in 2008 was replaced with the data from 2010. The results showed that, except for differences between the aquaculture pond data we classified in 2008 and 2022 and the publicly available data, there were no significant differences between the other land cover data we classified for other years and the publicly available data (Figure 2). After further examination, the reasons for the difference include: firstly, the publicly available data did not entirely match the years of our data. Secondly, in the publicly available data of 2022, the classification standard of aquaculture ponds was different from the classification standard in general studies.

3.1.2 Land cover maps and dynamic changes

The distribution of land use types in the study area from 1990 to 2022 is shown in Figure 3A. In 1990, large areas of tidal flats were distributed in the Dandou Sea except for Zone G. In 2000, most of the exposed tidal flats were covered by mangroves. After 2008, the expansion of mangrove forests mainly occurred in the tidal flat around the aquaculture ponds in Zone B and the coastal tidal flat in Zone I. Compared with the period before 2008, the expansion trend is not obvious. In 2000, *S. alterniflora* appeared in Zone D and Zone G. *S. alterniflora* spread in the Dandou Sea in 2008 and gradually threatened the mangroves in Zone C. Table 5 shows the area of mangroves and other land cover types in the study area from 1990 to 2022. From 1990 to 2022, the area of mangroves increased from 235.26 ha to 873.27 ha. From 1990 to 2008, the growth rate of the mangrove area was 198.85%, and from 2008 to 2022, the growth rate decreased to 24.2%.

Figure 3B shows the conversion between mangroves and other land cover during 1990-2022. From 1990 to 2022, 667.35 ha and 716.88 ha of other land types were converted into mangroves and *S. alterniflora*, respectively, among which 84.59% and 76.61% were

TABLE 4 Producer's accuracy (PA), user's accuracy (UA) and F1-score of land cover classes.

	1990			2000			2008			2015			2022		
	PA	UA	F1	PA	UA	F1	PA	UA	F1	PA	UA	F1	PA	UA	F1
MF	0.78	0.95	0.86	0.94	0.98	0.97	0.95	0.96	0.95	0.88	0.91	0.89	0.92	0.92	0.91
TF	0.90	0.96	0.93	0.93	0.95	0.94	0.96	0.97	0.96	0.98	0.89	0.93	0.95	0.96	0.96
SA	–	–	–	0.92	0.92	0.92	0.92	0.83	0.87	0.89	0.89	0.89	0.84	0.84	0.84
WB	0.96	0.94	0.95	0.98	0.98	0.98	0.96	0.96	0.96	0.93	0.98	0.96	0.97	0.98	0.98
WL	0.92	0.84	0.88	0.96	0.87	0.97	0.91	0.93	0.92	0.86	0.90	0.89	0.90	0.91	0.91
AP	0.97	0.76	0.85	0.95	0.97	0.96	0.98	0.96	0.97	0.90	0.96	0.93	0.92	0.95	0.94
BL	0.85	0.89	0.87	0.90	0.90	0.90	0.78	0.87	0.82	0.83	0.83	0.83	0.95	0.91	0.93
GL	0.90	0.92	0.91	0.91	0.94	0.93	0.93	0.90	0.92	0.93	0.83	0.88	0.92	0.84	0.88
OA	0.92			0.95			0.95			0.92			0.94		

MF, mangrove forest; TF, tidal flat; SA, *S. alterniflora*; WB, water body; WL, woodland; AP, aquaculture pond; BL, built-up land; GL, grassland.

converted from tidal flats. A total of 148.91 ha of mangroves were converted into non-mangroves, among which 19.3 ha was converted to aquaculture ponds, mainly distributed in the joint area between mangroves and aquaculture ponds, accounting for 12.96% of the mangrove conversion. Table B (Supplementary, Table B) presents the estimation of mangrove area change produced from stratified random sampling and mangrove change map for 1990-2022. From 1990 to 2022, The estimated area of mangrove gain was 594.80 ha (± 113.74 ha).

3.2 Distribution and dynamic changes of MREI

The average MREI values for the five evaluation phases (1990-2000, 2000-2008, 2008-2015, 2015-2022, 1990-2022) were positive: 0.48, 0.24, 0.29, 0.17, and 0.72. The percentage of grid in the 'Area increase' category of MREI decreases gradually from 1990-2000 to 2015-2022. The percentage of grid is the highest in the category of 'Worse growth' during 2015-2022, while during 2008-2015, the 'Better growth' category has the highest percentage of all phases (Figure 4A).

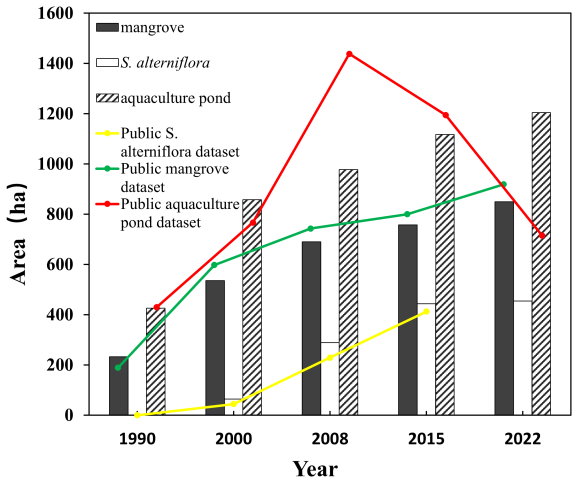

FIGURE 2
Comparison of our resultant map with the publicly available data.

Figures 4B–E show the grid percentage of MREI values in different intervals. In the (0.5 ~ 1.0) range, the MREI values concentrated between 0.7 ~ 1.0 (Figure 4B). In the (-1.0 ~ -0.5) range, the MREI values for 2008-2015 and 2015-2022 are both distributed between -1.0 and -0.8 (Figure 4C). Within the (0 ~ 0.5) range, the MREI values of 1990-2000 and 2000-2008 were distributed in the low-value range (0 ~ 0.2), while the MREI values of the remaining stages were distributed in the high-value range (0.2 ~ 0.5) (Figure 4D). The MREI values from 2015 to 2022 have a larger grid area in the (-0.5 ~ 0) range, but the MREI values of 90.16% of the grid are between the middle range (-0.3 ~ 0.2) (Figure 4E).

The spatial distribution of MREI in five evaluation phases based on the grid scale is shown in Figure 5. From 1990 to 2000, the mangroves located in the southern part of Zone G had MREI values between 0 and -0.5. During this period, the mangrove area in the zone did not change (Figure 3A), but the vegetation coverage decreased. Similarly, from 2000 to 2008, the MREI value of mangroves in Zone C was between 0 and -0.5, and the mangrove vegetation coverage decreased, but the area did not change (Figure 3A). From 2008 to 2015, the MREI values of mangroves in Zone C and Zone E were less than -0.5. During this period, *S. alterniflora* invaded these two zones and the mangrove area decreased (Figure 3A). From 2015 to 2022, the MREI values of Zone A were less than -0.5, resulting in a decrease in the area of mangrove forests located around aquaculture ponds (Figure 3A). From 1990 to 2022, except for the mangroves in the southern part of Zone G and the mangroves in Zone J, whose MREI values range from 0 to 0.5, all other regions had MREI values greater than 0.5.

Figure 6 shows the spatial distribution of average MREI for each zone over five evaluation phases. Zones with an average MREI value greater than 0 were the most common during the five evaluation phases. From 1990 to 2000, the average MREI value in Zone J was -0.5 ~ 0, while the values in other zones were greater than 0,

10.3389/fmars.2023.1280373

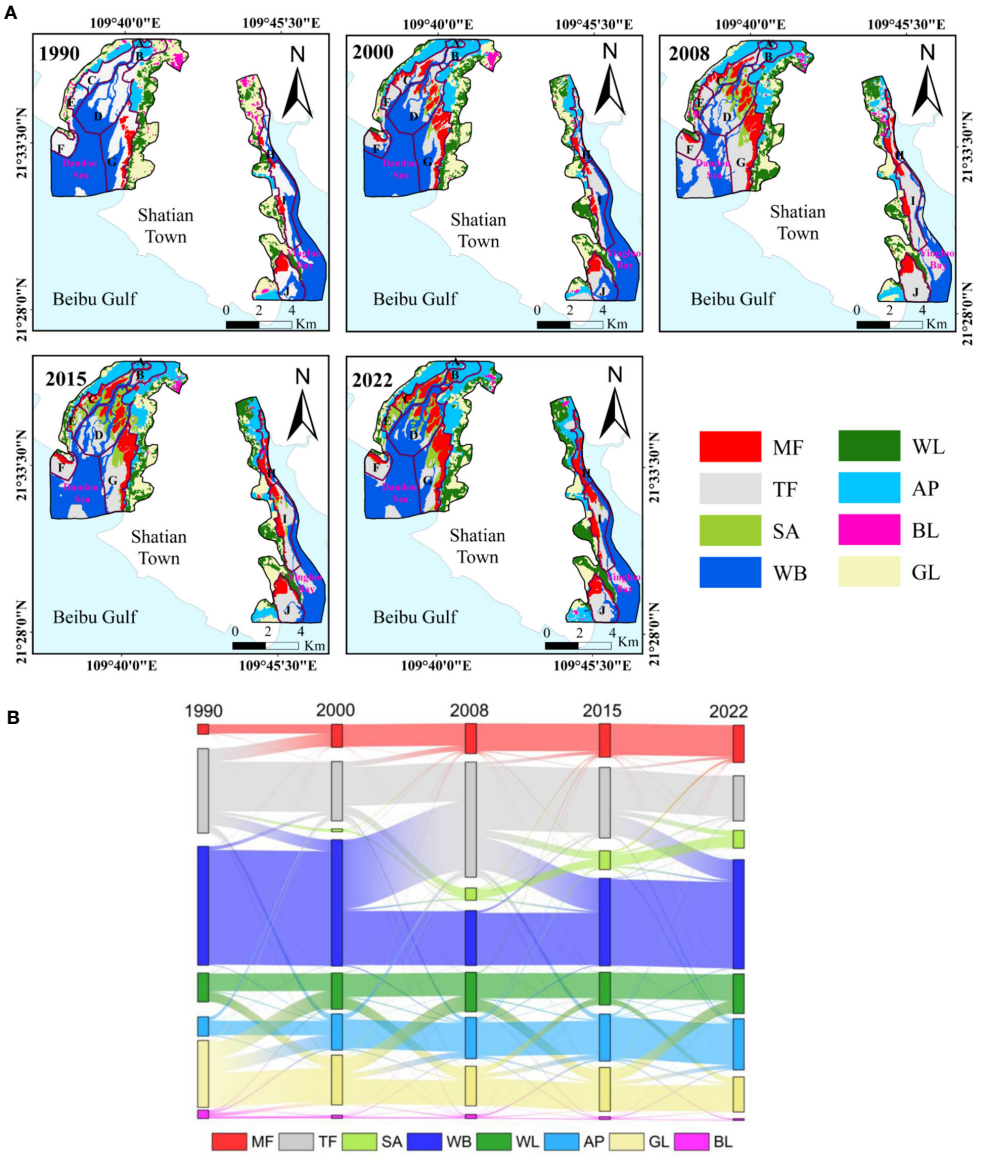

FIGURE 3
Land cover classification results. **(A)** Land cover maps of the reserve in 1990-2022 **(B)** Conversion between mangrove forest and other land cover types in 1990-2022.

TABLE 5 The area (ha) of mangroves and other land cover of the reserve in 1990-2022.

Year	MF	TF	SA	WB	WL	AP	BL	GL
1990	235.26	1981.89	0	2802.65	687.33	462.33	201.87	1573.38
2000	541.8	1386.36	65.7	2986.25	856.53	859.5	75.6	1172.97
2008	703.08	2715.3	284.76	1303.16	930.69	977.22	98.64	931.86
2015	785.43	1660.59	433.89	2065.46	770.67	1122.39	68.58	1037.7
2022	873.27	1069.74	412.38	2575.31	928.89	1211.49	45.72	827.91

MF, mangrove forest; TF, tidal flat; SA, *S. alterniflora*; WB, water body; WL, woodland; AP, aquaculture pond; BL, built-up land; GL, grassland.

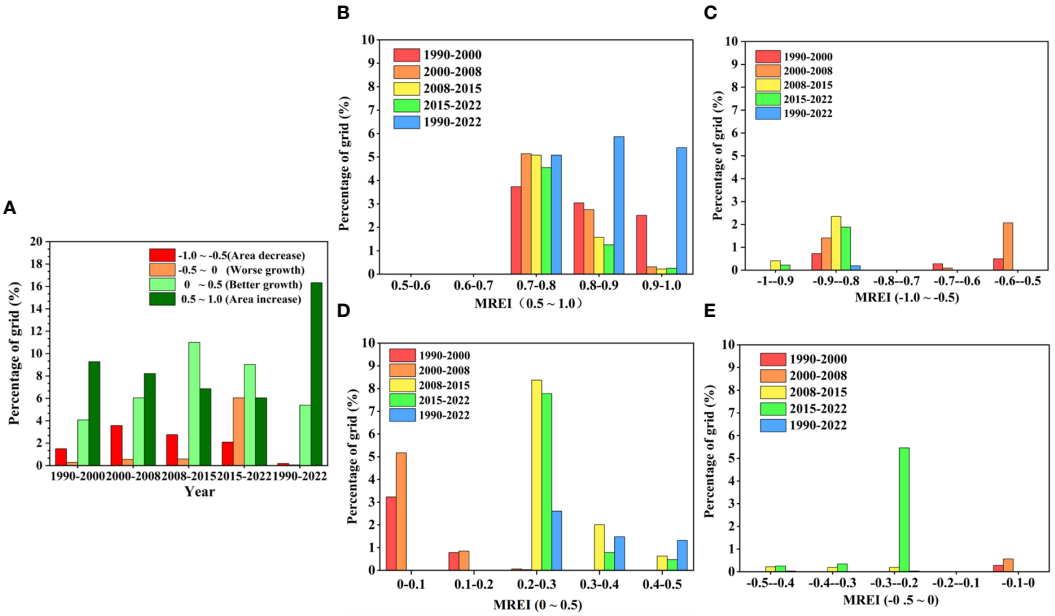

FIGURE 4
Grid percentage of MREI in different categories and different intervals. **(A)** Grid percentage for the four MREI categories; **(B)** Distribution of MREI values for 'Area increase' category (0.5 ~ 1.0); **(C)** Distribution of MREI values for 'Area decrease' category(-1.0 ~ -0.5); **(D)** Distribution of MREI values for 'Better growth' category (0 ~ 0.5); **(E)** Distribution of MREI values for 'Worse growth' category (-0.5 ~ 0).

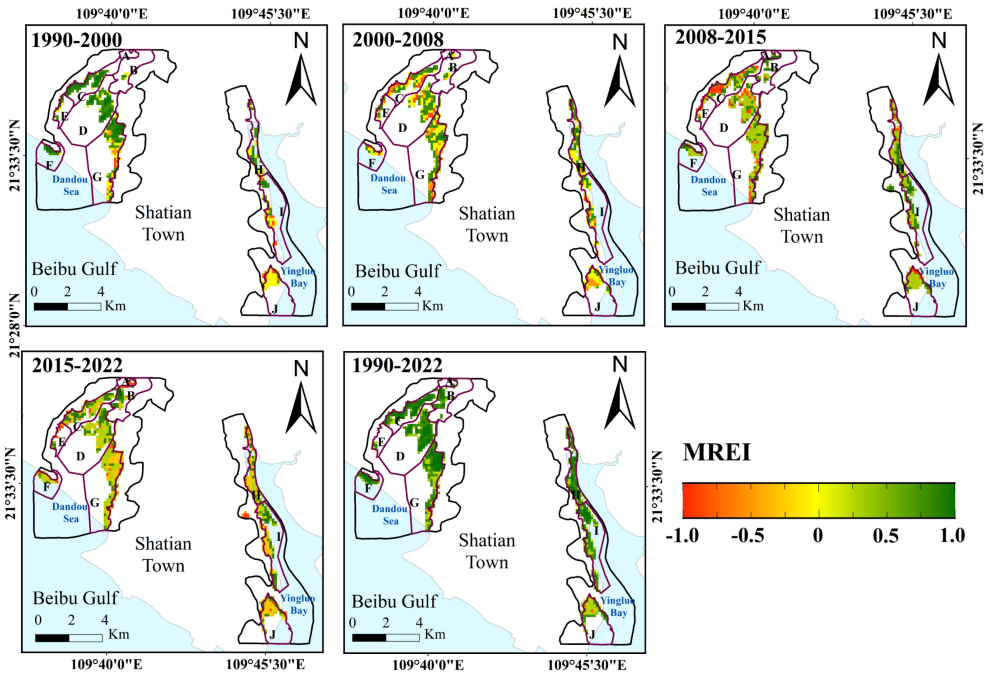

FIGURE 5
The spatial distribution of MREI in five evaluation phases (grid-scale).

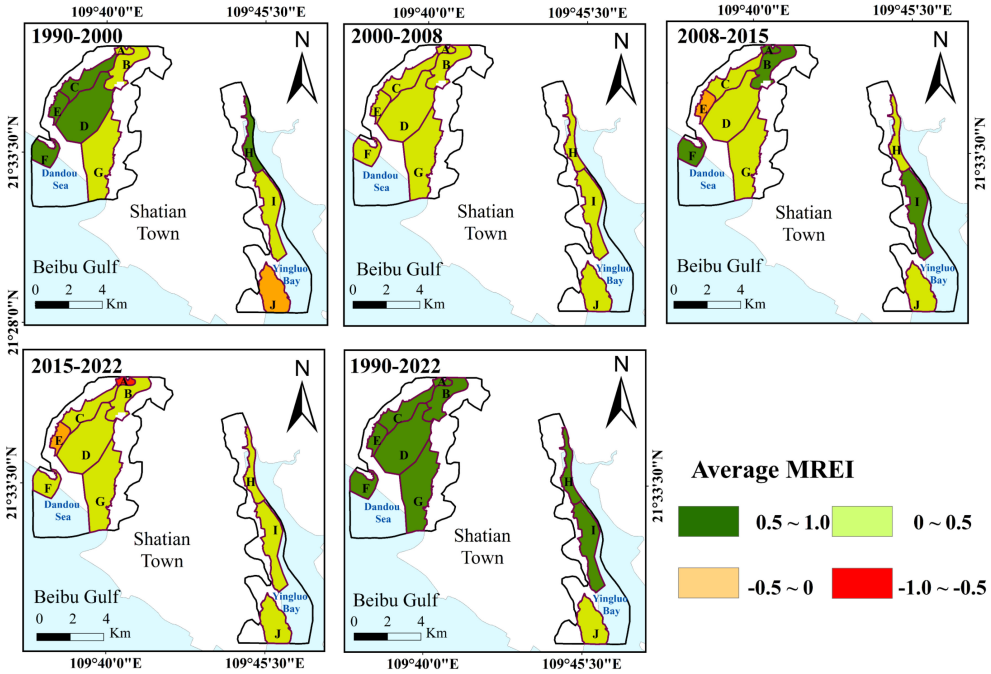

FIGURE 6
The spatial distribution of average MREI in five evaluation phases (village-scale).

indicating relatively poor restoration effectiveness in Zone J; From 2000 to 2008, the average MREI values in all zones were 0 to 0.5; From 2015 to 2022, the restoration effectiveness in Zone A was the worst, with an average MREI value of less than -0.5. From 1990 to 2022, only the average MREI value in Zone J was less than 0.5, while values in the other zones were greater than 0.5.

3.3 Validity of MREI

The accuracy of MREI was examined by analyzing Google Earth and PlanetScope images. The distribution of MREI before and after the third phase of NCSSCP (2015-2022) is displayed in Figure 7A. The six Locations (I-VI) in the figure represent typical areas selected for validation. Detailed MREI values for the four locations (I- IV) and their corresponding high-resolution images are presented in Figures 7B–E. It should be noted that some images from 2015 and 2022 had poor quality or even missing. The area of mangroves does not change significantly in a short period, so available images taken from September to December in 2016 and 2021 were used to replace these missing images to verify whether the indication of MREI values is consistent with the actual changes in mangroves. In some zones, the mangrove area has not changed significantly, but the vegetation and canopy cover changed, such as in Locations V and VI. To examine the validity of MREI at these locations, we also used maximum NDVI images. Figures 7F, G show the MREI values and their corresponding NDVI for locations V and VI.

Location I is near the tidal flat around the northern aquaculture pond of Dandou Sea, with an average MREI of -0.87. It can be found from Google Earth images that from 2015 to 2022, mangrove forest was degraded, especially on the right side of the tidal flat, where mangroves almost disappeared. Location II is located on the west side of Dandou Sea, with an average MREI value of -0.74. We can see the loss of mangroves on the PlanetScope images in Figure 7C. The reason for the loss of mangroves may be related to the expansion of *S. alterniflora*. Location III is near the tidal flat around the aquaculture pond in the north of Dandou Sea, with an average MREI of 0.85. An increase in the area of mangrove forests near the aquaculture pond was observed at the location III. Location IV is located in the central part of Yingluo Bay, and many areas have MREI values greater than 0.5, with an average MREI value of 0.76. From Google Earth images, it can be seen that mangrove forests expanded from 2015 to 2022, and we suspect that there is tree planting activity here. On the side near the coastline, there is less land pollution in living areas, industrial areas, agricultural areas, and other areas, and the concentration of heavy metals in sediment can also become lower due to marine dynamic factors (Xie et al., 2022). Therefore, the MREI value on the seaward side of location IV is higher than on the land side. The mangrove area of Locations V and VI did not change significantly from 2015 to 2022, but the MREI is a good indicator of the changes in their vegetation cover (expressed as NDVI). The average MREI value of location V is -0.21, and NDVI decreased from 2015 to 2022 (Figure 7F). The average MREI value of location VI is 0.37, and NDVI increased from 2015 to 2022 (Figure 7G). Both location V and location VI are mainly distributed in natural mangrove forests, where the increase in mangrove patches is not significant and large-scale tree planting activities are unlikely. Location V is close to the land side, while Location VI is close to the coastline, so the MREI value of location V is lower than that of location VI.

10.3389/fmars.2023.1280373

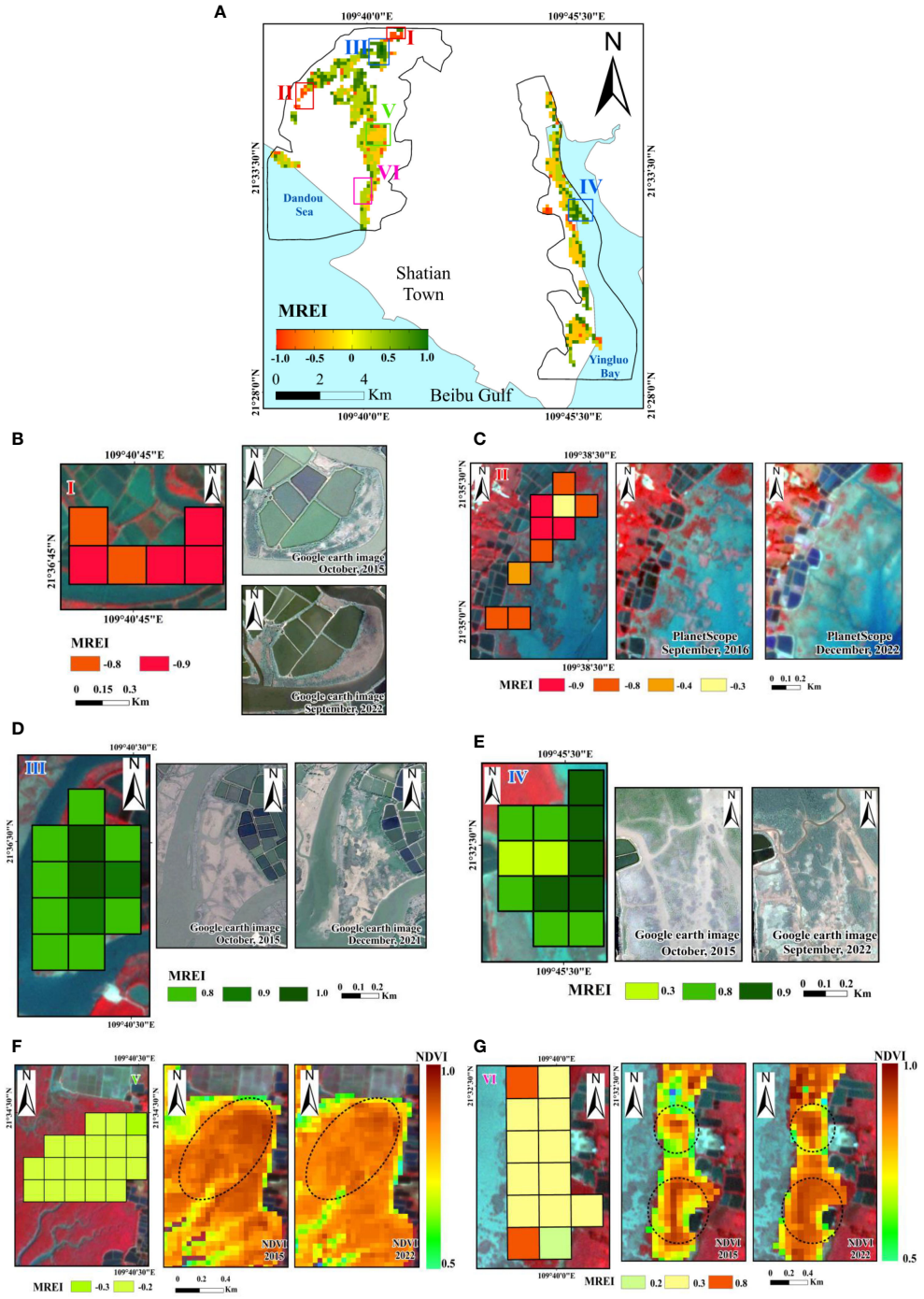

FIGURE 7
Verification of MREI values based on high-resolution images and maximum NDVI images. **(A)** Distribution of MREI (2015-2022) and typical Locations I-VI; MREI values of **(B)** Location I, **(C)** Location II, **(D)** Location III, **(E)** Location IV verified based on high-resolution images; MREI values of **(F)** Location V, **(G)** Location VI verified based on maximum NDVI images.

3.4 Persistence of restoration effectiveness

The PRE distribution in entire afforestation phases is shown in Figure 8A. Figure 8B shows the grid percentage of different PRE categories. The percentage of 'excellent PRE' grids is the highest, relatively concentrated in zones B, D, I, and H, accounting for 44.17% of the total grid area. The grid number of 'Poor PRE' was 40, accounting for 5.24% of the total grid number, which was mainly distributed in the mudflat of Zone C. The grid number of 'Good PRE' was 148, accounting for 19.40% of the total grid number. The grid of 'Average PRE ', with varying degrees of distribution in different zones, accounting for 31.19% of the total grid number. The PREI values of ten zones within the reserve indicated (Figure 8C) that for Zone A and Zone E, the PREI values were 0 and 0.38

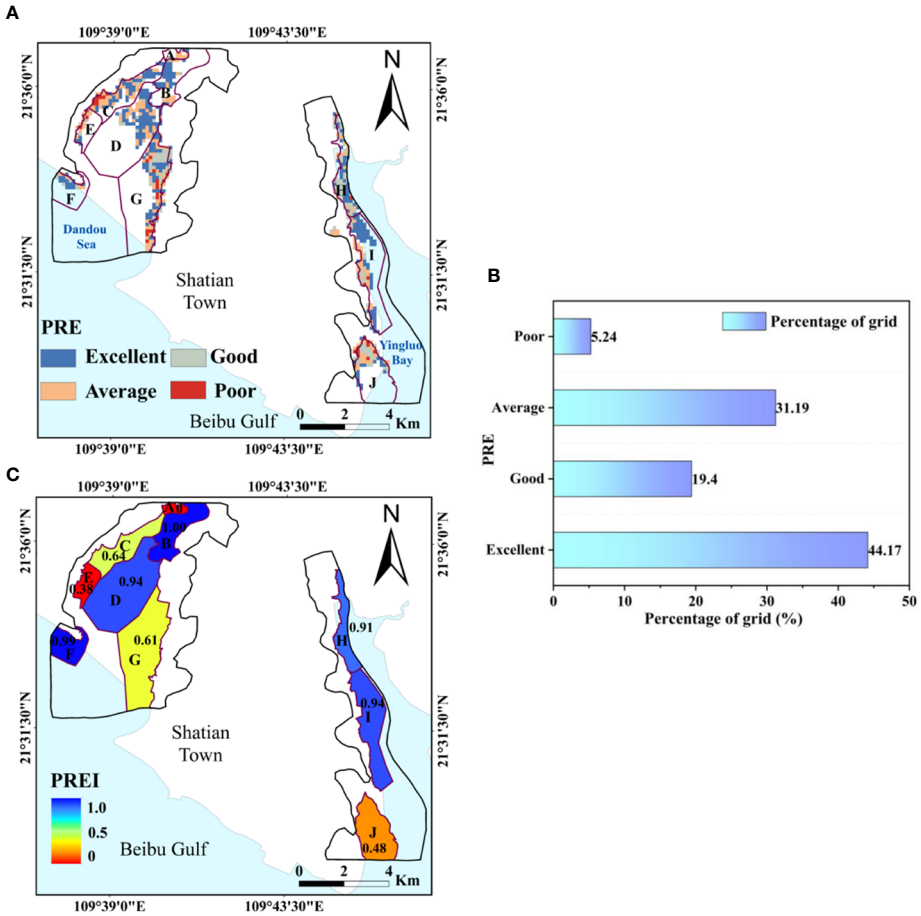

FIGURE 8
The persistence of mangrove restoration effectiveness (PRE). **(A)** The PRE based grid-scale; **(B)** The grid percentage of different PRE categories; **(C)** The PRE based on village-scale.

respectively; Zone J with PREI value of 0.48; the PREI values of Zone C and Zone G were 0.64 and 0.61 respectively; Five regions (Zones H, I, D, F, B) showed PREI values near 1.0.

4 Discussion

4.1 Reasons for changes in mangrove restoration effectiveness

The survival rate and preservation rate of mangroves are two important factors that affect the effectiveness of restoration projects focused on mangrove planting. We found that 84.59% of the mangrove area was converted from tidal flats within the reserve. However, this conversion process may face many challenges in the future. GSMNNR is the area with the highest sea salinity along the coast of Guangxi. Although mangroves have salt tolerance and the ability to absorb heavy metals, excessive salinity or heavy metal concentrations in water can also have adverse effects on mangroves, leading to a decrease in mangrove biomass and seedling death (Niu et al., 2020). In addition, mangrove ecosystems are particularly sensitive to sea-level rise, converted mangrove land on exposed coastlines can be highly vulnerable to erosion. The impact of sea level rise on mangroves mainly depends on the relationship between the speed of sea level rise and sediment accumulation (Wang, 2021). According to Li et al. (2015), the rise in sea level will affect mangroves with lower sedimentation rates in the Dandou Sea on the west side of the reserve by 2025. Those mangrove communities in the higher intertidal zone will be lost, converted into lower communities, tidal flats, or will become inundated.

The challenges in the transformation of mudflat to mangroves also include the threat of human activities and alien species. During our fieldwork in GSMNNR and communication with relevant experts in Guangxi, we found that the growth of mangrove seedlings in the reserve is poor, with a survival rate of planting for three years at about 30%, mainly threatened by *S. alterniflora* and aquaculture ponds (Figure 9). The aquaculture pond is directly connected to the mangrove forests, and sewage from the aquaculture pond is directly discharged into the mangrove habitat through valves (Figure 9D), which is likely the reason for the area reduction of mangrove forests outside the aquaculture pond in Zone A between 2015 and 2022 (Figure 3A). However, similar to the study by Shi et al. (2023), we found an interesting phenomenon that not all mangroves around aquaculture ponds have low preservation

FIGURE 9
Photographs of some typical landscapes in the reserve (captured on April 11th, 2023). **(A)** Mangrove seedlings planted in the reserve; **(B)** Mangrove seedlings invaded by *S. alterniflora*; **(C)** aquaculture pond; **(D)** Water control valves for aquaculture ponds.

rates. For example, mangroves have grown well, and the area has even increased significantly from 2015 to 2022 on the mudflats near the aquaculture ponds in Zone B (Figure 3A). This may be due to the nutrients contained in sewage being absorbed by mangroves, thereby promoting their growth (Jia, 2014). The alien species in the GSMNNR are *S. alterniflora*, mainly distributed in the Dandou tidal flat and Yingluo tidal flat. *S. alterniflora* competes with mangroves for sunlight and growth space, making it easy to shade the low mangrove plants.

In addition, we have sorted out some events that may cause changes in the area and growth (vegetation coverage and canopy cover) of mangroves in GSMNNR after 1990 (Figure 10). During NCSSCP Phase I (1990-2000), 1093 ha of mangroves were planted along the coast of Guangxi, with a survival rate of 71%. There were large areas of exposed mudflat in the reserve (Figure 3A), so it was less difficult to plant mangroves. In 1990, The GSMNNR was established. Around 1995, the emergence of aquaculture ponds in Guangxi led to extensive mangrove deforestation. The

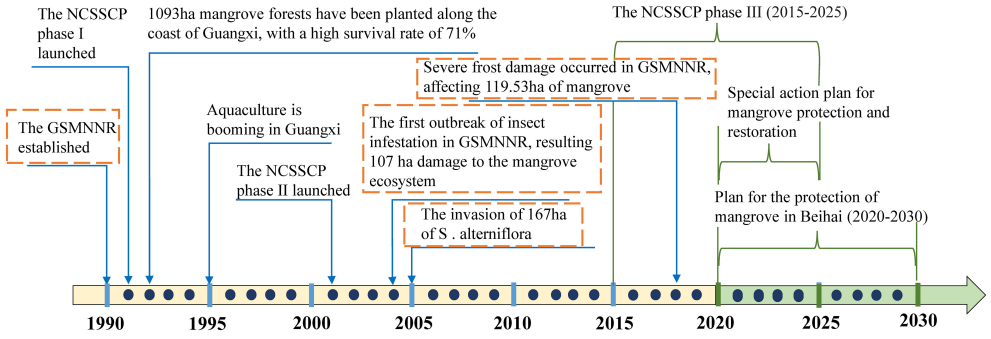

FIGURE 10
Important time points for mangrove area and growth changes in GSMNNR. Dashed boxes indicate events that only occur within the GSMNNR.

establishment of reserve has to some extent reduced the direct deforestation of mangroves within the protected areas (Wang et al., 2021). Mangroves are easy to grow, coupled with the strict management of mangroves in the reserve. From 1990 to 2000, the average MREI value in the reserve was 0.48, which is the highest among the four afforestation phases.

The afforestation area was 2615.5 ha in Guangxi from 2002 to 2007, and it was 1333 ha from 2008 to 2015, but only 37.11% and 26.63% of the artificial afforestation area have been preserved (Fan and Mo, 2018). Pest invasion can lead to the withering of mangrove leaves, and even cause the death of mangroves. In 2004, the first outbreak of pests destroyed 107 ha of mangroves in the reserve (Wei et al., 2019). In 2008, the most severe pest disaster occurred between 2004 and 2018, with an area of 264 ha affected. The main pest species of the two pest disasters were *Oligochroa cantonella*, and the main threat to the mangrove tree species was *Avicennia marina* (Wei et al., 2019). Subsequently, in 2005, the invasion area of *S. alterniflora* exceeded 167 ha, which had adverse effects on the mangrove seedlings. Compared to the NCSSCP Phase I, the impact of this invasion, combined with pests, may result in low preservation rates for the two afforestation attempts in the NCSSCP Phase II. The average MREI for 2000-2008 and 2008-2015 was slightly lower than the NCSSCP Phase I. It is worth noting that in the mudflats of Zone C and Zone E, the MREI value changed from positive to negative and even dropped below -0.5.

The average MREI in the reserve of the NCSSCP Phase III is the lowest, only 0.17. The reason for the lowest MREI value is the deterioration of mangrove growth and a decrease in vegetation coverage in the southern part of Zone G (Figure 5). However, the results of our further exploration (Figure 4E) indicate that although vegetation coverage decreased, the overall decrease was not significant, 90.16% of the MREI values in the negative range were distributed in the grid (-0.3 ~ -0.2). We tried to explain the reason for the relatively low MREI value in the third afforestation stage. The NCSSCP Phase III focuses on ecological restoration, and the intensity of planting mangroves has decreased. After years of planting recovery, the remaining direct afforestation of mudflats is limited, and the planting difficulty increases. In addition, the threat of *S. alterniflora* and insect pests is still ongoing, and the northern part of Zone E, which is close to Zone C, is gradually being affected.

4.2 Advantages of MREI in mangrove restoration effectiveness evaluation and implication for management

The increase or decrease in mangrove area is often used to directly reflect the restoration effectiveness of mangroves. An increase in area indicates a good restoration effectiveness, while a decrease in area indicates a poor restoration effectiveness. For example, Zhang R. et al. (2022) analyzed the mangrove conservation effectiveness by mapping the land cover of China's Mangrove National Nature Reserve from 2016 to 2020 and analyzing the changes in mangrove area and land cover transformation. In addition, vegetation indices such as NDVI and EVI have also been widely used in monitoring vegetation coverage, canopy closure, and vegetation health, which reflect vegetation growth. Healthy and well-growing vegetation absorbs red light and reflects near-infrared light due to the chlorophyll and cellular structure in its leaves, resulting in lower red band reflectance and higher near-infrared band reflectance. Poor growth and unhealthy vegetation have opposite characteristics. NDVI can reflect some vegetation state parameters that are positively correlated with leaf area index, biomass, and vegetation coverage based on this principle. These state parameters are also closely related to the restoration effectiveness of mangroves. Ruan et al. (2022) analyzed the global NDVI changes in mangroves using the Modify Resolution Imaging Spectrometer (MODIS) Normalized Difference Vegetation Index (NDVI) dataset and Landsat Global Mapping of Mangrove Forests (GMMF) from 2000-2018 to identify the Mangrove health conditions and dynamics. Zhu et al. (2021) used the NDVI time series analysis method and combined it with land cover change to divide the changes in mangroves in Qinglangang Nature Reserve, Hainan into three stages. However, there is currently no indicator that combines mangrove NDVI with area to evaluate the mangrove restoration effectiveness. This combination is necessary for understanding the growth status and restoration effectiveness of some mangroves that have not undergone significant changes in area but have undergone changes in growth and health. Based on the distribution characteristics of MREI values in each interval and the spatial distribution characteristics of MREI, we concluded that there were more areas where mangroves had better growth between 2008 and 2015, mainly distributed in Zone D of the Dandou Sea, and Zone G, J of the Yingluo Bay. Between 2015 and 2022, there were many areas with poor growth, mainly distributed in the northeast of Zone G and Zone J of the Dandou Sea, with 90.16% of the growth declining slightly (Figures 4, 5). PREI obtained the persistence of restoration effectiveness of the entire afforestation phase based on village-scale by classifying the trajectory of MREI. These two indices enable a more comprehensive analysis of the restoration effectiveness of mangroves using specific values. The accuracy of MREI had been examined on high-resolution images and NDVI maximum images. Furthermore, this index also takes into account the errors generated during the classification process, making the evaluation results more in line with the real situation. Remote sensing technology provides an effective way to obtain information on mangrove growth during historical periods lacking data. The evaluation method framework based on GIS provides a way for future research on the spatiotemporal changes in the restoration effectiveness, mainly focusing on changes in mangrove area and growth. This method framework can be easily applied to analyze and evaluate different time periods in other regions and has strong replicability.

The results of MREI show the improvement of mangrove growth and area during each afforestation period. Managers should further evaluate the restoration effectiveness based on the actual afforestation statistics of each period, such as afforestation date, time, and area. The results of PRE show several sites with poor

persistence of mangrove restoration effectiveness. It is important to focus on these sites, investigate the mudflat elevation, hydrological conditions, sediment environment, etc., and determine whether they are suitable for mangrove growth. At present, the mudflat suitable for afforestation in the reserve has been greatly reduced, and the mangrove area has been slowly increased. On the one hand, mangrove restoration participants should actively explore new ideas for mangrove restoration, such as the policy of "returning ponds to mangroves"; On the other hand, emphasis should be placed on ecological restoration. In addition, the effectiveness of community-based mangrove restoration management has been confirmed in many studies. Managers can refer to the results of PRE and conduct pilot work on villages with good persistence of restoration effectiveness to establish successful mode.

4.3 Limitations and implications for future work

The study represents a case study conducted within a single reserve, yet it holds the potential for broader application across multiple reserves on a larger scale. The index can encompass both within and outside the reserve, in order to study the differences in the mangrove restoration effectiveness inside and outside the reserve, and to explore the impact of the establishment of reserve on the mangrove restoration effectiveness. Moreover, three primary approaches to mangrove restoration exist direct planting, integration of coastal engineering techniques, and hydrological connectivity restoration. Our research background is mangrove planting activities, Therefore, The MREI model specifically focuses on the most pronounced changes, namely mangrove area and vegetation cover, before and after the restoration project based on planting. We only considered the restoration status of mangrove vegetation, ignoring the restoration of animal communities, habitat conditions, the elimination of threatened organisms, and the restoration of ecosystem functions.

During the United Nations Decade of Ecosystem Restoration (2021-2030), countries worldwide are embarking on initiatives to restore mangrove forests. In particular, China is actively engaged in the Special Action Plan for Mangrove Protection and Restoration (2020-2025), which plans to plant and restore 18800 ha of mangrove forests by 2025. In Guangxi's mangrove protection and special restoration plan, it is planned to plant 1000 ha and restore 3500 ha of mangrove forests by 2025. Mangrove planting strategies include planting on mudflat and returning ponds to mangroves. At present, there are few mudflats suitable for afforestation. The difficulty of mangrove planting and restoration lies in the selection of suitable planting areas and the implementation of the policy of returning ponds to mangroves (Wang et al., 2021). In the future, multi-source remote sensing data, combined with drone and SAR data, can be used to overcome the limitations of remote sensing spatial resolution and weather, evaluate areas with high potential for mangrove planting and restoration, and timely monitor the success rate of mangrove restoration from ponds and the survival rate of mangrove planting.

5 Conclusion

In this study, we proposed a novel approach for assessing the mangrove restoration effectiveness, which involves integrating changes in mangrove areas and vegetation coverage (represented as NDVI). Taking GSMNNR as a study case, new indices MREI and PREI were constructed to quantitatively evaluate the mangrove restoration effectiveness of each afforestation phase during 1990-2022. Through the dynamic changes of MREI in a single afforestation phase and multiple afforestation phases, combined with land cover change, a method framework for evaluating the effectiveness of mangrove restoration based on grid-scale and village-scale was attempted to be explored.

Through the analysis of land cover and its mutual transformation, we concluded that the mangrove area in the reserve increased from 235.26 ha in 1990 to 873.27 ha in 2022, and 84.59% of mangroves were converted from tidal flats. The MREI we constructed can represent area and vegetation coverage of mangroves, effectively evaluating the effectiveness of planting restoration. The average value of MREI in the five evaluation phases was 0.48, 0.24, 0.29, 0.17, and 0.72, respectively. The results show that the NCSSCP is effective as a whole, and the first phase of the project NCSSCP had the best restoration effectiveness. There are fewer suitable tidal flats in the reserve now, the survival rate of mangrove planting is low, and the effectiveness of the third phase of the afforestation project is not as good as the first two phases. Managers should seek new ideas for mangrove restoration, such as "returning ponds to mangroves". By analyzing the dynamic changes of MREI over multiple phases, we have concluded that 5.42% of the areas within the reserve have poor persistence of restoration effectiveness; 44.17% of the regions have excellent persistence of restoration effectiveness. Sites with poor persistence of restoration effectiveness should be given special attention. A recovery demonstration area should be established for the sites with excellent persistence of restoration effectiveness. From the perspective of spatial distribution of PREI, the zones with poor to excellent persistence of restoration effectiveness within the reserve were as follows: A, E, J, G, C, H, I (D), F, B. The high value zones of PREI were mainly distributed in the central of the Dandou Sea and the northern part of the Yingluo Bay. The low value zones were distributed in the northwest of the Dandou Sea.

This paper indicates that the MREI index and PREI index can comprehensively evaluate the effectiveness of mangrove restoration in terms of mangrove area, coverage changes, and long-term persistence. We expect that the indices presented in this study have great potential to be applied in broader regions as mangrove restoration efforts have been carried out worldwide. The mangrove restoration in GSMNNR has been carried out for nearly 40 years. Although the overall restoration effectiveness is good, there are still some areas with poor restoration effectiveness and persistence.

With the reduction of mudflat suitable for afforestation and the threat of *S. alterniflora* invasion, the afforestation of GSMNNR mangroves is becoming more and more difficult, which is also a problem that other regions in the world will face. In the future, in addition to the restoration of mangrove area, we hope to focus on improving the functionality of mangroves and develop remote sensing methods to monitor changes in mangrove function.

Data availability statement

The raw data supporting the conclusions of this article will be made available by the authors, without undue reservation.

Author contributions

YW: Writing – original draft, Conceptualization, Data curation, Formal analysis, Methodology, Writing – review & editing. XW: Data curation, Formal analysis, Writing – review & editing. SK: Project administration, Supervision, Writing – review & editing. DZ: Conceptualization, Methodology, Project administration, Supervision, Writing – review & editing. YK: Conceptualization, Methodology, Project administration, Supervision, Writing – review & editing.

Funding

The author(s) declare financial support was received for the research, authorship, and/or publication of this article. This work was supported by the National Natural Science Foundation of China (No. 42071396), and Beijing Science and Technology Planning Project (No. Z201100006720001).

Acknowledgments

The authors acknowledge the data support from "National Earth System Science Data Center, National Science & Technology Infrastructure of China". We are also thankful to the Landsat imagery data provided by the USGS through the Google Earth Engine (GEE). We also thank the Planet Labs Education and Research program for providing PlanetScope satellite imagery.

Conflict of interest

The authors declare that the research was conducted in the absence of any commercial or financial relationships that could be construed as a potential conflict of interest.

Publisher's note

All claims expressed in this article are solely those of the authors and do not necessarily represent those of their affiliated organizations, or those of the publisher, the editors and the reviewers. Any product that may be evaluated in this article, or claim that may be made by its manufacturer, is not guaranteed or endorsed by the publisher.

Supplementary material

The Supplementary Material for this article can be found online at: https://www.frontiersin.org/articles/10.3389/fmars.2023.1280373/full#supplementary-material

References

Baloloy, A. B., Blanco, A. C., Ana, R. R. C. S., and Nadaoka, K. (2020). Development and application of a new mangrove vegetation index (MVI) for rapid and accurate mangrove mapping. *ISPRS J. Photogramm. Remote Sens.* 166, 95–117. doi: 10.1016/j.isprsjprs.2020.06.001

Bao, S., and Yang, F. (2022). Spatio-temporal dynamic of the land use/cover change and scenario simulation in the Southeast coastal shelterbelt system construction project region of China. *Sustainability* 14, 8952. doi: 10.3390/su14148952

Bunting, P., Rosenqvist, A., Hilarides, L., Lucas, R. M., Thomas, N., Tadono, T., et al. (2022). Global mangrove extent change 1996–2020: global mangrove watch version 3.0. *Remote Sens. (Basel)* 14, 3657. doi: 10.3390/rs14153657

Cadier, C., Bayraktarov, E., Piccolo, R., and Adame, M. F. (2020). Indicators of coastal wetlands restoration success: A systematic review. *Front. Mar. Sci.* 7. doi: 10.3389/fmars.2020.600220

Carugati, L., Gatto, B., Rastelli, E., Lo Martire, M., Coral, C., Greco, S., et al. (2018). Impact of mangrove forests degradation on biodiversity and ecosystem functioning. *Sci. Rep.* 8, 13298. doi: 10.1038/s41598-018-31683-0

Du, C., Khan, S., Ke, Y., and Zhou, D. (2023). Assessment of spatiotemporal dynamics of mangrove in five typical mangrove reserve wetlands in Asia, Africa and Oceania. *Diversity* 15, 148. doi: 10.3390/d15020148

Duke, N. C., Meynecke, J. O., Dittmann, S., Ellison, A. M., Anger, K., Berger, U., et al. (2007). A world without mangroves? *Science* 317, 41–42. doi: 10.1126/science.317.5834.41b

Fan, H., and Mo, Z. (2018). The history, achievements and lessons learnt for mangrove restoration in Guangxi, China. *Guangxi Sci.* 25, 363–371,387. doi: 10.13656/j.cnki.gxkx.20180918.001

Friess, D. A., Rogers, K., Lovelock, C. E., Krauss, K. W., Hamilton, S. E., Lee, S. Y., et al. (2019). The state of the world's mangrove forests: past, present, and future. *Ann. Rev. Environ. Resour.* 44, 89–115. doi: 10.1146/annurev-environ-101718

Gatt, Y. M., Andradi-Brown, D. A., Ahmadia, G. N., Martin, P. A., Sutherland, W. J., Spalding, M. D., et al. (2022). Quantifying the reporting, coverage and consistency of key indicators in mangrove restoration projects. *Front. For. Glob. Change* 5. doi: 10.3389/ffgc.2022.720394

Gerona-Daga, M. E. B., and Salmo, S. G. (2022). A systematic review of mangrove restoration studies in Southeast Asia: Challenges and opportunities for the United Nation's Decade on Ecosystem Restoration. *Front. Mar. Sci.* 9. doi: 10.3389/fmars.2022.987737

Gevana, D., Camacho, L., Carandang, A., Camacho, S., and Im, S. (2015). Land use characterization and change detection of a small mangrove area in Banacon Island, Bohol, Philippines using a maximum likelihood classification method. *For. Sci. Technol.* 11, 197–205. doi: 10.1080/21580103.2014.996611

Gilani, H., Naz, H. I., Arshad, M., Nazim, K., Akram, U., Abrar, A., et al. (2021). Evaluating mangrove conservation and sustainability through spatiotemporal, (1990–2020) mangrove cover change analysis in Pakistan. *Estuar. Coast. Shelf Sci.* 249, 107128. doi: 10.1016/j.ecss.2020.107128

Giri, C., Ochieng, E., Tieszen, L. L., Zhu, Z., Singh, A., Loveland, T., et al. (2011). Status and distribution of mangrove forests of the world using earth observation satellite data. *Glob. Ecol. Biogeogr.* 20, 154–159. doi: 10.1111/j.1466-8238.2010.00584.x

Ha, T. T. T., van Dijk, H., and Bush, S. R. (2012). Mangrove conservation or shrimp farmer's livelihood? The devolution of forest management and benefit sharing in the Mekong delta, Vietnam. *Ocean Coast. Manage.* 69, 185–193. doi: 10.1016/j.ocecoaman.2012.07.034

Hamilton, S. E., and Casey, D. (2016). Creation of a high spatio-temporal resolution global database of continuous mangrove forest cover for the 21st century (CGMFC-21). *Glob. Ecol. Biogeogr.* 25, 729–738. doi: 10.1111/geb.12449

Huang, H., Chen, K., Wang, A., and Wu, K. (2023). Historical changes, problems and protection countermeasures of mangrove in China. *Ocean. Coast. Manage.* 40, 125–132. doi: 10.20016/j.cnki.hykfygl.2023.02.011

Jia, M. (2014). *Remote Sensing analysis of China's mangrove forests dynamics during 1973 to 2013* (China: University of Chinese Academy of Sciences). dissertation/ Doctoral thesis.

Jia, M., Wang, Z., Mao, D., Huang, C., and Lu, C. (2021). Spatial-temporal changes of China's mangrove forests over the past 50 years: An analysis towards the Sustainable Development Goals (SDGs). *Chin. Sci. Bull.* 66, 3886–3901. doi: 10.1360/TB-2020-1412

Jia, M., Wang, Z., Zhang, Y., Mao, D., and Wang, C. (2018). Monitoring loss and recovery of mangrove forests during 42 years: The achievements of mangrove conservation in China. *Int. J. Appl. Earth Obs. Geoinf.* 73, 535–545. doi: 10.1016/j.jag.2018.07.025

Kamali, B., and Hashim, R. (2011). Mangrove restoration without planting. *Ecol. Eng.* 37, 387–391. doi: 10.1016/j.ecoleng.2010.11.025

Li, L., Liu, W., Tao, Y., Xu, X., Fu, W., and Dong, J. (2021). Diffusion dynamics and driving forces of *Spartina alterniflora* in the Guangxi Shankou Mangrove Reserve. *Acta Ecol. Sin.* 41, 6814–6824. doi: 10.5846/stxb202101260275

Li, S., Meng, X., Ge, Z., and Zhang, L. (2015). Evaluation of the threat from sea-level rise to the mangrove ecosystems in Tieshangang Bay, southern China. *Ocean Coast. Manage.* 109, 1–8. doi: 10.1016/j.ocecoaman.2015.02.006

Liu, M. (2018). *Remote Sensing analysis of Spartina alterniflora in the coastal areas of China during 1990 to 2015* (China: University of Chinese Academy of Sciences). dissertation/Ph D Thesis.

Liu, X., Yang, X., Zhang, T., Wang, Z., Zhang, J., Liu, Y., et al. (2022). Remote sensing based conservation effectiveness evaluation of mangrove reserves in China. *Remote Sens. (Basel)* 14, 1386. doi: 10.3390/rs14061386

Lu, C., Li, L., Wang, Z., Su, Y., Su, Y., Huang, Y., et al. (2022). The national nature reserves in China: Are they effective in conserving mangroves? *Ecol. Indic.* 142, 109265. doi: 10.1016/j.ecolind.2022.109265

Min, Y., Ke, Y., Yue, H., Xiaolan, Y., and Demin, Z. (2023). Dynamic monitoring of invasive *Spartina alterniflora* clearance *via* fusion of Sentinel-2 and GF-1 time series images. *Natl. Remote Sens. Bull.* 27, 1467–1479. doi: 10.11834/jrs.20232279

Niu, A., Gao, Y., and Xu, S. (2020). Effects of heavy metal pollution on the carbon content of surface sediments of mangroves in the Pearl River Estuary. *Acta Ecologica. Sinica.* 40, 8549–8558. doi: 10.5846/stxb202002240322

Olofsson, P., Foody, G. M., Herold, M., Stehman, S. V., Woodcock, C. E., and Wulder, M. A. (2014). Good practices for estimating area and assessing accuracy of land change. *Remote Sens. Environ.* 148, 42–57. doi: 10.1016/j.rse.2014.02.015

Peng, Y., Zhou, Y., and Chen, G. (2008). The restoration of mangrove wetland: a review. *Acta Ecol. Sin.* 28, 786–797. doi: 10.3321/j.issn:1000-0933.2008.02.041

Planet Team (2022). *Planet Application Program Interface: In Space for Life on Earth* (San Francisco, CA). Available at: https://api.planet.com.

Polidoro, B. A., Carpenter, K. E., Collins, L., Duke, N. C., Ellison, A. M., Ellison, J. C., et al. (2010). The loss of species: mangrove extinction risk and geographic areas of global concern. *Plos. One* 5, e10095. doi: 10.1371/journal.pone.0010095

Primavera, J. H., and Esteban, J. M. A. (2008). A review of mangrove rehabilitation in the Philippines: successes, failures and future prospects. *Wetlands Ecol. Manage* 16, 345–358. doi: 10.1007/s11273-008-9101-y

Rouse, J. W., Haas, R. H., Schell, J. A., and Deering, D. W. (1974). Monitoring vegetation systems in the Great Plains with ERTS. NASA. Goddard Space Flight Center 3d ERTS-1 Symp., Vol. 1, Sect. A. [online] Available at: https://ntrs.nasa.gov/citations/19740022614.

Roy, D. P., Huang, H., Houborg, R., and Martins, V. S. (2021). A global analysis of the temporal availability of PlanetScope high spatial resolution multi-spectral imagery. *Remote Sens. Environ.* 264, 112586. doi: 10.1016/j.rse.2021.112586

Ruan, L., Yan, M., Zhang, L., Fan, X., and Yang, H. (2022). Spatial-temporal NDVI pattern of global mangroves: a growing trend during 2000–2018. *Sci. Total Environ.* 844, 157075. doi: 10.1016/j.scitotenv.2022.157075

Seto, K. C., and Fragkias, M. (2007). Mangrove conversion and aquaculture development in Vietnam: A remote sensing-based approach for evaluating the Ramsar Convention on Wetlands. *Glob. Environ. Change* 17, 486–500. doi: 10.1016/j.gloenvcha.2007.03.001

Shi, M., Li, H., and Jia, M. (2023). Spatio-temporal variations in mangrove forest in the Shankou Mangrove Nature Reserve based on the GEE cloud platform and Landsat data. *Remote Sens. Nat. Res.* 35, 61–69. doi: 10.6046/zrzyyg.2022209

Suyadi,, Gao, J., Lundquist, C. J., and Schwendenmann, L. (2018). Characterizing landscape patterns in changing mangrove ecosystems at high latitudes using spatial metrics. *Estuar. Coast. Shelf Sci.* 215, 1–10. doi: 10.1016/j.ecss.2018.10.005

Veettil, B. K., Pereira, S. F. R., and Quang, N. X. (2018). Rapidly diminishing mangrove forests in Myanmar (Burma): a review. *Hydrobiologia* 822, 19–35. doi: 10.1007/s10750-018-3673-1

Wang, L., Jia, M., Yin, D., and Tian, J. (2019). A review of remote sensing for mangrove forests: 1956–2018. *Remote Sens. Environ.* 231, 111223. doi: 10.1016/j.rse.2019.111223

Wang, L., Shi, C., Tian, J., Song, X., Jia, M., Li, X., et al. (2018). Researches on mangrove forest monitoring methods based on multi-source remote sensing. *Bio. Sci.* 26, 838–849. doi: 10.17520/biods.2018067

Wang, W., Fu, H., Lee, S. Y., Fan, H., and Wang, M. (2020). Can strict protection stop the decline of mangrove ecosystems in China? From rapid destruction to rampant degradation. *Forests* 11, 55. doi: 10.3390/f11010055

Wang, W., Zhang, L., Zhang, Y., and Wang, M. (2021). Research progress of pond-to-mangrove restoration. *J. Xiamen University(Natural Science)* 60, 348–354. doi: 10.6043/j.issn.0438-0479.202011015

Wang, Y. (2021). Impacts, challenges and opportunities of global climate change on mangrove ecosystems. *J. Trop. Oceanogr.* 40, 1–14. doi: 10.11978/YG2020006

Wei, J., Liu, W., Huang, Q., Chen, Q., and Su, B. (2019). Investigation of main insect pests in Shankou national mangrove reserve of Guangxi in recent 15 years. *J. Fujian Forestry Sci. Technol.* 46, 66–69. doi: 10.13428/j.cnki.fjlk.2019.04.015

Wodehouse, D. C. J., and Rayment, M. B. (2019). Mangrove area and propagule number planting targets produce sub-optimal rehabilitation and afforestation outcomes. *Estuar. Coast. Shelf Sci.* 222, 91–102. doi: 10.1016/j.ecss.2019.04.003

Worthington, T. A., Zu Ermgassen, P. S. E., Friess, D. A., Krauss, K. W., Lovelock, C. E., Thorley, J., et al. (2020). A global biophysical typology of mangroves and its relevance for ecosystem structure and deforestation. *Sci. Rep.* 10, 14652. doi: 10.1038/s41598-020-71194-5

Xiao, H., Su, F., Fu, D., Yu, H., Ju, C., Pan, T., et al. (2021). *10-M GLOBAL MANGROVE CLASSIFICATION PRODUCTS OF 2018-2020 BASED ON BIG DATA [DS/OL]* Vol. V1 (China: Science Data Bank). Available at: https://cstr.cn/31253.11.sciencedb.01019.

Xie, Z., Zhu, G., Xu, M., Zhang, H., Yi, W., Jiang, Y., et al. (2022). Risk assessment of heavy metals in a typical mangrove ecosystem - a case study of Shankou mangrove national natural reserve, southern China. *Mar. pollut. Bull.* 178, 113642. doi: 10.1016/j.marpolbul.2022.113642

Xu, H. (2005). A study on information extraction of water body with the modified normalized difference water index (MNDWI). *Natl. Remote Sens. Bull.* 9, 589–595. doi: 10.3321/j.issn:1007-4619.2005.05.012

Xu, R., Zhao, S., and Ke, Y. (2021). A simple phenology-based vegetation index for mapping invasive *spartina alterniflora* using google earth engine. *IEEE J. Sel. Top. Appl. Earth Obs. Remote Sens.* 14, 190–201. doi: 10.1109/JSTARS.2020.3038648

Zha, Y., Ni, S., and Yang, S. (2003). An effective approach to automatically extract urban land-use from TM imagery. *Natl. Remote Sens. Bull.* 7, 37–40. doi: 10.3321/j.issn:1007-4619.2005.05.012

Zhang, R., Jia, M., Wang, Z., Zhou, Y., Mao, D., Ren, C., et al. (2022). Tracking annual dynamics of mangrove forests in mangrove National Nature Reserves of China based on time series Sentinel-2 imagery during 2016–2020. *Int. J. Appl. Earth Obs. Geoinf.* 112, 102918. doi: 10.1016/j.jag.2022.102918

Zhang, Z., Xu, N., Li, Y., and Li, Y. (2022). Sub-continental-scale mapping of tidal wetland composition for East Asia: A novel algorithm integrating satellite tide-level and phenological features. *Remote Sens. Environ.* 269, 112799. doi: 10.1016/j.rse.2021.112799

Zhao, C., and Qin, C. (2022). A detailed mangrove map of China for 2019 derived from sentinel-1 and -2 images and google earth images. *Geosci. Data J.* 9, 74–88. doi: 10.1002/gdj3.119

Zhen, J. (2019). *Monitoring and dynamic analysis of mangrove forests in Hainan Island using multi-temporal remote sensing images* (China: University of Chinese Academy of Sciences). dissertation/Master's thesis.

Zhu, B., Liao, J., and Shen, G. (2021). Combining time series and land cover data for analyzing spatio-temporal changes in mangrove forests: A case study of Qinglangang Nature Reserve, Hainan, China. *Ecol. Indic.* 131, 108135. doi: 10.1016/j.ecolind.2021.108135

frontiers | Frontiers in Marine Science

TYPE Mini Review
PUBLISHED 19 December 2023
DOI 10.3389/fmars.2023.1304000

OPEN ACCESS

EDITED BY
Milko Alberto Jorquera,
University of La Frontera, Chile

REVIEWED BY
Marcos Rubal,
University of Minho, Portugal
Kathryn Schoenrock,
University of Galway, Ireland

*CORRESPONDENCE
Pedro A. Quijón
pquijon@upei.ca

RECEIVED 28 September 2023
ACCEPTED 29 November 2023
PUBLISHED 19 December 2023

CITATION
Gibbons EG and Quijón PA (2023) Macroalgal features and their influence on associated biodiversity: implications for conservation and restoration.
Front. Mar. Sci. 10:1304000.
doi: 10.3389/fmars.2023.1304000

Macroalgal features and their influence on associated biodiversity: implications for conservation and restoration

Emily G. Gibbons and Pedro A. Quijón*

Department of Biology, University of Prince Edward Island, Charlottetown, PEI, Canada

Studies examining the relationship between seaweeds and the diversity of associated organisms have been attempted far less than those focusing on the influence of terrestrial plants. That is troublesome considering the growing number of studies reporting the decline or local loss of macroalgae because of ocean warming and climate change. Since the fate of macroalgae will have an influence on associated organisms, this brief overview examined the different roles played by macroalgae, making the distinction between morphological features associated with individual seaweed species and those associated with populations or habitats. Most studies at both (individual and population) levels have identified positive relationships between morphological features such as structural complexity (including fractal dimensions) and invertebrate biodiversity, and the abundance of various faunistic groups. Some of these relationships are stronger than others, often with complex outcomes, suggesting that the current and future ecological benefits provided by macroalgae are strongly species- and habitat-dependent. While the displacement or local-scale loss of seaweeds may continue because of climate change, the features identified here may become useful in light of conservation and restoration efforts.

KEYWORDS

seaweeds, biodiversity, abundance, conservation, restoration, climate change

1 Introduction

Many macroalgal species function as ecosystem engineers or foundation species (*sensu* Marzinelli et al., 2016) and are therefore central to restoration and sustainability goals (Ellison et al., 2005; Marzinelli et al., 2016). These macroalgae create direct or indirect food sources (Tano et al., 2016), space suitable for attachment, growth, or reproduction (Gallardo et al., 2021), refuge from predators (Best et al., 2014), and altered (often ameliorated) physical conditions for marine invertebrates (Brawley and Adey, 1981; Christie et al., 2003; Schmidt and Scheibling, 2006; Best et al., 2014; Schaal et al., 2016; Tano et al., 2016; Gallardo et al., 2021; El-Khaled et al., 2022) and vertebrates (e.g., Norderhaug et al., 2005), including seabirds and mammals (Lorentsen et al., 2010;

Christensen-Dalsgaard et al., 2017). Despite their importance, studies addressing the biodiversity associated with marine macroalgae have been attempted considerably less than those associated with terrestrial plants (Parker et al., 2001; Goodsell et al., 2004; Best et al., 2014; Gallardo et al., 2021). However, there is a need for these studies given ongoing climate events and anthropogenic disturbances, which are resulting in accelerated loss of species across coastal habitats worldwide (Bates and DeWreede, 2007). In this changing scenario, quantifying the contribution of macroalgae to biodiversity, both as individual algae or as clumps, beds, or populations, is undeniably important (Bates and DeWreede, 2007; El-Khaled et al., 2022).

Several macroalgal morphological or structural features have been directly or indirectly associated with the colonization and use of macroalgae by infaunal and epifaunal organisms (Bates and DeWreede, 2007; Duarte et al., 2020). However, these features have not been thoroughly explored in the context of biodiversity levels and their change in a warming ocean (Chemello and Milazzo, 2002). An examination of these features at the individual and population levels is not only important from a research perspective. It may also help conservation efforts, particularly in the case of macroalgal species that are threatened or are experiencing long-term declines (Lilley and Schiel, 2006; Marzinelli et al., 2014; Tummon Flynn et al., 2019). For those species, evidence showing their contribution to biodiversity and the features that enhance biodiversity levels, can support claims calling for their further protection and restoration (Marzinelli et al., 2014; Buršić et al., 2019; El-Khaled et al., 2022). Therefore, the goal of this minireview was to examine whether macroalgae influence biodiversity, and to identify the characteristics of individual seaweeds, or seaweed populations, that have an influence on any aspect of biodiversity. For this review, "biodiversity" was quantified using various measures, including species richness, diversity and/or species evenness, and biomass and abundance of organisms, among other metrics.

The influence of macroalgae on biodiversity is outlined in Table 1 and includes a compilation of 62 published studies (as of November 2023) deemed representative rather than comprehensive of those addressing seaweed-biodiversity relationships. We focused primarily on physical or structural features, including fractal dimensions (e.g. Davenport et al., 1996; Tokeshi and Arakaki, 2012) when measured, but did not account for a distinct branch of studies on algal chemical products (e.g. Hay and Fenical, 1996). These chemical products have evolved from the interaction between seaweeds, consumers, hosts, or colonizers (often as defenses against herbivory) at every coastal region and latitude (see e.g., Amsler, 2008 and Amsler et al., 2014). Their influence on species interactions and biodiversity has been comprehensively reviewed by other authors (Amsler, 2008 and chapters and references therein; Ianora et al., 2006; Hay, 2009; and Sotka et al., 2018, among others). Studies focusing primarily on aquatic plants outside of the realm of marine macroalgae were not considered either. For instance, species such as *Zostera marina* often overlap and interact with various marine macroalgae (Richard and Quijon, 2023). However, they belong into a distinct group of flowering plants with root systems, which has been examined by other authors (e.g., Hansen et al., 2010) and was deemed beyond the scope of this minireview. The articles examined here were obtained using search engines such as OneSearch and Google Scholar, networks (e.g., ResearchGate), and cross-listed references within articles and other online resources. Key words used in these searches included "seaweed" or "algae" or "kelp," "rhodoliths", "biodiversity" or "diversity" "invertebrates" or "epifauna" or "infauna", and various combinations among them. Our review uses rather loosely the terms algae and seaweeds, but in all instances, we are referring to marine macroalgae. Likewise, our review includes studies on algae identified as "foundation species" or "ecosystem engineers", but these terms were not used as keywords given their widely known importance (e.g., Dayton, 1985; Stachowicz, 2001; Ellison et al., 2005) and much broader influence, often above the level of communities.

2 The influence of individual seaweed features

Out of the studies compiled in Table 1, a large majority suggests that seaweed's structural complexity (measured for instance as branching, physical rugosity or fractal dimensions) contributes to various metrics of invertebrate diversity and abundance. Higher structural complexity has been causally linked with increased invertebrate biodiversity (Chemello and Milazzo, 2002; Frame et al., 2007; Schaal et al., 2016; Mancuso et al., 2023a), species richness (Gee and Warwick, 1994; Duarte et al., 2020), and organisms' abundance (Russo, 1990; Davenport et al., 1996; Chemello and Milazzo, 2002; Frame et al., 2007; Schaal et al., 2016; Dijkstra et al., 2017; Duarte et al., 2020). The reported influence of complexity is variable, resulting in increases of nearly 58% in Shannon-Wiener diversity (Chemello and Milazzo, 2002) to increases in biodiversity levels ranging between 52% and 115%, depending on the time of year (Schaal et al., 2016). Algal complexity has also resulted in increases that ranged from 40% (Dijkstra et al., 2017) to an almost eight-fold increase in abundance (Chemello and Milazzo, 2002). Consistent with this, seaweed's fractal dimensions have been also shown to have an influence on invertebrate abundance and taxon richness (Mancuso et al., 2023a) regardless of host identity (Veiga et al., 2014). However, some studies have also found mixed results, with strong positive correlations between community structure and algal complexity features such as holdfast diameter and frond length, and negative correlations with features such as the number of stipes (Velasco-Charpentier et al., 2021).

A few studies have found that algal structural complexity had little influence on e.g. invertebrate species richness (Russo, 1990; Dijkstra et al., 2017) or abundance (Russo, 1990; Lenzo et al., 2023), while others have found that these relationships change temporarily. According to Da Rocha et al. (2006), similar assemblages could be associated with structurally different macroalgae, but complexity still have an influence on the biology of the dominant groups of invertebrates. Due to life cycles, macroalgal morphological features change seasonally (Leite and Turra 2003; Mancuso et al., 2023b) and this has prompted studies examining the influence of these changes on associated epifaunal

TABLE 1 A summary of studies identifying relationships between macroalgae or their features and various aspects of coastal organism biodiversity levels. In addition to location and type of habitat, seaweed species and features, responses measured, target taxa (or groups of taxa) and reported effects on biodiversity are presented for 62 studies (reference #s are organized alphabetically by authors' last names and are identified in the footnote of this Table).

Location	Habitat	Seaweed(s)/ feature(s)	Measured response	Target taxa	Effect on faunal diversity	#
US/CA	Kelp forests	*M. pyrifera, understory algae*/ Canopy, density, shade	Other seaweeds, sessile invertebrate diversity	Invertebrate communities	Canopy of kelp in multiple sites influenced other algae and invertebrate diversity and abundance. Indirect facilitation processes.	1
Canada/BC	Intertidal seaweed system	*A. leptophyllum, A. japonicus, others*/Species & functional richness, functional composition	Small epifaunal species composition, functional groups	Amphipods, copepods	Invertebrate composition and diversity were related to seaweed identity in simple monocultures (functional composition).	2
US/CA	Mid-high intertidal	*M. papillatus, C. columbiana, P. limitata*/ Identity, richness, total cover	Invertebrate species richness, abundance	Amphipods, isopods	Richness and abundance were higher in polycultures than in monocultures. Richness increased with cover. Densely branched algae held highest density.	3
Croatia	Coralline turf/ intertidal	*C. officinalis*/ Within-habitat biodiversity	Invertebrate density, taxonomic groups	Amphipods, polychaetes	*Corallina officinalis* supported a high diversity of invertebrates.	4
Germany	Rocky shore, tidal flats	*S. muticum, H. siliquosa, other*/complexity & invasive status	Epibiota species richness	Gastropods, amphipods	Diversity was correlated with algal complexity, regardless of native non-native status.	5
Spain	Rocky intertidal habitats	*Sargassum muticum* and *Laminaria ochroleuca*/ structural complexity and habitat position	Density, taxa abundance, and diversity	Gastropods, malacostracenematodes	When comparing mid to low shore position, there was significant differences in number of taxa with less in the mid shore than low.	6
Brazil	Euphotic and mesophotic	Rhodolith beds/ Structural characteristics of zones	Macroinvertebrates spp. diversity, abundance	Polychaeta, crustacea	Euphotic rhodolith beds supported twice the abundance and number of taxa than mesophotic.	7
Italy	Rocky plateau	*S. vulgare, C. spinosa, D. fasciola*/ Branching, ramuli, leaves, algal and stem width	Mollusk abundance, diversity	Neotaenio-glossa	More complex plants had higher abundances and richness. Structural complexity was related to degree of branching, width, and log of stem width.	8
Australia	Fringing reef	*Sargassum*/Canopy size	Epifaunal abundance and biomass	Crustaceans and molluscs	There was a positive correlation between canopy size & associated epifaunal community.	9
Norway	Kelp forests	*iliolatenrea*/ Distribution on lamina, stipe & holdfast	Mobile invertebrate diversity, abundance	Amphipods, gastropods	Holdfasts hosted highest number of species, while stipes had the highest abundance. Lamina had the lowest diversity and abundance.	10
Brazil	Rocky beach	*Sargassum polyceratium, others*, sediments/ Physical structure	Shannon-Wiener index, density, and genera richness	Nematodes	No significant difference in phytal nematofauna between habitats but dominant genera in each suggests that complexity influence organism biology	11
South Georgia	Subtidal habitat	*Macrocystis pyrifera, Desmarestia menziesi, others*/ Fractal dimensions	Abundance & biomass	Copepods, peracarids, bivalves	The most complex algae (by fractal dimensions), supported highest abundance and biomass.	12
Australia	Intertidal sheltered shore	*Corallina, Hormosira, Entermorpha*/Fractal dimensions and emersion	Abundance	Copepods	Most complex algae had highest abundance and when emerged had the lowest rates of migration.	13
US/ ME/NH	Rocky subtidal	Native: *S. latissima, Ulva* sp.… Introduced: *B. hamifera*…/ Structural complexity, height	Meso-invertebrate abundance, richness	Amphipods	Seaweed complexity accounted for 93% of abundance & 71% spp. richness. Introduced algae were more complex & enhanced density.	14

(Continued)

TABLE 1 Continued

Location	Habitat	Seaweed(s)/ feature(s)	Measured response	Target taxa	Effect on faunal diversity	#
Brazil	Estuary	*G. domingensis, S. filiformis, G. cuneata, D. ciliolateata*),/ Habitat complexity index	Mollusk composition, richness, diversity, abundance	Gastropods, bivalves.	Habitat complexity was positively correlated with mollusk abundance & richness.	15
Italy	Algal assemblages	*P. crispa, P. oceanica*/ Leaves and rhizomes	Sessile invertebrate abundance, diversity, phenotype richness	Invertebrates	*P. crispa's* holobionts, leaves & rhizomes had highest abundances, while its mats had higher Simpson diversity & phenotype richness.	16
US/CA	Rocky intertidal	*S. multicum, Z. farlowii, Others and turf-forming algae*	Species richness and density per algal weight unit	Ostracods	Structurally complex algae held more ostracods. Turf-forming algae held more richness.	17
US/CA	Rocky reefs, subtidal	Rhodoliths/Rhodoliths beds vs crushed rhodolith sands	Invertebrate density and abundance	Tanaids	Rhodolith beds supported higher abundance than the less complex crushed rhodolith beds.	18
Spain	Rocky subtidal bar	*H. scoparia, H. filicina, C. fragile, C. bursa, S. coronpifolius…*/ Soft or hard calcareous thallus	Invertebrate species richness, abundance	Annelids, Arthropods, Molluscs	Higher biodiversity was found in hard than soft algae, possibly due to the structure of the thalli and the microhabitats it provides.	19
England	Intertidal zone	*Chondrus crispus, Laurencia pinnatifida, others*/ Fractal dimensions	Macro- & meiofauna abundance and richness	Copepods/nematodes	Changes in thallus structure affected meiofauna more than macrofauna. Complex substrate results in increased diversity.	20
Spain	Lower intertidal	*B. bifurcate*, *S. muticum*, others/ Presence of invasive species	Epifaunal abundance, richness, diversity	Gastropods, isopods	*B. bifurcate* held the highest diversity whereas *S. polyschides* held the highest biomass of epifauna.	21
French Polynesia	Coral reef-lagoon	*L. kotschyanum*/Branch density, thallus rugosity, interstitial volume	Assemblage abundance	Crustaceans	Host morphology was most important in defining cryptofaunal assemblages.	22
Australia	Subtidal rocky costs	*E. radiata*/ Habitat configuration	Invertebrate density, species richness	Assemblages	Invertebrate assemblages, but not spp. richness, differed between *E. radiata* mono-specific and interspersed strands and clumped strands.	23
US/CA	Rocky mid-intertidal	*P. fastigiate* Size	Invertebrate richness, abundance	Copepods, amphipods	Higher biodiversity was positively associated with seaweed size.	24
US/ME	Rocky shore, tidepools	*U. lactuca, C. rubrum, C. crispus, C. officinalis, L. digitata …* mimics/ Degree of branching	Amphipod density	Amphipods	Branched algae had the highest densities, possibly due to the higher amount of habitable space available between fronds.	25
Australia	Rhodolith beds	*H. rupestre, Lithothamnion, others*/Foliose vs fruticose forms	Cryptofaunal abundance	Polychaeta	Minor or no differences in assemblages. Higher rhodolith diversity not correlated with cryptofauna.	26
UK	Kelp beds	Artificial kelp holdfast/ Complexity of holdfast	Invertebrate diversity richness, abundance	Amphipods, gastropods	Holdfast complexity was associated with species richness, diversity & abundance.	27
Scotland	Intertidal zone	*Cladophora rupestris, Laminaria digita*, and *Fucus serratus*/Fractal dimensions and emersion	Abundance	Copepods, amphipods, bivalves	Most complex macroalgae had higher abundance of invertebrates. Emersion only affected the least complex seaweed, causing an increase in abundance.	28
US/CA	Kelp forests	*Egregia menziesii*/ Algal cover, canopies at multiple sites	Algal cover/ richness,	Other algae, invertebrate benthos	*Egregia* kelp has both positive and negative effects on benthic biodiversity in stressful and non-stressful habitats, respectively.	29

(Continued)

TABLE 1 Continued

Location	Habitat	Seaweed(s)/ feature(s)	Measured response	Target taxa	Effect on faunal diversity	#
			invertebrate diversity			
England	Mid-shore rock pool	*Coralline officinalis, Cladophora rupestris, others*/ Degree of branching	Density, abundance, diversity	Ostracod	Results show that structural complexity affects epifaunal communities in space and time	30
US/CA	Kelp forests	*M. pyrifera*/ Canopy in physical gradient	Invertebrate density, diversity, interactions	Epibionts, communities	Canopies of kelp along a physical gradient influenced epibionts, invertebrate density, diversity, and some of their trophic interactions.	31
Chile	Rocky intertidal shore	Coralline algal turf/ Habitat characteristics	Taxonomic richness and abundance	Polychaetes	Frond density and amount of sediment were the best variables to explain assemblage differences.	32
Brazil	Sandy beach	*Sargassum*/Biomass	Density	Gastropoda	There were variations in seaweed biomass and epifauna density throughout the year.	33
Italy	Shallow coastal areas	Native & invasive seaweeds/ PUAs & structural complexity	Meio- & microphytobenthic communities	Diatoms, copepods, macrofauna.	Invasive algae supported less diversity than native species. PUAs & structural complexity could not predict differences in meiobenthic assemblages.	34
New Zealand	Intertidal rocky shores	*Hormosira banksii*/ Presence or absence of dominant habitat-forming seaweed	Epifaunal abundance, species richness	Amphipods,Micro-snails copepods	Removal of dominant seaweed caused a decline in epifaunal species richness and abundance.	35
Spitsbergen	Arctic benthic communities	*L. digitata, A.* aff. *Flagellate*, etc./Abiotic and biotic factors	Invertebrate and species abundance, and invertebrate density	Bryozoa and Crustacea	Low diversity in shallow algae due to ice/ waves. Thallus morphology influenced epifauna, which was lower when compared to other regions.	36
Australia	Rocky intertidal	Invasive: *C. fragile fragile* Native: *C. fragile tasmanicum*…/Branching, thallus & holdfast S:A	Epifauna taxonomic richness, abundance	Gastropods, gammarid amphipods	Invasive seaweed's holdfasts hold highest taxa richness. Branching was correlated with taxa and abundance on native but not invasive seaweeds.	37
Italy	Temperate rocky coast	*Cystoseira montagnei*/ Habitat size	Richness, evenness, structure, composition, trophic guilds	Gastropods	Abundance, richness, and H' increased with patch-size. Best explanatory algal features were algal surface, thallus volume & biomass.	38
Italy	Intertidal habitat	*E. amentacea* & *Laurencia*/ Structural complexity	Species richness, H' index, Pielou's evenness	Amphipods	The most and least complex algae had more density and diversity, respectively. Due to allelochemicals.	39
Italy	Shallow rocky shore	*Gongolaria montagnei*/ Fractal analysis	Abundance and species richness	Molluscs	Fractal dimensions of algae change during its vegetative cycle, and these changes have the ability to alter assemblages of organisms using the algae.	40
Australia	Shallow rocky reefs	*P. comosa, E. radiata*/ Structural complexity	Commercial species relative abundance, biomass	Abalone, sea urchins, fish	*P. comosa* supported higher density of abalone and urchins than *E. radiata*. This seems related to alga's complexity or chemical cues.	41
Australia	Exposed, rocky reefs	*P. comosa, E. radiata, S. vestitum*/Extant native vs transplanted plants	Epifaunal number of taxa, individuals	Crustaceans, mollusks	Algae had different assemblages. Transplanted algae supported lower diversity than undisturbed algae but supported considerable diversity.	42
Russia	Red algae zone	*C. truncates, P. extensum, others*/ Presence of algae species	Taxon richness	Bryozoans	Zonation found in epibenthic organisms in the red algae zone. Differences in assemblages between sites could be due to hydrology and sediments.	43

(Continued)

TABLE 1 Continued

Location	Habitat	Seaweed(s)/ feature(s)	Measured response	Target taxa	Effect on faunal diversity	#
Brazil	Sandstone reefs	Rhodoliths/Complexity of microhabitats	Faunal richness and diversity (meiofauna and macrofauna)	Nematoda, polychaetes	Rhodoliths complex microhabitats supported higher richness and diversity than bare sediment.	44
Antarctic	Subtidal	*D. menziessi*, *A. utricularis*, others/Chemical defenses	Amphipod densities	Amphipods, sea stars	Seaweed with high density of amphipods developed deterrents. Amphipods used habitats as refuges.	45
Chile	Subtidal forests	*Macrocystis pyrifera*/ Holdfast size	Invertebrate species richness, diversity	Crustaceans, echinoderms	Species richness, diversity & abundance increased with size of holdfasts (up until a threshold)	46
US/VA	Seagrasses, algal assemblage	*Z. marina*, *R. maritima*, drift algae, green and red algae/ Seaweed richness, composition	Epifaunal density	Isopods, amphipods	In mixed habitats, epifauna abundance was higher on seaweeds than seagrasses. Plant composition was more influential than plant diversity.	47
US/VA	Estuarine Seagrass/ seaweeds	*G. verrucosa, Ulva* spp., *C. rubrum, S. filiformis*/ Diversity and surface area	Motile epifauna density, diversity/ evenness, biomass	Amphipods	Plant diversity influenced Simpson diversity. Plant surface enhanced biomass & abundance, but reduced evenness & Simpson diversity.	48
US/CA	Nearshore systems	*Sporolithon australe*/ Rhodoliths	Cryptofaunal abundance, taxon richness	Polychaetes, crustaceans	Living rhodolith habitats had higher diversity than dead rhodolith beds and bare sand.	49
US/HI	Reef platform	*P. japonica, D. crenulate, T. ornate, G. fastigiata…*/ Surface area, biomass, S: B ratio	Epifaunal amphipod abundance	Amphipods	Abundance was correlated with seaweed S:A and biomass. Amphipod abundance or richness were not correlated with S:A.	50
France	Rocky shore	*L. digitata, P. palmata, M. stellatus, E. elongate*/ Structural complexity	Invertebrate, abundance, richness	Amphipods, gastropods	Algal complexity was correlated with abundance, richness & diversity. More complex assemblages supported higher epifaunal diversity.	51
Canada, NS	Subtidal rocky reef	*C. fragile*, *L. longicruris*, *L. digitata*/Fronds, holdfasts, thalli	Epifaunal abundance	Gastropods	Assemblages on fronds and holdfasts differ among algae. Diversity on the fronds was also different.	52
Greenland	Arctic benthic communities	*Clathromorphum* sp., *S. longicururis*, etc./Kelp beds vs coralline algae	Invertebrate species diversity	Mixed	Interstitial communities in rhodolith habitats are different and more diverse than in kelp beds.	53
Australia	Temperate artificial rocky reefs	*E. radiata*, artificial kelp/ Density, patch size, position	Epifaunal secondary productivity, richness, diversity, structure	Epifauna	Patch size had positive effect on richness. Mimic patch edges had higher richness than center, their size influenced diversity in centrally located habitats.	54
Costa Rica	Shallow subtidal	Rhodoliths/ Aggregation level	Macrofauna richness. Abundance, H', composition.	Crustaceans, polychaetes, mollusks	Moderately and highly aggregated rhodoliths had highest richness. Highest abundance and H' found at moderately aggregated rhodoliths.	55
Brazil	Benthic habitats	Rhodolith beds/ Nodule densities and morphology	Macrofaunal diversity	Annelida, Crustacea, Mollusks	Density was similar between high-and low-density rhodolith beds. Density and trophic richness were higher on nodules compared to sediments below.	56
Tanzania	Rocky, soft sediment seaweeds	*T. conoides*, *S. aquifolium*/ Seagrass & seaweed combinations	Epifaunal abundance, biomass, taxa richness	Crustaceans, Annelids	Seaweed richness was correlated with epifaunal abundance, richness & biomass. Seaweeds had also higher biodiversity and fish than seagrasses.	57
New Zealand	Rocky subtidal	Brown and laminarian algae/ Thallus width, growth forms	Mobile epifauna density	Amphipods, isopods	Thallus width and density were inversely related. Thallus width and isopod shape were related. algal fine structured growth was related with abundance.	58

(Continued)

TABLE 1 Continued

Location	Habitat	Seaweed(s)/ feature(s)	Measured response	Target taxa	Effect on faunal diversity	#
Portugal	Rocky shore	Annual species; *Chondracnthus teedii, Codium tomentosum*, others/ Biomass and fractal measures	Abundance and taxa richness	Molluscs, crustaceans, polychaetas.	Biomass & fractal area of macroalgae had the biggest influence on shaping associated epifaunal communities.	59
Portugal	Intertidal rocky pools	Native and invasive seaweeds/ Macroalgal complexity	Taxa richness and abundance	Mixed epifauna	Abundance increased with algae's dry weight & fractal dimension, independent of algae identity, affected abundance & richness.	60
Chile	Subtidal subantarctic kelp forest	*Lessonia flavicans*	Species richness, abundance, community structure	Macrobenthic communities	Diversity and community structure correlated positively and negatively with distinct features of algal structural complexity	61
Sweden	Shallow hard bottoms	*F. vesiculosus*/ Presence or absence	Invertebrate biomass, abundance, richness	Gastropods, bivalves	The presence of *F. vesiculosus* was positively associated with the biomass but not the species richness of invertebrates.	62

Table reference numbers (#): Arkema et al. (2009)[1], Bates and DeWreede (2007)[2], Best et al. (2014)[3], Burščić et al. (2019)[4], Buschbaum and Chapman (2006)[5], Cacabelos et al. (2010)[6], Cerqueira Veras et al. (2020)[7], Chemello and Milazzo (2002)[8], Chen et al. (2020) [9], Christie et al. (2003)[10], Da Rocha et al. (2006)[11], Davenport et al. (1996)[12], Davenport et al. (1999) [13], Dijkstra et al. (2017) [14], Duarte et al. (2020)[15], El-Khaled et al. (2022)[16], Frame et al. (2007)[17], Gabara et al. (2018) [18], Gallardo et al., (2021)[19], Gee and Warwick (1994)[20], Gestoso et al. (2012)[21], Glanz (2021)[22], Goodsell et al. (2004)[23], Gunill (1982)[24], Hacker and Steneck (1990)[25], Harvey and Bird (2008)[26], Hauser et al. (2006)[27], Hooper and Davenport (2006)[28], Hughes (2010)[29], Hull (1997)[30], Karr (2011)[31], Kelaher and Castilla (2005)[32], Leite and Turra (2003)[33], Lenzo et al. (2023)[34], Lilley and Schiel (2006)[35], Lippert et al. (2001)[36], Lutz et al. (2019)[37], Mancuso et al. (2021)[38], Mancuso et al. (2023a)[39], Mancuso et al. (2023b)[40], Marzinelli et al. (2014)[41], Marzinelli et al. (2016)[42], Mikhaylova et al. (2019)[43], Neves and Costa (2022)[44], Núñez-Pons et al. (2012)[45], Ojeda and Santelices (1984)[46], Parker (1998)[47], Parker et al. (2001) [48], Robinson (2015)[49], Russo (1990)[50], Schaal et al. (2016)[51], Schmidt and Scheibling (2006)[52], Schoenrock et al. (2018)[53], Shelamoff et al. (2020)[54], Solano-Barquero et al. (2022)[55], Stelzer et al. (2021)[56], Tano et al. (2016)[57], Taylor and Cole (1994)[58], Torres et al. (2015)[59], Veiga et al. (2014)[60], Velazco-Charpentier et al. (2021)[61], Wikstrom and Kautsky (2007)[62].

assemblages (Hull, 1997; Leite and Turra 2003; Torres et al., 2015; Mancuso et al., 2023b). For instance, changes in fractal dimensions during the algal vegetative cycle have resulted in changes in associated gastropod communities (Mancuso et al., 2023b) and the timing of peak abundances of ostracod populations (Hull, 1997). The latter author, for example, found that ostracod densities in the most complex alga (*Ceramium nodulosum*) peaked in February, whereas in the least complex alga (*Chondrus crispus*) they peaked in December (Hull, 1997). Meanwhile, the seasonal variation in biomass of a different seaweed (*Sargassum* spp) appeared to be unrelated with the seasonal variation of its own associated epifauna (Leite and Turra 2003). Yet another study (Torres et al., 2015) found that a combination of two of the macroalgal features cited above (fractal area and biomass) were the best predictors of associated epifaunal assemblages.

While the studies cited above examined seaweed structural complexity at the individual level, others have focused on the complexity of specific traits of seaweeds (e.g., thallus and holdfast morphology). Such traits specifically include blades' surface area or density (Gunill, 1982; Russo, 1990; Parker et al., 2001; Kelaher and Castilla, 2005), degree of branching or number of blade branches (Hacker and Steneck, 1990; Chemello and Milazzo, 2002; Lutz et al., 2019), thallus characteristics (i.e., the morphology of full seaweeds) (Taylor and Cole, 1994; Schmidt and Scheibling, 2006; Gallardo et al., 2021), and holdfast characteristics (Ojeda and Santelices, 1984; Hauser et al., 2006; Schmidt and Scheibling, 2006; Lutz et al., 2019). The first features (seaweed surface area and density) have been found to have the strongest relationships with invertebrate assemblages (Kelaher and Castilla, 2005). These features have been shown to contribute to significant increases in invertebrate diversity (Gunill, 1982), from two to ten-fold increases in abundance (Russo, 1990; Gunill, 1982), and up to a 15-fold increase in biomass (Parker et al., 2001). Exceptions have been found, though, where surface area was shown to reduce invertebrate diversity and evenness (Parker et al., 2001).

Physiological features of seaweed thalli have also been linked with significant changes in invertebrate biodiversity (Gallardo et al., 2021) and density levels (Taylor and Cole, 1994). For example, comparing soft and hard thalli, Gallardo et al., (2021) reported a 20-50% increase in biodiversity levels in hard thalli species when compared to soft thalli species. Likewise, Taylor and Cole (1994) showed an inverse relationship between thallus width and invertebrate densities, with a density increase of nearly 300% from the widest to the narrowest thallus. Such a surprising relationships can be explained by the finely structured thinner thalli, which led to a higher small-scale structural complexity that favored epifaunal density (Taylor and Cole, 1994). The branching of the thalli also supported a higher number of taxa and individuals (Lutz et al., 2019), and higher overall abundances and biodiversity levels (Hacker and Steneck, 1990; Chemello and Milazzo, 2002). For example, the degree of branching increased the density of amphipods, among the most common epifaunal groups associated with seaweeds (e.g., Tummon Flynn et al., 2021), from ~2 individuals/100mL interstitial volume on seaweeds with large leathery thalli, to ~22 individuals/100mL interstitial volume on coarsely branched thalli (Hacker and Steneck, 1990).

Structural complexity has also been linked to a prominent group of red coralline algae, the Rhodoliths (Harvey and Bird, 2008; Stelzer et al., 2021; Neves and Costa, 2022). They create a porous habitat that enhances individual and bed physical complexity (Gabara et al., 2018, Cerqueira Veras et al., 2020),

supporting significantly higher diversities than non-living beds or adjacent bare sediments (Robinson, 2015; Stelzer et al., 2021; Neves and Costa, 2022), or even some kelp beds (Schoenrock et al., 2018). Along with complexity, the depth (shallow or deep, in tropical or polar latitudes, respectively; Mikhaylova et al., 2019; Cerqueira Veras et al., 2020) and density of these beds also contribute to biodiversity. Counter examples include studies where different rhodolith forms are only weakly associated with species assemblages (Harvey and Bird, 2008), or host morphology was the most important in determining crytofaunal assemblages associated with crustose coralline algae (Glanz, 2021). Lastly, regarding macroalgae that have holdfasts, it has been found that taxa richness (Lutz et al., 2019), number of species, species diversity, and abundance (Ojeda and Santelices, 1984; Hauser et al., 2006) all significantly increased in relation with holdfast structural complexity. For example, Hauser et al. (2006) found increases of nearly 170%, 250% and 260% in invertebrate species richness, diversity, and abundance, respectively, from the least to the most complex holdfasts of artificial kelps under comparison. Similarly, Lutz et al. (2019) found that a species of non-indigenous green alga (*Codium fragile* spp. *Fragile*), which possessed more complex holdfasts than native conspecifics (*C. fragile*), held twice the species richness. However, it is noteworthy that at least two studies have found no differences in invertebrate taxa (Schmidt and Scheibling, 2006) and assemblages (Lutz et al., 2019) in relation to the holdfast complexity, for kelp and green algae, respectively.

3 The influence of seaweed habitat features

In addition to features associated with individual seaweeds, several studies have focused on how the structure or makeup of entire seaweed communities (or habitats) contribute to invertebrate diversity. Various aspects of invertebrate communities, including biodiversity, have been associated with seaweed diversity and/or species richness (Parker, 1998; Bates and DeWreede, 2007; Best et al., 2014; Tano et al., 2016), seaweed identity and species composition (Parker, 1998; Lilley and Schiel, 2006; Wikstrom and Kautsky 2007; Bates and DeWreede, 2007; Marzinelli et al., 2016), seaweed assemblage structure (Goodsell et al., 2004; Frame et al., 2007), seaweed habitat size (Shelamoff et al., 2020; Chen et al., 2020; Mancuso et al., 2021), and habitat position in relation to tide level (Davenport et al., 1999; Hooper and Davenport, 2006; Cacabelos et al., 2010; Loke and Todd, 2016). The first of these features, seaweed species richness, has often been correlated with higher invertebrate species richness (Parker, 1998; Best et al., 2014). For instance, Best et al. (2014) found that while habitats with higher algal species richness had ~9% higher animal species richness, they tend to have lower animal abundance. At least two articles have found this association to be weak (Parker, 1998; Bates and DeWreede, 2007) and claimed that seaweed species composition (rather than richness) correlated better with increases in invertebrate diversity. With regards to the structure of seaweed assemblages, Goodsell et al. (2004) did not find causal effects on species richness, but the makeup of invertebrate communities was significantly different among distinct algal habitat configurations. Likewise, Frame et al. (2007) found that the abundance of ostracods was closely associated with the structural complexity of various algae, while their highest species richness was associated with turf-forming algae.

Macroalgae often form patches, beds, or habitats of limited dimensions. The size of these patches has been positively correlated with invertebrate species richness, abundance, and biomass (Shelamoff et al., 2020; Mancuso et al., 2021). The former author found that a decrease in seaweed patch size reduced animal species richness by 50%, while reducing Shannon-Wiener diversity by 20%, from the largest to the smallest patch (Shelamoff et al., 2020). Similarly, Chen et al. (2020) found that canopy volume in conjunction with algal weight, had a strong correlation with invertebrate abundance and biomass. Variation in biotic and abiotic factors due to differences in geographic location often accounts for part of these relationships. However, studies conducted in high (including polar) latitudes, follow the general trend observed in warmer coasts: bed size and structural complexity favors higher invertebrate diversity (Lippert et al., 2001; Schoenrock et al., 2018). Harsh physical conditions (including ice and wave stress) frequently limit overall diversity in shallow compared to deep habitats, increasing the likelihood of unstable, more fluctuating communities and favoring the development of barren habitats (Lippert et al., 2001; Mikhaylova et al., 2019). Despite that, most evidence suggests that the food, habitat, and refuge associated with complex seaweed beds also favors stability and ultimately local biodiversity (e.g., Lippert et al., 2001; Núñez-Pons et al., 2012; Mikhaylova et al., 2019). Locally, large seaweed beds, particularly kelp forests, display interesting (complex) relationships between canopies, physical conditions and species interactions and diversity. Karr (2011) found that *Macrocystis pyrifera* kelp forests most directly exposed to swell, supported larger density and diversity (and different assemblages) than less exposed forests. The same author suggested that kelp canopy's functional role was a nursery habitat for fish, that indirectly altered trophic interactions (Karr, 2011).

The role played by seaweed beds has also been associated with the presence or absence of certain species, including the giant kelp referred to above (Karr, 2011). For example, large canopies of giant kelp have strong direct and indirect effects on other seaweeds, and ultimately on invertebrate diversity and community structure (e.g., Arkema et al., 2009). As stated above, the influence of "foundation species" (Dayton, 1985; Stachowicz, 2001) exceeds community-level metrics such as biodiversity. Such influence is strong, but as described by Hughes (2010) for the brown alga *Egregia menziesii*, is also complex and varies with local physical conditions and spatial scale. When these key species are artificially removed or lost, they cause strong changes over multiple species and trophic levels (Ellison et al., 2005; Castorani et al., 2018; Montie and Thomsen, 2023). For example, Lilley and Schiel, 2006 found that when a dominant habitat forming seaweed species was removed, the period following removal (up to two years afterwards), was characterized by a significant decrease in the number of invertebrate taxa. In fact, two

years after these experiments, removal plots had ~40% less taxa than control (non-removal) plots (Lilley and Schiel, 2006). Effects on different trophic levels resulting from kelp harvesting in Norway have been reported by Lorentsen et al. (2010) and Christensen-Dalsgaard et al. (2017). Likewise, Perälä et al. (2023) have highlighted the negative influence of the harvesting of *Laminaria hyperborea* forests from the Northeast Atlantic on the survival of Atlantic cod and European lobsters. All those results are closely related with those documented by Wikstrom and Kautsky (2007), who showed that in the absence of a common seaweed, the biomass of associated invertebrates was significantly lower. In addition, Marzinelli et al. (2016) focused on a related aspect with practical implications for biodiversity: these authors found that when transplanted seaweed species are brought into an area, they often support less diversity than the same species in their "undisturbed" condition.

Many macroalgae and the habitats they create are associated with intertidal systems, and therefore, are exposed to periodic emersion. Not surprisingly, several studies have examined how macroalgal structural complexity influences associated assemblages in relation with their position across the intertidal gradient (Davenport et al., 1999; Hooper and Davenport, 2006; Cacabelos et al., 2010). In sheltered shorelines of South Australia, the periodic emersion of three species of macroalgae caused a significant reduction in associated epifaunal numbers. However, macroalgal structural complexity ameliorated these reductions: for organisms associated with the simplest alga (*Enteromorpha*) 44 times as many animals were present when submerged than when emersed, a ratio strikingly higher than the one measured in animals associated with the most complex algae (*Corallina*) for which the submerged to emersed ratio was only 1.8 (Davenport et al., 1999). The reduced losses observed in complex algae was partially attributed to water retention which likely prevents desiccation potential effects. However, trends like these are not necessarily consistent across studies. Hooper and Davenport (2006) compared three macroalgae of distinct structural complexity (as measured by fractal dimensions) and although the most complex alga had the richest associated communities, there were no differences in terms of epifaunal emigration levels during low tide emersion.

4 Implications for conservation, restoration, and monitoring

As the bulk of the information summarized in Table 1 indicates, most research to date shows that macroalgae and the habitats they create contribute to an increase in at least some measure of biodiversity. While those increases range widely from weak to very strong, and the influence of non-native seaweeds or other factors add an additional level of complexity (e.g., Veiga et al., 2016; Lutz et al., 2019; Ndhlovu et al., 2021; Lenzo et al., 2023), seaweeds generally improve rather than hinder associated communities. The most consistent promoter of faunal diversity seems to be the complexity of identifiable features within a seaweed itself (e.g., branching or holdfast morphology; Hacker and Steneck, 1990; Hauser et al., 2006; Lutz et al., 2019: Velasco-Charpentier et al., 2021) or the complexity achieved by the presence of several individuals or species coming together into a discernable habitat (Best et al., 2014; Tano et al., 2016). Algal structural complexity-biodiversity relationships have also been examined using fractal dimensions, and the outcome of several key studies have provided added support to these relationships (e.g., Mancuso et al., 2023b). However, some of this research has also identified exceptions and highlighted outcome variations, partly due to the strong influence of organisms' size and spatial scale on fractal dimensions (e.g., Gee and Warwick, 1994). Among the above refereed studies, tide distribution or seasonal variation associated with life cycles, in addition to various concurrent factors (e.g., Ndhlovu et al., 2021) suggest that algal structural complexity is one but not the sole predictor of associated biodiversity levels (Torres et al., 2015).

From a conservation and restoration point of view, such features gain relevance in coastal areas where seaweeds and seaweed habitats are in decline, or otherwise where lasting populations of rare, threatened, or endangered species of seaweeds can be found. Given the importance of these species, some of them coined foundation species (*sensu* Wikström and Kautsky, 2007; Dijkstra et al., 2017; El-Khaled et al., 2022) or ecosystem engineers (Schmidt and Scheibling, 2006; Schaal et al., 2016; Shelamoff et al., 2020), their loss likely entails escalating changes on associated communities. Based on most of the evidence reviewed here, such changes are most likely detrimental to diversity or abundance metrics (Ellison et al., 2005; Norderhaug et al., 2005; Marzinelli et al., 2016). Conserving or restoring by protecting, planting, or transplanting key seaweed species is complex, resource intensive, and provides variable levels of success due to many unaccounted factors (Marzinelli et al., 2016; Whitaker et al., 2023). However, when facing the accelerated loss or displacement of seaweed species caused by climate change (see Bindoff et al., 2019), they represent the best approach for protecting the ecological services they provide and a diversity of reliant organisms that otherwise may be lost as well. The results of this review also suggest that the monitoring of estuarine or coastal fauna should focus heavily on the sampling of seaweed habitats, particularly those holding complex species- or bed-related features. As highlighted above, such features generally contribute to richer associated communities (Christie and Kraufvelin 2004; Frame et al., 2007; Shelamoff et al., 2020; Mancuso et al., 2023a) by providing shelter against harsh physical conditions (e.g., the brown alga *Phyllospora comosa* in exposed rocky reefs of Australia; Marzinelli et al., 2016), or refuge against predators (e.g., a variety of the red alga *Chondrus crispus* in sedimentary bottoms of Atlantic Canada; Tummon Flynn et al., 2020).

Our call for surveys that include the careful examination of seaweed habitats applies to every type of organism. However, our review incidentally found that meiofaunal groups warrant further attention (see e.g., Da Rocha et al., 2006; Veiga et al., 2016), and a particular group among macrofaunal organisms, the amphipods, has been the most recurrently found, sampled, and studied in relation to seaweed characteristics (Table 1). Similar conclusions were highlighted in Christie et al. (2009)'s review of organisms associated with macrophytes, including macroalgae. These authors

showed that amphipod abundances were dynamic (due to dispersal, colonization, and behavior) but consistently among the highest. Likewise, complex interactions between chemically defended macroalgae and amphipods have been documented in multiple regions, including Antarctic habitats (Brawley, 1992; Núñez-Pons et al., 2012). It follows that in a scenario of further seaweed declines due to climate change, amphipods (and the consumers relying on these small crustaceans for food) will be among the most directly affected. Considering the plausibility of monitoring, we argue that among the macrobenthic taxa associated with macroalgae, amphipods may be among the species to be studied as recurrent users of rugose habitats such as those provided by many morphologically complex algae.

This overview made also evident a potential geographic gap: most of the studies examined were conducted in warm, low-mid latitudes, such as southern U.S.A., the Mediterranean coasts or Australia (Hacker and Steneck, 1990; Russo, 1990; Taylor and Cole, 1994; Lutz et al., 2019; Shelamoff et al., 2020), although a representative number of studies from high (including polar) latitudes have been also considered (e.g., Lippert et al., 2001; Núñez-Pons et al., 2012; Velasco-Charpentier et al., 2021). Often, the diverse complement of seaweeds found in low-mid latitude regions support rich associated communities, making the influence of features such as physical complexity potentially more evident. The lower representation of higher latitude (potentially less diverse) seaweed-invertebrate communities may mask additional relationships in those regions, and merits further examination. Similarly, there was a relatively high number of studies conducted in rocky shores (e.g., Taylor and Cole, 1994; Buschbaum and Chapman, 2006; Schaal et al., 2016; Dijkstra et al., 2017) in comparison to those conducted in sedimentary habitats. Despite obvious differences, physical complexity of seaweeds or seaweed morphological features remained consistently related with biodiversity levels. Still, distinct ecosystems warrant further attention and open a potential venue for future comparative studies to help us better understand how these relationships operate. As forecasted (Bindoff et al., 2019), climate events will continue to displace and locally exclude seaweed species, so knowledge on the seaweed features that contribute the most to the biodiversity of associated organisms should quickly transition to practice. Ultimately, ongoing seaweed losses should be matched by further monitoring, conservation, and restoration efforts.

Author contributions

EG: Data curation, Formal analysis, Investigation, Writing – original draft, Writing – review and editing. PQ: Conceptualization, Formal analysis, Funding acquisition, Investigation, Supervision, Writing – original draft, Writing – review and editing.

Funding

The author(s) declare financial support was received for the research, authorship, and/or publication of this article. A CGS-M fellowship (EG) and a Discovery grant (PQ) both from the Natural Sciences and Engineering Research Council of Canada (NSERC) provided support during the preparation of this Minireview.

Acknowledgments

We thank Paula Tummon Flynn and K. Devon Lynn (UPEI), and two reviewers for their feedback on earlier versions of this manuscript.

Conflict of interest

The authors declare that the research was conducted in the absence of any commercial or financial relationships that could be construed as a potential conflict of interest.

The author(s) declared that they were an editorial board member of Frontiers, at the time of submission. This had no impact on the peer review process and the final decision.

Publisher's note

References

Amsler, C. D. (2008). *Algal chemical ecology. Vol. 468* (Berlin: Springer).

Amsler, C. D., McClintock, J. B., and Baker, B. J. (2014). Chemical mediation of mutualistic interactions between macroalgae and mesograzers structure unique coastal communities along the western Antarctic Peninsula. *J. phycology* 50, 1–10. doi: 10.1111/jpy.12137

Arkema, K. K., Reed, D. C., and Schroeter, S. C. (2009). Direct and indirect effects of giant kelp determine benthic community structure and dynamics. *Ecology.* 90, 3126–3137. doi: 10.1890/08-1213.1

Bates, C. R., and DeWreede, R. E. (2007). Do changes in seaweed biodiversity influence associated invertebrate epifauna? *J. Exp. Mar. Biol. Ecology.* 344, 206–214. doi: 10.1016/j.jembe.2007.01.002

Best, R. J., Chaudoin, A. L., Bracken, M. E. S., Graham, M. H., and Stachowicz, J. J. (2014). Plant-animal diversity relationships in a rocky intertidal system depend on invertebrate body size and algal cover. *Ecology.* 95, 1308–1322. doi: 10.1890/13-1480.1

Bindoff, N. L., Cheung, W. W. L., Kairo, J. G., Aristegui, J., Guinder, V. A., Hallberg, R., et al. (2019). "Changing ocean, marine ecosystems, and dependent communities," in *IPCC Special Report on the Ocean and Cryosphere in a Changing Climate*. Eds. H.-O. Portner, D. C. Roberts, V. Masson-Delmotte, P. Zhai and M. Tignor (Cambridge, UK and New York, NY, USA: Cambridge University Press), 447–587.

Brawley, S. H. (1992). "Mesoherbivores," in *Plant-Animal Interactions in the Marine Benthos*. Eds. D. John, S. Hawkins and J. Price (Oxford: Oxford University Press), 235–263.

Brawley, S. H., and Adey, W. H. (1981). The effect of micrograzers on algal community structure in a coral reef microcosm. *Mar. Biol.* 61, 167–177. doi: 10.1007/BF00386656

Buršić, M., Iveša, L., Jaklin, A., and Arko Pijevac, M. (2019). A preliminary study on the diversity of invertebrates associated with *Corallina officinalis* Linnaeus in southern Istrian peninsula. *Acta Adriatica.* 60, 127–136. doi: 10.32582/aa.60.2.2

Buschbaum, C., and Chapman, A. S. (2006). How an introduced seaweed can affect epibiota diversity in different coastal systems. *Mar. Biol.* 148, 743–753. doi: 10.1007/s00227-005-0128-9

Cacabelos, E., Olabarria, C., Incera, M., and Troncoso, J. S. (2010). Effects of habitat structure and tidal height on epifaunal assemblages associated with macroalgae. *Estuarine Coastal Shelf Science.* 89, 43–52. doi: 10.1016/j.ecss.2010.05.012

Castorani, M. C., Reed, D. C., and Miller, R. J. (2018). Loss of foundation species: disturbance frequency outweighs severity in structuring kelp forest communities. *Ecology* 99, 2442–2454. doi: 10.1002/ecy.2485

Cerqueira Veras, P., Pierozzi-Jr, I., Lino, J. B., Amado-Filho, G. M., Senna, A. R., Santos, C. S. G., et al. (2020). Drivers of biodiversity associated with rhodolith beds from euphotic and mesophotic zones: Insights for management and conservation. *Perspect. Ecol. Conserv.* 18, 37–43. doi: 10.1016/j.pecon.2019.12.003

Chemello, R., and Milazzo, M. (2002). Effect of algal architecture on associated fauna: some evidence from phytal molluscs. *Mar. Biol.* 140, 981–990. doi: 10.1007/s00227-002-0777-x

Chen, Y. Y., Cooper, P., and Fulton, C. J. (2020). Sargassum epifaunal communities vary with canopy size, predator biomass and seascape setting within a fringing coral reef ecosystem. *Mar. Ecol. Prog. Series.* 640, 17–30. doi: 10.3354/meps13282

Christensen-Dalsgaard, S., Mattisson, J., Bekkby, T., Gundersen, H., May, R., Rinde, E., et al. (2017). Habitat selection of foraging chick-rearing European shags in contrasting marine environments. *Mar. Biol.* 164, 1–12. doi: 10.1007/s00227-017-3227-5

Christie, H., Jorgensen, N. M., Norderhanug, K. M., and Waage-Nielsen, E. (2003). Species distribution and habitat exploitation of fauna associated with kelp (*Laminaria hyperborea*) along the Norwegian coast. *J. Mar. Biol. Assoc. United Kingdom.* 83, 1–13. doi: 10.1017/S0025315403007653h

Christie, H., and Kraufvelin, P. (2004). Mechanisms regulating amphipod population density within macroalgal communities with low predator impact. *Scientia Marina.* 68, 189–198. doi: 10.3989/scimar.2004.68s1189

Christie, H., Norderhaug, K. M., and Fredriksen, S. (2009). Macrophytes as habitat for fauna. *Mar. Ecol. Prog. Series.* 396, 221–233. doi: 10.3354/meps08351

Da Rocha, C. M. C., Venekev, V., Bezerra, T. N. C., and Souza, J. R. B. (2006). Phytal marine nematode assemblages and their relation with the macrophytes structural complexity in a Brazilian tropical rocky beach. *Hydrobiologia.* 553, 219–230. doi: 10.1007/s10750-005-0923-9

Davenport, J., Butler, A., and Cheshire, A. (1999). Epifaunal composition and fractal dimensions of marine plants in relation to emersion. *J. Mar. Biol. Assoc. United Kingdom.* 79, 351–355. doi: 10.1017/S0025315498000393

Davenport, J., Pugh, P. J. A., and McKechnie, J. (1996). Mixed fractals and anisotropy in subantarctic marine macroalgae from South Georgia: implications for epifaunal biomass and abundance. *Mar. Ecol. Prog. Series.* 136, 245–255. doi: 10.3354/meps136245

Dayton, P. K. (1985). Ecology of kelp communities. *Annu. Rev. Ecol. Systematics.* 16, 215–245. doi: 10.1146/annurev.es.16.110185.001243

Dijkstra, J. A., Harris, L. G., Mello, K., Litterer, A., Wells, C., and Ware, C. (2017). Invasive seaweeds transform habitat structure and increase biodiversity of associated species. *J. Ecology.* 105, 1668–1678. doi: 10.1111/1365-2745.12775

Duarte, R. C. S., Mota, E. L. S., and Dias, T. L. P. (2020). Algal complexity positively affects the abundance, richness and diversity of molluscan assemblages of a semiarid hypersaline mangrove. *Aquat. Ecology.* 54, 1001–1013. doi: 10.1007/s10452-020-09789-3

El-Khaled, Y. C., Daraghmeh, N., Tilstra, A., Roth, F., Huettel, M., Rossbach, F. I., et al. (2022). Fleshy red algae mats act as temporary reservoirs for sessile invertebrate biodiversity. *Commun. Biol.* 5, 579. doi: 10.1038/s42003-022-03523-5

Ellison, A. M., Bank, M. S., Clinton, B. D., Colburn, E. A., Elliott, K., Ford, C. R., et al. (2005). Loss of foundation species: consequences for the structure and dynamics of forested ecosystems. *Front. Ecol. Environ.* 3, 479–486. doi: 10.1890/1540-9295(2005)003[0479:LOFSCF]2.0.CO;2

Frame, K., Hunt, G., and Roy, K. (2007). Intertidal meiofaunal biodiversity with respect to different algal habitats: a test using phytal ostracodes from Southern California. *Hydrobiologia.* 586, 331–342. doi: 10.1007/s10750-007-0707-5

Gabara, S. S., Hamilton, S. L., Edwards, M. S., and Steller, D. L. (2018). Rhodolith structural loss decreases abundance, diversity, and stability of benthic communities at Santa Cataline Island, CA. *Mar. Ecol. Prog. Series.* 595, 71–88. doi: 10.3354/meps12528

Gallardo, D., Oliva, F., and Ballesteros, M. (2021). Marine invertebrate epibionts on photophilic seaweeds: importance of algal architecture. *Mar. Biodiversity.* 51, 16. doi: 10.1007/s12526-020-01151-y

Gee, J. M., and Warwick, R. M. (1994). Metazoan community structure in relation to the fractal dimensions of marine macroalgae. *Mar. Ecol. Prog. Series.* 103, 141–150. doi: 10.3354/meps103141

Gestoso, I., Olabarria, C., and Troncoso, J. S. (2012). Effects of macroalgal identity on epifaunal assemblages: native species *versus* the invasive species *Sargassum muticum*. *Helgoland Mar. Res.* 66, 159–166. doi: 10.1007/s10152-011-0257-0

Glanz, J. S. (2021). *Relationship between a branch-forming crustose coralline algae, associated small motile invertebrates, and water flow* (Northridge: California State University).

Goodsell, P. J., Fowler-Walker, M. J., Gillanders, B. M., and Connell, S. D. (2004). Variations in the configurations of algae in subtidal forests: Implications for invertebrate assemblages. *Austral Ecol.* 29, 350–357. doi: 10.1111/j.1442-9993.2004.01372.x

Gunill, F. C. (1982). Effects of plant size and distribution on the numbers of invertebrate species and individuals inhabiting the brown alga *Pelvetia fastigiata*. *Mar. Biol.* 69, 263–280. doi: 10.1007/BF00397492

Hacker, S. D., and Steneck, R. S. (1990). Habitat architecture and the abundance and body-size dependent habitat selection of a phytal amphipod. *Ecology.* 71, 2269–2285. doi: 10.2307/1938638

Hansen, J. P., Sagerman, J., and Wikstrom., S. A. (2010). Effects of plant morphology on small-scale distruction of invertebrates. *Mar. Biol.* 157, 2143e2155. doi: 10.1007/s00227-010-1479-4

Harvey, A. S., and Bird, F. L. (2008). Community structure of a rhodolith bed from cold-temperature waters (southern Australia). *Aust. J. Botany.* 56, 437–450. doi: 10.1071/BT07186

Hauser, A., Attrill, M. J., and Cotton, P. A. (2006). Effects of habitat complexity on the diversity and abundance of macrofauna colonising artificial kelp holdfasts. *Mar. Ecol. Prog. Series.* 325, 93–100. doi: 10.3354/meps325093

Hay, M. E. (2009). Marine chemical ecology: chemical signals and cues structure marine populations, communities, and ecosystems. *Annu. Rev. Mar. Science.* 1, 193–212. doi: 10.1146/annurev.marine.010908.163708

Hay, M. E., and Fenical, W. (1996). Chemical ecology and marine biodiversity: Insights and products from the sea. *Oceanography* 9, 10–20. doi: 10.5670/oceanog.1996.21

Hooper, G. J., and Davenport, J. (2006). Epifaunal composition and fractal dimensions of intertidal marine macroalgal in relation to emersions. *J. Mar. Biol. Assoc. United Kingdom.* 86, 1297–1304. doi: 10.1017/S0025315406014329

Hughes, B. B. (2010). Variable effects of a kelp foundation species on rocky intertidal diversity and species interactions in central California. *J. Exp. Mar. Biol. Ecology.* 393, 90–99. doi: 10.1016/j.jembe.2010.07.003

Hull, S. L. (1997). Variable effects of a kelp foundation species on rocky intertidal diversity and species interactions in central California. *Marine Ecology Progress Series* 161, 71–82. doi: 10.3354/meps161071

Ianora, A., Boersma, M., Casotti, R., Fontana, A., Harder, J., Hoffmann, F., et al. (2006). New trends in marine chemical ecology. *Estuaries Coasts.* 29, 531–551. doi: 10.1007/BF02784281

Karr, K. A. (2011). *Patterns, mechanisms and community consequences of variation in kelp forest canopies* (Santa Cruz: University of California).

Kelaher, B. P., and Castilla, J. C. (2005). Habitat characteristics influence macrofaunal communities in coralline turf more than mesoscale coastal upwelling on the coast of Northern Chile. *Estuarine Coast. Self Science.* 63, 155–165. doi: 10.1016/j.ecss.2004.10.017

Leite, F.P.P., and Turra, A. (2003). Temporal variation in Sargassum biomass, Hypnea epiphytism and associated fauna. *Braz. Arch. Biol. Technol.* 46, 665–671. doi: 10.1590/S1516-89132003000400021

Lenzo, D., Colangelo, M. A., Pasteris, A., Rindi, F., Pistocchi, R., and Pezzolesi, L. (2023). Understanding the role of macroalgal complexity and allelochemicals production in invasive and non-invasive macroalgae in the North-Western Adriatic Sea: effect on the associated communities. *Water.* 15, 1697. doi: 10.3390/w15091697

Lilley, S. A., and Schiel, D. R. (2006). Community effects following the deletion of a habitat-forming alga from rocky marine shores. *Oecologia.* 148, 672–681. doi: 10.1007/s00442-006-0411-6

Lippert, H., Iken, K., Rachor, E., and Wiencke, C. (2001). Macrofauna associated with macroalgae in the Kongsfjord (Spitsbergen). *Polar Biol.* 24, 512–522. doi: 10.1007/s003000100250

Loke, L. H., and Todd, P. A. (2016). Structural complexity and component type increase intertidal biodiversity independently of area. *Ecology.* 97, 383–393. doi: 10.1890/15-0257.1

Lorentsen, S. H., Sjøtun, K., and Grémillet, D. (2010). Multi-trophic consequences of kelp harvest. *Biol. Conserv.* 143, 2054–2062. doi: 10.1016/j.biocon.2010.05.013

Lutz, M. L., Minchinton, T. E., and Davis, A. R. (2019). Differences in architecture between native and non-indigenous macroalgae influence associations with epifauna. *J. Exp. Mar. Biol. Ecology.* 514, 76–86. doi: 10.1016/j.jembe.2019.03.006

Mancuso, F. P., Lo Brutto, S., Chemello, R., Sarà, G., and Mannino, A. M. (2023a). Effects of structural complexity on epifaunal assemblages associated with two intertidal Mediterranean seaweeds. *Plant Biosystems.* 157, 812–820. doi: 10.1080/11263504.2023.2200775

Mancuso, F. P., Milazzo, M., and Chemello, R. (2021). Decreasing in patch-size of *Cystoseira* forests reduces the diversity of their associated molluscan assemblage in Mediterranean rocky reefs. *Estuarine Coast. Shelf Science.* 250, 107163. doi: 10.1016/j.ecss.2020.107163

Mancuso, F. P., Milazzo, M., Sarà, G., and Chemello, R. (2023b). Bi- and three-dimensional fractal analysis of the brown seaweed *Gongolaria montagnei* and their

relationship with gastropod molluscs assemblage. *Mar. pollut. Bulletin.* 186, 114396. doi: 10.1016/j.marpolbul.2022.114396

Marzinelli, E. M., Campbell, A. H., Verges, A., Coleman, M. A., Kelaher, B. P., and Steinberg, P. D. (2014). Restoring seaweeds: does the declining fucoid *Phyllospora comosa* support different biodiversity than other habitats? *J. Appl. Phycology.* 26, 1089–1096. doi: 10.1007/s10811-013-0158-5

Marzinelli, E. M., Leong, M. R., Campbell, A. H., Steinberg, P. D., and Verges, A. (2016). Does restoration of a habitat-forming seaweed restore associated faunal diversity? *J. Soc. Ecol. Restoration.* 24, 81–90. doi: 10.1111/rec.12292

Mikhaylova, T. A., Aristov, D. A., Naumov, A. D., Malavenda, S. S., Savchenko, O. N., and Bijagov, K. L. (2019). Diversity and structure of epibenthic communities of red algae zone in the White Sea. *Polar Biol.* 42, 953–968. doi: 10.1007/s00300-019-02488-2

Montie, S., and Thomsen, M. S. (2023). Long-term community shifts driven by local extinction of an iconic foundation species following an extreme marine heatwave. *Ecol. Evol.* 13, e10235. doi: 10.1002/ece3.10235

Ndhlovu, A., Lathlean, J. A., McQuaid, C. D., and Seuront, L. (2021). Indirect effects shape macroalgal epifaunal communities. *Ecol. Evol.* 11, 15141–15152. doi: 10.1002/ece3.8195

Neves, S. B., and Costa, K. G. (2022). Diversity of benthic fauna of rhodoliths and sediments deposited on sandstone reefs in Southeast Brazil. *Ocean Coast. Res.* 70, e:22010. doi: 10.1590/2675-2824070.21029sbn

Norderhaug, K. M., Christie, H., Fosså, J. H., and Fredriksen, S. (2005). Fish – macrofauna interactions in a kelp (*Laminaria hyperborea*) forest. *J. Mar. Biol. Assoc. UK.* 85, 1279–1286. doi: 10.1017/S0025315405012439

Núñez-Pons, L., Rodríguez-Arias, M., Gómez-Garreta, A., Ribera-Siguán, A., and Avila, C. (2012). Feeding deterrency in Antartic marine organisms: bioassays with the omnivore amphipod *Cheirimedon femoratus*. *Mar. Ecol. Prog. Series.* 462, 163–174. doi: 10.3354/meps09840

Ojeda, F. P., and Santelices, B. (1984). Invertebrate communities in holdfasts of the kelp *Macrocystis pyrifera* from southern Chile. *Mar. Ecol. Prog. Series.* 16, 65–73. doi: 10.3354/meps016065

Parker, J. D. (1998). *Does plant diversity control animal diversity? an experimental approach*. MSc Thesis. (Virginia, USA: The College of William and Mary). doi: 10.25773/v5-1y50-6034

Parker, J. D., Duffy, J. E., and Orth, R. J. (2001). Plant species diversity and composition: experimental effects on marine epifaunal assemblages. *Mar. Ecol. Prog. Series.* 224, 55–67. doi: 10.3354/meps224055

Perälä, T., Pesari, S. N. K., Ahti, P. A., Lehtinen, S. O., Schoenrock, K. M., and Kuparinen., A. (2023) Non-trophic interactions amplify kelp harvest-induced biomass oscillations and biomass changes in a kelp forest ecological network model. *Mar. Ecol. Prog. Ser.* 722, 19-36. doi: 10.3354/meps14438

Richard, M., and Quijón, P. A. (2023). Seagrass-macroalgal interactions in a changing ocean. *Front. Clim.* 5, 1283305. doi: 10.3389/fclim.2023.1283305

Robinson, K. M. (2015). *Motile cryptofaunal invertebrate assemblages in Catalina Island's rhodolith beds in relation to physical structure and live rhodoliths* (Monterey Bay: California State University).

Russo, A. R. (1990). The role of seaweed complexity in structuring Hawaiian epiphytal amphipod communities. *Hydrobiologia.* 194, 1–12. doi: 10.1007/BF00012107

Schaal, G., Leclerc, J. C., Droual, G., Leroux, C., and Riera, P. (2016). Biodiversity and trophic structure of invertebrate assemblages associated with understorey red algae in a *Laminaria digitata* bed. *Mar. Biol. Res.* 12, 513–523. doi: 10.1080/17451000.2016.1164318

Schmidt, A. L., and Scheibling, R. E. (2006). A comparison of epifauna and epiphytes on native kelps (*Laminaria* species) and an invasive alga (*Codium fragile* spp. *tomentosoides) Nova Scotia Canada. Botanica Marina.* 49, 1–16. doi: 10.1515/BOT.2006.039

Schoenrock, K. M., Vad, J., Muth, A., Pearce, D. M., Rea, B. R., Schofield, J. E., et al. (2018). Biodiversity of kelp forests and coralline algae habitats in Southwestern Greenland. *Diversity.* 10, 1–20. doi: 10.3390/d10040117

Shelamoff, V., Layton, C., Tatsumi, M., Cameron, M. J., Edgar, G. J., Wright, J. T., et al. (2020). Kelp patch size and density influence secondary productivity and diversity of epifauna. *Oikos.* 129, 331–345. doi: 10.1111/oik.06585

Solano-Barquero, A., Sibaja-Cordero, J. A., and Cortés, J. (2022). Macrofauna associated with a rhodolith bed at an Oceanic Island in the Eastern Tropical Pacific (Isla del Coco National Park, Costa Rica). *Front. Mar. Science.* 9, 1–16. doi: 10.3389/fmars.2022.858416

Sotka, E. E., Jormalainen, V., and Poore, A. G. B. (2018). "The evolution of marine herbivores in response to algal secondary metabolites," in *Chemical ecology: the ecological impacts of marine natural products*. Eds. M. P. Puglisi and M. A. Becerro (Boca Raton, FL, USA: CRC Press), 193–220.

Stachowicz, J. J. (2001). Mutualism, facilitation, and the structure of ecological communities. *BioScience.* 51, 235–246. doi: 10.1641/0006-3568(2001)051[0235:MFATSO]2.0.CO;2

Stelzer, P. S., Mazzuco, A. C. A., Gomes, L. E., Martins, J., Netto, S., and Bernardino, A. F. (2021). Taxonomic and functional diversity of benthic macrofauna associated with rhodolith beds in SE Brazil. *PeerJ Life Environ.* 9, e:11903. doi: 10.7717/peerj.11903

Tano, S., Eggertsen, M., Wikstrom, S. A., Berkstrom, C., Buriyo, A. S., and Halling, C. (2016). Tropical seaweed beds are important habitats for mobile invertebrate epifauna. *Estuarine Coast. Shelf Science.* 183, 1–12. doi: 10.1016/j.ecss.2016.10.010

Taylor, R. B., and Cole, R. G. (1994). Mobile epifauna on subtidal brown seaweeds in northeastern New Zealand. *Mar. Ecol. Prog. Series.* 115, 271–282. doi: 10.3354/meps115271

Tokeshi, M., and Arakaki, S. (2012). Habitat complexity in aquatic systems: fractals and beyond. *Hydrobiologia.* 685, 27–47. doi: 10.1007/s10750-011-0832-z

Torres, A. C., Veiga, P., Rubal, M., and Sousa-Pinto, I. (2015). The role of annual macroalgal morphology in driving its epifaunal assemblages. *J. Exp. Mar. Biol. Ecology.* 464, 96–106. doi: 10.1016/j.jembe.2014.12.016

Tummon Flynn, P., Lynn, K. D., Cairns, D., and Quijón, P. A. (2019). The role of the non-indigenous green crab (*Carcinus maenas*) in the decline of a unique strain of Irish moss (*Chondrus crispus*): direct and indirect effects. *ICES J. Mar. Science.* 76, 2338–2348. doi: 10.1093/icesjms/fsz130

Tummon Flynn, P., Lynn, K. D., Cairns, D., and Quijón, P. A. (2021). Mesograzer interactions with a unique strain of Irish moss Chondrus crispus: colonization, feeding, and algal condition-related effects. *Mar. Ecol. Prog. Series.* 669, 83–96. doi: 10.3354/meps13737

Tummon Flynn, P., McCarvill, K., Lynn, K. D., and Quijón, P. A. (2020). The positive effect of coexisting ecosystem engineers: a unique seaweed-mussel association provides refuge for native mud crabs against a non-indigenous predator. *PeerJ.* 8, e10540. doi: 10.7717/peerj.10540

Veiga, P., Rubal, M., and Sousa-Pinto, I. (2014). Structural complexity of macroalgae influences epifaunal assemblages associated with native and invasive species. *Mar. Environ. Res.* 101, 115–123. doi: 10.1016/j.marenvres.2014.09.007

Veiga, P., Sousa-Pinto, I., and Rubal, M. (2016). Meiofaunal assemblages associated with native and non-indigenous macroalgae. *Continental Shelf Res.* 123, 1–8. doi: 10.1016/j.csr.2016.04.007

Velasco-Charpentier, C., Pizarro-Mora, F., Navarro, N. P., and Valdivia, N. (2021). Disentangling the links between habitat complexity and biodiversity in a kelp-dominated subantarctic community. *Ecol. Evol.* 11, 1214–1224. doi: 10.1002/ece3.7100

Whitaker, S. G., Ambrose, R. F., Anderson, L. M., Fales, R. J., Smith, J. R., Sutton, S., et al. (2023). Ecological restoration using intertidal foundation species: Considerations and potential for rockweed restoration. *Ecosphere.* 14, e4411. doi: 10.1002/ecs2.4411

Wikstrom, S. A., and Kautsky, L. (2007). Structure and diversity of invertebrate communities in the presence and absence of canopy-forming *Fucus vesiculosus* in the Baltic Sea. *Estuarine Coast. Shelf Science.* 72, 168–176. doi: 10.1016/j.ecss.2006.10.009

frontiers | Frontiers in Marine Science

TYPE Original Research
PUBLISHED 20 December 2023
DOI 10.3389/fmars.2023.1305763

OPEN ACCESS

EDITED BY
Tian Xie,
Beijing Normal University, China

REVIEWED BY
Vera G. Fonseca,
Fisheries and Aquaculture Science (CEFAS), United Kingdom
Siyuan Yang,
Beijing Institute of Applied Meteorology, China

*CORRESPONDENCE
Yan Xu
grawain007@163.com
Jie Zhu
zhujie03@caas.cn

RECEIVED 02 October 2023
ACCEPTED 04 December 2023
PUBLISHED 20 December 2023

CITATION
Xu Y, Huang F, Zhou M, Gu R, Zhu J, Rong Q and Cai Y (2023) Recognizing topological attributes and spatiotemporal patterns in spotted seals (*Phoca largha*) trophic networks based on eDNA metabarcoding. *Front. Mar. Sci.* 10:1305763. doi: 10.3389/fmars.2023.1305763

Recognizing topological attributes and spatiotemporal patterns in spotted seals (*Phoca largha*) trophic networks based on eDNA metabarcoding

Yan Xu[1]*, Fei Huang[1], Mingliang Zhou[1], Rui Gu[1], Jie Zhu[2]*, Qiangqiang Rong[3] and Yanpeng Cai[4]

[1]College of Marine Science and Technology, China University of Geosciences, Wuhan, China, [2]Institute of Environment and Sustainable Development in Agriculture, Chinese Academy of Agricultural Sciences, Beijing, China, [3]Research Center for Eco-environmental Engineering, Dongguan University of Technology, Dongguan, China, [4]Guangdong Provincial Key Laboratory of Water Quality Improvement and Ecological Restoration for Watersheds, Institute of Environmental and Ecological Engineering, Guangdong University of Technology, Guangzhou, China

Spotted seals, a protected species, face multifaceted threats to their habitat, which in turn impact the closely associated trophic networks. These threats will lead to irreversible structural variations within the ecosystem. Therefore, investigating the topological variability of trophic networks in spotted seals is important. Applying environmental DNA methods, field sample collection was conducted in 2021 during both the sea fishing moratorium period and the fishing period to decode fish diversity. Assessing the current status of fish resources by using the multivariate statistics approach. Applying dietary information establishes the spotted seals' trophic network. Selecting 12 network indexes to analyze the spatiotemporal patterns of network topological attributes. As a result, about 51 families, and 76 genera species were identified. During the sea fishing moratorium and the fishing period, there are 12 and 18 different food resources available for spotted seals, respectively. The diversity index revealed that the FP had greater species richness and diversity than the SP. Comparatively, the Fishing period exhibited higher species richness and biodiversity, likely influenced by habitat heterogeneity and anthropogenic activities. Additionally, the topological features of networks reflected the high clustering coefficients (CC=0.35) and the proportion of omnivorous species (O≈60%), indicating that the network structure in this region tends to form higher trophic-level clustering patterns, which facilitate the formation of weaker interactions between clusters, enhancing the robustness of the network. The higher connectivity complexity index during the fishing period (SC=12.3) supported that the spotted seal's trophic network was relatively more stable in this period. Thus, during the fishing period, it is crucial to pay more attention to the intensity of human fishing on mid-to-high trophic-level omnivorous fish resources to ensure the sustainability of these potential food resources for spotted seals. This comprehensive study achieved three

key objectives: (a) utilizing eDNA to characterize fish diversity during distinct periods, (b) establishing trophic networks of spotted seals, and (c) discerning topological attributes and spatiotemporal patterns within the ecological network. Overall, this study can provide technical and data support for integrated ecological network management and propose suggestions for protecting and recovering spotted seals.

KEYWORDS

eDNA metabarcoding, spotted seals, trophic network, biodiversity, ecological network analysis, Liaodong bay

1 Introduction

The spotted seal (Latin name: *Phoca largha*), a marine pinniped mammal belonging to the *Phocidae* family, primarily preying on fish, inhabits mid to high-latitude nearshore regions of the North Pacific (Lowry et al., 2000). Since the 16th century, extensive human hunting activities have pushed it to the brink of extinction. Despite conservation efforts, such as the implementation of CITES (Convention on International Trade in Endangered Species of Wild Fauna and Flora) in 1975 (Huxley, 2013), which effectively curbed hunting and contributed to population recovery, and being elevated to first-class national protected species in China, the species still confronts multiple external disruptions (Hendrix et al., 2021). These external disturbances pose severe threats to its habitat and survival (Zhu et al., 2000). Research indicates that nearly 50% of marine species in high-latitude regions are on the brink of extinction (Karlson et al., 2020). First and foremost, the issue of ocean acidification resulting from climate change has led to a reduction in water pH, directly impacting foundational organisms in the marine food chain (i.e., phytoplankton and zooplankton), and subsequently affecting other spotted seal prey resources through trophic cascades (Fassbender et al., 2017; Guzzo et al., 2017). Furthermore, the ongoing expansion of fishing activities not only results in accidental bycatch of spotted seals and habitat disruption but also impacts their foraging resources, diminishing the food resources availability, consequently causing irreversible alterations in the structure and functioning of the nutritional network (Farriols et al., 2016; Pires et al., 2016; D'Alessandro and Mariani, 2021). There is a high probability of inducing resource homogenization within the food web, significantly increasing the system's vulnerability and diminishing its stability (Xu et al., 2023). Therefore, the conservation and attention to the spotted seal are urgently needed.

Being regarded as top predators, spotted seals play a pivotal and intricate ecological role within food webs (Albouy et al., 2017). Ecosystems facilitate the flow of energy, information transmission, and material cycling through food webs (Trussell et al., 2006). Top predators, in turn, regulate the population of lower-level prey, influencing the flow of material energy within the food web (Danger et al., 2022). This contributes to maintaining material energy balance within ecosystems. Through these trophic cascades, top-down effects prevent overpopulation of prey and excessive harm to primary producers. From an evolutionary perspective, top-level predators promote species' adaptive evolution within prey populations, as exemplified by the interaction between the Atlantic flounder and cod (Orio et al., 2020). In recent years, the role of top predators in food webs has garnered increasing attention from researchers (Avila et al., 2018). Some studies have suggested the use of the dynamics of top-level predators as one of the indicators for assessing the health of marine ecosystems (Bossart, 2011; Parsons et al., 2015). However, relying solely on population dynamics can be challenging in revealing the state of nutritional networks and interspecies interactions. Hence, network-based systematic analysis methods have emerged as a valuable tool (Brose and Dunne, 2009). Previous research has shown significant quantifiable functional relationships between the topological metrics of different nutritional networks and species richness (Riede et al., 2010; Marina et al., 2018). This relationship aids in identifying both local and overall system states. By quantifying the topological attributes of networks, it has been observed that nutritionally complex networks, such as the food web of Beagle Channel, exhibit less local stability (Rodriguez et al., 2022). It is contributes to verify the diversity-stability debate in ecosystems (McCann, 2000; Bascompte, 2009). Therefore, studying the spatiotemporal patterns of diversity and topological attributes within the trophic network of spotted seals can serve as a reflection of the ecosystem state characteristics. It also provides valuable data support and theoretical guidance for the development of system-based marine biodiversity conservation and management strategies.

The objective of this study is to identify the spatiotemporal patterns of diversity and topological attributes within the trophic network of spotted seals (*Phoca largha*) and quantify the network state. We selected 6 typical spotted seal habitats considered as our study area, located in Liaodong Bay, China. Applying environmental DNA (eDNA) methods, field sample collection was conducted in 2021 during both the sea fishing moratorium period (SP) and the fishing period (FP), with the collection of three

samples from different locations surrounding each habitat. In total, 36 samples and part of the biological samples were collected. Fish diversity was decoded through PCR amplification and high-throughput sequencing techniques. Calculating biodiversity in the study area and assessing the current status of fish resources by using the PCA approach. Additionally, dietary information for species was obtained through database research and stomach content analysis, enabling the construction of the spotted seal's nutritional network. 12 network topological metrics were selected to analyze the spatiotemporal patterns of network topological attributes. This study enhanced the traditional method in terms of (a) characterizing fish diversity during different periods using eDNA, (b) establishing the high-resolution nutritional network of spotted seals, and (c) discerning the topological attributes and spatiotemporal patterns within the ecological network. The above improvements have overcome the shortcomings of time-consuming, cumbersome and costly sampling faced by traditional sampling.At the same time, Edna has less wear and tear on the collected samples, making it suitable for long-term monitoring.Overall, this research can provide technical and data support for integrated ecological network management and propose recommendations for the conservation and recovery of spotted seals.

2 Materials and methods

2.1 Sampling sites and collections

The Liaodong Bay spotted seal (hereinafter referred to as the "spotted seal"), also known as the Western Pacific spotted seal, is a species that migrates to the Bohai Sea and Liaodong Bay region of China (Han, 2009). It is the only marine pinniped species that breeds in China. Each year (Zhuang et al., 2023). During the winter and spring seasons, the spotted seals migrate to the Liaodong Bay region for overwintering and breeding (Barman et al., 2020). The region has several habitats that support spotted seal populations, with larger populations found in areas like Panjin and Lvshun (Zhuang et al., 2023).

In this study, we employed environmental eDNA technology to monitor fish resource diversity (Kda et al., 2015; Yates et al., 2021). Compared to traditional taxonomic identification-based monitoring methods, the eDNA approach offers advantages such as high sensitivity and detection rates (Yang et al., 2021). Additionally, for endangered species like the spotted seal, the eDNA method reduces the risk associated with lethal biological sampling (Rourke et al., 2022).

According to the migration route and main habitats of spotted seals, six sampling areas (P1: Lvshun nearshore, P2: Fuzhou River estuary, P3: Daliao River estuary, P4: Liao River estuary, P5: Xiaoling River estuary, P6: Penglai nearshore) were designated for this study, as shown in Figure 1. A total of 36 samples were collected from May to June (the sea fishing moratorium period, SP) and September to October (the fishing period, FP) in 2021, with the collection of three samples from different locations surrounding each habitat. Surface environmental water samples (5L per sample) were collected at each sampling area using a water collector. Prior to each sample collection, the water collector was washed with surface water three times. The collected water was then poured into a clean wide-mouth bottle and immediately stored in a vehicle refrigerator at a low temperature (Qu et al., 2020).

To prevent contamination by exogenous eDNA, the following measures were taken: (1) All water bottles and filtration devices were cleaned with a 10% bleach solution between each sampling

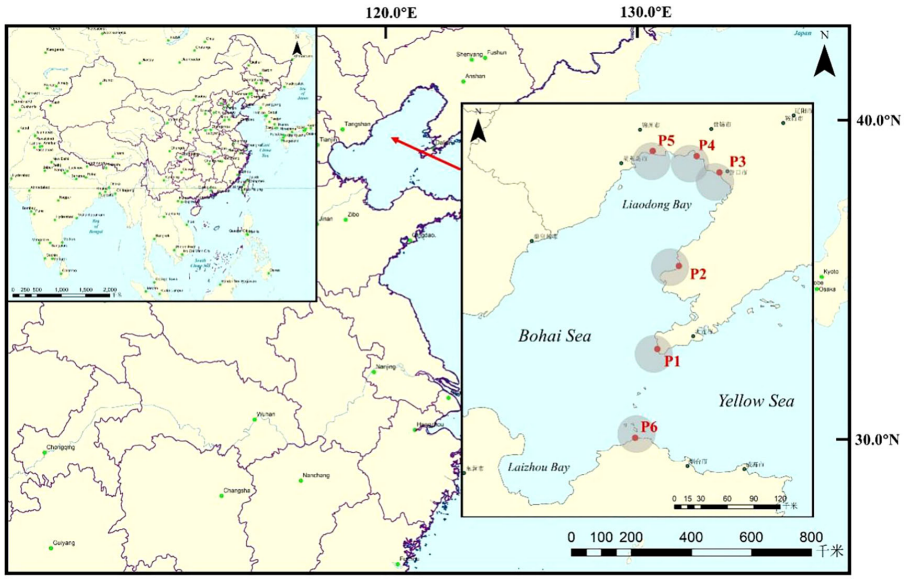

FIGURE 1
The location of the study area and distribution of sampling regions, Bohai Bay, China. (P1: Lvshun, P2: Fuzhou River, P3: Daliao River, P4: Liao River, P5: Xiaoling River, P6: Penglai).

(DiBattista et al., 2017); (2) Researchers changed disposable gloves between different samples during the collection process; (3) A negative control was included in all sampling areas, using 3L of deionized water as the sample. Within 24 hours after sampling, eDNA was enriched on a filter membrane with a pore size of 0.45μm using a vacuum pressure pump (Liu et al., 2021). After filtration, the filter membrane of each sample was carefully folded inward with tweezers, placed in a 50ml centrifuge tube, labeled, and stored in separate plastic bags at -20°C until eDNA extraction. The geographic coordinates of each sampling area were recorded using a handheld GPS device, and water quality parameters such as total dissolved solids (TDS), oxidation-reduction potential (ORP), salinity (S), pH, temperature (T), and dissolved oxygen concentration (O) were measured using a HQ30d portable water quality tester for subsequent analysis and research.

2.2 DNA extraction and PCR amplification

Total DNA in the sample was extracted using the FastDNA® Spin Kit for Soil (MP Biomedicals) extraction kit. DNA extracts were validated on 1% agarose gel and DNA concentration and purity were determined using a NanoDrop 2000 UV-vis spectrophotometer. ABI GeneAmp® 9700 PCR thermocycler using primers MiFish - U - F(5'- GTCGGTAAAACT CGTGCCAGC - 3') and MiFish - U- R (5'- CATAGTGGGGTA TCTAATCCCAGTTTG - 3) PCR amplification was carried out on the variable region. The reaction system is 5×FastPfu Buffer 4μL, 2.5mM dNTPs 2μL, forward primer (5μM) 0.8μL, reverse primer (5μM) 0.8μL, TransStart FastPfu DNA polymerase 0.4μL, BSA 0.4μL, 10ng template DNA supplemented with ddH2O to 20μL. The reaction parameters were as follows: initial denaturation at 95 °C for 5 min, denaturation at 94 °C for the 30s, annealing at 51 °C for 30s, extension at 72 °C for 32 times, then stable extension at 72 °C for 18 min, and finally preservation at 10 °C. There were 3 replicates per sample, and the products of the 3 replicates were mixed. PCR products were extracted from 2% agarose gel and purified using the AxyPrep DNA Gel Extraction Kit. The recovered products were quantified by Quantus™ Fluorometer.

2.3 High throughput sequencing and species annotation

We further sent the samples to Majorbio Bio-Pharm Technology Co. Ltd. (Shanghai, China) for high-throughput sequencing. We used an Illumina MiSeq PE300 platform/ NovaSeq PE250 platform and pool purified amplicons in an equimolar fashion and sequenced them paired-end. We used FASTP version 0.20.0 (Chen et al., 2018) (https://github.com/OpenGene/fastp) to control the original sequencing sequences quality; used FLASH version 1.2.7 (Magoc and Salzberg, 2011) (http://www.cbcb.umd.edu/software/flash) for assembling; used UPARSE version 7.1 (Edgar, 2013) (http://drive5.com/uparse) to perform OTU clustering of sequences according to 97% similarity and eliminate chimeras. There were 3 parallel samples in each sampling area. In the statistical process, the three sequence results of a sampling area are added together, and the total sequence value obtained is taken as the final sequence result of the sampling area. The subsequent analysis is based on this value. Species classification annotation was performed for each sequence using RDP Classifier version 2.2 (Wang et al., 2007) (http://rdp.cme.msu.edu). Subsequently, referring to the Fishbase database (https://www.fishbase.se) and the related literature (Liu, 2019) to record and refer to relevant historical documents, further annotate the fish data, screen and improve the taxonomic information of fish, and finally sort out and obtain the list of fish resources in the habitat of spotted seals in Liaodong Bay.

2.4 Statistical analyses

Since there are some sequences in the collected samples that do not match the sequences in the library, we need to eliminate them and calculate the percentage of valid sequences out of the total sequences. Here, we calculated the percentage of each fish's effective sequences in each sample, and the histogram of fish composition at each sampling region was drawn. We calculated Alpha diversity such as Richness, Chao1 index, ACE index, Shannon index, Pielou index, Invisimpson index, and Coverage index to assess and evaluate the degree of fish diversity at various sampling sites. See Appendix A1 for the exact calculation formula. These indexes reflected community richness, diversity, and community coverage, respectively. Additionally, based on the corresponding abundance data of OTU in each sample, this study estimated the Bray-Curtis distance to explore community composition difference and similarities between various groups of collections, calculated and mapped the principal coordinates PCOA (Principal Co-ordinates Analysis). Besides, this study calculated t-test to recognize the similarity between communities in different regions. RDA (Redundancy analysis) was used to explore the primary environmental elements influencing where fish communities are found. All analyses were performed and visualized on the Excel, Origin, and Tutools platform (https://www.cloudtutu.com). In addition, the dominance index (Y) of the fish community in two periods was calculated by the dominance formula (Yang et al., 2022), the equation as follow:

$$Y = \frac{T_i}{T} \times \frac{n_i}{N} \quad (1)$$

where T_i is the number of sample points where the fish i appears; T is the total number of sample points; n_i is the sequence abundance of the fish i; N is the total sequence abundance.

2.5 Biological network

2.5.1 Establishing trophic network

We established trophic networks by analyzing eDNA metabarcoding data obtained from our sampling. To achieve a high-resolution feeding web for spotted seals, we refrained from species aggregation. To identify consumer-resource interactions, we conducted

a comprehensive literature review using various web databases including Web of Science (https://www.webofscience.com) and Google Scholar (https://scholar.google.com). We identified 52 scientific papers that provided trophic interaction information at the species level. During the sampling process, we collected a subset of biological samples and conducted stomach content analysis using traditional microscopic examination methods. To address concerns about the limitations of our sampling data, we supplemented our findings with stomach content data referenced from relevant literature. Furthermore, additional feeding data were sourced from the World Fish Database website (www.fishbase.de). After sorting out data, we revealed that the diet of spotted seals in the region consisted of 19 fish species belonging to 4 orders, 7 families, and 15 genera (Supplementary Table S1).

Next, we categorized all the data, with species data serving as nodes and trophic relationships as links. We constructed a trophic network determined by an interaction adjacency matrix consisting of S rows and S columns, where S represents the total number of species and taxa involved in the study, and the order of species among rows corresponds to that among columns. The value at the intersection of the ith row and jth column in the food web matrix is either 0 or 1, denoted as a_{ij}, indicating whether species j preys on species i, where a_{ij}=0 signifies the absence of a feeding relationship between i and j. From this matrix, a directed graph with L trophic links connecting S nodes can be derived, and visualized graphs by Cytoscape (version 3.9.1) (Shannon et al., 2003).

To analyze highly connected clusters of interaction networks in the constructed food web, we utilized the program 'Molecular Complex Detection' (MCODE) (Liu et al., 2017). MCODE is a graph-theory-based clustering algorithm that employs the vertex-weighting method to filter out regions of high density by using the density of a map as a weighting factor. This algorithm is commonly used to identify large molecular complexes within protein structures (Nomura et al., 2021). In the graph G=(V, E), |V| represents the number of nodes in the graph, and |E| represents the weight of the interacting connected edges. The network consists of |V| nodes, and the maximum weight of |E| is defined as:

$$|E|_{max} = \frac{|V|(|V|+1)}{2} \tag{2}$$

The density of the graph is defined as follows:

$$DG = \frac{|E|}{|E|_{max}} \tag{3}$$

MCODE efficiently identifies sections of interaction networks that are highly linked based solely on connectivity data (Bader and Hogue, 2003) to find highly interconnected areas, which reflect the density of nodes and surrounding nodes with the score value of nodes. Besides, we selected the high-score value sub-network and considered it as the stable core sub-network in a food web.

2.5.2 Topological network analysis

To describe the complexity and structural characteristics of a food web (Rodriguez et al., 2022; Cordone et al., 2020), we chose the following 12 topological indexes:

(1) Species (S): total number of species and groups;

(2) Links (L): total number of interactions or nutritional linkages;

(3) Linkage density (D): the number of interactions for each species;

$$D = \frac{L}{S} \tag{4}$$

(4) Connectance (C): connectivity or trophic links divided by the total number of possible interactions;

$$C = \frac{L}{S^2} \tag{5}$$

(5) Percentage of top species (T): percentage of species with prey but without predators;

$$T = \frac{S_T}{S} \times 100\,\% \tag{6}$$

Where S_T is the number of top species;

(6) Percentage of intermediate species (I): percentage of species with prey and predators;

$$I = \frac{S_I}{S} \times 100\,\% \tag{7}$$

Where S_I is the number of intermediate species;

(7) Percentage of basal species (B): percentage of species with predators but without prey;

$$B = \frac{S_B}{S} \times 100\,\% \tag{8}$$

Where $S_B$is the number of basal species;

(8) Percentage of omnivorous species (O): percentage of species that eat prey from more than one trophic level;

$$O = \frac{S_0}{S} \times 100\,\% \tag{9}$$

Where S_O is the number of omnivorous species;

(9) Mean trophic level (MTL): weighted average of trophic levels for all species;

$$T_{TL_j} = 1 + \sum_{i=1}^{S} l_{ij} \frac{T_{TL_i}}{n_j} \tag{10}$$

$$MTL = \frac{\sum_{i=1}^{S} T_{TL_i}}{S} \tag{11}$$

Where T_{TL_j} and T_{TL_i} represent the trophic levels of species j and i; for column j and row i, l_{ij} is the connection matrix of row S and column S. If species j prey on species i, l_{ij}= 1; If species j do not prey on species i, l_{ij}= 0; n_j is the number of species j capture food species;

(10) Connection complexity index (SC): describing food web stability;

$$SC = S \times \frac{2L}{S^2 - S} \tag{12}$$

(11) Characteristic path length (ChPath): the average shortest path length between all species pairs;

$$ChPath = \frac{2}{S(S-1)}\sum_{i=1}^{S}\sum_{j=1}^{S}ChPat_{min}(i,j) \quad (13)$$

(12) Clustering coefficient (CC): the average number of species pairs connected to the same species and to each other to describe the clustering coefficient of species nodes in the food web.

$$CC_i = \frac{2E_i}{K_i(K_i-1)} \quad (14)$$

$$CC = \frac{1}{S}\sum_{i=1}^{S}CC_i \quad (15)$$

Where K_i represents all the edges connecting node i to other K_i nodes, if all K_i are neighbors, the maximum is $K_i(K_i-1)$, E_i represents the actual number of neighbors.

3 Results

3.1 Species diversity

3.1.1 Fish species composition monitored by eDNA

In this study, 85 fish species from 16 orders, 51 families, and 76 genera were identified by eDNA metabarcoding (Supplementary Table S2). The total number of species detected in different sampling regions in the two periods is shown in Figure 2. It was found that more fish species were monitored in the FP than in the SP.

From Figure 3A, 54 fish species were present throughout the SP, and they belonged to 51 genera, 36 families, and 11 orders. *Perciformes* (25 species) comprised around 46.3% of all fish species on the level of order, followed by *Scorpaeniformes* (7 species), which accounted for roughly 13% of the species richness. While other families were discovered with fewer species, *Engraulidae* and *Carangidae* had 4 species (7.4%) found on the family level. According to Table 1, the top 15 species represented 95.11% of all sequences and had the highest relative abundance. *Trichiurus lepturus*, which made up 45.43% of the series in the SP, was the most frequently observed species, followed by *Protosalanx chinensis* (15.49%) and *Remorina albescens* (8.67%).

From Figure 3B, the biodiversity was higher during the FP when 74 species, 68 genera, 49 families, and 17 orders were detected. On order level, 33 species from *Perciformes* were identified, occupying 44.6% of the total species richness, followed by 8 species (10.8%) from *Clupeiformes*. On the family level, *Gobiidae* and *Engraulidae* each had 6 species (8.1%), while the remaining families had fewer species (1-3). Table 1 showed that the top 15 species' relative abundance accounted for 93.03% of total sequences. *Trichiurus lepturus* (37.11%) still had the highest relative abundance in the environment, 19.27% and 7.81% of sequences were identified as *Engraulis japonicus* and *Seriola lalandi*.

According to Equation 1, the index of dominant species Y was used to identify the predominant fish species communities during the two time periods, the results (Y>0.2) are shown in Table 2. During the SP, we regarded 5 species as dominant species, the top 3 species were *Trichiurus lepturus*, *Protosalanx chinensis*, and *Remorina albescens*, respectively. There were 8 dominant species

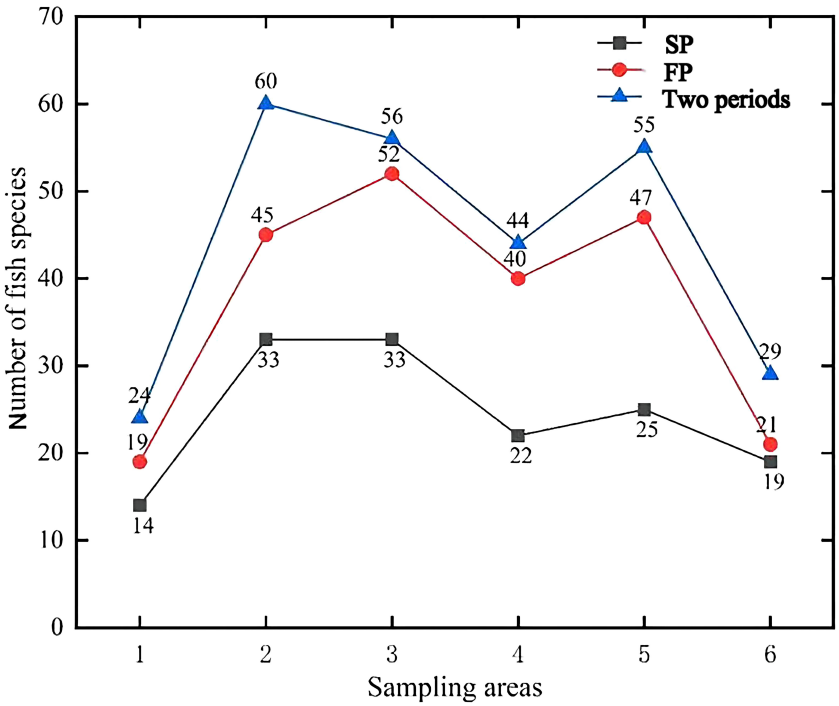

FIGURE 2
The species line chart for the number of fish species detected by eDNA metabarcoding in different sampling areas in the two periods. (1: Lvshun nearshore, 2: Fuzhou River estuary, 3: Daliao River estuary, 4: Liao River estuary, 5: Xiaoling River estuary, 6: Penglai nearshore).

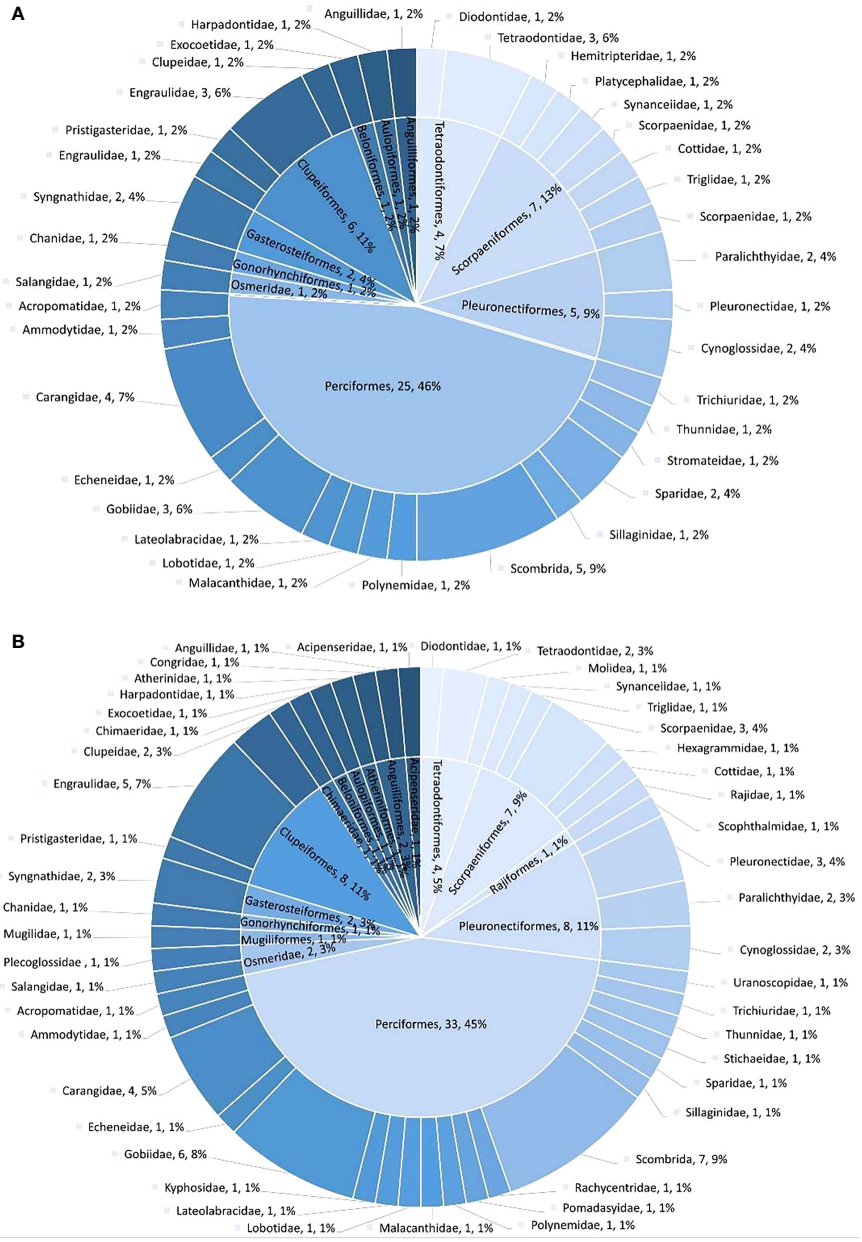

FIGURE 3
The number and proportion at the taxonomic level of order and family in two periods: **(A)** SP; **(B)** FP.

found in the FP, and *Trichiurus lepturus*, *Engraulis japonicus*, and *Seriola lalandi* outcompeted other species. Moreover, we found that 3 species were dominant in both periods: *Protosalanx chinensis*, *Coilia mystus*, and *Seriola lalandi*.

3.1.2 Spatial and temporal patterns of fish biodiversity

A total of 43 (50.59%) species were found through both two periods, while 11 (12.94%) and 31 (36.47%) species were detected in the SP and the FP, respectively (Figure 4A). Besides, we found 5 fish species in all samples: *Coilia mystus*, *Protosalanx chinensis*, *Seriola lalandi*, *Trichiurus lepturus*, and *Scomber japonicu* (Figure 4B). The sequence of the fish species abundance in the top five were *Trichiurus lepturus*, *Engraulis japonicus*, *Protosalanx chinensis*, *Seriola lalandi*, *Coilia mystus*. In particular, the amounts of their sequences showed spatial and temporal differences (Figure 4C).

Alpha diversity of the fish community was compared between the SP and the FP. All samples' coverage ranged from 0.988-0.999 (Supplementary Table S3), demonstrating that sequencing covered all species so that the results could reflect the actual community. Chao1 ranged from 14 to 54.17, while ACE ranged from 14 to 55.81. These two indices showed a similar trend. The results of Shannon's (0.36-2.57) and Simpson's range (0.12-0.89) also show a resemblance. The highest species richness was found in the

TABLE 1 The top 15 fish in the percentage of abundance in the Sealing period and the Fishing period, respectively.

	No.	Scientific Name	Order level	Abb	Percentage of abundance	Occurrence rate
Sealing period	1	*Trichiurus lepturus*	Perciformes	Trle	45.43%	100%
	2	*Protosalanx chinensis*	Osmeridae	Prch	15.49%	100%
	3	*Remorina albescens*	Perciformes	Real	8.67%	50%
	4	*Acanthogobius hasta*	Perciformes	Acha	5.21%	33%
	5	*Coilia mystus*	Clupeiformes	Comy	3.98%	100%
	6	*Seriola lalandi*	Perciformes	Sela	3.38%	100%
	7	*Johnius belangerii*	Perciformes	Jobe	2.29%	50%
	8	*Seriola dumerili*	Perciformes	Sedu	1.85%	83%
	9	*Scomberomorus niphonius*	Perciformes	Scni	1.67%	67%
	10	*Parastromateus niger*	Perciformes	Pani	1.64%	67%
	11	*Engraulis japonicus*	Clupeiformes	Enja	1.40%	67%
	12	*Takifugu rubripes*	Tetraodontiformes	Taru	1.28%	50%
	13	*Scomber japonicus*	Perciformes	Scja	1.25%	100%
	14	*Sillago sihama*	Perciformes	Sisi	0.86%	67%
	15	*Konosirus punctatus*	Clupeiformes	Kopu	0.72%	83%
Fishing period	1	*Trichiurus lepturus*	Trichiuridae	Trle	37.11%	100%
	2	*Engraulis japonicus*	Engraulidae	Enja	19.27%	83%
	3	*Seriola lalandi*	Carangidae	Sela	7.81%	100%
	4	*Coilia mystus*	Engraulidae	Comy	6.98%	100%
	5	*Sillago sihama*	Sillaginidae	Sisi	5.22%	100%
	6	*Nibea albiflora*	Sciaenidae	Nial	3.38%	83%
	7	*Protosalanx chinensis*	Salangidae	Prch	3.06%	100%
	8	*Konosirus punctatus*	Clupeidae	Kopu	2.54%	100%
	9	*Acanthogobius hasta*	Gobiidae	Acha	1.88%	100%
	10	*Johnius belangerii*	Sciaenidae	Jobe	1.75%	100%
	11	*Takifugu rubripes*	Tetraodontidae	Taru	1.10%	83%
	12	*Cheilopogon cyanopterus*	Exocoetidae	Chcy	0.84%	100%
	13	*Remorina albescens*	Echeneidae	Real	0.79%	83%
	14	*Anguilla japonica*	Anguillidae	Anja	0.70%	67%
	15	*Hippocampus coronatus*	Syngnathidae	Hico	0.59%	83%

Abb refers to the abbreviation of the Scientific Name; Percentage of abundance refers to the proportion of sequence abundance; Occurrence rate refers to the frequencies of fish detected in the six sampling regions.

Daliao River estuary (52) in the FP, and the lowest in Lvshun nearshore (14) in the SP. The t-test results of diversity are shown in Supplementary Table S4. Overall, different samples, including 6 indexes, Richness, Shannon, Simpson, Pielou, Invsimpson, and Coverage, showed no significant differences ($p>0.05$). It means there is no difference between samples for all of them, showing consistency. However, there is a significant value for Chao1 and ACE indexes in the samples ($p<0.05$). For these two indexes, the average value of the FP was higher than that of the SP. These findings showed that there were more species overall during the FP than during the SP, indicating a higher level of community variety during the FP.

Based on all sampling sites' sequence abundance, the Bray standardized similarity coefficient matrix Bray-Curtis distance was used for PCoA analysis to compare similarity and differentiation within samples. Bray standardized similarity refers to the application of the Bray-Curtis distance metric to assess the similarity and differentiation within samples based on the

TABLE 2 Dominance index of dominant species in two periods.

Sealing period		Fishing period	
Scientific Name	Dominance index(Y)	Scientific Name	Dominance index(Y)
Trichiurus lepturus	0.4534	*Trichiurus lepturus*	0.37111
Protosalanx chinensis	0.1546	*Engraulis japonicus*	0.16060
Remorina albescens	0.0432	*Seriola lalandi*	0.07806
Coilia mystus	0.0397	*Coilia mystus*	0.06978
Seriola lalandi	0.0338	*Sillago sihama*	0.04353
		Protosalanx chinensis	0.03063
		Nibea albiflora	0.02815
		Konosirus punctatus	0.02541

abundance of sequences across various sampling sites. It's a way to measure how samples compare to each other in terms of their composition. The result shows that two principal coordinates explained 52.39% of the differentiation, and some separate trends can be found between the two periods (Figure 5A). The results showed that the sampling regions were more dispersed during the SP, indicating that the species differences within the community were large. The opposite is true for the sampled data during FP.For almost all sampling areas, some distance also can be found between the two periods, reflecting seasonal differences in species composition. However, SP1 (Lvshun nearshore in the SP) and FP1 (Lvshun nearshore in the FP) were close in the PCoA analysis, indicating that the composition of fish species in P1 (Lvshun nearshore) was similar in the two periods.

Differences in the regional and temporal distributions of the species were shown by the heatmap of their relative sequencing abundances (Figure 6A). Briefly, the composition of the community differed among samples. *Trichiurus lepturus* and *Engraulis japonicus* had the highest relative abundance and most extensive distribution, whereas *Cynoglossus graciliss*, *Larimichthys polyactis*, and *Collichthys niveatus* distributed narrower. Each sampling site had some specialists, for example, *Rachycentron canadum* (Raca) only appeared in FP1(Lvshun nearshore), and *Acanthogobius hasta* (Acha) had a higher abundance in SP4 (Liao river estuary) compared to other samples.

The diagram based on sequence abundance showed the distribution of fish species is similar at some sites with actual differences (Figure 6B). In Lvshun nearshore (P1), high similarity fish compositions that *Trichiurus lepturus* dominated, as same as the trend reflected by the results of PCoA analysis. However, the Daliao River estuary (P3) showed a considerable discrepancy compared to Lvshun nearshore, *Protosalanx chinensis* (Prch) and *Remorina albescents* (Real) were the dominant species during the SP, which switched to *Trichiurus lepturus* (Trle) and *Engraulis japonicus* (Enja) in the FP. Besides, *Protosalanx chinensis* (Prch) was the main species during the SP, while the FP showed high diversity in Xiaoling River estuary (P5).

3.1.3 Relationship of fish diversity with environmental factors

In this study, 8 different environmental factors were collected, such as total dissolved soil (TDS), the potential of hydrogen (pH), oxidation-reduction potential (ORP), salinity (S), dissolved oxygen (DO), conductivity (C), dissolved oxygen saturation (O) and temperature (T). The measurement results of environmental factors are shown in Supplementary Table S5. The water temperature in each area ranges from 23.6-26.8 °C with an average value of 25.52 °C during the SP and ranges from 18.9°C to 23.6 °C with an average value of 21.73 °C during the FP. The comparison of environmental factor t-test results (mean ± standard deviation) between sampling areas is shown in Supplementary Table S6. It can be seen from the test results that the average values of TDS, S, C, and O in the SP are higher than those in the FP, but ORP, pH, and DO are opposites. The two periods had no significant difference in the above environmental factors. Still, the water was substantially warmer during the SP than it was during the FP ($p<0.01$).

Using data from the top 8 abundant species found in the two periods and the set of five environmental parameters, RDA analysis was used to highlight the correlations between the environmental factors and the fish species. From Figure 5B, the two RDA axes can explain 39.07% of the structural differences. By studying this figure, it can be found that the samples in the SP and the FP show high dispersion, and there is no consistent relationship between environmental conditions and species distribution. The first-ranking axis and each of the five environmental factors were adversely connected, however, the second-ranking axis was positively correlated. DO has the longest ray arrow, the strongest correlation with the distribution of fish community, and the greatest influence on it, so it is the key environmental factor affecting fish assemblage. This axis is closely related to C, O, and TDS. Furthermore, DO has a strong negative correlation with samples in the FP, but a strong positive correlation with some sampled areas in the SP.

3.2 Trophic network of spotted seals

3.2.1 Network structure analyzing

As shown in Figure 7, the total food webs in the SP and the FP were respectively constructed. Through the food web structure chart, it was clear that the network structure of the FP was more complex than that of the SP, with a high number of connections between *Cephalopods* and fishes. During the SP period, the total number of nodes in the network was 68, with a total of 353 links. In the FP period, the total number of nodes increased to 88, with a total of 535 links. Among the detected fish species, spotted seals (*Phoca largha*) preyed on 12 species during the SP, constituting 17.64% of the total node count; and 18 species during the FP, accounting for 20.45% of the total node count. Among them, 11 species existed in both periods.

According to Equations 1, 2, we selected the sub-network with a high score value and considered it as the stable core sub-network in

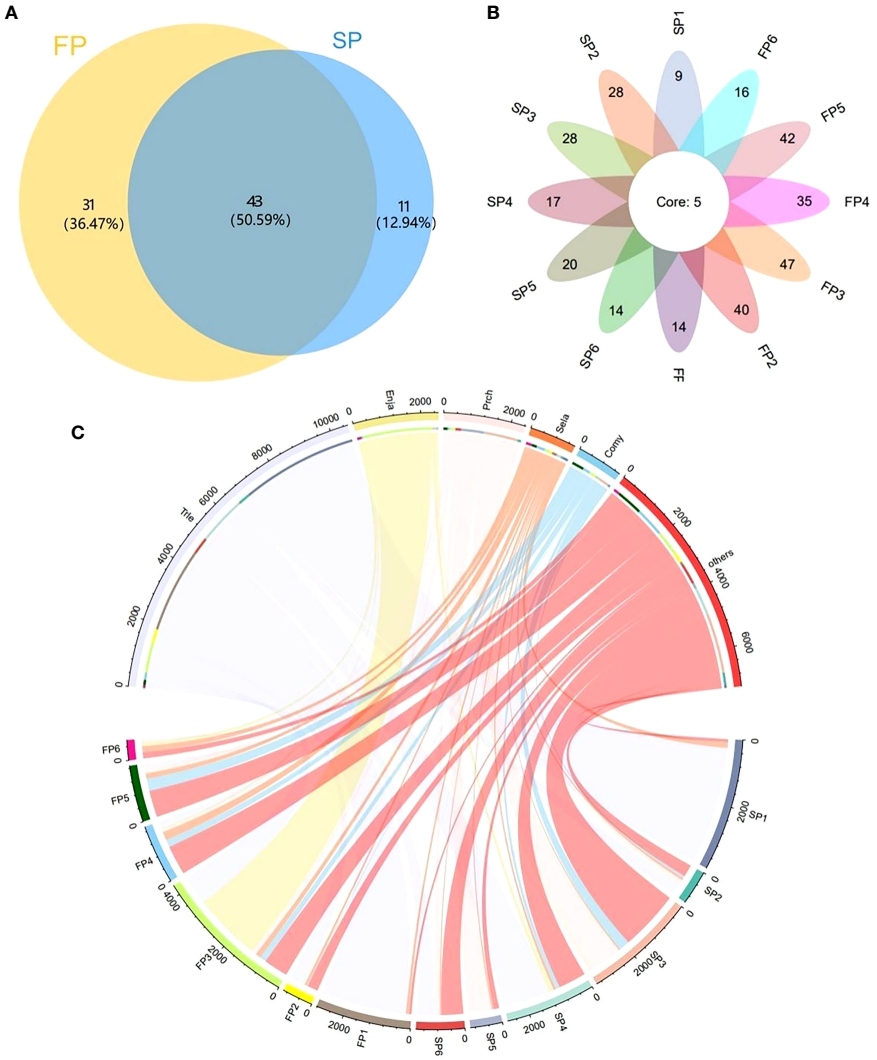

FIGURE 4
The number of fish species identified during the SP and the FP. **(A)** Venn diagrams of FP and SP; **(B)** Venn diagrams of points in both periods; **(C)** chord diagrams based on sequence abundance.

a food web from 12 food webs in two periods based on the use of the Cytoscape MCODE program (Figure 8). Through these sub-networks, we discovered that the core sub-network scores in the SP higher than these in the FP. Overall, based on the 12 food webs' partially stable structures, *Cephalopods* (Ceph) were identified as keystone species 3 times and *Coilia mystus* (Comy) two times, which were the species that *Phoca largha* preyed on. Spatially, Comy could be found in the stable structures from P1 and P6, while Ceph appeared in P5, these two species both play critical roles in P2 and P3. Whereas, P4 showed a fluctuation and caused no species could become the critical prey in the food web during two periods.

3.2.2 Topological network analysis

According to Equations 4–15, from Table 3, we detected the structural characteristics and complexity of the spotted seals' food webs. The food web in the SP contained 68 species, while 88 species during the FP. On the one hand, the number of links during the FP (L=535) is almost 1.5 times that of the SP (L=353), but the connectance of the former (C=0.076) is higher than that of the latter (C=0.069); On the other hand, the mean trophic level of the food web in the FP (MTL=3.00) was higher than that in the SP (MTL=2.92). It is worth noting that although the two food networks contain different numbers of species, the proportions of species assigned to the two food webs were very similar: top species (T%, 13% during the SP; 14% during the FP), intermediate species (I%, 83.8% the SP; 83.0% the FP), basal species (B%, 2.9% the SP; 2.3% the FP) and omnivorous species (O%, 58.8% the SP; 61.4% the FP). Intermediate species far outnumber top and basal species, meaning most species were both predators and prey. Besides, the network topological attributes: the characteristic path length (ChPath, 1.98 during the SP; 1.96 during the FP) and the clustering coefficient (CC, 0.345 during the SP; 0.352 during the FP) were similar.

Through t-test results of network parameters (Supplementary Table S7), we discovered that the number of food web nodes in two periods did not differ significantly (P=0.074). However, the mean number of nodes in the FP was higher (51.33 ± 13.98) than in the SP

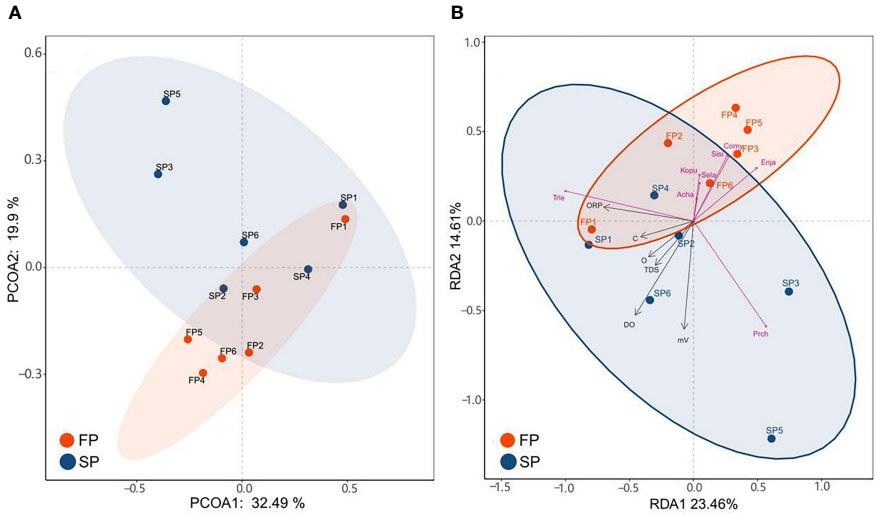

FIGURE 5
(A) The result of PCoA analysis shows the diversity of fish communities between the two periods. **(B)** The heatmap showed the relative abundance of fish species at each sampling region.

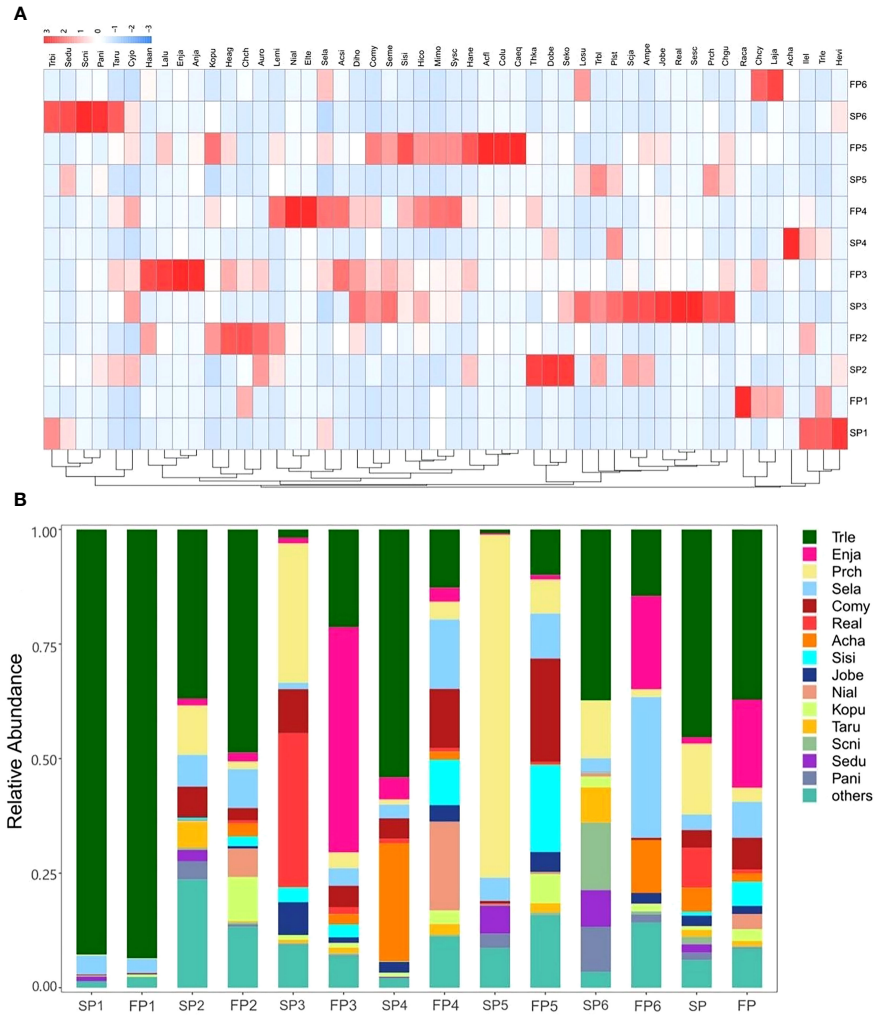

FIGURE 6
(A) The RDA diagram of the relationship between fish and six environmental factors for two periods. **(B)** The relative abundance (%) of fish species in different seasons detected in every sampling site.

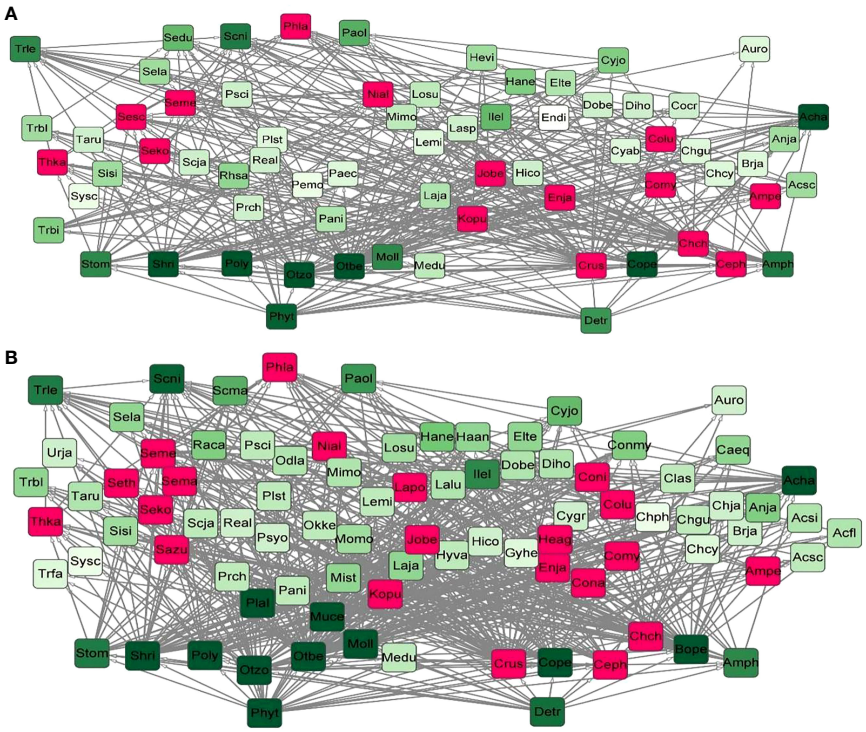

FIGURE 7
(A) The total food web in the SP. **(B)** The total food web in the FP. The darker the node color indicated the higher the degree value of species; red nodes represented the feeding species of spotted seals.

(38.33 ± 7.63). For the number of food web links (the distribution range was 100-335), there were noticeable temporal variations in the quantity of food web links (P=0.034), links found in the FP (267.00 ± 82.09) were significantly higher than that in the SP (169.33 ± 52.94).

The number of links generally increased as node counts climbed, except at Xiaoling River estuary (P5) where they declined during the FP. Similar to the number of links (P=0.034), the distinct link density characteristics (P=0.026) of food webs at different times also showed significant differences, ranging from 3.57 to 5.54. In comparison to the SP (4.34 ± 0.61), the mean number of food web links during the FP (5.15 ± 0.46) was higher. Although there was no statistically significant difference between the two periods (P=0.544), the distribution of food web connectance ranged from 0.072 to 0.136, with the lowest and highest values observed during the FP.

4 Discussion

In this study, we focused on the habitats of spotted seals (*Phoca largha*) in Liaodong Bay and analyzed fish biodiversity during the closed fishing season (SP, May to June) and the fishing season (FP, September to October) in 2021, based on 36 samples. The results revealed the identification of a total of 85 fish species, with 54 species detected during SP and 74 species during FP. The primary prey species targeted by spotted seals included 12 species during the SP period, constituting 17.64% of the total node count. In the FP period, they consumed 18 species, accounting for 20.45% of the total node count. Comparison with historical records (Cheng, 2004; Liu et al., 2015) showed minimal differences in dominant fish species in the study area, underscoring the utility of eDNA technology. Moreover, the number of fish species discovered during FP significantly exceeded that observed during SP, as reflected in the biodiversity analysis results. A previous study by Wang et al. (2021) had already confirmed the positive impact of the fishing prohibition policy on promoting the recovery of fish populations. Furthermore, variations in fish biodiversity may also be attributed to differences in the habitat heterogeneity of fish species or manifestations of spatial niche differentiation. Notably, Bray-Curtis similarity analysis results indicated significant differences in fish biodiversity between sampling points P1 (Lvshun nearshore) and P6 (Penglai nearshore), revealing that the estuarine habitat environments offer more diverse and stable food resources for spotted seals, Figure 6. In other words, the spatial distribution pattern of fish resources is determined by the long-term influences of habitat heterogeneity, to which spotted seals have adapted through their evolutionary history.

Based on fish resource data, a trophic network for spotted seals was established. We selected 12 network topological measures to analyze the spatiotemporal patterns of network topological properties, describing the complexity characteristics of the network structure. Comparing with network parameters of food webs in other regions (Supplementary Table S8), it was found that the average trophic level (MTL) and clustering coefficient (CC) in the Liaodong Bay nutritional network were both higher than 87.5%

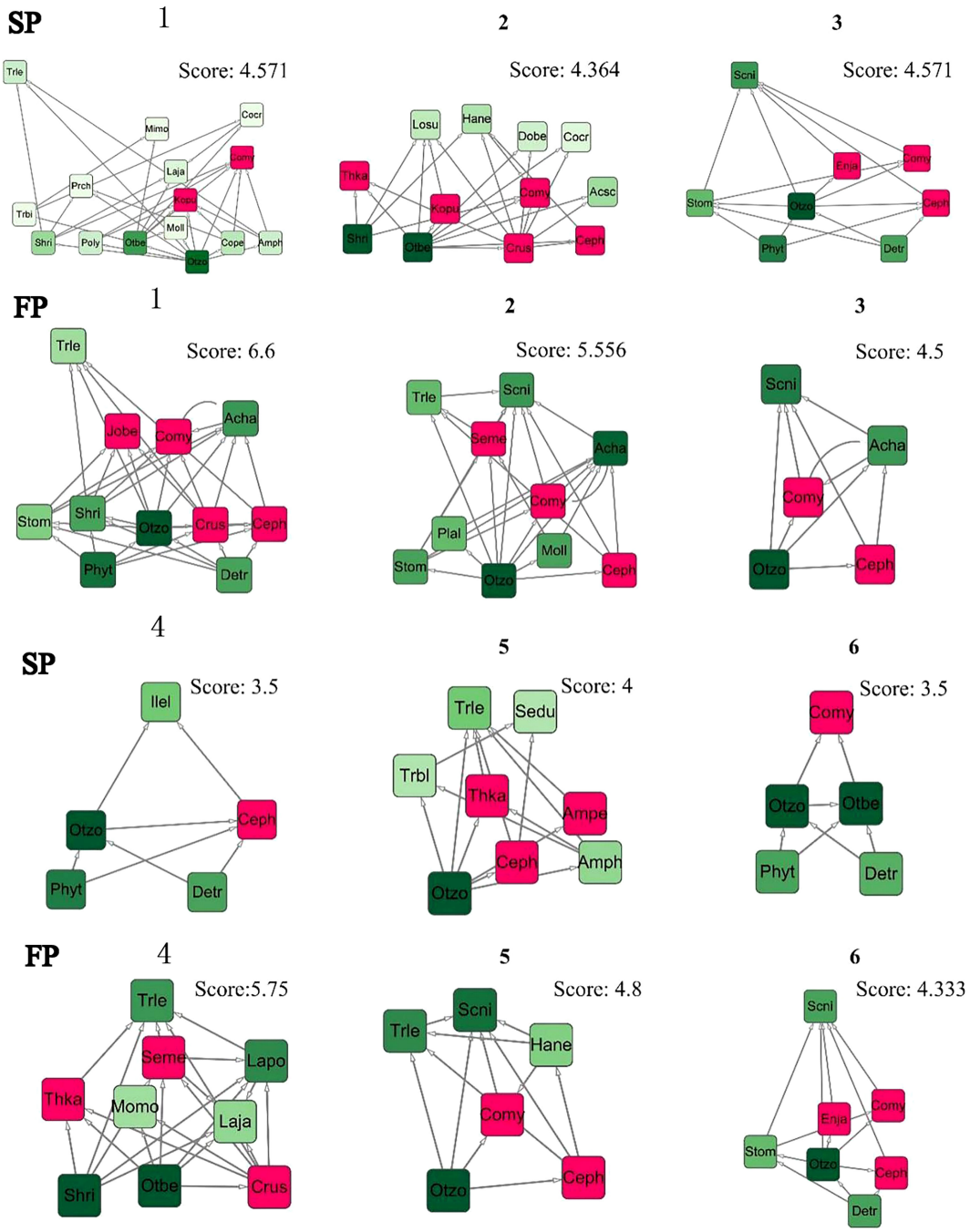

FIGURE 8
The core of stable sub-network selected with a high score value of the trophic network.

of other food webs. Additionally, the intermediate species ratio (I) was also relatively high (Supplementary Table S8). This indicates that the network structure in this region tends to form higher trophic-level clustering patterns, which facilitate the formation of weaker interactions between clusters, enhancing the robustness of the network. Furthermore, the proportion of omnivorous species (O) contributes to forming more links with limited nodes, increasing node degrees, and enhancing the topological importance of omnivorous nodes, which significantly benefits the stability of food webs (Norkko et al., 2007; Xu et al., 2020). Specifically, during both periods, the proportion of omnivorous species (O) reached approximately 60%, with slightly higher values during FP. Overall, the closure of fishing activities appears to have primarily contributed to the recovery of higher trophic-level omnivorous predators in the local fish resources (T increased by 1.6%), which largely fall within the prey category of spotted seals, promoting the complexity of the trophic network. This conclusion is supported by the significantly higher connectivity complexity index during FP (SC=12.3) compared to SP (SC=10.54). Previous studies have suggested that higher food web diversity leads to

TABLE 3 Network metric values in the Sealing period (SP) and the Fishing period (FP).

	S	L	D	C	T(%)	I(%)	B(%)	O(%)	MTL	SC	ChPath	CC
SP1	28	100	3.57	0.128	14.3	78.6	7.1	42.9	2.68	7.41	1.87	0.46
SP2	47	229	4.87	0.104	14.9	80.9	4.3	53.2	3.07	9.96	1.91	0.34
SP3	47	232	4.94	0.105	12.8	83.0	4.3	53.2	3.02	10.09	1.89	0.36
SP4	36	173	4.81	0.133	11.1	83.3	5.6	50.0	2.83	9.89	1.82	0.33
SP5	39	148	3.79	0.097	15.4	79.5	5.1	53.8	2.96	7.79	1.98	0.44
SP6	33	134	4.06	0.123	18.2	75.8	6.1	45.5	2.96	8.38	1.85	0.35
SP	68	353	5.19	0.076	13.2	83.8	2.9	58.8	3.23	10.54	1.98	0.35
FP1	33	148	4.48	0.136	15.2	78.8	6.1	42.4	2.74	9.25	1.82	0.34
FP2	59	329	5.58	0.095	11.9	84.7	3.4	61.0	3.08	11.34	1.90	0.34
FP3	66	313	4.74	0.072	15.2	81.8	3.0	59.1	3.20	9.63	1.99	0.37
FP4	54	299	5.54	0.103	16.7	79.6	3.7	59.3	3.09	11.28	1.88	0.39
FP5	61	335	5.49	0.090	9.8	86.9	3.3	57.4	3.10	11.17	1.93	0.38
FP6	35	178	5.09	0.145	14.3	80.0	5.7	48.6	2.80	10.47	1.77	0.36
FP	88	535	6.08	0.069	14.8	83.0	2.3	61.4	3.26	12.30	1.96	0.35

S is the total number of species and groups; L is the total number of interactions or nutritional linkages; D is the number of interactions for each species; C is the connectivity or trophic links divided by the total number of possible interactions; T denotes the percentage of top species; I denotes the percentage of intermediate species; B denotes the percentage of basal species; O denotes the percentage of omnivorous species; MTL represents the mean trophic level; SC represents the connection complexity index Price category of scientific species; ChPath represents the characteristic path length; CC represents the clustering coefficient.

greater stability (McCann, 2000), indicating that the spotted seal's trophic network is relatively more stable during FP.

We also found that the food web in Liaodong Bay has a longer characteristic path length compared to most food webs. This suggests that there are longer material energy flow paths and higher ecosystem assimilation efficiency. As a result, the food web has increased redundancy and resistance to disturbances (Marina et al., 2018). The structural analysis of sub-networks revealed that food resources related to spotted seals are often part of highly connected and hierarchical sub-net units, which consist of various omnivorous predators (Figure 8). These sub-net units tend to have higher stability scores. This could be attributed to the fact that species with numerous associations in the food web are linked to specific species, forming multiple interacting clusters (Delmas et al., 2019). In conclusion, our findings suggest that the sources of food for spotted seals in different seasons are not significantly affected by the current fishing ban policy. When winter arrives and spotted seals migrate to the Liaodong Bay area for overwintering and breeding, the network structure they form with local species remains relatively stable. This stability contributes to the recovery of the spotted seal population. However, during the fishing period (FP), it is crucial for the government and species conservation organizations to pay more attention to the intensity of human fishing on mid-to-high trophic-level omnivorous fish resources. This attention is necessary to ensure the sustainability of these potential food resources for spotted seals during the winter season.

In our study, we acknowledge several limitations. Firstly, the degradation process of eDNA can be influenced by various environmental factors, which may potentially affect the experimental results (Mauvisseau et al., 2022). Secondly, we encountered difficulties in identifying many detected sequence fragments through eDNA barcoding, possibly due to insufficient data in the genetic databases. Thirdly, we did not consider predation differences due to age structure, such as the fact that adults and juveniles often feed on different prey, which could impact the network topology. To address these limitations, our future plans include conducting long-term monitoring of the food web structure in Liaodong Bay and expanding the existing database. Additionally, we aim to investigate the effects of network structure variations on spotted seals. Furthermore, we intend to expand the ecological database through long-term field surveys.

5 Conclusion

In conclusion, we conducted in Liaodong Bay, China, using environmental DNA (eDNA) methods and high-throughput sequencing techniques revealed significant findings about the spotted seal habitats and their associated fish diversity.

(a) We identified 85 fish species in total, with Perciformes dominating at 46%. During the sea fishing moratorium period (SP), 54 species were identified, while the fishing period (FP) recorded 74 species, indicating higher species richness in FP across all sampling areas.

(b) The study also constructed and analyzed spotted seals trophic networks, highlighting a more complex structure during

FP with increased connections between Cephalopods and fishes. Phoca largha preyed on 12 species during SP and 18 species during FP. The network analysis indicated high clustering coefficients for both periods, suggesting the formation of higher trophic-level clustering patterns, enhancing network robustness. The proportion of omnivorous species (O=60%) contributed to increased stability by forming more links with limited nodes.

(c) Structural analysis of sub-networks revealed that food resources related to spotted seals were part of highly connected and hierarchical sub-net units, consisting of various omnivorous predators. The study emphasized that the spotted seal's trophic network is relatively more stable during FP, supported by a significantly higher connectivity complexity index. The conclusion emphasized the importance of attention to human fishing intensity on mid-to-high trophic-level omnivorous fish resources during FP for the sustainability of spotted seals' winter food sources. Overall, the research provides valuable insights for integrated ecological network management and suggestions for the protection and recovery of spotted seals.

Data availability statement

The original contributions presented in the study are publicly available. The Coastal eDNA Genome sequencing can be found here: NCBI with Accession: PRJNA1026063, https://www.ncbi.nlm.nih.gov/bioproject/PRJNA1026063.

Author contributions

YX: Conceptualization, Funding acquisition, Investigation, Methodology, Project administration, Supervision, Writing – original draft, Writing – review & editing. FH: Formal Analysis, Investigation, Methodology, Software, Writing – original draft. MZ: Investigation, Visualization, Writing – review & editing. RG: Writing – review & editing. JZ: Funding acquisition, Project administration, Supervision, Writing – review & editing. QR: Resources, Validation, Writing – review & editing. YC: Supervision, Writing – review & editing.

Funding

The author(s) declare financial support was received for the research, authorship, and/or publication of this article. This research was supported by: National Natural Science Foundation of China (No. 42277470, 42007185), Open fund of Key Laboratory of Ecological Prewarning, Protection and Restoration of Bohai Sea, Ministry of Natural Resources (No. 2022106), Foundation of State Environmental Protection Key Laboratory of Coastal Ecological Environment, National Marine Environmental Monitoring Center of China (202310), Knowledge Innovation Program of Wuhan-Shuguang Project (No. 2022020801020210). We also thanked the Majorbio Bio-Pharm Technology Co. Ltd. (Shanghai, China) for supporting high-throughput sequencing.

Conflict of interest

Author YX was assisted by the Majorbio Bio-Pharm Technology Co. Ltd. for high-throughput sequencing.

The remaining authors declare that the research was conducted in the absence of any commercial or financial relationships that could be construed as a potential conflict of interest.

Publisher's note

Supplementary material

The Supplementary Material for this article can be found online at: https://www.frontiersin.org/articles/10.3389/fmars.2023.1305763/full#supplementary-material

References

Albouy, C., Delattre, V. L., Merigot, B., Meynard, C. N., and Leprieur, F. (2017). Multifaceted biodiversity hotspots of marine mammals for conservation priorities. *Divers. Distrib.* 23, 615–626. doi: 10.1111/ddi.12556

Avila, I. C., Kaschner, K., and Dormann, C. F. (2018). Current global risks to marine mammals: Taking stock of the threats. *Biol. Conserv.* 221, 44–58. doi: 10.1016/j.biocon.2018.02.021

Bader, G. D., and Hogue, C. W. (2003). An automated method for finding molecular complexes in large protein interaction networks. *BMC Bioinf.* 4 (1), 1–27. doi: 10.1186/1471-2105-4-2

Barman, P. P., Yanan, H., and Liu, Q. (2020). Dynamic characteristics of community structure and seasonal variation of fishery species in the Bohai Sea, China. *Appl. Ecol. Env. Res.* 18 (1), 817–837. doi: 10.15666/aeer/1801_817837

Bascompte, J. (2009). Disentangling the web of life. *Science* 325, 416–419. doi: 10.1126/science.1170749

Bossart, G. D. (2011). Marine mammals as sentinel species for oceans and human health. *Vet. Pathol.* 48, 676–690. doi: 10.1177/0300985810388525

Brose, U., and Dunne, J. A. (2009). "37Chapter 3 Modelling the dynamics of complex food webs," in *Community Ecology: Processes, Models, and Applications*. Eds. H. A. Verhoef and P. J. Morin (United States: Oxford University Press). Available at: https://academic.oup.com/book/11078.

Chen, S., Zhou, Y., Chen, Y., and Gu, J. (2018). FASTP: an ultra-fast all-in-one FASTQ preprocessor. *Bioinformatics* 34, i884–i890. doi: 10.1093/bioinformatics/bty560

Cheng, J. S. (2004). *Ecological environment and biomes in coastal waters of the Yellow Sea and Bohai Sea* (China: Qingdao Ocean University Press). Available at: https://www.zhangqiaokeyan.com/book-cn/081501157090.html.

Cordone, G., Salinas, V., Marina, T. I., Doyle, S. R., Pasotti, F., Saravia, L. A., et al. (2020). Green vs brown food web: Effects of habitat type on multidimensional stability proxies for a highly-resolved Antarctic food web. *Food Webs* 25, e00166. doi: 10.1016/j.fooweb.2020.e00166

D'Alessandro, S., and Mariani, S. (2021). Sifting environmental DNA metabarcoding data sets for rapid reconstruction of marine food webs. *Fish Fish.* 22, 822–833. doi: 10.1111/faf.12553

Danger, M., Bec, A., Spitz, J., and Perga, M.-E. (2022). Questioning the roles of resources nutritional quality in ecology. *Oikos* 2022, e09503. doi: 10.1111/oik.09503

Delmas, E., Besson, M., Brice, M.-H., Burkle, L. A., Dalla Riva, G. V., Fortin, M.-J., et al. (2019). Analysing ecological networks of species interactions: Analyzing ecological networks. *Biol. Rev.* 94, 16–36. doi: 10.1111/brv.12433

DiBattista, J. D., Coker, D. J., Sinclair-Taylor, T. H., Stat, M., Berumen, M. L., and Bunce, M. (2017). Assessing the utility of eDNA as a tool to survey reef-fish communities in the Red Sea. *Coral Reefs* 36, 1245–1252. doi: 10.1007/s00338-017-1618-1

Edgar, R. C. (2013). UPARSE: highly accurate OTU sequences from microbial amplicon reads. *Nat. Methods* 10, 996–998. doi: 10.1038/nmeth.2604

Farriols, M. T., Ordines, F., Somerfield, P. J., Pasqual, C., Hidalgo, M., Guijarro, B., et al. (2016). Bottom trawl impacts on Mediterranean demersal fish diversity: Not so obvious or are we too late? *Cont. Shelf Res.* 137, 84–102. doi: 10.1016/j.csr.2016.11.011

Fassbender, A. J., Sabine, C. L., and Palevsky, H. I. (2017). Nonuniform ocean acidification and attenuation of the ocean carbon sink: NonUniform Ocean Acidification. *Geophys. Res. Lett.* 44, 8404–8413. doi: 10.1002/2017GL074389

Guzzo, M. M., Blanchfield, P. J., and Rennie, M. D. (2017). Behavioral responses to annual temperature variation alter the dominant energy pathway, growth, and condition of a cold-water predator. *PNAS* 114, 9912–9917. doi: 10.1073/pnas.1702584114

Han, J. (2009). "Studies on Population Resources and Molecular Genetic Characteristics of Spotted Seals (*Phoca largha*)," in *Chinese Waters* (China: Institute of Oceanology, Qingdao, The Chinese Academy of Sciences). Available at: https://d.wanfangdata.com.cn/thesis/Y1613257.

Hendrix, A. M., Lefebvre, K. A., Quakenbush, L., Bryan, A., Stimmelmayr, R., Sheffield, G., et al. (2021). Ice seals as sentinels for algal toxin presence in the Pacific Arctic and subarctic marine ecosystems. *Mar. Mammal Sci.* 37, 1292–1308. doi: 10.1111/mms.12822

Huxley, C. (2013). "CITES: the vision," in *Endangered species threatened convention: the past, present and future of CITES, the convention on international trade in endangered species of wild Fauna and Flora* (Washington, Routledge: Earthscan Press). Available at: https://books.google.hu/books?hl=en&lr=&id=2Xr7AQAAQBAJ&oi=fnd&pg=PA3&dq=+CITES:+the+vision.&ots=bpo6oxHftf&sig=zYWJqzmYa_AdeJLn09II1jvbMTA&redir_esc=y#v=onepage&q=CITES%3A%20the%20vision.&f=false.

Karlson, A. M. L., Gorokhova, E., Gårdmark, A., Pekcan-Hekim, Z., Casini, M., Albertsson, J., et al. (2020). Linking consumer physiological status to food-web structure and prey food value in the Baltic Sea. *Ambio* 49, 391–406. doi: 10.1007/s13280-019-01201-1

Kda, B., Jcw, B., Em, A., and Faa, C. (2015). Choice of capture and extraction methods affect detection of freshwater biodiversity from environmental DNA. *Biol. Conserv.* 183, 53–63. doi: 10.1016/j.biocon.2014.11.018

Liu, J. (2019). *Fishes of Bo Hai. Beijing* (China: Science Pres). Available at: https://www.abebooks.com/Fishes-Bo-Liu-Jing/30537577381/bd.

Liu, X., Li, Y., Wang, W., Duan, Y., Chai, Y., and Dong, J. (2015). The fish community structure and diversity in the north of Liaodong Bay. *Jornal Fisheries China* 39, 1155–1165. doi: 10.11964/jfc.20150309766

Liu, B., Wang, H., Qin, B., Fan, Z., Xiong, W., and Chen, Y. (2021). Environmental DNA metabarcoding-based monitoring of fish diversity and screening invasion risk of non-native fishes in the Beijing area. *J. Biosafety* 30, 220–229. doi: 10.3969/j.issn.2095-1787.2021.03.011

Liu, H., Wei, Q., Huang, C., Zhang, Y., and Guo, Z. (2017). Potential roles of intrinsic disorder in maternal-effect proteins involved in the maintenance of DNA methylation. *Int. J. Mol. Sci.* 18, 1898. doi: 10.3390/ijms18091898

Lowry, L. F., Burkanov, V. N., Frost, K. J., Simpkins, M. A., Davis, R., DeMaster, D. P., et al. (2000). Habitat use and habitat selection by spotted seals (*Phoca largha*) in the Bering Sea. *Can. J. Zoo.* 78 (11), 1959–1971. doi: 10.1139/z00-138

Magoc, T., and Salzberg, S. L. (2011). FLASH: fast length adjustment of short reads to improve genome assemblies. *Bioinformatics* 27, 2957–2963. doi: 10.1093/bioinformatics/btr507

Marina, T. I., Salinas, V., Cordone, G., Campana, G., Moreira, E., Deregibus, D., et al. (2018). The Food Web of Potter Cove (Antarctica): complexity, structure and function. *Estuar. Coast. Shelf Sci.* 200, 141–151. doi: 10.1016/j.ecss.2017.10.015

Mauvisseau, Q., Harper, L. R., Sander, M., Hanner, R. H., Kleyer, H., and Deiner, K. (2022). The multiple states of environmental DNA and what is known about their persistence in aquatic environments. *Environ. Sci. Technol.* 56, 5322–5333. doi: 10.1021/acs.est.1c07638

McCann, K. S. (2000). The diversity-stability debate. *Nature* 405 (6783), 228–233. doi: 10.1038/35012234

Nomura, J., Mardo, M., and Takumi, T. (2021). Molecular signatures from multi-omics of autism spectrum disorders and schizophrenia. *J. Neurochem.* 159 (4), 647–659. doi: 10.1111/jnc.15514

Norkko, A., Thrush, S. F., Cummings, V. J., Gibbs, M. M., Andrew, N. L., Norkko, J., et al. (2007). Trophic structure of coastal antarctic food webs associated with changes in sea ice and food supply. *Ecology* 88, 2810–2820. doi: 10.1890/06-1396.1

Orio, A., Bergström, U., Florin, A. B., Šics, I., and Casini, M. (2020). Long-term changes in spatial overlap between interacting cod and flounder in the Baltic Sea. *Hydrobiologia* 847 (11), 2541–2553. doi: 10.1007/s10750-020-04272-4

Parsons, E. C. M., Baulch, S., Bechshoft, T., Bellazzi, G., Bouchet, P., Cosentino, A. M., et al. (2015). Key research questions of global importance for cetacean conservation. *Endanger. Species Res.* 27, 113–118. doi: 10.3354/esr00655

Pires, A. P. F., Marino, N. A. C., Srivastava, D. S., and Farjalla, V. F. (2016). Predicted rainfall changes disrupt trophic interactions in a tropical aquatic ecosystem. *Ecology* 97, 2750–2759. doi: 10.1002/ecy.1501

Qu, C., Stewart, K. A., Clemente-Carvalho, R., Zheng, J., Wang, Y., Gong, C., et al. (2020). Comparing fish prey diversity for a critically endangered aquatic mammal in a reserve and the wild using eDNA metabarcoding. *Sci. Rep.* 10, 16715. doi: 10.1038/s41598-020-73648-2

Riede, J. O., Rall, B. C., Banasek-Richter, C., Navarrete, S. A., Wieters, E. A., Emmerson, M. C., et al. (2010). "Scaling of Food-Web Properties with Diversity and Complexity Across Ecosystems," in *Advances in Ecological Research, Vol 42: Ecological Networks*. Ed. G. Woodward (United States: Academic Press), 139–170. doi: 10.1016/B978012381363-3.00003-4

Rodriguez, I. D., Marina, T. I., Schloss, I. R., and Saravia, L. A. (2022). Marine food webs are more complex but less stable in sub-Antarctic (Beagle channel, Argentina) than in Antarctic (Potter cove, Antarctic peninsula) regions. *Mar. Environ. Res.* 174 (1), 105561. doi: 10.1016/j.marenvres.2022.105561

Rourke, M. L., Fowler, A. M., Hughes, J. M., Broadhurst, M. K., DiBattista, J. D., Fielder, S., et al. (2022). Environmental DNA (eDNA) as a tool for assessing fish biomass: A review of approaches and future considerations for resource surveys. *Environ. DNA* 4 (1), 9–33. doi: 10.1002/edn3.185

Shannon, P., Markiel, A., Ozier, O., Baliga, N. S., Wang, J. T., Ramage, D., et al. (2003). Cytoscape: A software environment for integrated models of biomolecular interaction networks. *Genome Res.* 13, 2498–2504. doi: 10.1101/gr.1239303

Trussell, G. C., Ewanchuk, P. J., and Matassa, C. M. (2006). The fear of being eaten reduces energy transfer in a simple food chain. *Ecology* 87, 2979–2984. doi: 10.1890/0012-9658(2006)87[2979:TFOBER]2.0.CO;2

Wang, Q., Garrity, G. M., Tiedje, J. M., and Cole, J. R. (2007). Naïve Bayesian Classifier for Rapid Assignment of rRNA Sequences into the New Bacterial Taxonomy. *Appl. Environ. Microbiol.* 73, 5261–5267. doi: 10.1128/AEM.00062-07

Wang, R., Lin, L., Li, H., Zhang, R., and Li, Y. (2021). Potential use of environmental DNA methods in Arctic marine fish diversity research. *Chin. J. Polar Res.* 33 (1), 148–155. doi: 10.13679/j.jdyj.20200018

Xu, Y., Huo, X. M., Jordán, F., Zhou, M. L., Cai, Y. P., and Sun, J. (2023). Identifying marine food web homogenization patterns. *Front. Mar. Sci.* 10, 1245513. doi: 10.3389/fmars.2023.1245513

Xu, C., Liu, Y., Cheng, Y., Xu, B. F., Zhang, C. L., Ren, Y. P., et al. (2020). Structure and complexity of Haizhou Bay food web based on topological network analysis. *Haiyang Xuebao* 42 (4), 47–54. doi: 10.3969/j.issn.0253-4193.2020.04.006

Yang, K., Ding, C., Chen, X., Ding, L., Huang, M., Chen, J., et al. (2022). Fish diversity and spatial distribution pattern in the Nujiang River Basin. *Biodivers. Sci.* 30, 21334. doi: 10.17520/biods.2021334

Yang, J., Zhang, X., Jin, X., Seymour, M., Richter, C., Logares, R., et al. (2021). Recent advances in environmental DNA-based biodiversity assessment and conservation. *Divers. Distrib.* 27 (10), 1876–1879. doi: 10.1111/ddi.13415

Yates, M. C., Cristescu, M. E., and Derry, A. M. (2021). Integrating physiology and environmental dynamics to operationalize environmental DNA (eDNA) as a means to monitor freshwater macro-organism abundance. *Mol. Ecol.* 30 (24), 6531–6550. doi: 10.1111/mec.16202

Zhu, Q., Jiang, B., and Tang, T. Y. (2000). Species, distribution and conservation strategies of Marine mammals in China. *Mar. Sci.* 24 (9), 35–39. doi: 10.3969/j.issn.1000-3096.2000.09.014

Zhuang, H., Shao, F., Zhang, C., Xia, W., Wang, S., Qu, F., et al. (2023). Spatial-temporal shifting patterns and in *situ* conservation of spotted seal (*Phoca largha*) populations in the Yellow Sea ecoregion. *Integr. Zool.* 0, 1–12. doi: 10.1111/1749-4877.12731

frontiers | Frontiers in Marine Science

TYPE Original Research
PUBLISHED 22 April 2024
DOI 10.3389/fmars.2024.1301612

OPEN ACCESS

EDITED BY
Tian Xie,
Beijing Normal University, China

REVIEWED BY
Marco Yévenes,
University of Los Lagos, Chile
Davide Agnetta,
National Institute of Oceanography and Applied Geophysics, Italy

*CORRESPONDENCE
Ferenc Jordán
ferencvalter.jordan@unipr.it

RECEIVED 25 September 2023
ACCEPTED 08 April 2024
PUBLISHED 22 April 2024

CITATION
Jordán F, Capelli G, Primicerio R and Bodini A (2024) Strongly asymmetric interactions and control regimes in the Barents Sea: a topological food web analysis.
Front. Mar. Sci. 11:1301612.
doi: 10.3389/fmars.2024.1301612

Strongly asymmetric interactions and control regimes in the Barents Sea: a topological food web analysis

Ferenc Jordán[1,2*], Greta Capelli[1,3], Raul Primicerio[3] and Antonio Bodini[1]

[1]Department of Chemistry, Life Sciences and Environmental Sustainability, University of Parma, Parma, Italy, [2]KeyNode Research Ltd, Budapest, Hungary, [3]Department of Arctic and Marine Biology, The Arctic University of Norway, Tromsø University, Tromsø, Norway

Introduction: Increasing temperature of the global ocean alters the spatial behavior of a number of species. From the northern Atlantic Ocean, species may shift their area towards the poles. This results in the atlantification of the Barents Sea, raising questions about possible changes in species composition, community structure and community control.

Methods: We address the question whether possible changes in community control can be detected and quantified based on simple network analytical measures applied to the food web. Based on unweighted (binary) and undirected (symmetric) data, we quantify the strength of direct and indirect interactions in the network, represent the most asymmetric effects in the asymmetry graph composed of directed and weighted links and study the overlap among trophic niches of organisms.

Results and discussion: We support earlier findings suggesting that the ecosystem can possibly be characterized by wasp-waist control. This would mean that focusing management efforts on intermediate trophic levels is of high importance, providing indirect benefit for organisms also at lower and higher trophic levels.

KEYWORDS

bottom-up, top-down, wasp-waist control, food web, network centrality, asymmetric interactions, regular equivalence

1 Introduction

Organisms influence each other in ecological communities by strong and weak, direct and indirect, positive and negative, bottom-up and top-down as well as trophic and non-trophic effects. Complex behavior is a result of the multiplicity of these parallel, combined and overlapping effects, among others (e.g. the number of species, spatial heterogeneity,

niche dimensionality). It is quite challenging to make predictions at this level of complexity, despite of massive progress in ecological modelling and related supporting bioinformatic techniques (Karsenti et al., 2011). Yet, testable predictions are essential for scientific understanding and management. Research towards simplifying and handling complexity is, thus, important if over-simplifications are avoided and predictability can be increased (Odenbaugh, 2006).

Network analysis is widely used and increasingly available tool in modelling various types of inter-connected ecological systems (Fath et al., 2007; Jordán, 2022). Most of the current methods focus on graph nodes in various contexts, including research on network modules (Gjata et al., 2012), diversity of functional groups (Lin et al., 2022), central nodes (Estrada, 2007), keystone species (Jordán, 2009), functional organization (Xu et al., 2023) but also the distribution of traits in various network positions (Endrédi et al., 2021). Other approaches focus more on interactions and the roles they play in community control. These include research on cycling (Finn, 1976), the analysis of distribution and variability of interaction strength (e.g. bimodal: Sala and Graham, 2002), the dominator tree structure of food webs (Allesina and Bodini, 2004; Allesina et al., 2006), the distinction between functional and redundant links (Allesina et al., 2006; Bondavalli and Bodini, 2014), quantifying direct and indirect control (Ulanowicz and Puccia, 1990), detecting long indirect interaction chain effects (Estes et al., 1998) and applying process-based modelling tools (Livi et al., 2011). It is clear that important nodes and crucial links cannot really be separated, so most approaches consider them equally, including Ecopath with Ecosim (Christensen and Walters, 2004), ATLANTIS (Audzijonyte et al., 2019) and OSMOSE (Shin and Cury, 1999). We use and develop our earlier approach that simplifies complexity by predicting critically important, predictable interactions, based on their topology-based asymmetry (Jordán et al., 2014). While quantifying and detecting either key nodes or key interactions is useful simplification, the price is loss of information and details.

For better understanding community dynamics, at a larger scale, one needs to know the dominant control regime in the system. Bottom-up control means the prevalence of dynamical regulation by resource availability, while top-down control implies the prevalence of regulative action by the consumers. The pattern of the two regimes is of particular interest (Hairston et al., 1960; Oksanen et al., 1981; Hunter and Price, 1992). Thus, one critically important property of an inter-specific interaction is its orientation from the viewpoint of trophic flows. Trophic interactions can be oriented in either bottom-up or top-down directions, while indirect interaction chains can be of mixed orientation. For example, a trophic cascade is composed of two top-down interactions (Ripple et al., 2016), while apparent competition is composed of one bottom-up and one top-down interactions (Holt and Bonsall, 2017). In particular ecosystems, either bottom-up or top-down effects may dominate, defining a control regime. In the case of wasp-waist control, the dominant controlling organisms exert both bottom-up and top-down effects on the food web. This mechanism is probably most typical in pelagic upwelling ecosystems, where a few species occupy the wasp-waist position (e.g. sardine, anchovy, jellyfish), exerting mixed-control (Cury et al., 2000), partly as a consequence of food web topology (Jordán et al., 2005). This regime has already been suggested also for the North Sea food web (Fauchald et al., 2011).

We suggest a novel approach to determining the dominant control regime, based on network analysis. Focusing on the most asymmetric relationships might be a way to reduce and manage complexity, by focusing on a few, quantitatively determined critical links in the interaction network (see a similar approach in Taruttis et al., 2015). In symmetric or only weakly asymmetric interactions between a pair of species i and j, effects can propagate in both directions, both from species i to species j and from species j to species i. This means that clearly identifying causes and effects in a large and complex network is not easy. However, strong asymmetry from i to j means that we expect flows mostly (if not excusively) only in one direction. Whether a „cause" in i will inevitably lead to an „effect" in j is not automatic, so in this sense „causality" is not guaranteed; it only helps interpretation. Yet, the flow of effects in these asymmetric interactions might be easier to predict, thus, the asymmetry graph may depict a subsystem with slightly more predictive food web models. For the majority of symmetric or only slightly asymmetric interactions, trophic effects propagate in every direction: indirect chain effects are less predictable. Understanding the structure to dynamics relationship is generally a notoriously difficult task (Endrédi et al., 2018) but there might be parts of the food web where topology correlates better with dynamics.

In the Barents Sea, human impact (mostly fisheries) is clearly unavoidable and increasingly important in ecosystem dynamics. This means that the future of this ecosystem depends to a large extent on wise decision-making based on simple and clear scientific support. In order to manage complexity, at least at the level of communication, strong simplifications are needed. One way to go is to quantitatively identify key elements (system components) governing ecosystem dynamics, with the hope that understanding and managing these key elements will have predictable and desirable effects. Earlier research on the Barents Sea food web focused on a number of key network properties, including node degree, connectance, clustering, modules and connectors (Kortsch et al., 2019). For quantifying the strength of indirect interactions among organisms, network analysis offers methods also beyond simply considering the number of neighbors (i.e. direct interactors, node degree). There is an increasing literature of key nodes in food webs (Jordán, 2009), here we focus on key interactions. These can be important because of their topological positions (Allesina and Bodini, 2004) or strength (Gjata et al., 2012). Also, we suggest that interactions of high asymmetric effects between species i and j can be critically important for predictability of single-species disturbances on community dynamics. While multiple direct and indirect effects may propagate between species i and j in complex food webs (in both directions), if the topological relationship between these species is highly asymmetric, identifying the cause (the species affecting the other) and the effect (the affected species) can be more predictable. Possibly neither these species nor the interaction(s) between them are of extreme importance, but at least this interaction can be highly predictable. Thus, these can be useful for establishing and communicating simple messages about complex systems.

Making fisheries sustainable would imply the protection of their resource base, avoiding an excess exploitation. This is a complex problem difficult to handle for policy-makers (ICES, 2022), mostly because of contrasting interests, and especially in a multi-species framework (e.g. MSY assessment, May et al., 1979). A contribution to this end may come from the understanding of the role species play as controlling factors. To this end, identifying critically important interactions and control regimes are of highest importance.

In this paper, we focus on the Barents Sea food web with the aim to quantify the strength and asymmetry of trophic effects, based on the topology of the food web. We determine the most asymmetric interactions composing the „asymmetry graphs". We discuss the consequences of reciprocity in asymmetric interactions, we explain how it is related to predictability and the dominant control regime and we provide ecological interpretation in the context of the Barents Sea. The final aim is to support better understanding of the atlantification process and the effects of multiple drivers of change.

2 Methods

2.1 Study area

The Barents Sea is a highly productive shelf area of the Arctic Ocean, having two major zones, an arctic and a boreal one (see Pecuchet et al., 2020a). It sustains the fisheries of 12 nations although Norway and Russia have the greatest share of the resources. Fishing activity targets several species, being the capelin (*Mallotus villosus*) the largest pelagic fish population in this ecosystem. Also marine mammals such as seals and whales are targets of fisheries. Currently, the Barents sea ecosystem faces major challenges, including overfishing, invasion by alien organisms and the effects of climate change (Pedersen et al., 2021). Warming is twice as fast as the global average and invasion intensity is five times more than the global average (Fossheim et al., 2015). The atlantification of the local fauna, for example, manifest in changing species composition coupled with re-arrangement of inter-specific interactions (Fossheim et al., 2015; Pecuchet et al., 2020a; 2020b), with a transition zone between Atlantic and Arctic waters East of Greenland (Emblemswag, 2022). Changes in species composition and altered interactions may finally lead to switching the control regime. Thus, several local effects may sum up to different system-level properties.

2.2 Trophic data and network construction

Trophic data were described based on stomach content analyses of samples got from bottom trawl surveys (Pecuchet et al., 2020a; 2022b; Kortsch et al., 2019). The meta-network for the whole ecosystem, composed by all available data, contained N=238 nodes. We analyzed an aggregated version of N=21 nodes in which we collapsed the original 238 trophic components. Original nodes were assigned to these 21 functional groups as shown in Supplementary Material A. In this, lower-resolution, parsimonious version of the food web, graph nodes are functional groups typically containing several species (occasionally only a single one, e.g. CAP: capelin). Aggregation was based mostly on trophic similarity (e.g. PELF: pelagic planktivorous fish), with conservation (e.g. RED: redfish) and economic (HER: herring) viewpoints that we also considered. Table 1 lists all the 21 functional groups. Food web links are based on statistical co-occurrence in the samples, enabled by traditional ecological knowledge and literature data.

2.3 Network analysis

In food webs, trophic links can be understood as either material transfers (with purely bottom-up effects) or reciprocal trophic effects between a pair of interacting populations (with one negative top-down and one positive bottom-up effects). In the latter sense, a web of interacting populations can be considered an undirected network, as control effects propagate in both directions. In any case, only the direct interactions are shown and indirect chain effects emerge as consequences of two or more direct links.

TABLE 1 The codes for the network nodes (functional groups).

CAP	capelin
COD	cod
D	detritus
HAD	haddock
HER	herring
LBEN	large benthivorous fish
LDEP	large deposit suspension feeding invertebrate
MACZO	macrozooplankton
PELF	pelagic planktivorous fish
PIF	piscivorous fish
PL	plankton
PRED	predatory feeding invertebrate
RED	redfish
SBEN	small benthivorous fish
SBIR	seabirds
SDEP	small deposit suspension feeding invertebrate
SEAL	seals
TOPP	top predators
WHF	fish eater whales
WHZ	zooplankton eater whales
ZOO	zooplankton

2.3.1 Interaction strength and centrality

Since strong indirect effects can appear in community dynamics, the number of direct partners offers only a limited view on network position (D: degree, the number of neighbors, connected by direct interactions). Indirect chain effects (Wootton and Emmerson, 2005) can be mapped and quantified in the network (see also Ulanowicz and Puccia, 1990). Based on an earlier approach focusing on apparent competition (Müller et al., 1999), calculating the strength and asymmetry of indirect effects was generalized (topological importance, TI, Jordán et al., 2003) for longer indirect chains (up to n steps). The binary (unweighted) version of the topological importance index measures the non-local (indirect up to n steps) position of species and uses undirected data. It provides complementary information to local scale (i.e., degree) and whole system approaches (i.e., closeness and betweenness). Topological importance was originally derived from the analysis of two-step long, horizontal, apparent competition interactions in host-parasitoid networks (Müller et al., 1999). When the species j can be reached from i in m steps, the effect is $r_{m,ij}$. In case of a direct effect (m = 1), topological importance is expressed as the inverse of degree ($TI_{m,ij} = 1/D_j$). Indirect effects are multiplicative and additive. In case of 2-step pathways (m = 2), if species j can be affected by i through two pathways that cross species k (i → k → j) and h (i → h → j), then the effect of each pathway is measured as the product of the direct effects (i.e., $TI_{1,ik} \cdot TI_{1,kj}$ and $TI_{1,ih} \cdot TI_{1,hj}$; multiplicative property). The total effect of i on j is obtained by summing up the contribution of the two pathways passing through k and h in m steps: $TI_{2,ij} = TI_{1,ik} \cdot TI_{1,kj} + TI_{1,ih} \cdot TI_{1,hj}$ (additive principle). When all pathways are quantified up to m steps (each $TI_{m,ij}$ is known), one can quantify (1) the strength of interaction between a pair of nodes i and j, (2) the asymmetry of the interaction between the node pairs (see below) and (3) the sum of interactions for each node, providing a measurement of node centrality (as a function of m). This latter is called TI_i, i.e. the topological importance of node *i* (Jordán et al., 2003; Jordán, 2009). It is noted that the same calculations can be performed for weighted networks (weighted importance, WI). Based on earlier research, indirect chain effects of 2 and 3 steps seem to be most relevant, both empirically and theoretically (see Brose et al., 2005), so we used m=3.

2.3.2 Interaction asymmetry and causality

In the TI matrix containing values of m-step-long mixed effects, asymmetry is quite typical between TI_{ij} and TI_{ji} values (unlike in the food web matrix, where consumer-resource effects most typically go in only one direction). This asymmetry is defined as

$$A = \left| TI_{ij}^3 - TI_{ji}^3 \right|$$

Applying a threshold value for A (c), we define the asymmetry graph as the subset of nodes and the most asymmetric effects between them such that

$$A \geq c$$

Theoretically, this threshold can be either a constant or a variable; if it is a constant, it could be determined empirically (for a similar approach, see Taruttis et al., 2015). However, values of TI, and thus of A, depend on N (network size), so it is better to define them as a function of the actual TI-matrix. We defined the c threshold as $c = 2/3^*A_{max} = 0.1$ ($A_{max} = 0.15$) but we explored also several other threshold values to study the sensitivity of the results. At c = 0.1, the asymmetry graph contains 8 highly asymmetric interactions out of (21*20)/2 = 210 un-ordered pairs of nodes (3.8%). Earlier we considered the most asymmetric 5% of simulated effects, with $A_{max} = 0.13$, N = 48 and 56 effects in the asymmetry graph (Jordán et al., 2014). While these c values seem to be appropriate for finding meaningful patterns (not too few and not too many highly asymmetric links), others can still be informative (see Supplementary Materials C, D).

Applying a particular threshold level, the asymmetry graph can be obtained, containing the most asymmetric effects (direct and indirect, bottom-up and top-down). These interactions are probably important and predictable, while the nodes of the asymmetry graph form a core of the community that is likely to be important for control. The ratio of bottom-up effects in the asymmetry graph quantifies the dominant control regime from this simple topological perspective. Experimental results could best validate this approach and mesocosm experiments are in preparation (beyond the scope of the present theoretical exercise).

We emphasize that the topology of an originally undirected (since we are interested in trophic control regimes, we consider undirected effects, otherwise no top-down effects can be defined) and unweighted (the database has no information on the magnitude of trophic flows) network defines directed and weighted measures for both interaction strength and asymmetry.

2.3.3 Trophic niche overlap

To understand whether species with strongly asymmetric effects have overlapping roles and functions (Cirtwill et al., 2018), it may be of interest to see the similarity of their network positions. For quantifying the similarity of network positions, we used the measure of regular equivalence (REGE, Everett and Borgatti, 1991), used already in ecological research (Luczkovich et al., 2003; Endrédi et al., 2018). This measure quantifies the similarity between the positions of network nodes i and j based on their network neighborhood, providing information about functional redundancy and niche diversity. The two kinds of indirect competition (exploitative and apparent) are explicitly used for calculating REGE. We used the UCINET software and studied the dendrograms (Borgatti et al., 2002). Two nodes are said to be regular equivalent if they are connected with the same types of nodes. In ecology terms, two species are more regularly equivalent if they have similar (but not necessarily the same) predators and preys: for example, two canopy-living insects feeding on leaves and consumed by birds. A REGE matrix S is the output of such an analysis, where the ij^{th} element, S_{ij}, expresses the extent of similarity between nodes i and j. Based on an output dendrogram, we can apply cutoff levels in order to compare the number of branches for different networks. This is a measure of functional diversity (the number of functional groups), while the number of graph nodes in a branch quantifies redundancy within a group. If a single species

constitutes a branch at a given cutoff level, it may be considered a keystone species (sensu Bond, 1994).

3 Results

3.1 Centrality

Based on the original trophic matrix (Supplementary Material B), we built up the associated food web (Figure 1A). The TI^3-matrix (Supplementary Material B) shows the strength of mixed and indirect interactions up to 3 steps and the corresponding network is shown in Figure 1B In the TI-matrix, only 4 values are zero, out of 21*21 = 441 effects (considering direction and self-loops). These are from zooplankton eater whales to large benthivorous fish, from large benthivorous fish to top predators, from large benthivorous fish to zooplankton eater whales and from large benthivorous fish to small benthivorous fish. This means that zooplankton eater whales and large benthivorous fish is the only pair of nodes that are independent of each other if indirect effects are not considered beyond three steps.

Based on the topological importance (TI^3) index, the most central functional groups are shown in Table 2. The three mostly connected, key organisms are haddock, cod and herring, while the least central ones are large deposit suspension feeding invertebrates (LDEP), small deposit suspension feeding invertebrates (SDEP), zooplankton eater whales and large benthivorous fish. These are the strongest and weakest interactors in the system, respectively. Earlier studies showed that according to local, direct measures (i.e. D degree, the number of neighbors), the key players are cod, haddock and redfish in the boreal, while detritus, plankton, *Boreogadus saida* (assigned to pelagic planktivorous fish) and *Pandalus borealis* (assigned to predatory feeding invertebrates) in the arctic waters (Kortsch et al., 2019).

3.2 Causality

Based on the asymmetry matrix (Supplementary Material B) at the c = 0,1 threshold level, the asymmetry graph is shown in Figure 1C (the list of links is given in Table 3, according to all A ≥ c). Here, nodes are arranged in the layout as in Figures 1A, B but Figure 1D shows a more intuitive layout for the asymmetry graph, clearly showing the affectors and the affected organisms in these mostly asymmetric relationships. Here, the spatial layout of the nodes does not follow that in the original food web; instead, affectors and affected are grouped at two different levels. The asymmetry graph contains 8 links at this threshold level (Figure 1D). These are from haddock to large benthivorous fish (A = 0,15), from haddock to LDEP, from haddock to SDEP, from cod to LDEP and from cod to SDEP (A = 0,13), macrozooplankton to zooplankton eater whales and from zooplankton to zooplankton eater whales (A = 0,11) and from redfish to large benthivorous fish (0,1). These 8 most asymmetric interactions link 5 affectors (haddock, cod, macrozooplankton, zooplankton, redfish) and 4 affected (large benthivorous fish, LDEP, SDEP, zooplankton eater whales) functional groups. These are close to the top and at the bottom of the TI-rank (respectively, see Table 2), the affectors being the most central and the affected nodes being the least central nodes in the food web. This pattern corresponds to wasp-waist community control in a structural sense.

Contrary to earlier results (Jordán et al., 2014), where the most asymmetric effect was an indirect one, all of the effects documented

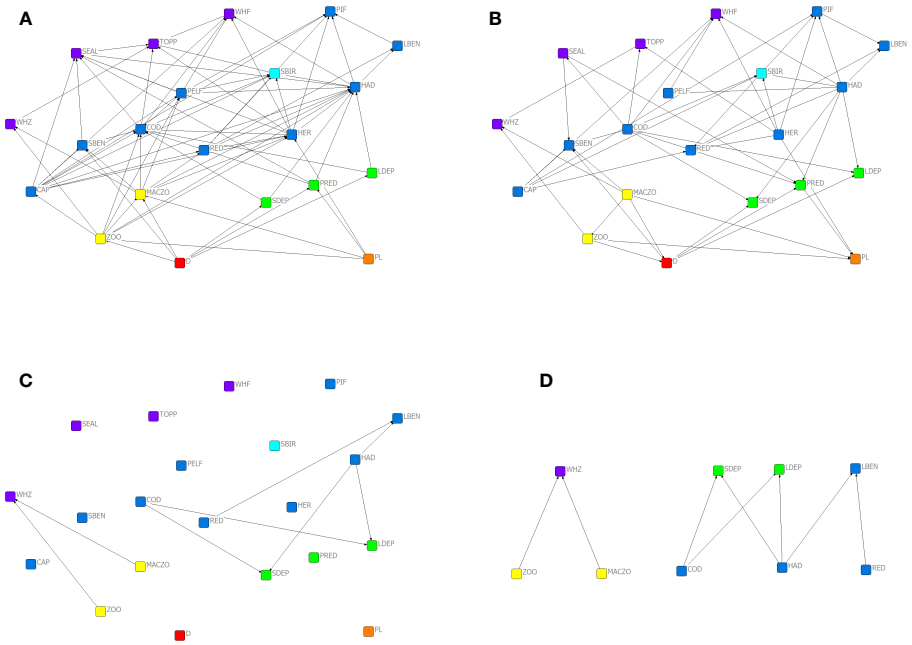

FIGURE 1
Interaction networks for the Barents Sea ecosystem: the food web **(A)**, the network of topological interactions based on TI **(B)**, the asymmetry graph at c = 0,1 **(C)** and the latter re-arranged for better visualization **(D)**.

TABLE 2 The TI-rank for all functional groups in the Barents Sea food web.

	TI
HAD	2,1
COD	1,91
HER	1,64
CAP	1,46
MACZO	1,46
ZOO	1,28
PELF	1,18
SEAL	1,08
D	1,01
RED	0,98
SBIR	0,89
TOPP	0,84
PIF	0,83
WHF	0,75
PRED	0,72
SBEN	0,67
PL	0,55
WHZ	0,42
LDEP	0,42
SDEP	0,42
LBEN	0,41

Colored background marks functional groups in the asymmetry graph (affectors in green, affected ones in red).

here are mixed (direct and indirect) interactions and there is no strong asymmetry between organisms that are only indirectly influencing each other.

Gradually decreasing the threshold level would add weaker and weaker links to the asymmetry graph, as shown in Supplementary Material C. Here, we also show the asymmetry graphs for c = 0,05

TABLE 3 The list of the 8 links in the asymmetry graph at c = 0.1.

A	effect
0,15	HAD → LBEN
0,13	COD → LDEP
	COD → SDEP
	HAD → LDEP
	HAD → SDEP
0,11	MACZO → WHZ
	ZOO → WHZ
0,1	RED → LBEN

Grey background marks top-down effects.

with 36 links (Supplementary Material D). This shows that results clearly depend on the value of the c threshold. The original purpose was to simplify network complexity to a level that can make communication clearer. The set of the most asymmetric effects should contain neither a single interaction nor a complex network of effects. Here, more information is shown but the original complexity of the food web is not reduced significantly.

3.3 Trophic niche overlap

The five affectors of the asymmetry graph are quite dispersed in the REGE dendrograms (Figure 2), haddock, cod and redfish (the invasive boreal species) having overlapping roles but zooplankton and macrozooplankton being isolated. The most unique organisms have the longest non-branching segments in the dendrogram, these are zooplankton eater whales, capelin and herring: their trophic roles are the least replaceable, these are key organisms in this sense. Considering the functional groups mostly sensitive to trawlers (LDEP, piscivorous fish), their strong perturbation can be partly compensated by other groups with high functional overlap (SDEP and top predators, respectively).

4 Discussion and conclusions

Our analysis is based on identifying the most asymmetric topological relationships in predator-prey interactions. This has been already explored also for plant-pollinator (Jordano, 1987) and host-parasite (Lafferty et al., 2006) interactions. We quantified asymmetry based purely on topology (unequal positions in the network) but it is noted that the approach presented here can be applied also for weighted interaction networks. Our results and conclusions are thus based on a modelling approach, based on solid field studies.

The asymmetry graph is composed of 4 top-down and 4 bottom-up effects, all originated from organisms at intermediate trophic levels. This might support earlier findings about the possibility of mixed, wasp-waist control (Cury et al., 2000) of haddock in this ecosystem (Fauchald et al., 2011). Wasp-waist control becomes more likely also with increasing biomass of krill and jellyfish (Pedersen et al., 2021) and the poleward shift of generalist species (Kortsch et al., 2015; Emblemswag, 2022).

Invasive fish species of Atlantic origin dominate in the topology of the meta-network, especially haddock and cod, but also redfish is quite central in the network. This supports that their invasion does really make an impact on the local community, as shown earlier (Kortsch et al., 2015).

Trawling influences a number of species in the Barents Sea ecosystem. These are assigned to 8 functional groups in our network model: LDEP and piscivorous fish with several sensitive species as well as 6 single species groups such as herring and capelin. LDEP is affected by strongly asymmetric effects of the invasive cod and haddock, so we can conclude that this functional group is the subject of double exposure (O'Brien and Leichenko, 2000).

The poleward shift of boreal species includes mostly generalists (*Argentina silus* in the pelagic planktivorous fish group and *Brosme brosme* in the large benthivorous fish group, see Supplementary

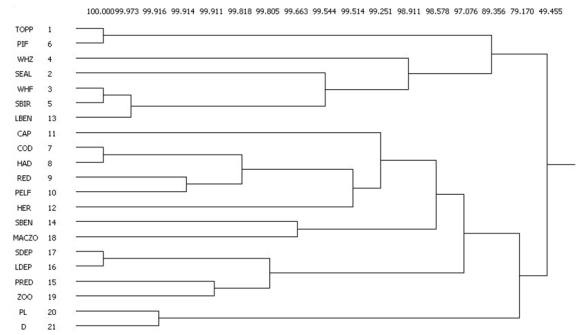

FIGURE 2
The REGE-based dendrogram showing the dissimilarities between the positions of organisms in the food web. For example, SDEP and LDEP are in very similar positions, while the positions of SDEP and WHF are quite different (values refer to similarity scores).

Material A), while benthivorous Arctic fish populations are decreasing (*Lycodes* spp. in the small benthivorous fish group and *Anarhichas denticulatus* in the large benthivorous fish group, see Supplementary Material A). This may change food web structure to more connected and more vulnerable state (Emblemswag, 2022). The increase of one and the decrease of another species within the large benthivorous fish group can be considered as a turnover of species from a functional point of view (i.e. relative abundances change at the species level but no major change at the functional group level). In other cases (pelagic planktivorous fish and small benthivorous fish), the similarity of network positions (Figure 2) may help to identify the key partners involved in the change, for example, competitors. If the pelagic planktivorous fish group increases, mostly redfish is influenced negatively (they are neighbors, forming a little branch), and for the same reasons, if small benthivorous fish decreases, mostly macrozooplankton is influenced positively. The similarity dendrogram helps the interpretation of changes at the level of trophic groups, from a more functional point of view. The strength of the expected competitive effects is proportional to the length of the segments in the dendrogram (i.e. close neighbors with short segments may imply stronger competition, cf. top predators and piscivorous fish versus small benthivorous fish and macrozooplankton). This suggests that the positive effect of declining small benthivorous fish on macrozooplankton may be slightly weaker.

An important component of the atlantification in the Barents Sea community may be similar to the changing control regime in the North Sea. Here, from predominantly bottom-up control (Fauchald et al., 2011), the system seems to being shifted towards mixed control, including some mid-trophic level species exerting wasp-waist control (with key bottom-up and top-down effects such as from haddock to large benthivorous fish and from haddock to LDEP, respectively, in our model). Wasp-waist topology does not automatically imply wasp-waist control (mixed bottom-up and top-down impact of a few species, Cury et al., 2000) but both may imply strong indirect interactions among species in the middle of the food web. If this is further supported by future studies, the chance of regime shifts and their dynamical consequences can be higher and needs further research.

If strong indirect and, especially, asymmetrical interactions are detected among commercially important fish species, the need for multi-species MSY assessment (May et al., 1979) is even stronger and developing policies considering these is more urgent. Here, food web theory and simulations can support policy-making (Legovic and Gecek, 2010; Legovic et al., 2010; Móréh et al., 2021).

In this article, we do not report on testing the predictions (e.g. by mesocosm experiments, time-series analyses) but we note that the approach is simple enough to potentially support indicator development or decision-making. Predictions can be tested on time-series, wherever available (like for reciprocity in plant-pollinator and plant-seed disperser networks, see Jordano, 1987). For fishing zones, data are probably available for testing the time-dynamics of links suggested here as being critical and predictable. Making and testing predictions is a generally hard task, especially in multi-species models, yet, simple predictions can be useful theoretical results (e.g. in loop analysis, Bodini and Clerici, 2016; Rodriguez et al., 2021; Fábián et al., 2022) generating and informing further empirical research.

Our future research on the Barents Sea ecosystem will focus on the spatial (e.g. Southern vs Northern region) and temporal (e.g. before and after the invasion of Atlantic species) variability of the food web (Frelat et al., 2022). Depending on the availability of high-quality time series (e.g. Kortsch et al., 2021), temporal changes may be described also in more than 2 stages (Uribe et al., 2021; Scotti et al., 2022). Further, we need a better topological description of the mathematical aggregation of species into functional groups (Abarca-Arenas and Ulanowicz, 2002) and loop analysis providing an alternative approach to crucial effects. The methodology used here can be performed also for weighted networks and it is a key question to see whether there is a major difference between the results for binary and weighted food webs (Scotti et al., 2007; Kortsch et al., 2021). In order to better explore the role of the c cutoff value, one potential solution is to define c as the smallest value where the asymmetry graph is still a DAG (directed acyclic graph), standardizing the definition and keeping the approach suitable for identifying clear cause-effect relationships.

Policy-making is based on simplified results and system-level indicators. Community control is an important property of ecological systems, providing crucial information to systems-based conservation and fisheries management. Whether top-down or bottom-up processes dominate has a major influence on the possible outcome of overfishing, for example. Our study aimed to contribute to developing the theoretical support for more predictive food web modelling, simplifying complexity by focusing on a few critical links in complex interaction networks. Our results provide support to the wasp-waist control of haddock, suggesting that special attention needs to be paid for this species. The high centrality of the boreal invaders (haddock, cod, redfish) means that even if these species show increasing tendencies in population size, they already have major community-wide effects in these Northern ecosystems. Zooplankton eater whales and large

benthivorous fish seem to be relatively unique in terms of their trophic niches. This suggests that overfishing these species may result in weak resilience, given the low level of overlap with other organisms.

Our results are based on a modelling exercise but, based on literature data and earlier findings, we suggest that these predictions may be quite feasible and realistic. Predictivity of results in food web research is always hard to justify, as experiments are of limited relevance in terms of spatio-temporal scales. We hope that our approach contributes to the development of systems-based, simple and quantitative toolkit of marine ecology.

Data availability statement

The original contributions presented in the study are included in the article/Supplementary Material. Further inquiries can be directed to the corresponding author.

Author contributions

FJ: Conceptualization, Methodology, Writing – original draft, Writing – review & editing. GC: Data curation, Methodology, Writing – review & editing. RP: Data curation, Investigation, Supervision, Writing – review & editing. AB: Funding acquisition, Methodology, Supervision, Writing – review & editing.

Funding

The author(s) declare financial support was received for the research, authorship, and/or publication of this article. The work of FJ was supported by the grant AtlantECO (H2020 BG-08-2018-2019, grant no. SEP-210591007) and also by a contract co-financed by the European Union - PON Research and Innovation 2014-2020 based on art. 24, paragraph 3, letter a) of the Law of 30 December 2010, Nr. 240 and subsequent amendments of Ministerial Decree of 10 August 2021 Nr. 1062.

Acknowledgments

We thank Marco Scotti for very useful advice on an earlier version of the manuscript and the anonymous reviewers for their excellent comments.

Conflict of interest

Author FJ was employed by the company KeyNode Research Ltd.

The remaining authors declare that the research was conducted in the absence of any commercial or financial relationships that could be construed as a potential conflict of interest.

Publisher's note

Supplementary material

The Supplementary Material for this article can be found online at: https://www.frontiersin.org/articles/10.3389/fmars.2024.1301612/full#supplementary-material.

References

Abarca-Arenas, L. G., and Ulanowicz, R. E. (2002). The effects of taxonomic aggregation on network analysis. *Ecol. Model.* 149, 285–296. doi: 10.1016/S0304-3800(01)00474-4

Allesina, S., and Bodini, A. (2004). Who dominates whom in the ecosystem? Energy flow bottlenecks and cascading extinctions. *J. Theor. Biol.* 230, 351–358. doi: 10.1016/j.jtbi.2004.05.009

Allesina, S., Bodini, A., and Bondavalli, C. (2006). Secondary extinctions in ecological networks: Bottlenecks unveiled. *Ecol. Model.* 194, 150–161. doi: 10.1016/j.ecolmodel.2005.10.016

Audzijonyte, A., Pethybridge, H., Porobic, J., Gorton, R., Kaplan, I., and Fulton, E. A. (2019). Atlantis: A spatially explicit end-to-end marine ecosystem model with dynamically integrated physics, ecology and socio-economic modules. *Methods Ecol. Evol.* 10, 1814–1819. doi: 10.1111/2041-210X.13272

Bodini, A., and Clerici, N. (2016). Vegetation, herbivores and fires in savanna ecosystems: A network perspective. *Ecol. Compl.* 28, 36–46. doi: 10.1016/j.ecocom.2016.10.001

Bond, W. J. (1994). "Keystone species," in *Biodiversity and ecosystem function*. Eds. E. D. Schulze and H. A. Mooney (Springer, Berlin, Germany), 255–270.

Bondavalli, C., and Bodini, A. (2014). How interaction strength affects the role of functional and redundant connections in food webs. *Ecol. Compl.* 20, 97–106. doi: 10.1016/j.ecocom.2014.09.004

Borgatti, S. P., Everett, M. G., and Freeman, L. C. (2002). *Ucinet for windows: software for social network analysis* (Harvard, MA: Analytic Technologies).

Brose, U., Berlow, E. L., and Martinez, N. D. (2005). Scaling up keystone effects from simple to complex ecological networks. *Ecol. Lett.* 8, 1317–1325. doi: 10.1111/j.1461-0248.2005.00838.x

Christensen, V., and Walters, C. J. (2004). Ecopath with Ecosim: methods, capabilities and limitations. *Ecol. Model.* 172, 109–139. doi: 10.1016/j.ecolmodel.2003.09.003

Cirtwill, A. R., Dalla Riva, G. V., Gaiarsa, M. P., Bimler, M. D., Cagua, E. F., Coux, C., et al. (2018). A review of species role concepts in food webs. *Food Webs* 16, e00093. doi: 10.1016/j.fooweb.2018.e00093

Cury, P., Bakun, A., Crawford, R. J. M., Jarre, A., Quiñones, R. A., Shannon, L. J., et al. (2000). Small pelagics in upwelling systems: patterns of interaction and structural changes in "wasp-waist" ecosystems. *ICES J. Mar. Sci.* 57, 603–618. doi: 10.1006/jmsc.2000.0712

Emblemswag, M. (2022). *Climate warming impact on the deep demersal fish community East of Greenland*. (PhD dissertation). The Arctic University of Norway, Tromsø.

Endrédi, A., Patonai, K., Podani, J., Libralato, S., and Jordán, F. (2021). Who is where in marine food webs? A trait-based analysis of network positions. *Front. Mar. Sci.* 8, 1315. doi: 10.3389/fmars.2021.636042

Endrédi, A., Senánszky, V., Libralato, S., and Jordán, F. (2018). Food web dynamics in trophic hierarchies. *Ecol. Model.* 368, 94–103. doi: 10.1016/j.ecolmodel.2017.11.015

Estes, J. A., Tinker, M. T., Williams, T. M., and Doak, D. F. (1998). Killer whale predation on sea otters linking oceanic and nearshore ecosystems. *Science* 282, 473–476. doi: 10.1126/science.282.5388.473

Estrada, E. (2007). Characterization of topological keystone species: Local, global and "meso-scale" centralities in food webs. *Ecol. Compl.* 4, 48–57. doi: 10.1016/j.ecocom.2007.02.018

Everett, M. G., and Borgatti, S. (1991). Role colouring a graph. *Math. Soc Sci.* 21, 183–188. doi: 10.1016/0165-4896(91)90080-B

Fábián, V., Reguly, I., and Jordán, F. (2022). Adding human impact to an ecological system model. *Ecol. Compl.* 50, 101000. doi: 10.1016/j.ecocom.2022.101000

Fath, B. D., Scharler, U. M., Ulanowicz, R. E., and Hannon, B. (2007). Ecological network analysis: network construction. *Ecol. Model.* 208, 49–55. doi: 10.1016/j.ecolmodel.2007.04.029

Fauchald, P., Skov, H., Skern-Mauritzen, M., Johns, D., and Tveraa, T. (2011). Wasp-waist interactions in the North Sea ecosystem. *PloS One* 6, e22729. doi: 10.1371/journal.pone.0022729

Finn, J. T. (1976). Measures of ecosystem structure and function derived from analysis of flows. *J. Theor. Biol.* 56, 363–380. doi: 10.1016/S0022-5193(76)80080-X

Fossheim, M., Primicerio, R., Johannesen, E., Ingvaldsen, R. B., Aschan, M. M., and Dolgov, A. V. (2015). Recent warming leads to a rapid borealization of fish communities in the Arctic. *Nat. Climate Change* 5, 673–677. doi: 10.1038/nclimate2647

Frelat, R., Kortsch, S., Kröncke, I., Neumann, H., Nordström, M. C., Olivier, P. E. N., et al. (2022). Food web structure and community composition: a comparison across space and time in the North Sea. *Ecography* 2022, e05945. doi: 10.1111/ecog.05945

Gjata, N., Scotti, M., and Jordán, F. (2012). The strength of simulated indirect interaction modules in a real food web. *Ecol. Compl.* 11, 160–164. doi: 10.1016/j.ecocom.2012.01.005

Hairston, N. G., Smith, F. E., and Slobodkin, L. B. (1960). Community structure, population control, and competition. *Am. Nat.* 94, 421–425. doi: 10.1086/282146

Holt, R. D., and Bonsall, M. B. (2017). Apparent competition. *Ann. Rev. Ecol. Evol. Syst.* 48, 447–471. doi: 10.1146/annurev-ecolsys-110316-022628

Hunter, M. D., and Price, P. W. (1992). Playing chutes and ladders: heterogeneity and the relative roles of bottom-up and top-down forces in natural communities. *Ecology* 73, 724–732. doi: 10.2307/1940152

ICES (2022). "Barents Sea ecosystem – fisheries overview," in *Report of the ICES Advisory Committee, 2022. ICES Advice 2022, section 5.2.* doi: 10.17895/ices.advice.21640814

Jordán, F. (2009). Keystone species in food webs. *Phil. Trans. R. Soc. London Ser. B* 364, 1733–1741. doi: 10.1098/rstb.2008.0335

Jordán, F. (2022). The network perspective: vertical connections linking organizational levels. Jörgensen review. *Ecol. Model.* 473, 110112. doi: 10.1016/j.ecolmodel.2022.110112

Jordán, F., Liu, W.-C., and van Veen, F. J. F. (2003). Quantifying the importance of species and their interactions in a host-parasitoid community. *Commun. Ecol.* 4, 79–88. doi: 10.1556/ComEc.4.2003.1.12

Jordán, F., Liu, W.-C., and Wyatt, T. (2005). Topological constraints on the dynamics of wasp-waist ecosystems. *J. Mar. Syst.* 57, 250–263. doi: 10.1016/j.jmarsys.2005.05.002

Jordán, F., Scotti, M., Mike, Á., and Ortiz, M. (2014). Strong asymmetry indicating causality in food web simulations. *Mar. Ecol. Prog. Ser.* 512, 89–98. doi: 10.1016/j.jmarsys.2005.05.002

Jordano, P. (1987). Patterns of mutualistic interactions in pollination and seed dispersal: Connectance, dependence asymmetries, and coevolution. *Am. Nat.* 129, 657–677. doi: 10.1086/284665

Karsenti, E., Acinas, S. G., Bork, P., Bowler, C., De Vargas, C., Raes, J., et al. (2011). A holistic approach to marine ecosystems biology. *PloS Biol.* 9, e1001177. doi: 10.1371/journal.pbio.1001177

Kortsch, S., Frelat, R., Pecuchet, L., Olivier, P., Putnis, I., Bonsdorff, E., et al. (2021). Disentangling temporal food web dynamics facilitates understanding of ecosystem functioning. *J. Anim. Ecol.* 90, 1205–1216. doi: 10.1111/1365-2656.13447

Kortsch, S., Primicerio, R., Aschan, M., Lind, S., Dolgov, A. V., and Planque, B. (2019). Food-web structure varies along environmental gradients in a high-latitude marine ecosystem. *Ecography* 42, 295–308. doi: 10.1111/ecog.03443

Kortsch, S., Primicerio, R., Fossheim, M., Dolgov, A. V., and Aschan, M. (2015). Climate change alters the structure of arctic marine food webs due to poleward shifts of boreal generalists. *Proc. R. Soc B* 282, 20151546. doi: 10.1098/rspb.2015.1546

Lafferty, K. D., Dobson, A. P., and Kuris, A. M. (2006). Parasites dominate food web links. *Proc. Natl. Acad. Sci. U.S.A.* 103, 11211–11216. doi: 10.1073/pnas.0604755103

Legovic, T., and Gecek, S. (2010). Impact of maximum sustainable yield on independent populations. *Ecol. Model.* 221, 2108–2111. doi: 10.1016/j.ecolmodel.2010.05.015

Legovic, T., Klanjscek, J., and Gecek, S. (2010). Maximum sustainable yield and species extinction in ecosystems. *Ecol. Model.* 221, 1569–1574. doi: 10.1016/j.ecolmodel.2010.03.024

Lin, W. H., Lai, S. M., Davis, A. J., Liu, W. C., and Jordán, F. (2022). A network-based measure of functional diversity in food webs. *Biol. Lett.* 18, 20220183. doi: 10.1098/rsbl.2022.0183

Livi, C. M., Jordán, F., Lecca, P., and Okey, T. A. (2011). Identifying key species in ecosystems with stochastic sensitivity analysis. *Ecol. Model.* 222, 2542–2551. doi: 10.1016/j.ecolmodel.2010.09.025

Luczkovich, J. J., Borgatti, S. P., Johnson, J. C., and Everett, M. G. (2003). Defining and measuring trophic role similarity in food webs using regular equivalence. *J. Theor. Biol.* 220, 303–321. doi: 10.1006/jtbi.2003.3147

May, R. M., Beddington, R. J., Clark, C. W., Holt, S. J., and Laws, R. M. (1979). Management of multispecies fisheries. *Science* 205, 267–277. doi: 10.1126/science.205.4403.267

Móréh, Á., Endrédi, A., Piross, I. S., and Jordán, F. (2021). Topology of additive pairwise effects in food webs. *Ecol. Model.* 440, 109414. doi: 10.1016/j.ecolmodel.2020.109414

Müller, C. B., Adriaanse, I. C. T., Belshaw, R., and Godfray, H. C. J. (1999). The structure of an aphid-parasitoid community. *J. Anim. Ecol.* 68, 346–370. doi: 10.1046/j.1365-2656.1999.00288.x

O'Brien, K. L., and Leichenko, R. M. (2000). Double exposure: assessing the impacts of climate change within the context of economic globalization. *Global Environ. Change* 10, 221–232. doi: 10.1016/S0959-3780(00)00021-2

Odenbaugh, J. (2006). The strategy of "The strategy of model building in population biology". *Biol. Philos.* 21, 607–621. doi: 10.1007/s10539-006-9049-3

Oksanen, L., Fretwell, S. D., Arruda, J., and Niemelä, P. (1981). Exploitation ecosystems in gradients of primary productivity. *Am. Nat.* 118, 240–261. doi: 10.1086/283817

Pecuchet, L., Lindegren, M., Kortsch, S., Całkiewicz, J., Jurgensone, I., Margonski, P., et al. (2020a). Spatio-temporal dynamics of multi-trophic communities reveal ecosystem-wide functional reorganization. *Ecography* 43, 197–208. doi: 10.1111/ecog.04643

Pecuchet, L., Blanchet, M.-A., Frainer, A., Husson, B., Jørgensen, L. L., Kortsch, S., et al. (2020b). Novel feeding interactions amplify the impact of species redistribution on an Arctic food web. *Global Change Biol.* 26, 4894–4906. doi: 10.1111/gcb.15196

Pedersen, T., Mikkelsen, N., Lindstrøm, U., Renaud, P. E., Nascimento, M. C., Blanchet, M.-A., et al. (2021). Overexploitation, recovery, and warming of the Barents Sea ecosystem during 1950–2013. *Front. Mar. Sci.* 8, 732637. doi: 10.3389/fmars.2021.732637

Ripple, W. J., Estes, J. A., Schmitz, O. J., Constant, V., Kaylor, M. J., Lenz, A., et al. (2016). What is a trophic cascade? *Trends Ecol. Evol.* 31, 842–849. doi: 10.1016/j.tree.2016.08.010

Rodriguez, M., Bodini, A., Escobedo, F. J., and Clerici, N. (2021). Analyzing socio-ecological interactions through qualitative modeling: Forest conservation and implications for sustainability in the peri–urban Bogota (Colombia). *Ecol. Model.* 439, 109344. doi: 10.1016/j.ecolmodel.2020.109344

Sala, E., and Graham, M. H. (2002). Community-wide distribution of predator–prey interaction strength in kelp forests. *Proc. Natl. Acad. Sci. U.S.A.* 99, 3678–3683. doi: 10.1073/pnas.052028499

Scotti, M., Bondavalli, C., Rossetti, G., and Bodini, A. (2022). Flow network indices signal a directional change in ecosystems: Evidence from a small mountain lake (Lake Santo, Northern Italy). *Ecol. Indic.* 139, 108896. doi: 10.1016/j.ecolind.2022.108896

Scotti, M., Podani, J., and Jordán, F. (2007). Weighting, scale dependence and indirect effects in ecological networks: a comparative study. *Ecol. Compl.* 4, 148–159. doi: 10.1016/j.ecocom.2007.05.002

Shin, Y. J., and Cury, P. (1999). "OSMOSE: a multispecies individual-based model to explore the functional role of biodiversity in marine ecosystems," in *Ecosystem approaches for fisheries management.* (Fairbanks: University of Alaska Sea Grant), 593–607.

Taruttis, F., Spang, R., and Engelmann, J. C. (2015). A statistical approach to virtual cellular experiments: improved causal discovery using accumulation IDA (aIDA). *Bioinformatics* 31, 3807–3814. doi: 10.1093/bioinformatics/btv461

Ulanowicz, R. E., and Puccia, C. J. (1990). Mixed trophic impacts in ecosystems. *Coenoses* 5, 7–16.

Uribe, R. A., Ortiz, M., and Jordán, F. (2021). Discrete steps of successional pathways differ in kelp forest and urchin barren communities. *Commun. Ecol.* 22, 41–54. doi: 10.1007/s42974-020-00035-2

Wootton, J. T., and Emmerson, M. (2005). Measurement of interaction strength in nature. *Ann. Rev. Ecol. Evol. Syst.* 36, 419–444. doi: 10.1146/annurev.ecolsys.36.091704.175535

Xu, Y., Huo, X., Jordán, F., Zhou, M., Cai, Y., and Sun, J. (2023). Identifying marine food web homogenization patterns. *Front. Mar. Sci.* 10, 1245513. doi: 10.3389/fmars.2023.1245513

Frontiers in Marine Science

Explores ocean-based solutions for emerging global challenges

The third most-cited marine and freshwater biology journal, advancing our understanding of marine systems and addressing global challenges including overfishing, pollution, and climate change.

Discover the latest Research Topics

See more →

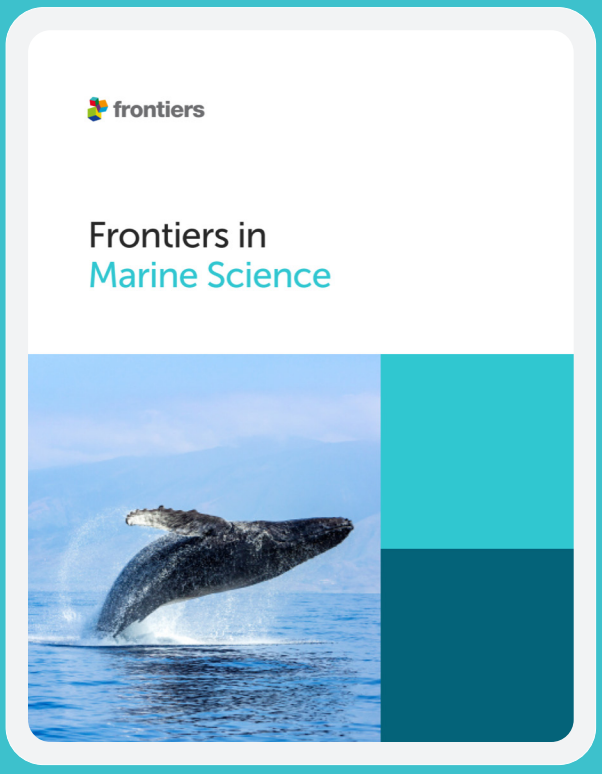

Frontiers

Avenue du Tribunal-Fédéral 34
1005 Lausanne, Switzerland
frontiersin.org

Contact us

+41 (0)21 510 17 00
frontiersin.org/about/contact